Effects of Functionality and Charge in the Design of Acrylic Polymers

Rebecca Huyck Brown

Dissertation submitted to the faculty of the Virginia Polytechnic Institute and State University in partial fulfillment of the requirements for the degree of

Doctor of Philosophy

In

Chemistry

Timothy E. Long, Chair
Richey M. Davis, Committee Member
Robert B. Moore, Committee Member
Judy S. Riffle, Committee Member
James M. Tanko, Committee Member

August 26, 2009

Blacksburg, Virginia

Keywords: living polymerization, n-butyl acrylate, organoaluminum, nitroxide mediated polymerization, zwitterion, sulfobetaine, ionomer, electrospinning, solution rheology

Effects of Functionality and Charge in the Design of Acrylic Polymers

Rebecca Huyck Brown

ABSTRACT

Use of a mixed triisobutylaluminum/1,1-diphenylhexyllithium intiator enabled the anionic polymerization of methyl methacrylate at room temperature, resulting in narrow molecular weight distributions and syndiorich structures. Polymerizations were controlled above Al:Li = 2, and control significantly decreased at elevated temperatures above 25 °C. A significant increase in T_g with increasing control of syndiotacticity demonstrated the ability to tailor polymer properties using this technique. Analysis with MALDI-TOF/TOF spectroscopy revealed the dominance of a back-biting side reaction at elevated temperatures.

Hydroxy-functional random and block copolymers of n-butyl acrylate (nBA) and 2-hydroxyethyl acrylate were synthesized using nitroxide mediated polymerization. Controlled polymerization was demonstrated, resulting in narrow polydispersities and linear molecular weight vs. conversion plots. In situ FTIR spectroscopy monitored the polymerizations and revealed pseudo first order rate kinetics for random copolymerizations. Protection of the hydroxyl using trimethylsilyl chloride alleviated isolation issues of amphiphilic polymer products.

For the first time zwitterion-containing copolymers were electrospun to form nanoscale fibers with diameters as low as 100 nm. Free radical copolymerization of nBA and sulfobetaine methacrylamide produced zwitterionic copolymers with 6-13 mol % betaine. Dynamic mechanical analysis revealed a rubbery plateau and biphasic morphology similar to ionomers. Electrospinning from chloroform/ethanol solutions (80/20 v/v) at 2-7 wt % afforded polymeric

fibers at viscosities below 0.02 Pa·s, which is the lowest viscosity observed for fiber formation in our laboratories. We hypothesized that intermolecular interactions rather than chain entanglements dominated the electrospinning process.

Solution rheology of zwitterionic copolymers containing 6 and 9 mol % sulfobetaine methacrylate functionality revealed two concentration regimes with a boundary at ~1.5 – 2.0 wt %, regardless of molecular weight. This transition occurred at an order of magnitude lower specific viscosity than the entanglement concentration (C_e) for poly(nBA), and correlated to the onset of fiber formation in electrospinning. Comparison to existing models for polymer solution dynamics showed closest agreement to Rubinstein's theory for associating polymers, in support of our hypothesis that zwitterionic interactions dominate solution dynamics.

The effect of ionic liquid (IL) uptake on mechanical properties and morphology of zwitterionic copolymers was explored using 1-ethyl-3-methylimidazolium ethylsulfate (EMIm ES). Dynamic mechanical analysis and impedance spectroscopy revealed a significant change in properties above a critical uptake of ~10 wt % IL. X-ray scattering revealed a significant swelling of the ionic domains at 15 wt % IL, with a 0.3 nm^{-1} shift in the ionomer peak to lower scattering vector. Results indicated the water-miscible IL preferentially swelled ionic domains of zwitterionic copolymers.

Acknowledgements

First I would like to acknowledge and thank my advisor, Dr. Tim Long, for many years of guidance and patience. He supported me in my career and life goals and challenged me to develop as a scientist and explore outside of my comfort zone. I am grateful for the numerous opportunities he gave me. I also want to thank Dr. Judy Riffle for her encouragement and assistance during my job search, as well as many helpful comments concerning my presentation and writing skills. I enjoyed my interactions with Dr. Jim Tanko concerning nitroxides/nitroxyls in the early years and appreciate his insight. I also thank Dr. Rick Davis and Dr. Bob Moore for their insight, helpful discussions, and valuable time.

I thank Kraton Polymers for financial support, especially Carl Willis and Donn Dubois for valuable discussions over the years. I also thank Eastman Chemical Company for the Eastman Fellowship, which has opened many doors of opportunity for me to travel and meet new people. In addition, I thank the NSF MILES IGERT program for financial support and fostering my interdisciplinary education through coursework and casual interactions. I especially thank Dr. Mary Dean Coleman, Dr. Jaehee Hong, and Annie Aigster in the MILES office for their help, friendship, and support over the years. I acknowledge Millie Ryan, Laurie Goode, Mary Jane Smith, and Tammy Jo Hiner for assisting with numerous tasks to make things run smoothly. These ladies saved me countless number of hours filing paper work, organizing events, and printing posters.

I am indebted to a number of key collaborators that contributed to this work. I thank Dr. Tony Giese at Vanderbilt for MALDI analysis, Dr. Karen Winey and Jae-Hong Choi at the University of Pennsylvania for many hours worth of valuable x-ray scattering data, and Dr. Bob

Moore and Jong Keun Park for carting samples to Korea for x-ray scattering as a kind favor. I also thank Steve McCartney and John MacIntosh of the NCFL for their amazing patience and expertise with microscopy and imaging. I also thank Tom Glass, formerly of Analytical Services, for his endless knowledge and guidance with NMR, and Vicky Long for assistance and training in the Polymer Laboratory.

My time in graduate school was truly blessed with an amazing group of scientists, coworkers, and friends with whom I had the pleasure to work with every day. I especially want to thank the ladies and gentlemen of Davidson Hall that made my time at VT unforgettable. I thank Dr. Scott Trenor and Dr. Jeremy Lizotte, my first mentors at Virginia Tech, for passing on a wealth of knowledge and leading me down the right path early in my career. More importantly, I appreciate the support and friendship they continue to give long after serving as my SURP mentors. Dr. Matt McKee and Dr. Ann Fornof showed me the ropes of the laboratory (and the local bars) and helped make Blacksburg feel like home. Dr. John Layman and Erika Borgerding provided countless hours of entertainment and conversations about life, love, and the pursuit of quality SEC data. I thank Dr. Matthew Cashion for humoring me during my many ramblings, for helping solve numerous problems in the lab and in life, and for keeping me grounded in reality. I am grateful to Matthew Hunley for dedicating many hours of hard work and brain power to my difficult rheology data, electrospinning and microscopy. Two of the chapters in this work were inspired by the expertise and knowledge of Matt. I will certainly miss Café Disco and the hottest tailgate in Blacksburg. I thank my good buddy Tianyu (Mr. T) Wu for his insatiable curiosity, probing questions, and many laughs. I was honored to mentor such a bright young scientist and good friend. I thank the rest of the Davidson crew, Dr. Bill Heath, Dr. Takeo Suga, Andy Duncan, and Ali Nebipasagil, for many lively discussions, fun gatherings, and

scientific insight. I also thank Matthew Dale Green and Michael Allen, frequent visitors and adopted members of the Davidson crew, for many lunch excursions, ridiculous conversations, and valuable contributions to my research.

The rest of the scientists working in the Long group also greatly influenced my time at Virginia Tech and helped make countless fond memories. I especially want to thank Dr. Sharlene Williams and Dr. Gozde Ozturk for many years of friendship and valuable discussions. I thank Dr. Tomonori Saito for training me for success with anionic polymerization. I thank Dr. Brian Mather and Shijing Cheng for sharing their expertise with nitroxide synthesis. Finally, I thank Dr. Sean Ramirez, Dr. Gene Joseph, Dr. Philipe Bissel, Mana Tamami, Steve June, Emily Anderson, Eveline van der Aa, and Nancy Zhang for all of their unique contributions to my scientific understanding, laboratory work, and personal growth.

My time in graduate school would have been empty and meaningless without the constant love and support of my wonderful husband, Jason. I dedicate the last 5 years and all that this experience will bring to our future to him. He has been supportive far beyond what I deserved and I am confident I would not have made it through without him.

I am here today thanks to two of the most important people in my life, my parents Bruce and Johannah Huyck. They have supported me unconditionally in every endeavor and maintained constant support in my success. I also want to give special thanks to my brother Nathan Huyck who has always believed that I would do great things, and my grandmother Winn Huyck who has supported me every step of the way through my education from grade school to graduate school. Her stories of my grandfather the chemist have always touched my heart and encouraged me in ways I can't explain.

Finally, I thank all of my extended family, in-laws, and friends who have been a constant source of encouragement, distraction, and comic relief when needed. To all those that go unnamed, thank you for the many ways you have impacted and blessed my life over the past five years.

Attribution

Many colleagues and coworkers aided in the research, preparation, and writing behind several chapters of this dissertation. A brief description of their background and contributions are included here.

Prof. Timothy E. Long- Ph.D. (Department of Chemistry, Virginia Tech) is the primary Advisor and Committee Chair. Prof. Long provided great insight, inspiration, and critical evaluation for all the work discussed herein.

Chapter 5: Electrospinning Zwitterion-containing Nanoscale Acrylic Fibers

Matthew T. Hunley- Ph.D. Candidate (Department of Chemistry, Virginia Tech) is currently a student in the author's group and contributed during his graduate studies to this chapter in terms of training the author in solution electrospinning of fibers, evaluating fibers with microscopy, and discussing electrospinning results in great detail.

Michael H. Allen- Graduate Student (Department of Chemistry, Virginia Tech) is currently a student in the author's group and served as an undergraduate researcher on this project. He was involved in the synthetic procedures and initial electrospinning of zwitterionic fibers.

Chapter 7: Effect of Ionic Liquid on Mechanical Properties and Morphology of Zwitterionic Copolymer Membranes

Andrew J. Duncan- Ph.D. Candidate (Department of Mechanical Engineering, Virginia Tech) aided in the evaluation of membrane conductivity and offered much insight in the use of ionic liquids with polymeric membranes.

Jae-Hong Choi- Graduate Student (Department of Materials Science and Engineering, University of Pennsylvania) performed the X-ray scattering of zwitterionic copolymers and was involved in the interpretation of results.

Jong K. Park- Graduate Student (Department of Chemistry, Virginia Tech) also performed X-ray scattering of zwitterionic membranes and assisted in the interpretation of scattering results.

Tianyu Wu- Graduate Student (Department of Chemistry, Virginia Tech) is a student in the author's group intricately involved in the zwitterion research project. He contributed to the synthesis and characterization of zwitterionic copolymers, as well as the discussion of analytical data.

Donald J. Leo- Ph.D. (Department of Mechanical Engineering, Virginia Tech) is a collaborator on this project that provided access to impedance spectroscopy for the evaluation of membrane conductivity in this work.

Karen I. Winey- Ph.D. (Department of Materials Science and Engineering, University of Pennsylvania) is a collaborator on this work that provided access to X-ray scattering instrumentation and numerous discussions of results.

Robert B. Moore- Ph.D. (Department of Chemistry, Virginia Tech) is a Committee Member and collaborator in the X-ray scattering of zwitterionomers. He was also involved in the critical analysis of data and editing of this work.

Table of Contents

Chapter 1: Introduction 1

1.1 Dissertation Overview 1

Chapter 2: Organoaluminum Additives in the Controlled and Stereospecific Anionic Polymerization of Methacrylates 3

2.1 Abstract 3

2.2 Scientific Perspective 4

2.3 Side Reactions in the Anionic Polymerization of Methacrylates 7

2.4 Reagent Selection in Controlling Anionic Polymerization of Methacrylates 9

2.4.1 Alkyl Lithiums and Aluminums 9

2.4.2 Lithium/Aluminum Complex 12

2.4.3 Polymerization Solvent 14

2.5 Mechanism of Polymerization Control in the Presence of Organoaluminums 14

2.5.1 Initiation and Termination 15

2.5.2 Role of Excess Aluminum in Monomer Activation 17

2.5.3 Formation of Coordinative Networks 19

2.6 Tacticity Control in the Presence of Organoaluminums 22

2.7 Block, Star, and Graft Copolymer Architectures via Screened Anionic Polymerization 24

2.8 Organoaluminums in the Controlled Anionic Polymerization of Acrylates 26

2.9 Application of Organoaluminums to Other Monomers in Anionic Polymerization 29

2.10 Retarded Anionic Polymerization of Styrene 30

2.11 Future Perspectives 31

2.12 References 33

Chapter 3: Factors Influencing the Room Temperature Anionic Polymerization of Alkyl Methacrylates in the Presence of Aluminum Alkyls 36

3.1 Abstract 36

3.2 Introduction 37

3.3 Experimental 38

3.3.1 Materials 38
3.3.2 Instrumentation 39
3.3.3 MALDI-TOF/TOF CID Measurements....39
3.3.4 Synthesis of 1,1-Diphenylhexyllithium (DPHL) 40
3.3.5 Measuring Initiator Concentration and Purity 40
3.3.6 Synthesis of Poly(methyl methacrylate) (PMMA) Homopolymers 41
3.4 Results and Discussion....42
3.4.1 Initiator Choice and Quality....42
3.4.2 Effect of Al:Li Ratio on Polymerization Control at Room Temperature 43
3.4.3 Effect of Temperature on Polymerization Control of MMA 46
3.4.4 In situ FTIR Monitoring of MMA Polymerization....52
3.5 Conclusions 57
3.6 Acknowledgements 58
3.7 References 58

Chapter 4: Nitroxide Mediated Polymerization of Hydroxy-functionalized Copolymers....59
4.1 Abstract 59
4.2 Introduction 59
4.3 Experimental 61
4.3.1 Materials 61
4.3.2 Instrumentation 62
4.3.3 Purification of HEA 62
4.3.4 Synthesis of silyl-protected HEA (HEA-TMS) 63
4.3.5 Synthesis of poly(n-butyl acrylate) (PnBA) with DEPN....63
4.3.6 Synthesis of poly((*n*BA-*co*-HEA-TMS)-*b*-styrene) 64
4.3.7 Synthesis of poly(nBA-*b*-HEA-TMS) 65
4.4 Results and Discussion....65
4.4.1 Homopolymerization of n-butyl acrylate....65
4.4.2 Copolymerization of nBA with HEA and HEA-TMS....67
4.4.3 Synthesis and Characterization of Block Copolymers....73

4.5 Conclusions 78
4.6 Acknowledgements 79
4.7 References 79

Chapter 5: Electrospinning Zwitterion-containing Nanoscale Acrylic Fibers 81

5.1 Abstract 81
5.2 Introduction 82
5.3 Experimental 85
5.3.1 Materials 85
5.3.2 Synthesis of poly(n-butyl acrylate-*co*-sulfobetaine methacrylamide) (PnBA-*co*-PSBMAm) 85
5.3.3 Synthesis of poly(*n*-butyl acrylate) (PnBA) 86
5.3.4 Electrospinning 86
5.3.5 Instrumentation 87
5.4 Results and Discussion 88
5.4.1 Synthesis of Zwitterionic Copolymers 88
5.4.2 Dynamic Mechanical Analysis of Zwitterionic Copolymers 91
5.4.3 Electrospinning Nanoscale Fibers 93
5.4.3.1 Effect of Solution Concentration on Fiber Morphology 93
5.4.3.2 Effect of Solution Concentration on Fiber Diameter 96
5.4.3.3 Influence of Zwitterion Aggregation on the Electrospinning Process Compared to Neutral PnBA 98
5.5 Conclusions 101
5.6 Acknowledgements 102
5.7 References 102

Chapter 6: Correlation of Solution Rheological Behavior with Electrospinning for Zwitterionomers 104

6.1 Abstract 104
6.2 Introduction 105
6.3 Experimental 107

6.3.1 Materials 107
6.3.2 Synthesis of sulfobetaine methacrylate-*co*-butyl acrylate copolymers.....108
6.3.3 Synthesis of poly(n-butyl acrylate) (PnBA) 108
6.3.4 Electrospinning 108
6.3.5 Instrumentation 109
6.4 Results and Discussion.....110
6.4.1 Synthesis and Characterization of Zwitterionomers.....110
6.4.2 Solution Rheology and Determination of Concentration Regimes for Zwitterionomers.....112
6.4.3 Electrospinning of Ester-linked Zwitterionomers to Form Nanoscale Fibers 123
6.5 Conclusions 129
6.6 Acknowledgement.....130
6.7 References 130

Chapter 7: Effect of Ionic Liquid on Mechanical Properties and Morphology of Zwitterionic Copolymer Membranes 133
7.1 Abstract 133
7.2 Introduction 134
7.3 Experimental 136
7.3.1 Materials 136
7.3.2 Synthesis of sulfobetaine methacrylate-*co*-butyl acrylate copolymers.....136
7.3.3 Membrane Preparation and Swelling in Ionic Liquid.....137
7.3.4 Instrumentation 137
7.4 Results and Discussion.....139
7.4.1 Synthesis and Characterization of Zwitterionomers.....139
7.4.2 Swelling of Zwitterionomers in Ionic Liquid 143
7.4.3 Mechanical Properties of Ionic Liquid Swollen Membranes 145
7.4.4 Morphological Changes in the Presence of Ionic Liquid.....148

7.4.5 Effect of IL Swelling on Membrane Conductivity 151
7.5 Conclusions 155
7.6 Acknowledgements 156
7.7 References 156

Chapter 8: Nitroxide Free Radicals in Synthetic and Biological Macromolecules.....158
8.1 Scientific Rationale and Perspective 158
8.2 Chemistry of Nitroxide Radicals 159
8.2.1 Structural requirements of nitroxides as stable free radicals 159
8.2.2 Reactivity of nitroxide free radicals.....163
8.3 Nitroxides as Mediators in the Synthesis of Macromolecules 166
8.3.1 Nitroxide Mediated Polymerization.....166
8.3.2 Commonly used nitroxides in NMP 168
8.3.3 Advantages of control with nitroxide mediators.....170
8.4 Nitroxides as Tags on Biological Macromolecules.....171
8.4.1 Site directed spin labeling and EPR spectroscopy.....171
8.4.2 Features of common tags used for biological macromolecules.....173
8.4.3 Probing molecular dynamics and motion with nitroxide tags 177
8.4.3.1 Studying protein structure and function relationships 177
8.4.3.2 Monitoring DNA dynamics through spin-labeled oligonucleotides.....179
8.5 Conclusions 180
8.6 References 181

Chapter 9: Overall Conclusions 185

Chapter 10: Future Work 192

10.1 Living Polymerization of Functional Triblock Copolymers.....192

10.2 Applications of Zwitterionic Copolymers in Electroactive Devices 198

10.3 Solution Rheology of Zwitterionic Copolymers.....201

10.4 Comparison of Zwitterionomers and Ammonium Cationic Polyelectrolyte Analogs.....202

10.5 References.....203

List of Figures

Figure 2.1 The chain end in methacrylate anionic polymerization features charge delocalization with two major resonance contributors, the carbanion and the enolate forms. 7

Figure 2.2 Intramolecular attack on an in-chain carbonyl terminates the chain with a six-membered ring 8

Figure 2.3 Nucleophilic attack on monomer carbonyl competes with initiation to form *t*-butyl isoprenyl ketone 8

Figure 2.4 Synthesis of (2,6-di-*tert*-butyl-4-methylphenoxy)diisobutylaluminum ($^{i}Bu_2Al(BHT)$) 11

Figure 2.5 Select organoaluminums for the formation of syndiorich poly(alkyl methacrylates) 12

Figure 2.6 Linking of Al and Li in the initiating complex occurs through carbon bridges 13

Figure 2.7 Coordination of the aluminum alkyl to ester groups of the monomer forms an activated monomer complex 18

Figure 2.8 Four resonance contributors of the MMA:Al adduct 18

Figure 2.9 Bimolecular chain propagation mechanism proposed by Rodriguez-Delgado and Chen for the polymerization of MMA using a lithium ester enonlaluminate/organoaluminum combination.....19

Figure 2.10 The interaction of aluminum alkyls and ester enolates in polymer coordinative networks.....20

Figure 2.11 Stereoregular chain structures of PMMA 23

Figure 3.1 SEC of PMMA samples produced with varying amounts of $^{i}Bu_3Al$.....45

Figure 3.2 Predominant polymer product structures expected in MALDI-TOF MS spectra. (**a**) Desired structure with initiator and proton endgroups. (**b**) Side product resulting from back-biting reaction to form a cyclic endgroup 48

Figure 3.3 MALDI-TOF MS spectra of PMMA synthesized at using $^{i}Bu_3Al$/DPHL 2.1:1; (a) 0 °C, (b) 25 °C, (c) 40 °C, (d) 50 °C.....50

Figure 3.4 *In situ* FTIR waterfall plot of the vinyl region of MMA during polymerization at 0 °C, where absorbance is decreasing with time 53

Figure 3.5 Kinetic analysis of the vinyl stretch at 1327 cm^{-1} for PMMA at 0 °C with Al:Li of 2.1 54

Figure 3.6 Kinetic analysis of the vinyl stretch at 1327 cm^{-1} for PMMA at 27.5 °C with Al:Li of 2.1.....55

Figure 3.7 SEC traces of PMMA synthesized at 27.5 °C with Al:Li 2.1 where the blue curve corresponds to PMMA monitored with in situ FTIR and the red curve represents a control experiment without in situ FTIR monitoring.....56

Figure 4.1 Molecular weight vs conversion for n-butyl acrylate, 130 °C in bulk, 2.5 excess DEPN:AIBN. Δ M_n ■ M_w/M_n.....67

Figure 4.2 SEC chromatograms of poly(nBA-*co*-HEA-TMS). Monomer conversion increases from right to left as molecular weight increases.....69

Figure 4.3 Molecular weight vs conversion for copolymerization of nBA and HEA-TMS, 130 °C in bulk, 2.5 excess DEPN:AIBN. Δ M_n ■ M_w/M_n.....70

Figure 4.4 In situ FTIR waterfall plot of monomer conversion (vinyl region 920-1020 cm^{-1}) ...72

Figure 4.5 Pseudo first order kinetic analysis for DEPN mediated copolymerizations at 988 cm^{-1}. ◊ Copolymerization of nBA and HEA-TMS ■ Hompolymerization of nBA ▲ Copolymerization of nBA and HEA.....73

Figure 4.6 SEC chromatograms showing the block addition of styrene to poly(nBA-*co*-HEA-TMS) (a), where (b) is the block copolymer product 74

Figure 4.7 SEC chromatograms showing successful block addition to poly(nBA) (a), to form poly(nBA-*b*-HEA-TMS) (b) 77

Figure 4.8 ^1H NMR of poly(nBA-*b*-HEA-TMS) in $CDCl_3$.....78

Figure 5.1 Reproducible SEC chromatograms of $PnBA_{90}$-*co*-$PSBMAm_{10}$.....90

Figure 5.2 Storage modulus at 1 Hz as a function of temperature for PnBA-*co*-PSBMAm containing 6, 10, and 13 mol% SBMAm.....92

Figure 5.3 FESEM images of $PnBA_{90}$-*co*-$PSBMAm_{10}$ electrospun fibers at various solution concentrations in chloroform/ethanol (80/20 v/v) 94

Figure 5.4 FESEM images of electrospun fibers of $PnBA_{94}$-*co*-$PSBMAm_6$ and $PnBA_{87}$-*co*-$PSBMAm_{13}$ at increasing solution concentrations in chloroform/ethanol (80/20 v/v) 95

Figure 5.5 Average fiber diameters of $PnBA_{94}$-*co*-$PSBMAm_6$, $PnBA_{90}$-*co*-$PSBMAm_{10}$, and $PnBA_{87}$-*co*-$PSBMAm_{13}$ as a function of solution concentration in chloroform/ethanol (80/20 v/v) 96

Figure 5.6 Dependence of fiber diameter on solution concentration for $PnBA_{90}$-*co*-$PSBMAm_{10}$ 97

Figure 5.7 FESEM images of low T_g PnBA (M_w 278,000 g/mol, M_w/M_n = 2.56) after attempted electrospinning from chloroform/ethanol (80/20 v/v) at different solution concentrations: (a) at 5.0 wt%, electrospraying of droplets onto collection grids occurred; (b) at 30 wt%, fibers were initially collected but flowed onto grid prior to analysis 99

Figure 5.8 Dependence of viscosity on shear rate for zwitterionomers and PnBA at concentrations (in 80/20 v/v chloroform/ethanol) equivalent to defect-free fiber formation.....100

Figure 6.1 Dependence of viscosity on shear rate for $PnBA_{91}$-*co*-$PSBMA_9$ (M_w = 265,000 g/mol) in chloroform at various concentrations.....113

Figure 6.2 Dependence of specific viscosity on concentration for PnBA (M_w = 283,000 g/mol) 114

Figure 6.3 Dependence of specific viscosity on concentration for $PnBA_{91}$-*co*-$PSBMA_9$ of varying molecular weights.....116

Figure 6.4 Dependence of specific viscosity on concentration for ◊ $PnBA_{94}$-*co*-$PSBMA_6$ M_w = 274,000 g/mol and ▲ $PnBA_{93}$-*co*-$PSBMA_7$ M_w= 447,000 g/mol.....118

Figure 6.5 Dependence of specific viscosity on concentration for $PnBA_{91}$-*co*-$PSBMA_9$ (M_w = 265,000 g/mol) under different solvent conditions. ■ chloroform; ▲ chloroform/ethanol 80/20 v/v 119

Figure 6.6 FESEM images of $PnBA_{91}$-*co*-$PSBMA_9$ (M_w = 324,000) electrospun fibers at various solution concentrations in chloroform/ethanol (80/20 v/v) 124

Figure 6.7 FESEM images of $PnBA_{94}$-*co*-$PSBMA_6$ (M_w = 447,000) electrospun fibers at various solution concentrations in chloroform/ethanol (80/20 v/v) 125

Figure 6.8 Dependence of fiber diameter on solution concentration for $PnBA_{91}$-*co*-$PSBMA_9$ and $PnBA_{94}$-*co*-$PSBMA_6$.....127

Figure 6.9 Comparison of fiber diameter dependence on solution concentration for $PnBA_{91}$-*co*-$PSBMA_9$ (M_w = 324,000) and $PnBA_{90}$-*co*-$PSBMAm_{10}$ (M_w = 344,000) 128

Figure 7.1 Structure of zwitterionic copolymers, (a) PnBA-*co*-PSBMA and (b) PnBA-*co*-PSBMAm.....139

Figure 7.2 X-ray scattering intensity vs. scattering vector (q) for PnBA-*co*-PSBMA (9 and 6 mol%), PnBA, and PSBMA 141

Figure 7.3 X-ray scattering intensity vs. scattering vector (q) for PnBA-*co*-PSBMAm (13, 9, and 6 mol%), PnBA, and PSBMAm 142

Figure 7.4 Chemical **s**tructure of 1-ehtyl-3-methylimidazolium ethylsulfate (EMIm ES).....143

Figure 7.5 Swelling behavior of $PnBA_{91}$-*co*-$PSBMA_9$ and $PnBA_{90}$-*co*-$PSBMAm_{10}$ in EMIm ES over a period of seven weeks 145

Figure 7.6 DMA storage modulus as a function of temperature for $PnBA_{91}$-*co*-$PSBMA_9$ at various levels of swelling in EMIm ES 146

Figure 7.7 Storage modulus vs. temperature profiles for $PnBA_{90}$-*co*-$PSBMAm_{10}$ (M_w 295,000 g/mol) at various swelling levels 148

Figure 7.8 X-ray scattering intensity vs. scattering vector (q) for $PnBA_{91}$-*co*-$PSBMA_9$ at increasing levels of IL content showing the shift in the ionomer peak; PnBA is also plotted for comparison of the high q region 149

Figure 7.9 X-ray scattering intensity vs. scattering vector (q) for $PnBA_{90}$-*co*-$PSBMAm_{10}$ at three swelling levels of IL showing a shift in the ionomer peak; PnBA is also plotted for comparison of the high q region 150

Figure 7.10 Semi-log plot of ionic conductivity vs. IL uptake for $PnBA_{91}$-*co*-$PSBMA_9$ membranes in EMIm ES 152

Figure 7.11 Ionic conductivity of $PnBA_{91}$-*co*-$PSBMA_9$ membranes in EMIm ES, plotted as a function of IL uptake, revealing a critical uptake transition 153

Figure 7.12 Semi-log plot of ionic conductivity vs IL uptake for $PnBA_{91}$-*co*-$PSBMA_9$ (◊, Δ) and $PnBA_{90}$-*co*-$PSBMAm_{10}$ (▲) membranes in EMIm ES 154

Figure 8.1 General structure of nitroxyl radicals, where R_1 and R_2 represent bulky alkyl substituents.....158

Figure 8.2 Resonance contributors of a stable nitroxide.....160

Figure 8.3 Examples of common stable nitroxides.....161

Figure 8.4 Alkoxyamine unimolecular initiators for NMP.....170

Figure 8.5 Spin labels are attached to proteins through the sulfhydryl group of cysteine. In order to maintain site label specificity, all native cysteines in a protein sequence which are not meant for spin label attachment must be replaced with amino acids of a similar size, mainly alanine and glycine.....173

Figure 8.6 Attachment of MTSSL to protein backbone through cysteine residues.....175

Figure 8.7 TEMPO-labeled uracil linked by a flexible ethyldiamino tether 176

Figure 10.1 Aqueous SEC of Poly(SBMA) synthesized using various DEPN:BlocBuilder ratios 198

Figure 10.2 Components of an ionic polymer transducer (IPT) device.....201

Figure 10.3 Monomers for comparison of zwitterion with structurally similar cationic monomers 203

List of Schemes

Scheme 3.1 Screened anionic polymerization of MMA in the presence of $^{i}Bu_3Al$ 43

Scheme 4.1 Bulk polymerization of n-butyl acrylate with excess DEPN.....66

Scheme 4.2 Nitroxide mediated polymerization of copolymers containing 10 mol % HEA or HEA-TMS.....68

Scheme 4.3 Synthesis of diblock copolymer, poly(nBA-*b*-HEA-TMS) 76

Scheme 5.1 Synthesis of poly(n-butyl acrylate-*co*-sulfobetaine methacrylamide) (PnBA-*co*-PSBMAm) 89

Scheme 6.1. Synthesis of P*n*BA-*co*-PSBMA copolymers 111

Scheme 8.1 Different oxidation states of nitroxides 165

Scheme 8.2 Three reaction rates (k_{act}, k_{deact}, and k_p) govern the TEMPO-mediated polymerization of styrene. Propagation occurs through the activated state, which exists at low concentrations due to an equilibrium favoring the deactivated form 167

Scheme 10.1 Sequential block addition of MMA and tBMA to form acrylic diblock copolymer using screened anionic polymerization.....193

Scheme 10.2 Synthesis of difunctional poly(nBA) using $DEPN_2$ difunctional alkoxyamine ...194

Scheme 10.3 Proposed synthesis of triblock copolymer through addition of HEA-TMS to poly(nBA) macroinitiator.....195

Scheme 10.4 Proposed synthetic route for the formation of zwitterionic block copolymers with n-butyl acrylate mid-block. 196

Scheme 10.5 Aqueous nitroxide mediated polymerization of SBMA using deprotonated BlocBuilder.....197

List of Tables

Table 3.1 Effects of Al:Li ratio on molecular weight control, yield, tacticity, and glass transition temperature (T_g) at 25 °C 44

Table 3.2 Characterization of PMMA synthesized at various temperatures with Al:Li 2.1 47

Table 3.3 Polymer properties of PMMA synthesized with and without in situ FTIR monitoring.... 56

Table 4.1 Molecular weight and composition of HEA/nBA copolymers 71

Table 4.2 Pseudo first order rate constants for the DEPN-mediated polymerization of nBA, nBA/HEA, and nBA/HEA-TMS 73

Table 4.3 Molecular weight characterization of block copolymers 77

Table 5.1 Summary of polymers and concentration ranges for electrospinning study 87

Table 5.2 Relative molecular weights of zwitterionic copolymers 91

Table 5.3 Fiber diameter scaling exponents for copolymers of various zwitterion concentrations 98

Table 6.1 Relative molecular weights of PnBA-*co*-PSBMA 112

Table 6.2 Concentration regimes for $PnBA_{91}$-*co*-$PSBMA_9$ as a function of molecular weight .116

Table 7.1 Relative molecular weights of zwitterionomers.....140

Table 7.2 Summary of scattering peaks and d-spacings for zwitterionomers, PnBA, and zwitterionic homopolymers 142

Table 7.3 Summary of scattering peaks and d-spacings for zwitterionomers swollen in IL 150

Table 10.1 Molecular Weight Characterization of Poly(nBA) prepared with $DEPN_2$ 194

Chapter 1: Introduction

1.1 Dissertation Overview

The design of polymeric materials with well-defined functionality is increasingly important with the growing demand for new technologies and high performance polymers and composites. Functional polymers with tailored performance properties are needed for new technological advances in many fields, including alternative energy, biomedicine, stimuli-responsive materials, biomimetics, and semiconductors. The overarching objective of this work is to utilize various forms of functionality in acrylic polymer design to afford new functional materials. Functionality is explored from three different perspectives. First, stabilization of the chain-end carbanion and radical in living polymerization of alkyl (meth)acrylates affords well-defined polymer structures. Second, incorporation of hydroxyls on the polymer chain enable tailored polymer properties through chemical modification. Finally, the use of zwitterions as sites for ionic interaction enables tailoring of polymer morphology and mechanical performance.

The first half of this dissertation covers the influence of both charge and functionality in the living polymerization of alkyl acrylates and alkyl methacrylates. The second chapter reviews the principles of organoaluminum mediated anionic polymerization of methacrylates, and highlights the progress in affording stereocontrolled polymerization through stabilization of the living chain end. The limits of control afforded in aluminum-mediated polymerization of methyl methacrylate as a function of aluminum:lithium ratio and temperature were explored in chapter 3. MALDI-TOF analysis was used to identify the degree of endgroup control at elevated temperatures of polymerization. In chapter 4, the technique of nitroxide mediated radical polymerization enabled the synthesis of n-butyl acrylate and 2-hydroxyethyl acrylate

copolymers. This work explores the synthesis of well-defined hydroxy-functional polyacrylates and the effects of the hydroxyl on the polymerization process.

The second half of this dissertation focuses on the effect of zwitterion functionalities as charge sites in low T_g acrylic copolymers on various polymer properties. Chapter 5 reports the electrospinning of zwitterionic copolymers for the first time, producing nanoscale fibers at very low solution concentrations and viscosities. We concluded that a mechanism other than chain entanglements was responsible for stabilization of the electrospinning jet at very low solution viscosities. Chapter 6 follows up on this hypothesis with solution rheological methods to explore the dynamics of zwitterionic copolymers in solution. Comparison of solution behavior with the behavior of the matrix polymer poly(n-butyl acrylate) confirmed that the physical phenomenon involved at the boundary between concentration regimes was not the same as chain entanglements for non-associating polymers. The interaction of zwitterion-containing copolymers with ionic liquids are explored in chapter 7, with implications in the design of a new class of acrylic copolymers for electroactive devices. X-ray scattering, impedance spectroscopy, and mechanical property analysis were correlated to explain the effect of ionic liquid content on copolymer properties.

Chapter 8 reviews the use of nitroxide functionality in polymerization processes and biological applications. Overall conclusions are summarized in chapter 9, followed by an overview of suggested experiments for the continuation of the reported work.

Chapter 2: Organoaluminum Additives in the Controlled and Stereospecific Anionic Polymerization of Methacrylates

2.1 Abstract

Poly(alkyl methacrylates) are widely used in numerous commercial applications. Anionic polymerization of methacrylates leads to well defined polymer structures, and block and star copolymer architectures. However, anionic polymerization of alkyl methacrylates requires extremely low temperatures (-78 °C) in order to suppress side reactions and afford molecular weight control. New methods that require less extreme temperatures and milder purification procedures are needed. Methods to control tacticity and other polymer properties in addition to molecular weight are also desired. Use of aluminum additives through *screened anionic polymerization* allows the fast and controlled polymerization of alkyl methacrylates and alkyl acrylates with high yields, good molecular weight control, and stereospecificity. Moreover, controlled polymerization at ambient temperatures is also achieved. In this review, we discuss the use of alkyllithium initiators with substituted aluminum alkyls in order to mediate the polymerization of alkyl methacrylates. The structural requirements of the initiators and organoaluminums are discussed, as well as the mechanism through which stereospecific polymerization occurs. Application of this synthetic method to form advanced polymer structures, and similar methods for other monomer classes, are also described.

2.2 Scientific Perspective

An ultimate goal of synthetic polymer chemistry is to mimic nature's impeccable control of macromolecular synthesis, including targeted molecular weights with extremely narrow distributions, precise chain structure and conformation, and endgroup functionality. Each of these parameters has a profound effect on polymer properties and performance, making controlled polymerization critical for many desired applications of synthetic polymers. To date, living anionic polymerization remains the premier synthetic technique to attain control of molecular weight, polydispersity, and chain architecture,[1,2] despite recent advances in many other living/controlled polymerization strategies.

Precise polymerization control of a variety of useful monomers has received significant interest since Szwarc introduced anionic polymerization in the 1950s.[3] The use of basic anion-forming initiators and high purity reagents leads to well-defined polymers with targeted molecular weight, narrow molecular weight distributions (<1.2), and quantitative monomer conversion. Several chain architectures (ie. linear, block, graft, star) are readily accessible via controlled endgroups and a variety of available initiators. However, anionic polymerizations must be completely free of protic impurities in order to reach 100% conversion and avoid initiator deactivation. While anionic polymerization is well suited for dienes and styrenic monomers, polymerization of more polar monomers like acrylates and methacrylates, which are difficult to purify and highly susceptible to side reactions, remains synthetically challenging.

Interest in the controlled polymerization of various monomers including (meth)acrylates spurred the development of living radical polymerization techniques, which were first introduced in the 1980s. Stable free radical polymerization (SFRP),[4,5] reversible addition-fragmentation chain transfer (RAFT),[6,7] and atom transfer radical polymerization (ATRP)[8,9] have significantly

expanded the range of monomers available for controlled polymerization to include styrenics, (meth)acrylates, acrylamides, 1,3-dienes, and many other polar or protic monomers. Careful selection of reaction conditions allows the synthesis of well-defined polymers with relatively narrow molecular weight distributions (1.1-1.5) and endgroup control, approaching the control previously afforded only by ionic methods. These techniques involve much less stringent purification techniques than ionic polymerizations and can tolerate a wide range of functionalities and solvents, making living radical polymerization a widely applicable and attractive methodology.

Despite numerous recent advances, living radical polymerization techniques have not been widely adapted to industrial processes for a number of practical and economical reasons. Living radical polymerization techniques require expensive or synthetically intensive mediator and initiator compounds specifically tailored to each monomer system. In addition, controlled radical polymerization techniques are limited to relatively low molecular weights and low monomer conversion due to the inherent reactivity and instability of radical species. In contrast, high molecular weight polymers reaching quantitative conversion are readily produced with anionic polymerization, which has been used to produce styrene- and diene-containing block copolymers and other polymer structures on industrial scales for many years.

Stereocontrol in living polymerizations is also highly desirable for precise control of polymer properties. Despite significant advances in the last decade, tacticity control in living radical polymerizations has not yet been realized for most monomer systems.[10] However, stereoregular polymers are readily produced using ionic techniques, depending on the polymerization temperature, initiator, and other additives. Because of this ability to make well-

controlled copolymers of various topologies while also controlling tacticity, research in the living ionic polymerization of (meth)acrylic monomers remains a topic of great interest.

Recent efforts to improve the anionic polymerization of methacrylates and acrylates have focused on the addition of various additives to help mediate the polymerization and control the various side reactions that plague ionic polymerization of polar monomers. Of these additives, organoaluminums have emerged as a promising class of compounds to aid in the precisely controlled and stereospecific polymerization of methacrylates. This technique was initially introduced by Hatada et al. as a strategy to produce highly syndiotactic PMMA using *t*BuLi and trialkylaluminums at the low temperatures typical of traditional anionic polymerization of methacrylates (≤-78 °C).[11] Slight changes in the alkyl aluminum structure and polymerization temperature resulted in drastic changes in stereocontrol, producing heterotactic, isotactic, or atactic polymers.[12,13] In 1992, Ballard and Haddleton et al. introduced a technique they called screened anionic polymerization, which allows syndiotactic polymerization of MMA at 0-40 °C using bulky alkoxy-substituted alkyl aluminums.[14] Screened anionic polymerization is very industrially and economically attractive, since it utilizes cheap and readily available reagents to control polymerization of methacrylates at near ambient temperatures in a chemically robust system. The structural requirements of organoaluminum additives in order to achieve stereospecific controlled anionic polymerization of alkyl methacrylates are reviewed herein. Application of organoaluminums in anionic polymerization of other monomers, including acrylates, functional methacrylates, and styrene, is discussed.

2.3 Side Reactions in the Anionic Polymerization of Methacrylates

The polarity and inherent functionality of methacrylate and acrylate monomers present a number of challenges to controlled polymerizations, especially in the presence of ionic initiators. Both the vinyl and ester carbonyl groups are susceptible to base attack, allowing a variety of possible reaction pathways for anionic polymerization, in addition to the desired propagation. After initiator attack on the first monomer unit, the charge on the propagating chain end is delocalized over the carbonyl π orbital, forming an enolate (Figure 2.1).[15] The favored resonance structure features the less basic, more stabilized enolate, while propagation only occurs through the carbanion form. The importance of the chain end structure is often overlooked; however, the nature of the chain end is essential in the discussion of aluminum-mediated polymerization. Methods to help stabilize the carbanion form of the propagating chain are commonly used to improve polymerization efficiency.

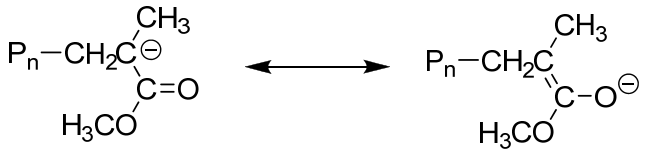

Figure 2.1 The chain end in methacrylate anionic polymerization features charge delocalization with two major resonance contributors, the carbanion and the enolate forms.

The primary side reaction that takes place during anionic polymerization of methacrylates is backbiting of an in-chain carbonyl to form a six-membered ring on the chain end, resulting in termination (Figure 2.2). This process releases a methoxide ion, which is a weak base and

therefore serves as a less active initiator unlikely to form new polymer chains. The reaction rate for cyclization decreases with steric hindrance or increasing chain length.[15]

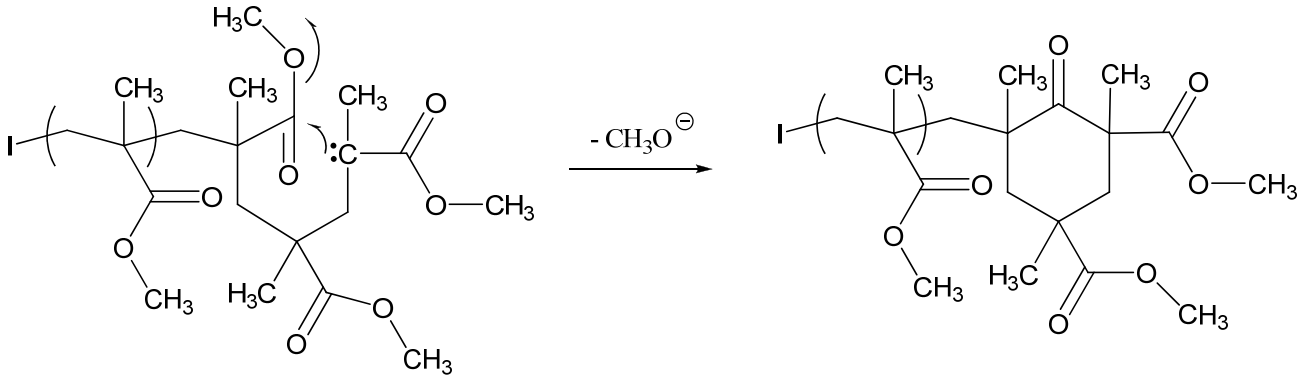

Figure 2.2 Intramolecular attack on an in-chain carbonyl terminates the chain with a six-membered ring.

A second important side reaction to avoid is nucleophilic attack of the initiator on the monomer carbonyl to form an alkenyl ketone. In the case of *t*-butyllithium and methyl methacrylate, the dead chain end *t*-butyl isoprenyl ketone is formed (Figure 2.3), which has a propagation rate too slow for polymerization to continue.[16]

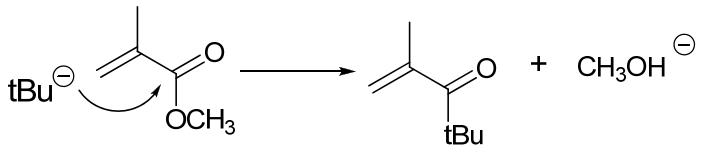

Figure 2.3 Nucleophilic attack on monomer carbonyl competes with initiation to form *t*-butyl isoprenyl ketone.

These side reactions must be minimized in order to control the anionic polymerization of methacrylates. Under classical anionic conditions, methacrylates are polymerized at very low temperatures (-78 °C) to dramatically retard the rate of side reactions in relation to propagation. Aluminum mediated anionic polymerization uses bulky additives such as trialkylaluminums to increase steric hindrance around the chain end and diminish the cyclization reaction, even at higher temperatures. Use of a bulky alkyllithium, such as *t*-butyllithium or 1,1-diphenylhexyllithium, in conjunction with the bulky alkyl aluminum provides the steric hindrance necessary to prevent carbonyl attack to form a ketone end.[17]

2.4 Reagent Selection in Controlling Anionic Polymerization of Methacrylates

2.4.1 Alkyl Lithiums and Aluminums

Anionic polymerization in the presence of organoaluminums occurs through a two-component initiation and mediation complex. First, an organolithium (RLi) is required to initiate polymerization, analogous to classical anionic polymerization. The traditional initiators used for anionic polymerization of (meth)acrylates include *t*-butyllithium, *sec*-butyllithium, ethyl α-lithioisobutyrate, and 1,1-diphenylhexyllithium.[18] The Haddleton and Hatada groups consistently used *t*-butyllithium as the initiator of choice for methacrylate systems. Haddleton and coworkers showed that using *n*-butyllithium resulted in a dramatic decrease in initiator efficiency (values less than 12%) and a reduction in polymerization control compared to the more sterically demanding *t*-butyllithium.[19] The less nucleophilic ethyl α-lithioisobutyrate (EiBLi) serves as a model for the living chain end and is often used for acrylate systems, where the presence of Lewis bases are required to afford improved control.[20] The controlled anionic

polymerization of acrylates using organoaluminum additives is specifically addressed in a later section.

The second component of the initiating and mediating complex is a bulky organoaluminum that acts as a Lewis acid, binding to enolates and carbonyl groups.[21] The bulkiness of the alkyl substituents is critical to formation of the initiating complex and the subsequent polymerization efficiency. Aluminum alkyls exist in equilibrium between monomeric and bridged forms.[15,22,23] This equilibrium complicates the efficiency of complexation due to varying availability of the Al centers for screening effects, as well as the Li centers for initiation after complex formation. Systematic studies of different aluminum alkyls suggest that the steric demands of the Al substituents may serve to drive this equilibrium toward monomeric species, which are free to complex with lithium alkyls in a form that supports polymerization. Haddleton and coworkers observed an increased control and efficiency of methyl methacrylate polymerization with increasing bulkiness of the aluminum alkyl substituent.[19] Under similar reaction conditions, $^{i}Bu_3Al$, $^{n}Pr_3Al$, and Et_3Al all led to 100% monomer conversion and high molecular weight polymer; however, the polydispersity increased significantly, from 1.08 for isobutyl to 1.44 and 1.50 for propyl and ethyl, respectively. In addition, SEC light scattering analysis of the resulting polymers showed bimodal distributions and secondary initiation taking place for less sterically demanding aluminum alkyls, Et_3Al and $^{n}Pr_3Al$. This result is consistent with the inability of $^{i}Bu_3Al$ to form aggregates. Therefore, the majority of reports on the polymerization of methacrylates in the presence of alkyl aluminums utilize $^{i}Bu_3Al$.

In addition to alkyl substituents, aluminum is easily modified with hindered phenolic groups, which may serve to drive the equilibrium toward monomeric species while screening the

active chain end (hence the term *screened anionic polymerization*). Ballard and coworkers modified $^{i}Bu_3Al$ with a common hindered phenol, 2,6-di-*tert*-butyl-4-methylphenol (BHT) featuring bulky *t*-butyl groups at the 2 and 6 positions (Figure 2.4).[14] Polymerization results showed that this bulky alkoxy aluminum effectively controlled polymerization of methacrylates with approximately 70% syndiotacticity and polydispersities below 1.20, at 0-40 °C in solution and up to 100 °C in the bulk.

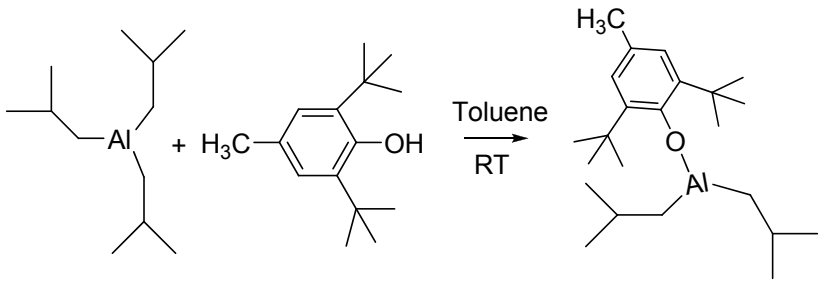

Figure 2.4 Synthesis of (2,6-di-*tert*-butyl-4-methylphenoxy)diisobutylaluminum ($^{i}Bu_2Al(BHT)$).

Later, Holmes and coworkers also studied the polymerization of methyl methacrylate in the presence of alkoxyaluminums[24] and organoaluminium amides.[25] Aluminum compounds were prepared with a reaction of $^{i}Bu_3Al$ and 1 or 2 equivalents of four different alcohols, including phenols, cyclohexanol, and a menthol derivative.[24] Only the reactions with ^{i}Bu or BHT ligands gave polymer in high yield with both low polydispersity and high syndiotacticity. The other alcohols resulted in high isotacticity and, in most cases, low conversions. NMR complexation studies revealed that $^{i}Bu_3Al$ and $^{i}Bu_2Al(BHT)$ formed complexes with the lithium enolate and free monomer to afford tacticity control, while the less hindered phenols were unable to complex the monomer and afford similar control. The electronic and steric nature of the ligand is very important in controlling the reactivity of dimeric aluminum compounds by

influencing aluminum bridge strength, and combinations of isobutyl and BHT ligands possess the best properties for effective polymerization of methacrylates. Similar studies with *N*-containing ligands to form $^{i}Bu_2Al(NRR')$ also resulted in the formation of syndio-rich PMMA with greater than 65% *rr* and narrow polydispersities.[25] Complexation with both the monomer and the enolate were required for controlled polymerization. Figure 2.5 contains a summary of organoaluminum structures that successfully afforded controlled polymerization of syndio-rich alkyl methacrylates.

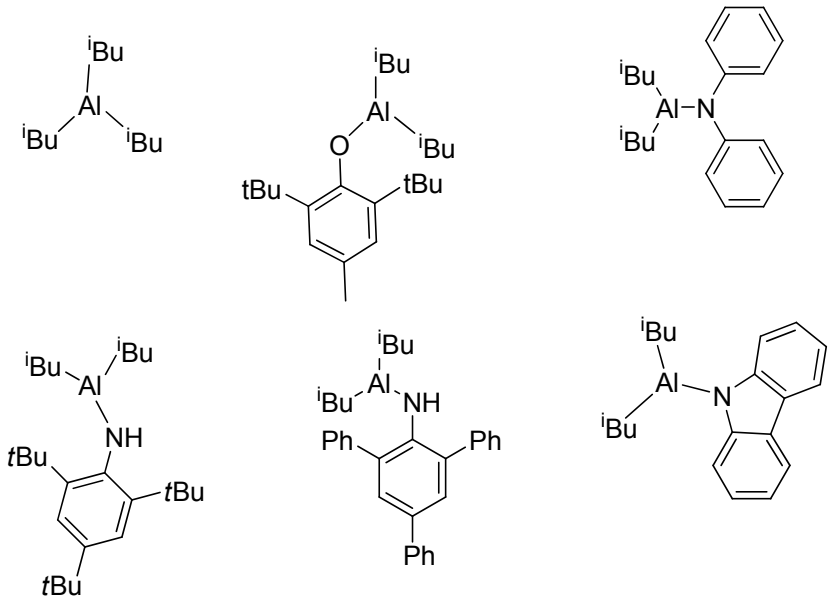

Figure 2.5 Select organoaluminums for the formation of syndiorich poly(alkyl methacrylates)

2.4.2 Lithium/Aluminum Complex

The initiating complex forms upon mixing of the alkyllithium and alkylaluminum species, with an exotherm indicating complex formation has occurred.[7] It is well known in organometallics that lithium aluminum alkyls are alternately linked through carbon bridges, resulting in oligomerization of $[LiAlR_n]_m$ depending on the solvent used (Figure 2.6).[14,22,23]

Hydrocarbon solvents such as toluene cause dissolution of the oligomer to form low molecular weight species, although some oligomers may persist. Low initiator efficiencies often observed indicate that more than one lithium-containing species is present in the polymerization media. In some cases the lithium is completely screened and cannot participate in polymerization, as in a dimeric species where only one lithium may be available to initiate a chain.

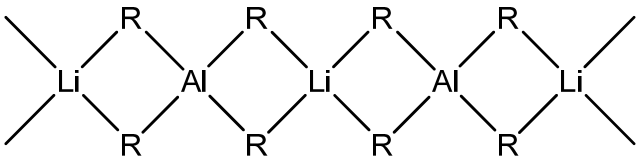

Figure 2.6 Linking of Al and Li in the initiating complex occurs through carbon bridges (adapted from ref. 14).[14]

The order of reagent addition was originally thought very important in terms of control and formation of the lithium/aluminium complex.[26] The preferred method of complex formation was premixing the lithium and aluminum species to form the complex *in situ* before adding the monomer. Some literature also supports premixing monomer with the aluminum alkyl, then adding both to the toluene/alkyllithium initiator solution equilibrated at the polymerization temperature. The premixing technique was implicated to scavenge impurities from the monomer prior to addition to the polymerization flask, requiring less stringent purification. Premixing the Al and Li species to form the initiating complex also avoided a large exotherm during polymerization, and led to a higher initiator efficiency. Otherwise, both methods were equally effective in controlling polydispersity, monomer conversion, and tacticity.[19]

The ratio of aluminum to lithium species in formation of the initiating complex is critical for controlled polymerization to occur. In the case of methacrylates, polymerization only proceeded to completion when an excess of aluminum was used. However, reaction efficiency declined when lithium was in excess, and syndiotacticity decreased with a corresponding increase in isotacticity, indicative of multiple reaction mechanisms.[14] When Al/Li was 2, no ketone formation or termination by cyclization was observed using MALDI-TOF MS.[16] Additional Al up to three equivalents (Al/Li =3) did not lend any additional reaction control other than possibly removing impurities.[14]

2.4.3 Polymerization Solvent

Unlike group transfer and classical anionic polymerization techniques, anionic polymerization with organoaluminums is conducted in nonpolar solvents, most often toluene, where the separation between the lithium cation and propagating anion is minimized. Common anionic solvents such as tetrahydrofuran and dimethoxyethane completely dissociate the Li-Al bridged structure, replacing it with Al and Li separately coordinated to the solvent ether oxygen and effectively inactivating the initiating complex. Toluene, however, allows the bridged system to remain intact and increases the association of the cation with the chain end, leading to a better screening effect which allows protection from side reactions and stereocontrolled monomer addition.[14]

2.5 Mechanism of Polymerization Control in the Presence of Organoaluminums

Through the selection of proper alkyl or alkoxy substituents and reaction conditions, good control of molecular weight, polydispersity, and tacticity are readily achieved in the organoaluminum mediated anionic polymerization of methacrylates. While the success of this

technique is well documented, the mechanism through which organoaluminums allow stereocontrolled and "living" anionic polymerization of methacrylates is less clear. Ballard, Haddleton, Hatada, and Müeller have all explored the polymerization mechanism in the presence of aluminum using various techniques, including model compounds, NMR studies, X-ray crystallography, and quantum chemical calculations, to name a few. The polymerization process is highly dependent on temperature and choice of aluminum additive. For example, at equivalent Al/Li and monomer/Li ratios, polydispersity increased markedly with increasing temperature, from 1.16 at 0 °C to 1.34 at 20 °C and 1.55 at 50 °C.[26] The rise in temperature also resulted in decreasing conversion and syndiotacticity. Therefore, different mechanisms may be applicable depending on reaction conditions.

2.5.1 Initiation and Termination

Two fundamental requirements of living polymerization are: 1) fast initiation with respect to propagation, and 2) the absence of termination reactions. One major concern for the use of organoaluminums in anionic polymerization is the possibility of secondary initiation through alkyl groups from the aluminum rather than the alkyllithium. However, Haddleton and coworkers determined that the alkyllithium fragment, not an alkyl group from the organoaluminum, comprised 100% of the polymer chain ends using both MALDI-TOF MS and an NMR study with MMA-d_8.[14,19,26,27]

Despite proof of alkyllithium initiation, the calculated molecular weight for the polymerization of methyl methacrylates in the presence of *t*-butyllithium and $^{i}Bu_3Al$ resulted in initiator efficiencies much less than 1, often as low as 0.5.[19] Low initiator efficiency indicates a non-living process with significant initiator quenching or side reactions. One proposed side

reaction responsible for initiator quenching is the competing reaction of butyllithium with methacrylate carbonyl to form *t*-butyl isoprenyl ketone.[16] However, MALDI-TOF MS analysis showed no evidence of ketone formation when an excess of 2:1 aluminum to lithium was used. If less than two equivalents of aluminum were used, the side reactions dominated leading to lower initiator efficiencies and significant ketone formation and secondary initiation detected with MALDI-TOF MS. Therefore, the low initiator efficiency was likely due to the formation of a new aluminum/lithium alkyl species, which contained multiple alkyllithiums with differing activities. The presence of screened, inactive alkyllithiums in the initiation complex is consistent with the complex structure proposed in section 3.2.[15,26]

The most accepted mechanism for anionic polymerization of methacrylates using bulky alkyllithium and organoaluminums containing bulky alkyl and alkoxy substituents involves the formation of a bimetallic "ate" complex in which the Al and Li centers are coordinated to the methacrylate ester oxygens. This complex then serves to both stabilize and deaggregate the lithium ester enolate chain ends so that controlled polymerization can occur. In order to further understand the structure and nature of the initiating complex, Chen and coworkers[28] synthesized for the first time various examples of monomeric lithium ester enolaluminates, and fully characterized their structures using X-ray diffraction and ^{13}C NMR studies. First, they synthesized isopropryl α-lithioisobutyrate as a model initiator for the living anionic polymerization of MMA. X-ray diffraction studies revealed a crystal structure featuring six initiator compounds and a hexagonal prism core of Li_6O_6. Following complex formation with the bulky organoaluminum compound $MeAl(BHT)_2$, a stable crystalline solid was isolated and X-ray diffraction studies revealed a monomeric, deaggregated structure. The addition of one molar equivalent of organoaluminum did not affect the structure of the 1:1 enolaluminate

complex. ^{13}C NMR studies also confirmed the "ate" complex structure, revealing an increased double bond character of C(α) and C(O) in the enolaluminate structure. Similar results were seen for the "ate" complex using $Al^{i}Bu_3$, however the complex was a colorless oil that did not crystallize for structural analysis. Overall, the study implies that the BHT ligand provides the necessary bulkiness and electron-donating character to the organoaluminum compound to form the monomeric non-aggregated "ate" complex. Using $MeAl(BHT)_2$ resulted in higher initiator efficiencies (~80%) at lower temperatures, confirming the presence of monomeric initiating species. Polymerization results also proved the living nature of the polymerization using $MeAl(BHT)_2$/lithium ester enolaluminate over a broad temperature range (-40 to 23 °C), reaching quantitative yields while maintaining molecular weight distributions below 1.2.

2.5.2 Role of Excess Aluminum in Monomer Activation

While the initiating "ate" complex forms at a 1:1 molar ratio, successful polymerization occurs only in the presence of excess aluminum. At least one molar excess of organoaluminum was required in order to achieve high conversions and narrow molecular weight distributions in the case of $^{i}Bu_3Al$.[14,19,26] Crystal structures and ^{13}C NMR studies of MMA:Al adducts featuring various ligands revealed that the excess aluminum coordinated the monomer ester carbonyl and activated the vinyl group toward monomer addition[28] (Figure 2.7). Detailed ^{13}C NMR analysis also revealed that the predominant resonance contributor within the MMA:Al adduct was the most active form (Figure 2.8, B) with a slight positive charge on the C(α) of the MMA vinyl group.

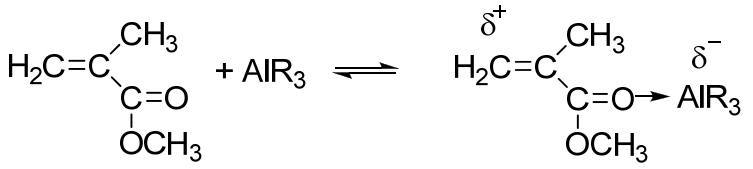

Figure 2.7 Coordination of the aluminum alkyl to ester groups of the monomer forms an activated monomer complex (adapted from ref. 29).[29]

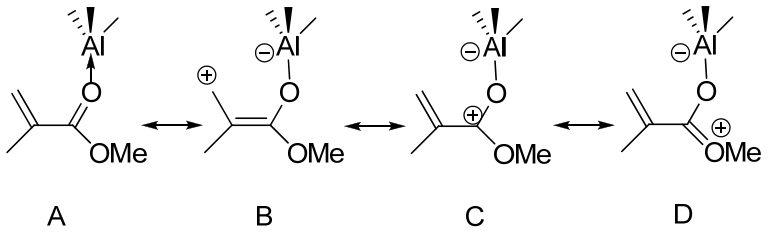

Figure 2.8 Four resonance contributors of the MMA:Al adduct (adapted from ref. 28).[28]

Schlaad and coworkers found a chemical shift downfield of the monomer carbonyl, methylene, and methoxy groups upon complexation with aluminum alkyl using ^{13}C NMR experiments.[29] Hatada and coworkers studied the copolymerization of acrylate and methacrylate pairs, MMA/*n*BA[30] and EMA/*t*BA[31], and found that a monomer-selective polymerization occurred at low temperatures leading to blocky structures. ^{13}C NMR analysis showed preferential complexation of the acrylates, leading to quantitative consumption of the acrylate prior to methacrylate block polymerization.[31] These studies further support the activated monomer mechanism of polymerization.

Using the premises of both monomer activation and monomeric ester enolaluminate formation, the bimolecular polymerization mechanism through a single-site propagation center was described according to Figure 2.9. The terminal unit carbonyl of a growing polymer chain P

is complexed to an aluminum to form the ester enolaluminate (G). An activated MMA unit (H) adds to the end of the polymer chain through a Michael addition reaction to form (I), where competitive binding between the monomer and polymer creates an equilibrium. Polymerization continues in this manner until all of the monomer is consumed.

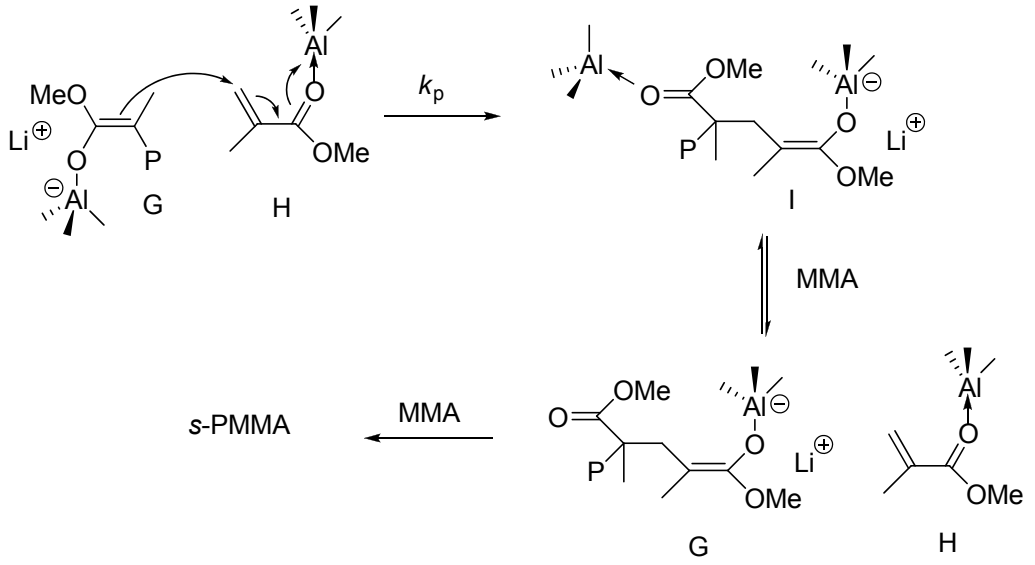

Figure 2.9 Bimolecular chain propagation mechanism proposed by Rodriguez-Delgado and Chen for the polymerization of MMA using a lithium ester enonlaluminate/organoaluminum combination (adapted from ref. 28).[28]

2.5.3 Formation of Coordinative Networks

Although the activated monomer mechanism seems to hold for initiating complexes incorporating bulky organoaluminums such as iBu_3Al, Schlaad and coworkers have discussed a different mechanism when less bulky organoaluminums are used. Less bulky aluminums such as $AlEt_3$ formed aggregated structures, and polymerizations resulted in substantial network or gel formation.

In the presence of methyl methacrylate, the initiating complex formed from EiBLi and $AlEt_3$ coordinated to ester enolate chain ends to form coordinative polymer networks at temperatures above -65 °C (Figure 2.10). These coordinative structures were elucidated using *ab initio* quantum chemical calculations and were consistent with ^{13}C NMR spectroscopy experiments.[32] The favored species was a dimer associating the lithiated chain end with an aluminum alkyl coordinated to another ester oxygen, not the unimeric "ate" complex of the propagating species.[20,32]

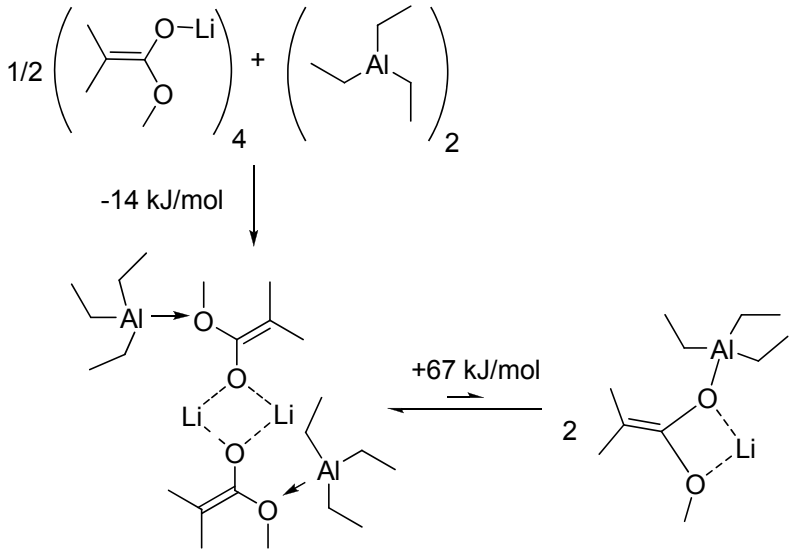

Figure 2.10 The interaction of aluminum alkyls and ester enolates in polymer coordinative networks (adapted from ref. 32).[32]

Additionally, Müller and coworkers described a deviation from first order kinetics in the polymerization of (meth)acrylates due to coordinative network formation.[20] This gel formation resulted in a kink in the time vs conversion plot, and was attributed to coordination of electron deficient lithium ions to Lewis bases in the reaction mixture, namely in-chain carbonyls.[32] The

equilibrium between polymer and gel shifted more to gel as conversion increased. However, addition of Lewis bases, such as crown ethers or methyl pivalate that are strong enough to compete with in-chain chelation, shifted this equilibrium back toward polymer, resulting in higher conversions and more controlled polymerizations.[33] No gelation was observed with esters, ethers, or amines; however, first order kinetics with unimodal and narrow molecular weight distributions were only achieved when using esters such as methyl pivalate.

In the polymerization of methyl methacrylate with EiBLi and Et_3Al at -78 °C, linearity of the time vs. conversion plot improved with increasing methyl pivalate concentration, but initiator efficiency also decreased as the amount of Lewis base increased.[32] With a toluene:methyl pivalate ratio of 3:1, no gel formed up to 0 °C and initiator efficiency was approximately 60%. Additionally, syndiotacticity increased to 90% above -60 °C as compared to 80% in pure toluene at -78 °C. However, at room temperature side reactions occurred, and low conversion and broad polydispersities were observed.

Hamada and coworkers included the use of Lewis bases such as ethers and polyamines to improve initiation, blocking efficiency, and livingness through suppression of network formation.[18] The preferred ethers included diethyl ether and 1,2-dimethoxyethane, as they improved polymerization rate without interfering with the organoaluminum complex. Cyclic ethers inactivated the aluminum complex. Polyamines such as *N,N,N',N'*-tetramethylethylene diamine were also cited to enhance the polymerization. Amounts of greater than 0.5 moles of Lewis base for every mole of anionic center is preferred, although too much may have an adverse effect on initiator efficiency.

2.6 Tacticity Control in the Presence of Organoaluminums

One critical aspect of controlled polymerizations is stereospecificity, since chain tacticity highly influences polymer properties (ie. glass transition temperature). Precise control of polymer backbone structure allows the tailoring of polymer properties over a wide range. In the case of PMMA, completely syndiotactic PMMA has a high T_g above 130 °C, while the T_g of isotactic PMMA is lower, ~45 °C.[34] Hatada and coworkers have studied stereospecific polymerization of methacrylates for more than two decades in order to understand fundamental relationships between tacticity and polymer properties. Isotactic specific polymerization using *t*-BuMgBr/$MgBr_2$ and syndiotactic specific polymerization with *t*BuLi/trialkylaluminum were discovered in the 1980s.[11,35] Heterotactic specific polymerization initiated with *t*-BuLi and methylaluminum bis(2,6-di-*t*-butylphenoxide) ($MeAl(ODBP)_2$) was found in the mid-1990s.[13,36] Heterotactic specific polymerization involves more sophisticated control than the others in order to form the alternating *meso (m)* and *racemo (r)* diad sequence (Figure 2.11).

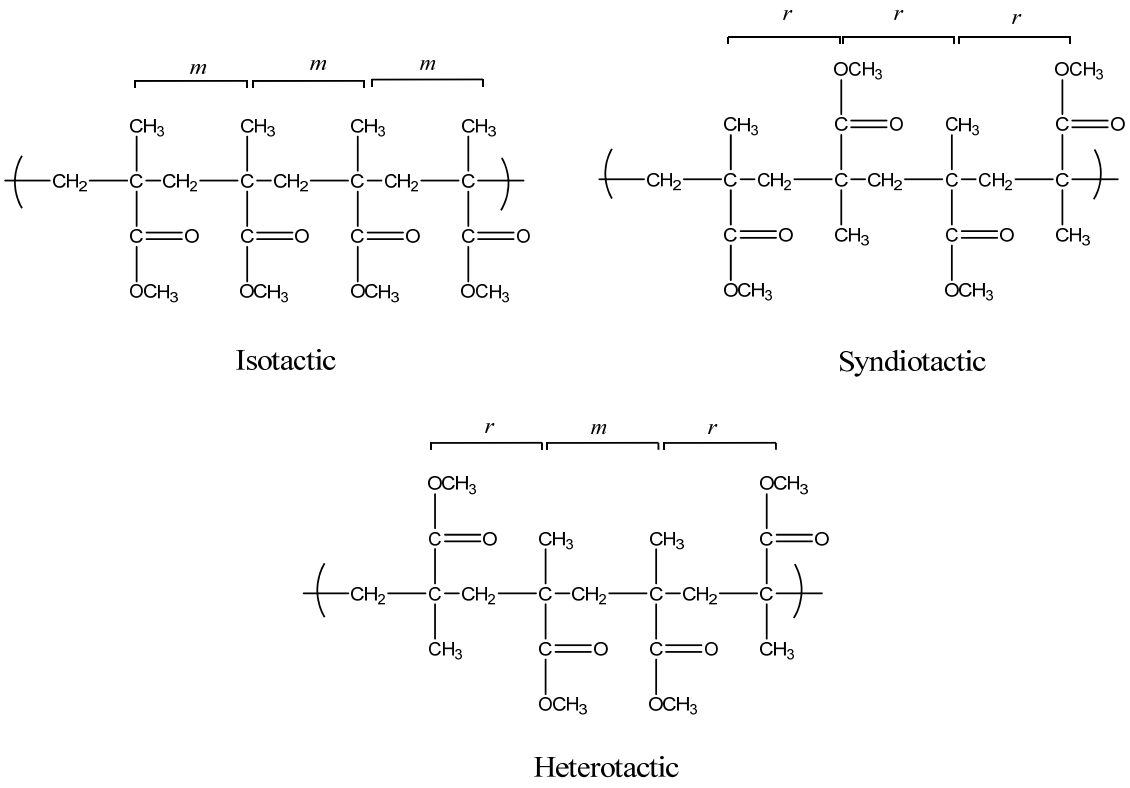

Figure 2.11 Stereoregular chain structures of PMMA.

The structure and Lewis acidity of the organoaluminum used greatly influences both polymerization control (polydispersity) and tacticity control of the resultant polymethacrylates.[37] Control of stereochemistry along the polymer backbone requires the ability of the organoaluminum to coordinate and activate the monomer toward preferred addition. Stereospecificity is maximized at low temperatures below -60 °C, but specificity in the range of 60-80% is still mainatained at higher temperatures depending on the ligand structure. The ligand type (i.e. alkyl, alkoxy, phenoxy) affects the bridge strength and aggregation behavior within the "ate" complex, influencing both the structure of the complex and the ability to activate the monomer effectively through complexation. Holmes and coworkers demonstrated the effect of sterics in a series of ligands using a lithium enolate initiator.[24] $^{i}Bu_3Al$, $^{i}Bu_2Al(BHT)$, and

^{i}BuAl(BHT)$_2$ gave syndiorich polymers, while polymerizations in the presence of phenoxy ligands yielded no polymer or isotactic structures. ^{13}C NMR studies confirmed the formation of an "ate" complex for systems with ^{i}Bu or BHT ligands, while no complexation was observed for phenoxy ligands.[24] This result is in agreement with the formation of isotactic polymers in the absence of "ate" complexes. Changing the *para* substituent (Me in BHT) to various sized groups also led to slight changes in tacticity, but stereospecificity was maintained.[12]

Monomer structure also influences the control of stereochemistry, where steric bulkiness of the pendant ester group plays a large role in the stereospecificity of polymerization. In the heterotactic polymerization of alkyl methacrylates at -78 °C using t-BuLi/Me(ODBP)$_2$, the length of the side chain in a series of different ester side chains drastically affected stereospecificity.[38] Heterotactic *mr* sequences were maximized between C-2 and C-4 esters (EMA and nBMA), and the polymerization of allyl methacrylate (C-3) led to *mr* content greater than 95% at -95 °C. Secondary alkyl methacrylates also formed highly heterotactic polymers with tBuLi/MeAl(ODBP)$_2$.[13] However, more bulky tertiary alkyl methacrylates, including t-butyl[13] and trimethylsilyl[39] methacrylates, resulted in a shift to highly syndiotactic microstructures.

2.7 Block, Star, and Graft Copolymer Architectures via Screened Anionic Polymerization

A main advantage of living polymerizations is direct synthesis of more complex chain architectures that have proven useful for a variety of applications. Several polymer architectures, including block, star, and graft copolymer structures, are accessible through anionic polymerization due to the living nature of the chain end, even in the presence of organoaluminum additives. Ballard and coworkers reported the synthesis of AB- and ABA-type

copolymers consisting of MMA and n-butyl methacrylate (*n*BMA) blocks at varying compositions and molecular weights using *t*BuLi and $^{i}Bu_3Al$.[14] Molecular weights reaching 86,000 g/mol were achieved while maintaining molecular weight distributions below 1.27, even after two sequential monomer additions. Later, Haddleton and coworkers reported a similar synthesis of diblock and triblock copolymers from a wide range of methacrylate monomers, including MMA, *n*BMA, hexyl methacrylate, 2-ethylhexyl methacrylate, cyclohexyl methacrylate, methoxy-PEG-methacrylate, and decylmethacrylate.[26] In all cases, 100% conversion was achieved, as indicated by ^{1}H NMR or the disappearance of the yellow color characteristic of the AlR_3-monomer complex. Block copolymers were successfully synthesized at Al:Li ratios of 1.5 to 2.0, resulting in polydispersities ranging from 1.17 to 1.5. Higher polydispersities were reported for polymers containing higher methacrylates, as these monomers contain high boiling impurities and are significantly more difficult to purify.

Star polymers were also readily formed from living PMMA chains using the "arm-first" approach, where the multifunctional monomer ethylene glycol dimethacrylate (EGDMA) was added at the end of the polymerization to form a crosslinked core with PMMA arms.[40,41] Using the *t*BuLi/$^{i}Bu_3Al$ initiator system, Crossman and Haddleton prepared PMMA star polymers with molecular weights >600,000 g/mol, corresponding to an estimated 39-56 arms based on the weight average molecular weights from SEC.[40] Stars with MMA-*n*BMA block copolymer arms with much higher molecular weights were also synthesized.

Hatada and coworkers have also reported the anionic preparation of PMMA star polymers using organoaluminum additives, with an emphasis on the stereoregularity of PMMA arms.[41-43] Using *t*BuLi/$^{n}Bu_3Al$ in toluene, coupling of syndiotactic arms with EGDMA was unsuccessful, while 139-arm syndiotactic PMMA stars were produced using butane-1,4-diol

methacrylate.[41] PMMA stars with isotactic arms were also synthesized using *t*BuMgBr as the anionic initiator for a direct comparison of the effects of tacticity on star polymer properties, especially viscosity effects. Lazzari and coworkers also synthesized PMMA star polymers using multifunctional bromomethylbenzenes as the core crosslinker to form controlled 4- and 6-armed star structures.[42]

In addition to stereoregular star structures, Hatada and coworkers have explored the synthesis of graft polymers to form combs with stereoregular main chain and arm structures.[36,44] Syndiotactic PMMA macromonomers were prepared using *t*BuLi/$^{n}Bu_3Al$ in toluene at -78 °C that were subsequently modified to form methacryloyl functional groups at the chain end.[44] The PMMA macromonomers were then polymerized with DPHL in THF to form graft copolymers with syndiotactic main chains as well as syndiotactic side chains. Similarly, polymerization of the macromonomers with *t*BuMgBr in toluene formed an isotactic main chain structure and a stereocomplex between the main chain and syndiotactic side chains.

2.8 Organoaluminums in the Controlled Anionic Polymerization of Acrylates

Controlled anionic polymerization of acrylates has received much less attention in the literature due to the higher reactivity of acrylate monomers compared to methacrylates. Acrylates lack the stabilizing effects of the α-methyl group, and instead feature an α-hydrogen that is susceptible to chain transfer reactions and enhances the probability of back biting side reactions. Substantial enol formation, which leads to back biting side reactions, increases with temperature; therefore, acrylates are controlled at lower temperatures than methacrylates (-60- -20 °C). The steric demand at the aluminum center is critical for stereoregulation in acrylic systems, with stronger coordination to ester alkyl leading to more sterospecific control.[45]

Using *t*-BuLi and trialkylaluminum (Me_3Al, Et_3Al, and $^{i}Bu_3Al$) at -78 °C in toluene, the polymerization of *n*-butyl acrylate (*n*BA) led to curved time vs conversion plots and incomplete conversions.[20] In the absence of aluminum, this polymerization proceeded to approximately 45% conversion with M_w/M_n of 14. With alkyl aluminum, 75% conversion was achieved with M_w/M_n between 1.8 and 2.5; however, the time vs. conversion plots remained curved, indicating an influence of coordinative networks. With the addition of methyl pivalate to this reaction, lower molecular weight distributions around 1.5 were achieved, and the reaction proceeded to completion while maintaining linear time vs. conversion plots. Polymerizations in the presence of methyl pivalate followed first order kinetics, which is consistent with the requirement that the concentration of propagating anionic chain ends remains constant in a living polymerization. The Lewis base effectively eliminated chain transfer and termination while increasing the reaction rate, but low temperatures and very high concentrations exceeding 2.0 M were required. The addition of methyl pivalate in the polymerization of *t*-butyl acrylate, however, did not have a pronounced effect. Additionally, MALDI-TOF analysis indicated the presence of significant backbiting and ketone formation. Switching the initiator to the less nucleophilic ethyl α-lithioisobutyrate effectively suppressed ketone formation. Therefore, this initiator is preferred in acrylate polymerizations.

Tabuchi and coworkers examined the effects of organoaluminum substituents and other reaction conditions in the polymerization of *n*BA, 2-ethylhexyl acrylate (EHA), and *t*-butyl acrylate (*t*BA).[45] Using *t*-butyllithium in toluene, $AlEt(BHT)_2$ allowed 100% conversion of highly syndiotactic polymer with narrow polydispersities below 1.15. However, use of $MeAl(BHT)_2$ resulted in heterotactic polymer at lower yields and polydispersities of 1.5-1.8. This result indicates the less bulky methyl group was unable to coordinate the chain end and

prevent back-biting side reactions. Additionally, monomer concentration generally had a significant effect on many aspects of the polymerization. As monomer concentration increased, the molecular weight and polydispersity also increased, while syndiotacticity decreased.

Due to the inherent reactivity difference between acrylates and methacrylates, Kitayama and coworkers were able to copolymerize *t*BA and EMA in a living and monomer-selective manner to form block-like copolymers with narrow molecular weight distributions using *t*BuLi/MeAl(ODBP)$_2$ between -40 and -30 °C.[31] At lower temperatures, the blocking efficiency was reduced resulting in a bimodal distribution with a low molecular weight fraction of *t*BA homopolymers and a higher molecular weight portion of a block-like structure. The blocking efficiency increased with temperature until -20 °C, at which point a random copolymer was formed while maintaining a narrow molecular weight distribution. ^{13}C NMR studies indicated that the aluminum species preferentially coordinated *t*BA for activation, giving rise to the selectivity of monomer addition. A similar result was obtained when copolymerizing a methacrylate with a primary acrylate, *n*BA, instead of the tertiary *t*BA.[30] In this case, monomer-selective and living block and copolymerizations were accessible using *t*BuLi/EtAl(ODBP)$_2$ instead of the MeAl(ODBP)$_2$, which resulted in low conversions and broad molecular weight distributions. Quantitative conversions and narrow molecular weight distributions were achieved from -60 to 0 °C for MMA/*n*BA copolymerizations. Therefore, *t*BuLi/EtAl(ODBP)$_2$ is an effective initiator system to afford syndiotactic control for both alkyl acrylates and methacrylates, and is useful for the synthesis of mixed acrylate/methacrylate polymers of both block and random monomer sequences.

2.9 Application of Organoaluminums to Other Monomers in Anionic Polymerization

Several researchers have expanded the capabilities of organoaluminum mediated anionic polymerization to include other classes of monomers beyond primary and tertiary alkyl (meth)acrylates. Among these monomers accessible for controlled polymerization through the alkyllithium/organoaluminum initiator system are acrylamides,[46,47] bicyclobutanes,[48] methacrylic acid,[39] hindered phenolic methacrylates,[49] and fluorinated methacrylates.[50]

Polyacrylamides are a good class of biocompatible polymers used in a variety of applications. While *N,N*-disubstituted acrylamides have been produced anionically in the past, mono- and un-substituted acrylamides bear an acidic proton that precludes anionic polymerization through the vinyl group. However, Kitayama et al. were able to polymerize a trimethylsilyl-protected acrylamide derivative in a highly isotactic manner (>90%) using *t*BuLi/trialkylaluminum (1/5) at -40 to 0 °C.[47] A bulkier bisphenoxy-based aluminum additive, $EtAl(ODBP)_2$, was also explored for the stereospecific polymerization of the protected acrylamide. While high isotacticity was achieved, lower yields indicated that bulky groups might actually hinder propagation. Interestingly, these highly isotactic polyacrylamides produced through anionic polymerization exhibited significantly different properties, especially solubility, than polymers produced with free radical methods.

Another silyl-protected monomer that has found significant relevance in anionic polymerization is trimethylsilyl methacrylate (TMSMA). The silyl group is easily hydrolyzed to form poly(methacrylic acid) (PMAD), which can be incorporated into a variety of amphiphilic block copolymers. Hatada et al. used stereospecific polymerization initiators at -78 °C to produce highly isotactic PMAD using *t*BuLi without Al, and syndiotactic PMAD with *t*BuLi/$MeAl(ODBP)_2$.[39] At the Al/Li ratio of 5, a syndiotacticity of >96% was achieved, one of

the highest percentages ever reported in anionic polymerizations of methacrylic monomers. Hatada et al. also reported the anionic polymerization of a hindered phenolic methacrylate featuring an unprotected hydroxyl functionality.[49] While *t*BuLi initiator was quenched by the phenolic monomer, modified less-reactive initiators such as oligomeric methacrylate anion or *t*BuLi/MeAl(ODBP)$_2$ successfully polymerized the phenolic methacrylate in a living manner with syndiotactic control at 0 °C, while the polymer produced at -78 °C comprised approximately 50% *mr* triads. The use of aluminum additives to reduce the quenching of alkyllithium in the presence of hydroxyl functionality is a significant development that could be exploited in future work.

Others have expanded anionic polymerization with aluminum compounds to include block polymerization of fluorinated methacrylates with PMMA for supercritical CO_2 and surfactant studies.[50,51] Using the colorimetric endpoint of MMA polymerization with *t*BuLi/Al^{i}Bu$_3$, well-defined PMMA blocks were produced in high yield. The color reappeared upon addition of the fluorinated monomer, and polymerization to form block copolymer surfactants proceeded over 45 minutes until the color disappeared.[51] These copolymers were subsequently used as stabilizers in the radical dispersion polymerization of MMA.

2.10 Retarded Anionic Polymerization of Styrene

Schade and coworkers at BASF also reported on the use of alkylaluminum species in anionic polymerization, but found that the combination of alkyllithiums and alkylaluminums resulted in retarded kinetic effects in the bulk polymerization of styrene at high temperatures (T > 50 °C).[52] Due to this rate effect in the presence of nonpolar monomers, the technique was referred to as "retarded anionic polymerization." The bulk anionic polymerization of styrene is a

desired process in industrial applications that leads to high molecular weight materials with improved properties. The challenge of this process is controlling the large exotherm of styrene polymerization to avoid runaway reactions.[52] The addition of organoaluminums helps slow down the polymerization so that control was maintained, even at elevated temperatures.

While this process is similar to screened anionic polymerization of methacrylates, different conditions are required to achieve control. In this technique, no polymerization occurs when Al/Li ≥ 1 due to the formation of an inactive 1:1 complex where no R-Li species are available for initiation.[52] However, ratios approaching 1, where the lithium species is still in excess, lead to narrower molecular weight distributions. The presence of the aluminate complex excludes thermal degradation through β-elimination and subsequent attack on the phenylallyl H, maintaining control in the polymerization of styrene at temperatures exceeding the T_g. Schade and coworkers also studied the effects of other organometallic species in the retardation of polystyrene, but with less success than the organoaluminum compounds. Dialkylmagnesium drastically reduced the rate of reaction while maintaining good control.[53] However, further studies also showed that initiation occurred through both addition to PSLi and insertion in Mg-R bonds, which complicated the molecular weight control of this technique.[54] Similar metal alkyls, alkylzinc and alkylboron, did not retard the polymerization rate while maintaining living control.[55]

2.11 Future Perspectives

Advances in the controlled anionic polymerization of alkyl methacrylates have allowed superior synthetic control in the design of acrylic macromolecules. The use of organoaluminum additives in screened anionic polymerization enables controlled polymerization with narrow

molecular weight distributions in addition to stereospecificity. Stereospecificity provides tailoring of polymer properties through the glass transition temperature. Hatada and coworkers have shown that the proper selection of initiator complex and organoaluminum leads to stereoregular structures, with greater than 90% heterotactic or syndiotactic diads.[38] This stereocontrol has led to very elegant studies that help elucidate the interplay of chain microstructure and bulk polymer properties.[41-43] The stereospecificity of screened anionic polymerization may be exploited in the future for the design of new block copolymer structures with highly stereoregular blocks and unique properties that were not previously achieved using other polymerization techniques.

Use of aluminum mediators in screened anionic polymerization allows for the stereospecific and controlled polymerization of a variety of functional monomers that were previously unavailable through anionic polymerization methods.[39,46,47,49] Continued work in this field will continue to expand the range of compatible monomers through the development of new bulky ligands and other additives that help tailor the initiator reactivity and inhibit side reactions. Holmes and coworkers introduced a new class of nitrogen-based ligands that provided greater stereospecificity while maintaining control.[25] More studies using this class of ligands may lead to new advances in monomer compatibility. Also, the successful synthesis of hydroxy-functional polymers through anionic polymerization makes new opportunities in polymer design available for functional materials.[49]

The energy and cost savings of room temperature anionic polymerization are important and substantial at the industrial scale. Additional increases in temperature may result from the introduction of new organoaluminum compounds, making this technique more viable for room temperature synthesis of novel acrylic polymers. All-acrylic triblock copolymers with properties

similar to styrene-butadiene block systems are of specific interest due to increased UV and oxidative stability and service temperature.[56-59] Screened anionic polymerization provides the necessary technology to synthesize these new classes of polymers with very good control. However, limitations in the controlled polymerization of alkyl acrylate monomers needed for the low T_g block of these systems still remain and require more attention.

2.12 References

(1) Braunecker, W. A.; Matyjaszewski, K. *Prog. Polym. Sci.* **2007**, *32*, 93-146.
(2) *Acs Symposium Series 768: Controlled/Living Radical Polymerization Progress in Atrp, Nmp, and Raft*; Matyjaszewski, K., Ed., 2000.
(3) Szwarc, M. *Carbanions, Living Polymers and Electron Transfer Processing*; Interscience: New York, 1968.
(4) Chevalier, C.; Guerret, O.; Gnanou, Y. *Living and Controlled Polymerization: Synthesis, Characterization and Properties of the Respective Polymers and Copolymers* **2006**, 51-63.
(5) Hawker, C. J.; Bosman, A. W.; Harth, E. *Chem. Rev.* **2001**, *101*, 3661-3688.
(6) Lowe, A. B.; McCormick, C. L. *Prog. Polym. Sci.* **2007**, *32*, 283-351.
(7) Moad, G.; Rizzardo, E.; Thang, S. H. *Aust. J. Chem.* **2005**, *58*, 379-410.
(8) Matyjaszewski, K.; Spanswick, J.; Sumerlin, B. S. *Living and Controlled Polymerization: Synthesis, Characterization and Properties of the Respective Polymers and Copolymers* **2006**, 1-37.
(9) Tsarevsky, N. V.; Matyjaszewski, K. *Chem. Rev.* **2007**, *107*, 2270-2299.
(10) Kamigaito, M.; Satoh, K. *Macromolecules* **2008**, *41*, 269-276.
(11) Kitayama, T.; Shinozaki, T.; Masuda, E.; Yamamoto, M.; Hatada, K. *Polym. Bull.* **1988**, *20*, 505-510.
(12) Kitayama, T.; Hirano, T.; Hatada, K. *Tetrahedron* **1997**, *53*, 15263-15279.
(13) Kitayama, T.; Zhang, Y.; Hatada, K. *Polym. J.* **1994**, *26*, 868-872.
(14) Ballard, D. G. H.; Bowles, R. J.; Haddleton, D. M.; Richards, S. N.; Sellens, R.; Twose, D. L. *Macromolecules* **1992**, *25*, 5907-5913.
(15) Davis, T. P.; Haddleton, D. M.; Richards, S. N. *J.M.S.-Rev. Macromol. Chem. Phys.* **1994**, *C34*, 243-324.
(16) Hunt, K. H.; Crossman, M. C.; Haddleton, D. M.; Lloyd, P. M.; Derrick, P. J. *Macromol. Rapid Commun.* **1995**, *16*, 725-732.
(17) Long, T. E.; Allen, R. D.; McGrath, J. E. In *Recent Advances in Mechanistic and Synthetic Aspects of Polymerization*; Fontanille, M., Guyot, A., Eds.; D. Reidel: Dordrecht, 1987.
(18) Hamada, K.; Ishiura, K.; Takahashi, T.; Yaginuma, S.; Akai, M.; Ono, T.; Shachi, K.; Kuraray Co., Ltd.: U.S. Patent Appl. 10/452,379, 2003.

(19) Haddleton, D. M.; Hunt, K. H.; Crossman, M. C. *Macromol. Symp.* **1996**, *107*, 177-188.
(20) Schmitt, B.; Schlaad, H.; Muller, A. H. E. *Macromolecules* **1998**, *31*, 1705-1709.
(21) Bi, X.; Wang, D.; Wu, Z. *J. Mol. Catal. A: Chem.* **2002**, *179*, 53-57.
(22) Yamamoto, O.; Hayamizu, K. *J. Phys. Chem.* **1968**, *72*, 822-828.
(23) Sirimanne, C. T.; Yu, Z.; Heeg, M. J.; Winter, C. H. *J. Organomet. Chem.* **2006**, *691*, 2517-2527.
(24) Peace, R. J.; Horton, M. J.; Peron, G. L. N.; Holmes, A. B. *Macromolecules* **2001**, *34*, 8409-8411.
(25) Peron, G. L. N.; Peace, R. J.; Holmes, A. B. *J. Mater. Chem.* **2001**, *11*, 2915-2918.
(26) Haddleton, D. M.; Muir, A. V. G.; O'Donnell, J. P.; Richards, S. N.; Twose, D. L. *Macromol. Symp.* **1995**, *91*, 93-105.
(27) Haddleton, D. M.; Hunt, K. H.; Lloyd, P. M.; Crossman, M. C. *Polym. Mater. Sci. Eng.* **1995**, *73*, 418-419.
(28) Rodriguez-Delgado, A.; Chen, E. Y.-X. *J. Am. Chem. Soc.* **2005**, *127*, 961-974.
(29) Schlaad, H.; Muller, A. H. E. *Macromol. Rapid Commun.* **1994**, *15*, 517-525.
(30) Kitayama, T.; Tabuchi, M.; Kawauchi, T.; Hatada, K. *Polym. J.* **2002**, *34*, 370-375.
(31) Kitayama, T.; Tabuchi, M.; Hatada, K. *Polym. J.* **2000**, *32*, 796-802.
(32) Schlaad, H.; Schmitt, B.; Muller, A. H. E.; Jungling, S.; Weiss, H. *Macromolecules* **1998**, *31*, 573-577.
(33) Schmitt, B.; Schlaad, H.; Muller, A. H. E.; Mathiasch, B.; Steiger, S.; Weiss, H. *Macromolecules* **1999**, *32*, 8340-8349.
(34) Thompson, E. V. *J. Poly. Sci., Polym. Phys.* **1966**, *4*, 199-208.
(35) Hatada, K.; Ute, K.; Tanaka, K.; Kitayama, T.; Okamoto, Y. *Polym. J.* **1985**, *17*, 977-980.
(36) Kitayama, T.; Nakagawa, O.; Hatada, K. *Polym. J.* **1996**, *28*, 150-154.
(37) Schlaad, H.; Muller, A. H. E. *Macromol. Symp.* **1996**, *107*, 163-176.
(38) Hirano, T.; Yamaguchi, H.; Kitayama, T.; Hatada, K. *Polym. J.* **1998**, *30*, 767-769.
(39) Kitayama, T.; He, S.; Hironaka, Y.; Iijima, T.; Hatada, K. *Polym. J.* **1995**, *27*, 314-318.
(40) Crossman, M. C.; Haddleton, D. M. *Macromol. Symp.* **1998**, *132*, 187-196.
(41) Hatada, K.; Kitayama, T.; Fujimoto, N.; Fukuoka, T.; Nakagawa, O.; Nishiura, T. *J. Macromol. Sci.- Pure Appl. Chem.* **2002**, *A39*, 801-814.
(42) Lazzari, M.; Kitayama, T.; Janco, M.; Hatada, K. *Macromolecules* **2001**, *34*, 5734-5736.
(43) Kitayama, T.; Nishiura, T.; Tsubota, M.; Nakanishi, H.; Hatada, K. *Polym. J.* **1999**, *31*, 1001-1004.
(44) Kitayama, T.; Nakagawa, O.; Kishiro, S.; Nishiura, T.; Hatada, K. *Polym. J.* **1993**, *25*, 707-720.
(45) Tabuchi, M.; Kawauchi, T.; Kitayama, T.; Hatada, K. *Polymer* **2002**, *43*, 7185-7190.
(46) Kitayama, T.; Katsukawa, K.-i. *Polym. Bull.* **2004**, *52*, 117-124.
(47) Kitayama, T.; Shibuya, W.; Katsukawa, K.-i. *Polym. J.* **2002**, *34*, 405-409.
(48) Kitayama, T.; Kawauchi, T.; Chen, X.-P.; Padias, A. B.; Hall, H. K. *Macromolecules* **2002**, *35*, 3328-3330.
(49) Kitayama, T.; Urbanek, S.; Yanagida, T.; Hatada, K. *Polym. J.* **1996**, *28*, 827-830.
(50) Yong, T.-M.; Hems, W. P.; van Nunen, J. L. M.; Holmes, A. B.; Steinke, J. H. G.; Taylor, P. L.; Segal, J. A.; Griffin, D. A. *Chem. Commun.* **1997**, 1811-1812.

(51) Hems, W. P.; Yong, T.-M.; van Nunen, J. L. M.; Cooper, A. I.; Holmes, A. B.; Griffin, D. A. *J. Mater. Chem.* **1999**, *9*, 1403-1407.
(52) Desbois, P.; Fontanille, M.; Deffieux, A.; Warzelhan, V.; Schade, C. *Macromol. Symp.* **2000**, *157*, 151-160.
(53) Desbois, P.; Fontanille, M.; Deffieux, A.; Warzelhan, V.; Latsch, S.; Schade, C. *Macromol. Chem. Phys.* **1999**, *200*, 621-628.
(54) Menoret, S.; Carlotti, S.; Fontanille, M.; Deffieux, A.; Desbois, P.; Schade, C.; Schrepp, W.; Warzelhan, V. *Macromol. Chem. Phys.* **2001**, *202*, 3219-3227.
(55) Deffieux, A.; Menoret, S.; Carlotti, S.; Fontanille, M.; Desbois, P.; Schade, C. *Macromol. Chem. Phys.* **2002**, *203*, 862-867.
(56) Moineau, C.; Minet, M.; Teyssie, P.; Jerome, R. *Macromolecules* **1999**, *32*, 8277-8282.
(57) Tong, J. D.; Moineau, G.; Leclere, P.; Bredas, J. L.; Lazzaroni, R.; Jerome, R. *Macromolecules* **2000**, *33*, 470-479.
(58) Leclere, P.; Moineau, G.; Minet, M.; Dubois, P.; Jerome, R.; Bredas, J. L.; Lazzaroni, R. *Langmuir* **1999**, *15*, 3915-3919.
(59) Leclere, P.; Rasmont, A.; Bredas, J. L.; Jerome, R.; Aime, J. P.; Lazzaroni, R. *Macromolecular Symposia* **2001**, *167*, 117-137.

Chapter 3: Factors Influencing the Room Temperature Anionic Polymerization of Alkyl Methacrylates in the Presence of Aluminum Alkyls

3.1 Abstract

The use of organoaluminum mediators in the anionic polymerization of alkyl methacrylates has enabled stereospecific polymerization with molecular weight control at ambient temperatures. Anionic polymerization of methyl methacrylate (MMA) with a mixed trialkylaluminum/alkyllithium initiator complex of triisobutylaluminum and 1,1-diphenylhexyllithium was performed at elevated temperatures (0-50 °C) to explore the limits of controlled polymerization in the presence of aluminum mediators. The effect of the aluminum:lithium ratio on parameters including molecular weight distribution, stereotacticity, and glass transition temperature was explored at 25 °C to reveal a drastic change in polymerization mechanism in the presence of excess aluminum. The effect of temperature on polymerization control was also explored using MALDI TOF/TOF CID spectroscopy to show the contribution of side reactions at elevated temperatures. Finally, polymerizations were monitored at 0 and 27.5 °C using in situ FTIR spectroscopy. Results show that chain termination through a back-biting side reaction dominated at temperatures above 25 °C, leading to broader molecular weight distributions and loss of desired chain end functionality.

3.2 Introduction

The controlled polymerization of acrylates and methacrylates is a highly desirable process for numerous industrial applications. Anionic polymerization is an appealing technique for the synthesis of well-controlled architectures, molecular weight distributions, and stereospecificity; however, the high sensitivity to impurities and extreme temperature requirements for control of acrylic monomers limit the industrial usefulness of this technique. Screened anionic polymerization (SAP) employs alkyllithium initiators with alkyl aluminum additives to control polymerization of acrylates and methacrylates in hydrocarbon solvents at ambient temperatures.[1-3] Bulky alkyl aluminums with large cross-sectional areas "screen" the propagating chain end from side reactions while complexing the acrylic monomer for stereospecific addition.[1]

Ballard and coworkers introduced SAP in the early 1990s with an initial report of controlled anionic polymerization of MMA at 0 °C in toluene using aluminum alkyls substituted with bulky 2,6-di-*tert*-butyl-4-methylphenol (BHT) groups.[1] Later, they reported that triisobutylaluminum ($^{i}Bu_3Al$) also effectively controlled polymerization,[4] but smaller alkyl substituents (methyl, ethyl, isopropyl) did not have sufficient size to screen the chain end at higher temperatures.[2,5] Rodriquez-Delgado and coworkers recently elucidated the mechanism of anionic polymerization in the presence of aluminum mediators using crystal structures of model compounds.[6] This work reaffirmed the role of excess organoaluminum with respect to alkyllithium initiator in order to achieve polymerization control. The first equivalent is involved in the stabilization of the living anion at the chain end, while the second is required for complexation of the monomer for stereospecific addition.[7-9] Excess aluminum also acts to

scavenge impurities in the reaction mixture, allowing for less rigorous purification techniques than those required in classical anionic polymerization.

Stereocontrol in the polymerization of methacrylates allows for the specific tailoring of thermal properties for use in advanced materials. Stereospecificity is best maintained at low temperatures, and greater than 90% syndiotactic poly(methyl methacrylate) (PMMA) was achieved using trialkylaluminum/alkyllithium initiators at -93 °C.[10] The goal of this study is to explore the limits of polymerization control and stereospecificity using $^{i}Bu_3Al$/alkyllithium at high temperatures, 0 – 50 °C in the polymerization of MMA. Polymerization control was evaluated based on molecular weight distribution, yield, and tacticity as a function of aluminum to lithium ratio and polymerization temperature. In addition, polymerizations were monitored using in situ FTIR spectroscopy to monitor polymerizations at 0 to 27.5 °C in real-time.

3.3 Experimental

3.3.1 Materials

Methyl methacrylate (MMA), 1,1-diphenylethylene (DPE), *sec*-butyllithium (*sec*BuLi, 1.40M solution in cyclohexane), triisobutylaluminum ($^{i}Bu_3Al$, 1.0M solution in toluene), 1,2-dibromoethane (99+%), and phenolphthalein were purchased from Aldrich Chemical Company. Industrial grade *sec*-BuLi in cyclohexane was kindly provided from FMC Lithium. MMA was passed through a neutral alumina column to remove inhibitors, distilled from CaH_2, and redistilled from triethylaluminum directly prior to use. DPE was distilled from *sec*-BuLi and stored in the freezer under nitrogen. Other reagents were used as received. Toluene was transferred under N_2 from an Innovative Technology, Inc. PureSolv-MD3 solvent purification system.

3.3.2 Instrumentation

^{1}H NMR spectra of the polymers were obtained on a Varian Unity 400 MHz spectrometer in $CDCl_3$. Size exclusion chromatography (SEC) was used to determine molecular weights at 40 °C in THF at 1 mL min^{-1} on a Waters SEC equipped with three Polymer Laboratories PLGel 5μm Mixed-C columns and an autosampler. Detectors included a Waters 2414 Refractive index (RI) detector and a Wyatt Technologies miniDAWN multiangle laser light scattering (MALLS) detector. Absolute molecular weights were determined using the MALLS detector and dn/dc values determined on-line. Differential scanning calorimetry (DSC) was performed on a TA Instruments Q100 at a heating rate of 10 C min^{-1} under nitrogen. The reported glass transition temperature represents the midpoint of the transition during the second heating cycle.

Insitu FTIR was performed with a Mettler Toledo ReactIR 4000 ATR apparatus equipped with a light conduit and a stainless steel insertion probe featuring a DiComp (diamond composite) probe tip. IR spectra were collected every minute with 256 scans per spectrum. Reaction analysis was performed with ReactIR 3.1 software from Mettler Toledo.

3.3.3 MALDI-TOF/TOF CID Measurements

PMMA samples were analyzed using a Voyager Elite DE STR MALDI-TOF MS (Applied Biosystems, Framingham, MA) equipped with a 337-nm N_2 laser. Spectra were obtained in the positive ion mode using an accelerating voltage of 20 kV and a laser intensity ~10% above threshold. Parameters including grid voltage, guide wire voltage, and delay time were optimized to achieve the best signal-to-noise ratio. Spectra were acquired in reflectron mode with a mass resolution greater than 3000 fwhm, with isotopic resolution throughout the entire mass range detected. External mass calibration was performed using protein standards

from a Sequazyme Peptide Mass Standard Kit (Applied Biosystems) and a five-point calibration method with masses ranging from 1296.69 Da to 5730.61 Da. Internal mass calibration was subsequently performed using a PEG standard (M*n* = 2000; Polymer Source, Inc.) to yield monoisotopic masses exhibiting a mass accuracy better than $\Delta m = \pm 0.1$ Da. The instrument was calibrated before every measurement for constant experimental conditions throughout the study. A dithranol (Aldrich) matrix doped with sodium trifluoroacetate (NaTFA, Aldrich) was used for all samples. Samples were prepared using the dried-droplet method with weight (mg) ratios of 50:10:1 (Dithranol:polymer:NaTFA) in tetrahydrofuran (THF).[11] The mixture was vortexed for 30 s, then 1 μL of the mixture was pipetted on the MALDI sample plate and allowed to air dry at room temperature. MS data were processed using Data Explorer 4.9 software from Applied Biosystems.

3.3.4 Synthesis of 1,1-Diphenylhexyllithium (DPHL)

Dry toluene (35 mL) and DPE (3.27 mmol, 0.59 mL) were added via cannula to a flame dried, 50-mL round bottomed flask equipped with a stir bar under a nitrogen atmosphere. The solution was titrated with 1.64M *sec*-butyllithium (*sec*BuLi) until a faint orange color persisted, then 2 mL (3.27 mmol) *sec*BuLi were added resulting in a deep maroon color. The solution stirred for 2h to ensure complete DPHL formation.

3.3.5 Measuring Initiator Concentration and Purity

Initiator concentration and quality were determined using the Gilman double titration method, according to published methods.[12] To determine the total content of base, a 1-mL

aliquot of DPHL synthesized in the previous step was quenched with 20 mL of degassed water under nitrogen. A few drops of phenolphthalein indicator were added, and the solution was titrated with standardized 0.1N HCl until the pink color disappeared. In a second flask, 0.2 mL of 1,2-dibromoethane were dissolved in 3 mL dry diethylether under nitrogen. A 1-mL aliquot of DPHL was added dropwise with stirring. The solution was diluted with 20 mL of water and then titrated in the same manner to determine the amount of residual base. The following equations were used to calculate DPHL concentration (1) and determine its quality (2), where c is concentration, V is volume, I represents the first step, and II represents the second step.

$$(1) \quad c_{(DPHL)} = [(V_{HCl\text{-}I} - V_{HCl\text{-}II}) \times c_{HCl}] / V_{aliquot}$$

$$(2) \quad \text{Residual base} = (V_{HCl\text{-}II} / V_{HCl\text{-}I}) \times 100\%$$

If the residual base content was greater than 10%, the initiator was deemed poor quality and not used for polymerization. The actual concentration of *sec*-BuLi used in the synthesis was determined in the same manner.

3.3.6 Synthesis of Poly(methyl methacrylate) (PMMA) Homopolymers

A representative polymerization of MMA is described. Toluene (30 mL), DPHL initiator solution (0.25 mmol), and $^{i}Bu_3Al$ solution (0.525 mL, 0.525 mmol) were sequentially added to a flame dried, 100-mL round bottomed flask. The solution was allowed to stir for 5 min in a water bath to equilibrate at 25 °C. Next, MMA (2.5 mL, 0.0234 mol) was added quickly and polymerization proceeded until the yellow color faded, approximately 1 h. The polymerization was quenched with the addition of 0.5 mL acidic methanol. Polymer product was precipitated in hexanes, filtered, washed with excess hexanes, and dried under vacuum overnight. For *insitu*

FTIR spectroscopy experiments, the reaction was performed in a 2-neck flask equipped with an airtight fitting for the FTIR probe.

3.4 Results and Discussion

3.4.1 Initiator Choice and Quality

Much of the reported literature on anionic polymerization of alkyl methacrylates in the presence of organoaluminums utilize *t*-butyllithium as the initiator for its high reactivity and steric bulk.[1,2,4,13-16] For the purposes of this study, we used 1,1-diphenylhexyllithium (DPHL), a sterically bulky initiator commonly used in the anionic polymerization of methacrylates.[17] In contrast to *t*-butyllithium, DPHL is less flammable and safer to use in the laboratory. However, DPHL is not commercially available and must be synthesized from commercially available *sec*BuLi and DPE. Therefore, the quality of DPHL initiator depends heavily on the purity of purchased *sec*BuLi.

The Gilman double titration method is a proven way to determine both concentration and overall reagent quality of alkyllithiums. Periodic titrations of *sec*BuLi stock solutions stored in the freezer revealed a marked degradation in initiator quality over short periods of time for the commercially available reagents, with greater than 20% residual base present after only a few months from purchase. FMCLithium industrial grade *sec*BuLi, however, remained stable over much longer periods with calculated residual base amounts typically less than 5%. Use of the high grade *sec*BuLi in the synthesis of DPHL afforded pure initiators with typically 3-8% residual base, leading to improved control in the polymerization of methacrylates.

3.4.2 Effect of Al:Li Ratio on Polymerization Control at Room Temperature

PMMA was synthesized via screened anionic polymerization in the presence of $^{i}Bu_3Al$ in toluene at 25 °C (Scheme 3.1). The ratio of aluminum to lithium (Al:Li) was systematically varied to explore its effects on polymerization control, including yield, molecular weight distribution, and stereotacticity. According to the early work of Haddleton,[1,2,13] and the mechanism proposed by Rodriguez-Delgado and Chen,[6] changes in the Al:Li ratio dramatically altered the polymerization behavior and a ratio greater than 2 was required for both molecular weight and tacticity control.

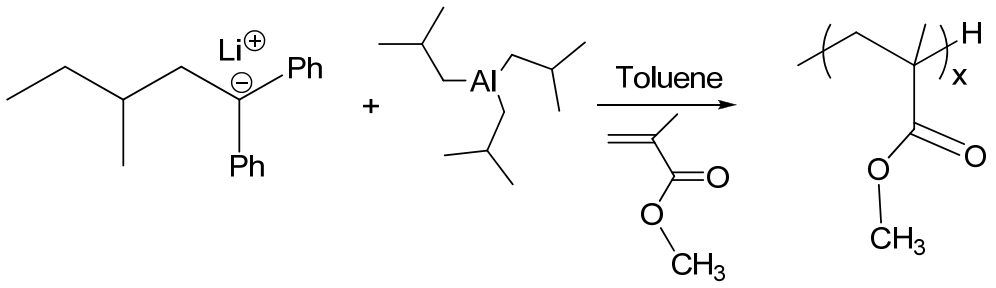

Scheme 3.1 Screened anionic polymerization of MMA in the presence of $^{i}Bu_3Al$.

In the absence of $^{i}Bu_3Al$, several side reactions dominated the anionic polymerization of MMA at ambient temperatures, leading to dead chain ends, uncontrolled molecular weights, and large polydispersities. This result was expected based on previous literature where alkyl methacrylates were polymerized at extreme temperatures below -78 °C to minimize adverse side reactions.[18] As shown in Table 3.1**,** polymerization in the absence of $^{i}Bu_3Al$ led to a broad molecular weight distribution and poor yield including the formation of an insoluble gel. The SEC chromatogram in Figure 3.1 confirms a high molecular weight fraction and very poor control over the polymerization process. In addition, polymerization in the absence of Al

resulted in a predominantly isotactic structure with 58% *rr* and only 19% *mr* diads, determined from ^{1}H NMR spectroscopy. It is well known that alkyllithium initiated polymerization of MMA in hydrocarbons leads to highly isotactic structures.

Table 3.1 Effects of Al:Li ratio on molecular weight control, yield, tacticity, and glass transition temperature (T_g) at 25 °C**.**

Temp (°C)	**Al:Li**	**M_n (g/mol)**	**M_w/M_n**	**Isolated Yield (%)**	**% Tacticity Syndio/Iso**	**T_g (°C)**
25	0	12700	11.7	50	19/58	71.0
25	1.1	12200	1.33	35	17/45	81.4
25	2.1	18700	1.12	95	57/7	121.2
25	3.0	14700	1.21	88	61/5	121.9
25	6.0	31300	1.27	97	66/7	126.2

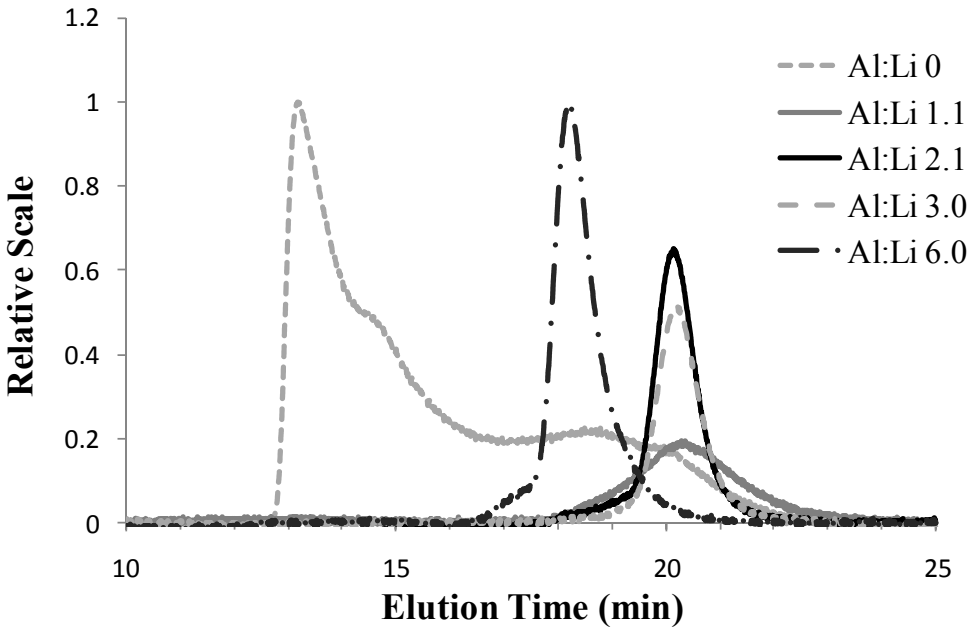

Figure 3.1 SEC of PMMA samples produced with varying amounts of $^{i}Bu_3Al$.

At Al:Li of 1.1, a relatively narrow molecular weight distribution was achieved, but with very low polymerization yield and little control of stereotacticity with 45% *rr* diads. The low yield indicated a poor degree of polymerization control, and the process was likely dominated by termination reactions leading to dead polymer chains. Polymerization with a ratio greater than 2 Al:Li achieved almost quantitative yields, syndiorich structures (~60% *mr*), and narrow molecular weight distributions. A corresponding increase in the sharpness of the SEC traces also represented improved polymerization control in the presence of excess Al (Figure 3.1). The excess Al available to complex MMA and promote stereoregular addition afforded the additional polymerization control, as expected based on the proposed polymerization mechanism. As the amount of excess Al increased to 6 equivalents, the syndiotacticity of PMMA also increased to 66%.

Stereoregularity drastically influences the ability of chains to order and crystallize, therefore affecting the glass transition temperature. The influence of stereoregularity in PMMA is especially pronounced, with a T_g difference of more than 70 °C between highly isotactic (50 °C at 96% *rr*) and syndiotactic structures (123 °C at 93% *mr*), as determined for uniform PMMA <5000 g/mol and extrapolated to T_g of infinite molecular weight.[10] The influence of stereocontrol on the T_g of PMMA synthesized via SAP is clearly observed in Table 3.1 as stereocontrol improved with increasing Al:Li. Entry 2 in Table 3.1 exhibited a T_g of 81.4 °C for an atactic structure with 45% *rr*. A lower T_g of 71.0 °C was observed for Entry 1, despite a higher *rr* content of 58%. The depression of the T_g for Entry 1 is due to the very broad molecular weight distribution. An increase in T_g of approximately 40 °C occurred between Entries 2 and 3 due to the enhanced control to form syndiorich structures. Syndiorich structures with 61 and 66% *mr* resulted in high T_gs of 121.9 °C and 126.2 °C, respectively. These values are higher than expected based on previous reports from Hatada and coworkers, where 123 °C was the maximum T_g expected for PMMA with very high *mr* content.[10] However, the previously reported T_gs were calculated from the onset of the transition, while the T_gs in this study are reported as midpoint values. This work demonstrates the ability to tune the T_g of methacrylates through simple selection of the temperature and Al:Li ratio for the design of new methacrylate-based materials with tailored thermal properties.

3.4.3 Effect of Temperature on Polymerization Control of MMA

In order to explore the temperature limits of polymerization control using $^{i}Bu_3Al$/DPHL, polymerizations were performed between 0 and 50 °C under otherwise constant conditions. An Al:Li of 2.1 was adopted as the ideal ratio to achieve narrow polydispersities with fair agreement

of targeted and actual molecular weights. Results at four different temperatures are summarized in Table 3.2. Increasing the polymerization temperature resulted in an overall decrease of isolated yield and increase in molecular weight distribution. Temperatures above 25 °C also resulted in a decrease of syndiotactic control, reaching only 44% *mr* at 50 °C. The observed decrease in polymerization control at elevated temperatures is not surprising and can be attributed to a very fast polymerization rate as well as the dominance of back-biting side reactions with increased temperatures. Haddleton and coworkers reported similar trends in polymer properties with increasing temperature, reaching 58% yield and 43% *mr* at 50 °C with a *t*-butyllithium/trialkylaluminum initiating complex.[4]

Table 3.2 Characterization of PMMA synthesized at various temperatures with Al:Li 2.1

T (°C)	Yield	M_n (SEC)	M_w/M_n	Syn	Iso
0	96	24600	1.18	48	13
25	95	18300	1.11	57	7
40	75	17900	1.49	50	10
50	58	9730	1.66	44	13

The contribution of the back-biting side reaction to the decrease in polymerization control at higher temperatures was evaluated using MALDI-TOF/ TOF CID. Two major structures were expected from the anionic polymerization of MMA initiated with DPHL, as shown in Figure 3.2. The desired structure derived from DPHL initiation and termination with acidic methanol features both initiator and proton endgroups (**a**). The predominant side reaction expected in

anionic polymerization of methacrylates is chain termination through a backbiting reaction at the terminal end to form a six-membered ring (**b**).[18] Structures **a** and **b** formed the basis of our MALDI-TOF analysis, where an increase in the appearance of **b** was expected with increasing polymerization temperature.

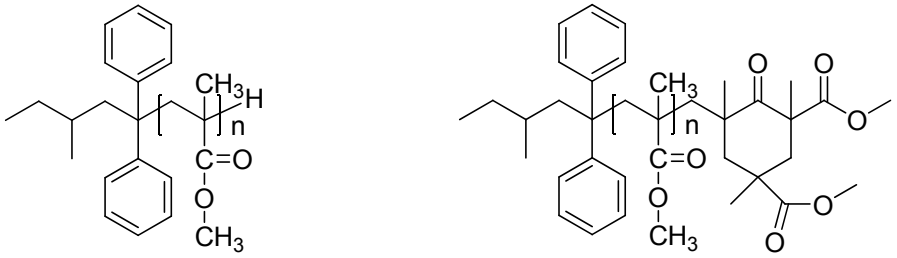

Figure 3.2 Predominant polymer product structures expected in MALDI-TOF MS spectra. (**a**) Desired structure with initiator and proton endgroups. (**b**) Side product resulting from back-biting reaction to form a cyclic endgroup.

The MALDI-TOF spectra for PMMA products polymerized at 0, 25, 40, and 50 °C are shown in Figure 3.3. A narrow mass range of 9025-9250 Da is shown for sake of clarity. The peaks corresponding to the proposed polymer structures are labeled **a** and **b**, for the desired controlled product and termination side products, respectively. The molecular weight difference between peaks of the major distributions corresponds to the molecular weight of the MMA repeating unit, 100.1 g/mol. The calculated endgroup mass for structure **a** is 238.2 Da ($C_{18}H_{21}$ + H). The calculated endgroup mass for structure **b** is 506.3 ($C_{18}H_{21}$ + $C_{14}H_{21}O_5$). Therefore, a sodiated 88-mer having the desired DPHL and H endgroups has a calculated mass of 88 x 100.1 ($C_5H_80_2$) + 238.2 ($C_{18}H_{22}$) + 22.99 (Na+) = 9069.99 Da. This is in agreement with the peak

labeled **a** observed at *m/z* 9069.9 for PMMA (Figure 3.3 a-c). Similarly, a sodiated 86-mer having the endgroups of the terminated **b** structure has a calculated mass of 86 x 100.1 ($C_5H_8O_2$) + 506.3 ($C_{32}H_{42}O_5$) + 22.99 (Na+) = 9137.89 Da. This is in agreement with the peak observed at *m/z* 9137.9, labeled **b** in Figure 3.3 a-d.

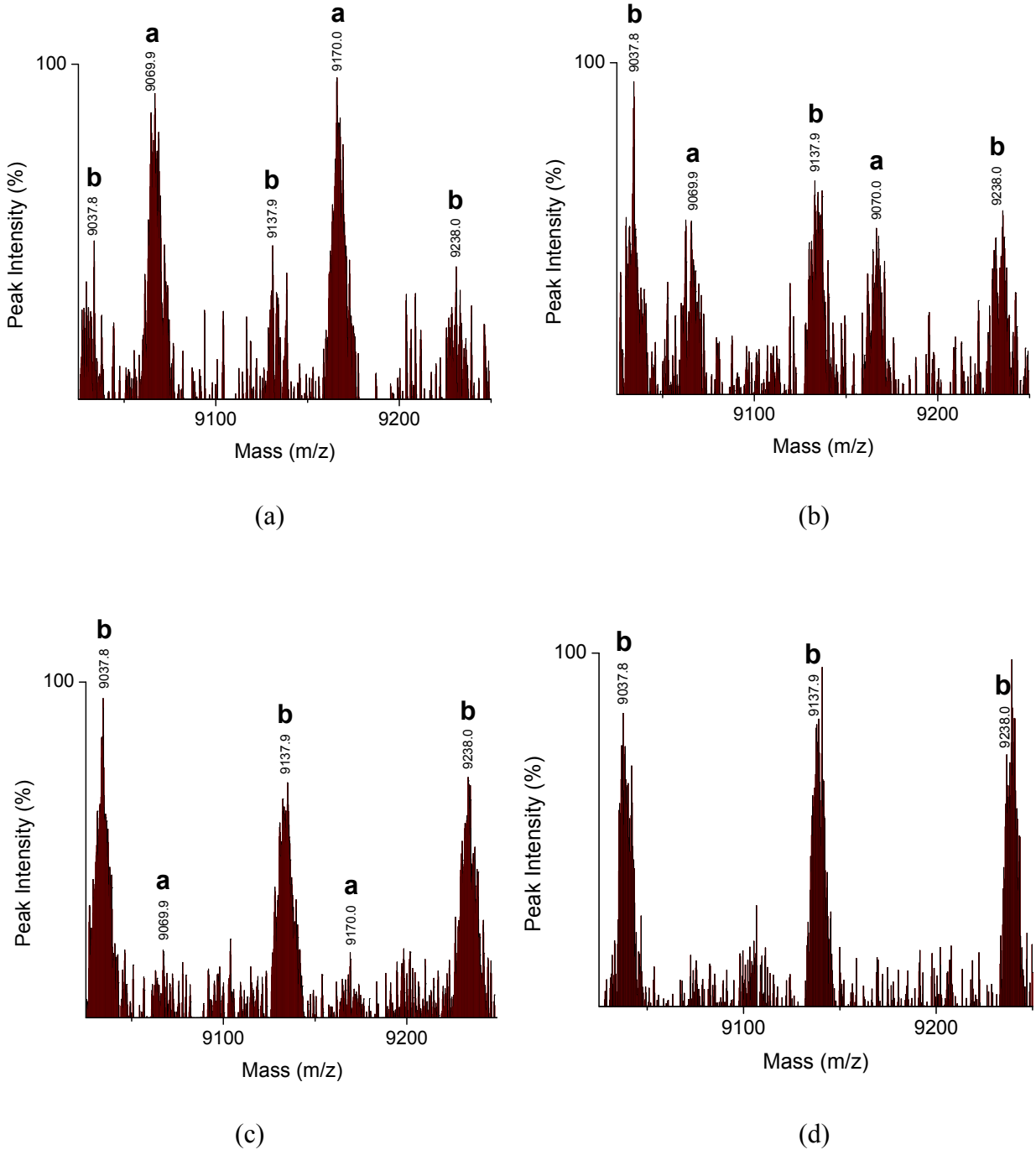

Figure 3.3 MALDI-TOF MS spectra of PMMA synthesized using $^{i}Bu_3Al$/DPHL 2.1:1; (a) 0 °C, (b) 25 °C, (c) 40 °C, (d) 50 °C

The contribution of the termination side product **b** increased with temperature and was the only product observed at 50 °C. At 0 °C, the predominant structure observed in the mass spectrum was the desired product **a**. However, a population of the termination side product was certainly visible at the lowest temperature, showing that endgroup control was not afforded at any temperature under the conditions studied. Comparable populations of both **a** and **b** structures were observed for PMMA polymerized at 25 °C, while **b** dominated the population at both 40 and 50 °C. The large amount of terminated chains at the higher temperatures accounted for the decreased yields and broader molecular weight distributions of the resultant PMMAs. These results show that the $^{i}Bu_3Al$/DPHL initiator complex was not effective in inhibiting side reactions to afford stereocontrolled anionic polymerization at temperatures above 25 °C. However, polymerizations at 0 and 25 °C afforded sufficient control to achieve narrow molecular weight distributions <1.2 and syndiorich structures. The drawback of this initiator system is that block additions will likely not be successful above 0 °C due to the large number of terminated chains unavailable for chain extension.

A major concern using organoaluminums in anionic polymerization has been the secondary initiation through alkyl groups from the aluminum rather than the alkyllithium. Haddleton and coworkers used MALDI-TOF endgroup analysis and NMR studies with MMA-d_8 to prove that all polymer chains contained alkyllithium initiator fragments, rather than isobutyl fragments from the aluminum species.[2,4,13,19] According to our preliminary calculations based on the expected structures and peak values observed in the MALDI spectra, the predominant PMMA structures observed were initiated with DPHL fragments while other forms of initiation did not occur.

3.4.4 In situ FTIR Monitoring of MMA Polymerization

In situ FTIR spectroscopy allows the real-time monitoring of reaction progress and kinetics without the hassle of removing samples for subsequent analysis. Screened anionic polymerization of MMA was monitored using *in situ* FTIR spectroscopy at 0 °C using a 5 mm IR probe inserted in the reaction vessel. The IR probe and reaction vessel were flamed and purged diligently to minimize the effects of impurities that are detrimental to anionic reactions. Regardless of these extra precautions, an excess of DPHL initiator was used in order to remove any impurities prior to the addition of $^{i}Bu_3Al$ in the flask, and the final amount of initiator added was determined through titration to the deep maroon color characteristic of DPHL.

Data collection started 1 minute before monomer addition. A large increase in absorption at the characteristic wavenumbers of MMA, including the vinyl region at 1307 and 1325 cm^{-1}, were immediately observed. As the reaction proceeded, the absorbance of these characteristic peaks decreased, revealing conversion of monomer to polymer (Figure 3.4). A plateau was observed at ~50 min, indicating the complete consumption of monomer. This plateau time coincided with a color change in the reaction mixture, from the pale yellow color of the MMA-Al complex to a clear solution indicative of complete monomer consumption. Haddleton and coworkers used this colorimetric endpoint to signal the end of reaction and time for addition of a new monomer in the formation of block copolymers.[4]

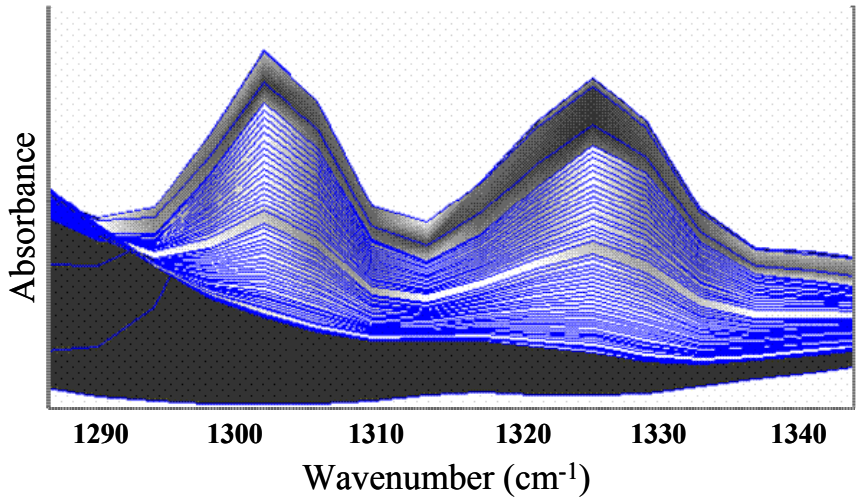

Figure 3.4 *In situ* FTIR waterfall plot of the vinyl region of MMA during polymerization at 0 °C, where absorbance is decreasing with time.

The rate of polymerization for a non-terminating, living anionic polymerization is expressed as the rate of propagation (R_p)

$$R_p = k_p^{app}[M^-][M]$$

where [M] is the monomer concentration and $[M^-]$ is the total concentration of living propagating chain ends. In the case of a truly living system with fast initiation, the concentration of $[M^-]$ remains constant until all monomer is consumed and/or the polymerization is terminated. Under this condition, the second-order propagation rate law becomes a pseudo-first order rate law where [M-] is represented as part of the observed rate constant (k_{obs}), where $k_{obs} = k_p^{app}[M^-]$. This pseudo-first order rate law allows for kinetic analysis of aluminum-mediated MMA polymerization with in situ FTIR spectroscopy, using the absorbance of the vinyl region of MMA.

Monomer conversion was plotted as a function of time for both monomer peaks at 1304 and 1327 cm^{-1}. Both plots exhibited a linear trend. The absorbance at 1327 cm^{-1} was chosen for pseudo-first order kinetic analysis. The monomer absorbance (A) at any given time was

normalized with the initial absorbance (A_0) recorded at the beginning of the reaction, and a plot of $-\ln(A/A_0)$ vs time (s) produced a straight line with a slope equal to the observed rate constant of polymerization, k_{obs} (Figure 3.5). At 0 °C and Al:Li of 2.1, the observed rate constant was 1.8 x 10^{-4} s^{-1}. This value is in reasonable agreement with reported observed rate constants on the order of 10^{-3} s^{-1} for the polymerization of MMA with *t*-butyllithium and $^{i}Bu_3Al$ (Al:Li 2.94) at -20 °C.[4]

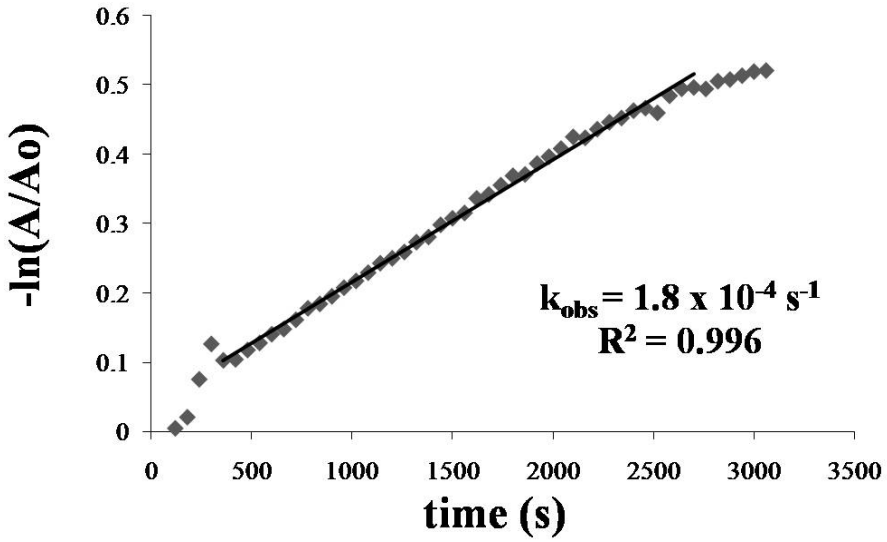

Figure 3.5 Kinetic analysis of the vinyl stretch at 1327 cm^{-1} for PMMA at 0 °C with Al:Li of 2.1.

SAP of MMA was also monitored using in situ FTIR at 27.5 °C, keeping Al:Li constant at 2.1 for comparison to data collected at 0 °C. Kinetic analysis of the vinyl stretch at 1327 cm^{-1} is shown in Figure 3.6. The observed rate constant over the linear range was 1.1 x10^{-3} s^{-1}. Significant deviation from pseudo-first order kinetics was observed after ~800 s (~13 min) of reaction time, which is likely due to an increasing contribution of side reactions and alternative

polymerization mechanisms later in the polymerization at this high temperature. This assumption is based on MALDI TOF analysis discussed earlier. The contribution of side reactions significantly affects [M^-] so that pseudo-first order analysis is no longer valid at elevated temperatures. The reaction was terminated after 37 minutes due to the disappearance of the yellow color as well as the observance of a plateau in the absorbance. Although not directly comparable due to differences in reaction conditions (ie. reagent concentration), the order of magnitude difference in k_{obs} agrees well with the shorter reaction time required for high conversion at 27.5 °C compared to 0 °C.

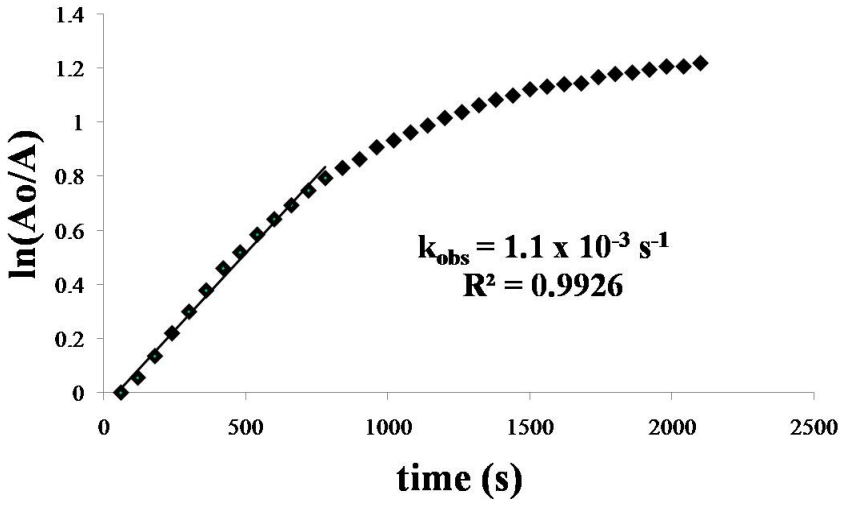

Figure 3.6 Kinetic analysis of the vinyl stretch at 1327 cm^{-1} for PMMA at 27.5 °C with Al:Li of 2.1.

A control reaction was performed simultaneously with the FTIR monitoring at 27.5 °C under equivalent conditions to confirm the same polymerization mechanisms applied regardless of the presence of the in situ probe. SEC chromatograms and the resulting polymer properties from both experiments at 27.5 °C are shown in Figure 3.7 and Table 3.3, respectively. The solid

lines of the SEC traces represent light scattering data, while the dashed lines are refractive index data. Peak shapes were very similar, and molecular weights matched closely, despite a sizeable increase in the molecular weight distribution to 1.29 for PMMA monitored with FTIR. A slight decrease in control was expected based on the excess DPHL used to titrate impurities at the start of reaction. A 10% decrease in yield is also consistent with an increase in termination reactions throughout the polymerization. However, stereoregularity matched very well between the two reactions, showing good agreement of the polymerization mechanism between the two methods.

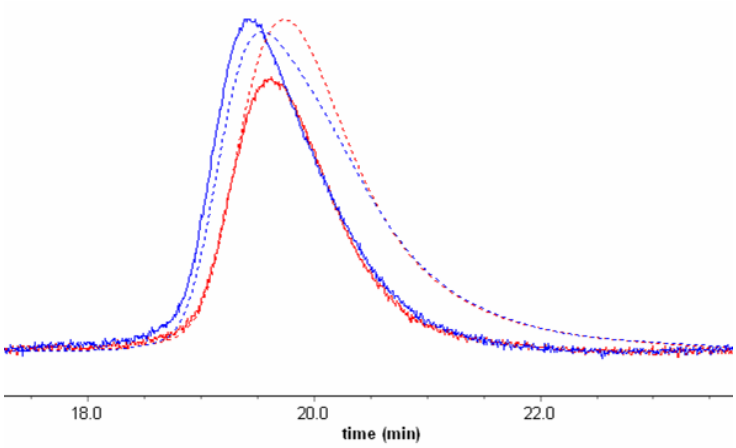

Figure 3.7 SEC traces of PMMA synthesized at 27.5 °C with Al:Li 2.1 where the blue curve corresponds to PMMA monitored with in situ FTIR and the red curve represents a control experiment without in situ FTIR monitoring.

Table 3.3 Polymer properties of PMMA synthesized with and without in situ FTIR monitoring.

	Yield (%)	M_n (g/mol)	M_w/M_n	Syndio (%)	Hetero (%)	Iso (%)
FTIR	82	19900	1.29	56	36	8
Control	91	22300	1.11	56	36	8

3.5 Conclusions

Syndiorich PMMA was synthesized via screened anionic polymerization at temperatures ranging from 0 to 50 °C using a mixed organoaluminum/alkyllithium initiator. Polymerization control was monitored as a function of Al:Li and temperature using parameters including yield, tacticity, and molecular weight distribution. The Al:Li ratio had a profound effect on the polymerization mechanism and control, and ratios >2 resulted in narrow molecular weight distributions, high yields, and syndiorich structures. Effectiveness of polymerization control decreased markedly at temperatures of 40 and 50 °C, resulting in low yields and poor molecular weight control. Additionally, MALDI-TOF/ TOF CID analysis revealed a predominance of chain termination through a back-biting reaction at increasing temperatures. At 50 °C, only chains with the cyclic chain terminated endgroup were detected. This study revealed a limit of control between 0 and 25 °C for the polymerization of PMMA using $^{i}Bu_3Al$/DPHL initiator, depending on desired application and endgroup control.

In situ FTIR spectroscopy enabled the real-time monitoring of MMA polymerizations at 0 and 27.5 °C. Analysis of the IR absorbance for the vinyl region at 1327 cm^{-1} revealed pseudo-first order kinetics with an observed rate constant (k_{obs}) of 1.8 x 10^{-4} s^{-1}. The observance of a plateau in the absorbance change at ~50 minutes also corresponded to the disappearance of the characteristic yellow Al-MMA complex, signifying complete consumption of monomer. In situ monitoring of polymerization at 27.5 °C revealed a k_{obs} of 1.1 x 10^{-3} s^{-1} and a deviation from pseudo-first order kinetics after ~13 min of reaction. The observed deviation in the kinetics plot is in agreement with the increased contribution of back-biting termination reactions determined with MALDI-TOF experiments at higher temperatures. The same mechanism of polymerization

was observed regardless of in situ monitoring, as evidenced by equivalent tacticity control with and without FTIR probe use.

3.6 Acknowledgements

The authors would like to acknowledge Kraton Polymers for unrestricted financial support of this research. We also thank Dr. Anthony Gies at Vanderbilt University for MALDI-TOF MS results.

3.7 References

(1) Ballard, D. G. H.; Bowles, R. J.; Haddleton, D. M.; Richards, S. N.; Sellens, R.; Twose, D. L. *Macromolecules* **1992**, *25*, 5907-5913.
(2) Haddleton, D. M.; Hunt, K. H.; Crossman, M. C. *Macromol. Symp.* **1996**, *107*, 177-188.
(3) Hamada, K.; Ishiura, K.; Takahashi, T.; Yaginuma, S.; Akai, M.; Ono, T.; Shachi, K.; Kuraray Co., Ltd.: U.S. Patent Appl. 10/452,379, 2003.
(4) Haddleton, D. M.; Muir, A. V. G.; O'Donnell, J. P.; Richards, S. N.; Twose, D. L. *Macromol. Symp.* **1995**, *91*, 93-105.
(5) Schmitt, B.; Schlaad, H.; Muller, A. H. E. *Macromolecules* **1998**, *31*, 1705-1709.
(6) Rodriguez-Delgado, A.; Chen, E. Y.-X. *J. Am. Chem. Soc.* **2005**, *127*, 961-974.
(7) Kitayama, T.; Tabuchi, M.; Hatada, K. *Polym. J.* **2000**, *32*, 796-802.
(8) Kitayama, T.; Tabuchi, M.; Kawauchi, T.; Hatada, K. *Polym. J.* **2002**, *34*, 370-375.
(9) Schlaad, H.; Muller, A. H. E. *Macromol. Rapid Commun.* **1994**, *15*, 517-525.
(10) Ute, K.; Miyatake, N.; Hatada, K. *Polymer* **1995**, *36*, 1415-1419.
(11) Gies, A. P.; Vergne, M. J.; Orndorff, R. L.; Hercules, D. M. *Macromolecules* **2007**, *40*, 7493-7504.
(12) Gilman, H.; Cartledge, F. K. *J. Organomet. Chem.* **1964**, *2*, 447-454.
(13) Haddleton, D. M.; Hunt, K. H.; Lloyd, P. M.; Crossman, M. C. *Polym. Mater. Sci. Eng.* **1995**, *73*, 418-419.
(14) Hatada, K.; Kitayama, T. *Polym. Int.* **2000**, *49*, 11-47.
(15) Kitayama, T.; Hirano, T.; Hatada, K. *Tetrahedron* **1997**, *53*, 15263-15279.
(16) Kitayama, T.; Nakagawa, O.; Kishiro, S.; Nishiura, T.; Hatada, K. *Polym. J.* **1993**, *25*, 707-720.
(17) Long, T. E.; Allen, R. D.; McGrath, J. E. In *Recent Advances in Mechanistic and Synthetic Aspects of Polymerization*; Fontanille, M., Guyot, A., Eds.; D. Reidel: Dordrecht, 1987.
(18) Davis, T. P.; Haddleton, D. M.; Richards, S. N. *J.M.S.-Rev. Macromol. Chem. Phys.* **1994**, *C34*, 243-324.
(19) Hunt, K. H.; Crossman, M. C.; Haddleton, D. M.; Lloyd, P. M.; Derrick, P. J. *Macromol. Rapid Commun.* **1995**, *16*, 725-732.

Chapter 4: Nitroxide Mediated Polymerization of Hydroxy-functionalized Copolymers

4.1 Abstract

The synthesis of new functional polymers are important for technological advances in a number of fields. Controlled radical polymerization techniques enable the synthesis of well-defined acrylic copolymers with various functionalities and are compatible with a wide range of solvent conditions. Nitroxide mediated polymerization was employed in this work using DEPN for the controlled synthesis of hydroxy-functional amphiphilic random and block copolymers containing 2-hydroxyethyl acrylate (HEA). Random copolymers of n-butyl acrylate (nBA) and 10 mol % HEA were synthesized in bulk conditions, and in situ FTIR spectroscopy monitored reactions in real-time. Pseudo first order rate kinetics were followed for all copolymerizations, and narrow polydispersities were obtained indicating a well controlled polymerization. Addition of a HEA block to nBA was also achieved with good monomer crossover, demonstrating the synthesis of amphiphilic functional diblock copolymers.

4.2 Introduction

2-hydroxyethyl acrylate (HEA) is a versatile acrylic monomer carrying a hydroxyl functionality useful in a variety of applications. HEA, and the methacrylate derivate 2-hydroxyethyl methacrylate (HEMA) are used in the synthesis of copolymers for many applications of functional materials, including hydrogels[1-5], contact lenses[6], drug delivery[7-9], coatings[10], and biomaterials.[2,11] A major requirement in the design of functional materials is controlled synthesis for tailoring of polymer properties, including topology, molecular weight

distribution, and end groups. HEA and HEMA are not polymerizable through group transfer or anionic polymerization techniques due to the presence of the labile proton. Advancements in controlled radical polymerization techniques have enabled the incorporation of HEA and HEMA into well-defined copolymers.

The advent of controlled radical polymerization has led to the synthesis of a myriad of copolymer structures and architectures with monomer families that were previously unaccessible. Techniques including reversible addition-fragmentation chain transfer (RAFT)[12,13], atom transfer radical polymerization (ATRP)[14,15], and nitroxide mediated polymerization (NMP)[16,17] are compatible with a variety of functional monomers and solvent conditions, including water. These polymerization techniques lead to well defined polymer architectures with control of molecular weights and distributions, end groups, and topologies. Matyjaszewski and coworkers have previously reported the synthesis of HEA and HEMA copolymers using ATRP with good control of molecular weight and molar mass distribution, as well as the formation of diblock copolymers with other (meth)acrylate monomers.[18,19] Bian and Cunningham[20] first utilized NMP in the homopolymerization of HEA in bulk, achieving high molecular weights with molecular weight distributions <1.3 and linear conversion with time up to 60% monomer conversion. Homopolymerizations were also successfully performed in water and *N,N*-dimethylformamide (DMF) with similar control, and block copolymers were formed with addition to poly(n-butyl acrylate) macroinitiators. This work demonstrated that NMP enabled the controlled polymerization of the functional monomer HEA, making this method applicable for the formation of amphiphilic and functional copolymers.

Lizotte and Long[21] previously reported an acceleration effect of hydroxyl-containing additives and monomers on the kinetics of NMP using in situ FTIR spectroscopy. They concluded that the incorporation of hydroxyl functionality during polymerization shifted the equilibrium toward active radical intermediates through hydrogen bonding stabilization of the nitroxide mediator, leading to increased monomer additions per activation cycle. This acceleration of the polymerization rate potentially leads to increased termination reactions and a decrease in polymerization control. Limited solubility of HEA in non-aqueous solvents also presents a potential challenge in the synthesis of HEA-containing copolymers using NMP. Protection of the hydroxyl with a trimethylsilyl group alters HEA solubility, making the monomer more compatible with other organic-soluble acrylate monomers. This method was previously used in ATRP and enabled the synthesis of poly(HEMA) under the same conditions used for methyl methacrylate polymerizations.[18] In this work, we report the synthesis of random and block copolymers of n-butyl acrylate (nBA) and HEA using nitroxide mediated polymerization. The resulting functional block and random copolymers may serve as precursors in the design of new functional polymers. Monitoring polymerization with in situ FTIR spectroscopy will also be discussed.

4.3 Experimental

4.3.1 Materials

n-Butyl acrylate (nBA), 2-hydroxyethyl acrylate (HEA), styrene, trimethylsilyl chloride, and triethylamine were purchased from Sigma-Aldrich. Dichloromethane and ethyl acetate were purchased from Fisher Scientific and used as received. DEPN was prepared according to previous literature methods.[22] nBA and styrene were passed through neutral alumina columns to

remove inhibitors and then distilled under reduced pressure from CaH_2. Triethylamine was distilled from CaH_2. *N,N*-dimethylformamide (DMF) was transferred under N_2 from an Innovative Technology, Inc. PureSolv-MD3 solvent purification system.

4.3.2 Instrumentation

^1H NMR spectra of the polymers were obtained on a Varian Unity 400 MHz spectrometer in $CDCl_3$. Size exclusion chromatography (SEC) was used to determine molecular weights at 40 °C in THF at 1 mL min^{-1} on a Waters SEC equipped with three Polymer Laboratories PLGel 5μm Mixed-C columns and an autosampler. Detectors included a Waters 2414 Refractive index (RI) detector and a Wyatt Technologies miniDAWN multiangle laser light scattering (MALLS) detector. Absolute molecular weights were determined using the MALLS detector and dn/dc values determined on-line.

Insitu FTIR was performed with a Mettler Toledo ReactIR 4000 ATR apparatus equipped with a light conduit and a stainless steel insertion probe with a DiComp (diamond composite) probe tip. IR spectra were collected every minute with 256 scans per spectrum. Reaction analysis was performed with ReactIR 3.1 software from Mettler Toledo.

4.3.3 Purification of HEA

HEA monomer was purified according to a modified literature procedure.[19] HEA (30 mL, 30.33 g) was dissolved in water (90 mL). Hydroquinone (0.32 g) was added to prevent thermal polymerization during purification. The aqueous solution was extracted with hexanes 10 times to remove diacrylate impurities. The aqueous solution was then salted with sodium chloride (30

g NaCl, 250 g/L). The monomer was separated from the aqueous layer with ether extractions (4 times) for the removal of acrylic acid. Hydroquinone was again added to the ether layer (0.7 wt %) to prevent thermal polymerization. $CaSO_4$ was added to remove residual water prior to removal of ethyl ether in vacuo. Purified HEA was stored under nitrogen in the freezer, and distilled under reduced pressure prior to use.

4.3.4 Synthesis of silyl-protected HEA (HEA-TMS)

The procedure for hydroxyl protection with trimethylsilyl chloride was adapted from Qiang et al.[23] HEA (12.5 mL, 0.11 mol, unpurified) and dichloromethane (125 mL) were added to a 250-mL, round-bottomed two-neck flask equipped with a stir bar and addition funnel. Freshly distilled triethylamine (20 mL, 0.14 mol) was added under nitrogen to the purged reaction vessel. The reaction solution was cooled to ~0 °C in an ice bath, and trimethylsilyl chloride (15.3 mL, 0.12 mol) was added dropwise via addition funnel over 30 minutes. Triethylammonium chloride salt precipitated out of solution as the reaction progressed. After 4 h, the reaction mixtures was filtered and rinsed with ethyl acetate. Dichloromethane was removed under reduced pressure, replaced with ~30 mL of ethyl acetate, and the reaction mixture was filtered again to remove residual salt impurities. Ethyl acetate was removed under reduced pressure to yield 18.51 g (90% yield) of HEA-TMS. Monomer was purified through fractional vacuum distillation at 45 °C and 50 mTorr to yield the pure product, a clear liquid.

4.3.5 Synthesis of poly(n-butyl acrylate) (PnBA) with DEPN

A typical polymerization procedure is described. nBA (25 mL, 0.174 mol), AIBN (12 mg, 0.073 mmol), and DEPN (53 mg, 0.180 mmol) were added to a 100-mL, round-bottomed flask

equipped with a magnetic stir bar. The reaction solution was subjected to three freeze pump thaw cycles to remove oxygen impurities prior to polymerization. The flask was placed in an oil bath at 130 °C for 150 min before quenching in an isopropyl alcohol/dry ice bath. ^{1}H NMR of the crude reaction revealed a monomer conversion of 30%. The reaction solution was diluted with 50 mL tetrahydrofuran (THF) and precipitated in 1 L of 10:1 methanol:water solution. The isolated polymer was dried at reduced pressure at 40 °C for 18 h to yield pure polymer. Copolymers incorporating HEA and in situ FTIR reactions were polymerized in a similar fashion with the addition of 10 mol % HEA or HEA-TMS monomers.

4.3.6 Synthesis of poly((*n*BA-*co*-HEA-TMS)-*b*-styrene)

Poly(nBA-*co*-HEA-TMS) macroinitiator was prepared through the bulk copolymerization of nBA and HEA-TMS (10 mol % in feed) at 130 °C with 2.5 xs DEPN as described above. The macroinitiator was precipitated in methanol:water and dried under reduced pressure for purification prior to block addition. Poly(nBA-*co*-HEA-TMS) macroinitiator (2 g, $2.334 * 10^{-5}$ mol chain end) and DEPN (1.1 mg, $3.74 * 10^{-6}$ mol) and styrene (10 mL, 0.087 mol) were added to a 100-mL, round-bottomed flask equipped with a magnetic stir bar. The reaction solution was subjected to three freeze pump thaw cycles to remove oxygen impurities prior to polymerization. The flask was placed in an oil bath at 125 °C for 70 min before quenching in an isopropyl alcohol/dry ice bath. ^{1}H NMR of the crude reaction revealed a styrene monomer conversion of 12%. The product was precipitated in methanol and dried at 40 °C under reduced pressure to yield pure polymer product.

4.3.7 Synthesis of poly(nBA-*b*-HEA-TMS)

PnBA macroinitiator (M_n 39,000 g/mol) was synthesized according to the method reported in 4.3.5. DEPN-functional PnBA (1 g, 2.56 * 10^{-5} mol chain ends), DEPN (15.3 mg, 5.20 * 10^{-5} mol), HEA-TMS (2.0 g, 0.011 mol), and DMF (10 g, 30 wt %) were added to a 100-mL, round-bottomed flask equipped with a magnetic stir bar. The reaction solution was stirred until PnBA fully dissolved in DMF, and was subjected to three freeze pump thaw cycles to remove oxygen impurities prior to polymerization. The flask was placed in an oil bath at 120 °C for 90 min before quenching in an isopropyl alcohol/dry ice bath. The product was precipitated in 5:1 methanol:water and dried at 40 °C under reduced pressure to yield 0.626 g.

4.4 Results and Discussion

4.4.1 Homopolymerization of n-butyl acrylate

The introduction of acyclic α-hydrido nitroxides, such as DEPN, has enabled the controlled polymerization of a diverse range of acrylates, including polar and functional monomers. Previous studies have shown that NMP of acrylates in the presence of DEPN require an excess of nitroxide mediator in order to achieve linear molecular weight versus conversion plots, and to maintain narrow polydispersities at high conversions. A fast coupling reaction between free nitroxide and free radicals in solution are required to maintain polymerization control and avoid radical-radical coupling.

n-Butyl acrylate (nBA) was polymerized in the bulk in the presence of 2.5 molar excess of DEPN (Scheme 4.1). DEPN-mediated polymerizations require temperatures above 115-120 °C for the thermally initiated homolytic cleavage of the alkoxyamine bond. Good

polymerization control with reproducible kinetics and targeted molecular weights were achieved at 130 °C, so this temperature was used for all bulk polymerizations in this work. Aliquots were removed from the reaction flask via syringe at systematic intervals throughout the polymerization, and monomer conversion was determined with ^{1}H NMR analysis of the crude reaction solution. Crude samples were also used directly for SEC analysis, which is a nice advantage of performing polymerizations in the bulk.

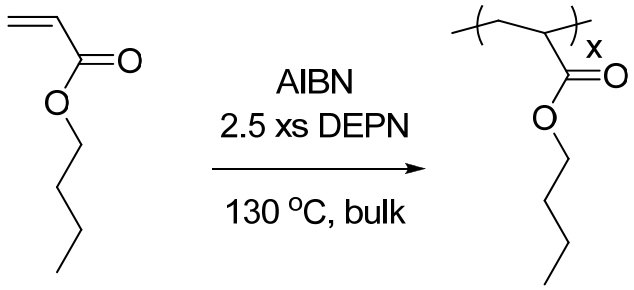

Scheme 4.1 Bulk polymerization of n-butyl acrylate with excess DEPN

The molecular weight and molecular weight distribution as a function of conversion are plotted in Figure 4.1 for the homopolymerization of nBA. The molecular weight increased with conversion in a linear fashion up to 75% monomer conversion, and molecular weight distributions remained <1.1. The synthetic conditions adopted for nBA led to high molecular weight polymer with good molecular weight control, and it is reasonable to apply the same conditions for the copolymerization of nBA with functional monomer, HEA.

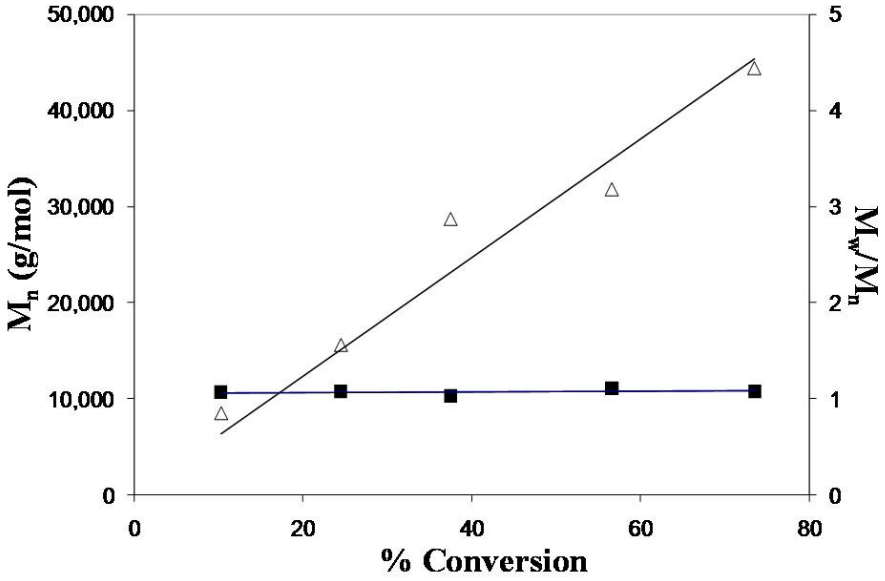

Figure 4.1 Molecular weight vs conversion for n-butyl acrylate, 130 °C in bulk, 2.5 excess DEPN:AIBN. Δ M_n ■ M_w/M_n

4.4.2 Copolymerization of nBA with HEA and HEA-TMS

Copolymerization of nBA with the functional acrylate, HEA, was explored for the synthesis of functional, low T_g polymers. A major issue in the use of HEA in controlled radical polymerization is the presence of impurities including diacrylate and acrylic acid in the unpurified monomer. Extractions to remove impurities are very tedious, and distillation is difficult because HEA is a viscous liquid with a very high boiling point due to hydrogen bonding of the hydroxyls. Attempts to distill HEA often led to thermal polymerization with very low yields of monomer. For this work, the purification procedure reported by Matyjaszewski et al.[19] was adapted with the addition of ample hydroquinone to avoid premature polymerization. Alternatively, protection of the hydroxyl was explored as a method to simplify the purification and alter the chemical properties of HEA for more facile synthetic conditions. Protection with

trimethylsilyl chloride through a one-step reaction afforded high yields and easy purification through vacuum distillation at ~40 °C.

Copolymerizations of nBA with both HEA and protected HEA (HEA-TMS) were performed using the same conditions as previously reported for homopolymerization of PnBA (Scheme 4.2). Both HEA and HEA-TMS were soluble in nBA, allowing for bulk polymerization with 10 mol % of the HEA comonomer in the feed. Other monomer feeds were not tested in this work, as the goal was to incorporate a relatively low concentration of functional groups along the polymer chain with sufficient space between reaction sites for potential introduction of new functionalities through chemical modification.

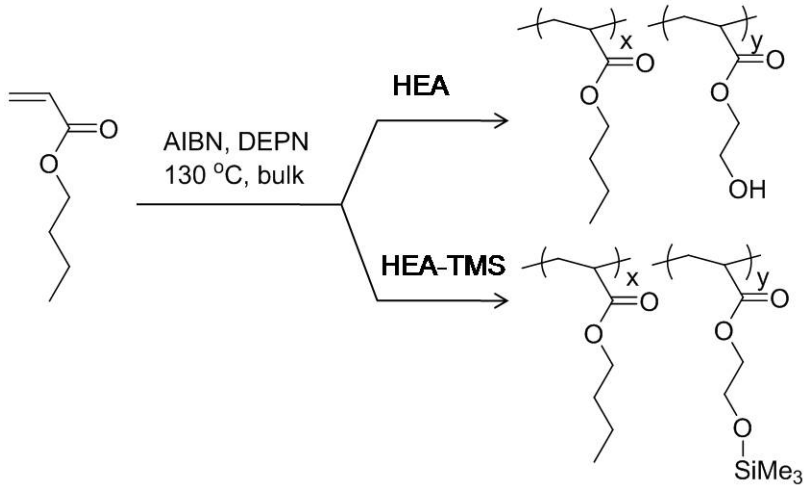

Scheme 4.2 Nitroxide mediated polymerization of copolymers containing 10 mol % HEA or HEA-TMS

Aliquots were removed from the reaction flask at systematic time intervals, and were analyzed with ^{1}H NMR and SEC to determine monomer conversion and molecular weight.

Figure 4.2 shows SEC traces for aliquots at various monomer conversions from the copolymerization of nBA and HEA-TMS. All traces were monomodal, and molecular weight increased systematically with reaction progress. A plot of molecular weight and molecular weight distribution as a function of monomer conversion for the copolymerization of nBA and HEA-TMS is shown in Figure 4.3. Similar to the homopolymerization of nBA, the change in molecular weight with conversion followed a linear trend, with some deviation from predicted behavior between 15 and 30 wt % conversion. Molecular weight distributions remained <1.2 up to 40% conversion of monomer to polymer. Monomer conversion was intentionally kept below 50% to maintain chain end integrity for subsequent block polymerization with these copolymers.

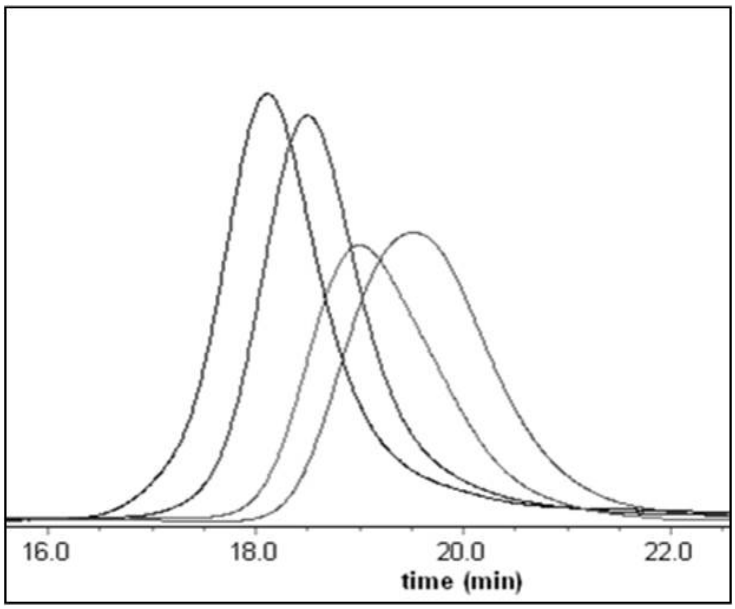

Figure 4.2 SEC chromatograms of poly(nBA-*co*-HEA-TMS). Monomer conversion increases from right to left as molecular weight increases.

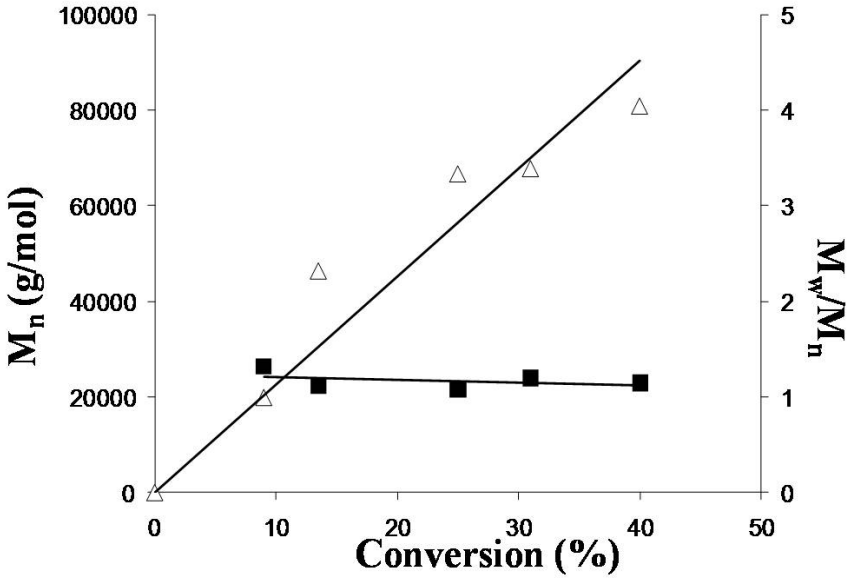

Figure 4.3 Molecular weight vs conversion for copolymerization of nBA and HEA-TMS, 130 °C in bulk, 2.5 excess DEPN:AIBN. Δ M_n ■ M_w/M_n

Copolymerizations with HEA also proceeded in a similar fashion to those with the protected monomer, affording high molecular weight polymer with narrow molecular weight distributions <1.32. A summary of copolymerization results is shown in Table 4.1. In all cases, the molar content of HEA in the polymer was higher than the feed. As noted previously, polymerizations were terminated prior to quantitative conversion, so the HEA enrichment is likely due to differences in reactivity ratios. The same HEA enrichment was observed in earlier studies, with more than 50% higher HEA incorporation than what was charged to the polymerization.[21]

Table 4.1 Molecular weight and composition of HEA/nBA copolymers

Monomer composition	Comonomer in feed (mol %)	Comonomer in polymer (mol %)	Mn (g/mol)	Mw/Mn
nBA	0	0	55,100	1.10
nBA	0	0	35,000	1.14
nBA/HEA	10	13	99,500	1.32
nBA/HEA	10	13	112,000	1.13
nBA/HEA-TMS	10	12	85,700	1.18
nBA/HEA-TMS	10	12	80,900	1.15

Homopolymerizations of nBA and copolymerizations with HEA monomers were monitored with in situ FTIR spectroscopy. This analytical technique is useful for the real-time monitoring of reactions to determine reaction kinetics and reaction endpoints, and look for production of side products. In this work, copolymerizations were monitored in order to measure polymerization kinetics and determine if the hydroxyl functionality influenced the DEPN equilibrium as previously reported by Lizotte and Long.[21] Reaction conditions were held constant for all polymerizations, and were the same as previous polymerizations (130 °C, 2.5 xs DEPN). A waterfall plot of the IR absorbance in the vinyl region for acrylates is shown in Figure 4.4 for copolymerization of nBA with 10 mol% HEA-TMS in the feed. Absorbances for the vinyl CH_2 of nBA, HEA, and HEA-TMS were not resolved, so the normalized overall conversion of monomer (A/A_o) was monitored using the C-H vinyl stretch at 988 cm^{-1} for kinetic analysis.

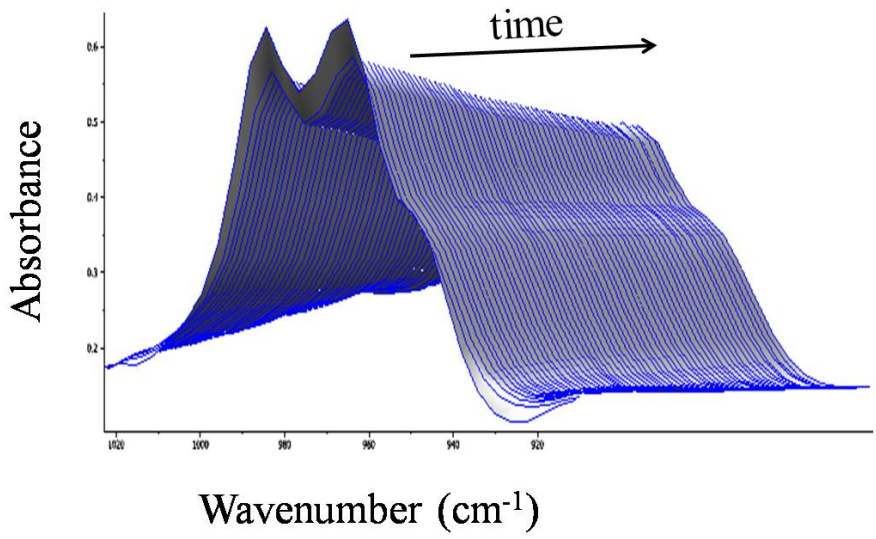

Figure 4.4 In situ FTIR waterfall plot of monomer conversion (vinyl region 920-1020 cm^{-1}).

Pseudo first order rate kinetic analysis of the monomer conversion profile resulted in a linear fit for the $-\ln(A/A_0)$ vs time (s) (Figure 4.5). Only monomer conversions up to 10% were included in the analysis, in order to eliminate viscosity effects of polymerization and drastic changes in monomer concentration. Similar analyses were also performed for the homopolymerization of nBA and copolymerization with HEA. The observed rate constants (k_{obs}) are shown in Table 4.2. The polymerization rate for homopolymerization of nBA was the highest value observed, 2.83 $*10^{-5}$ s^{-1}. This result was unexpected and is likely a result of slight variations in experimental conditions. Rates of polymerization were within error for the copolymerizations with HEA and HEA-TMS, showing no discernable effect of the hydroxyl on polymerization kinetics. Lizotte and Long reported k_{obs} of 2.50 $*10^{-5}$ s^{-1} for the homopolymerization of nBA in the bulk with DEPN, which is comparable to the current study (2.83 $*10^{-5}$ s^{-1}).[21] The effect of the hydroxyl on polymerization kinetics is also consistent with their report, where significant rate enhancements were not observed until 20 mol % of HEA or greater.

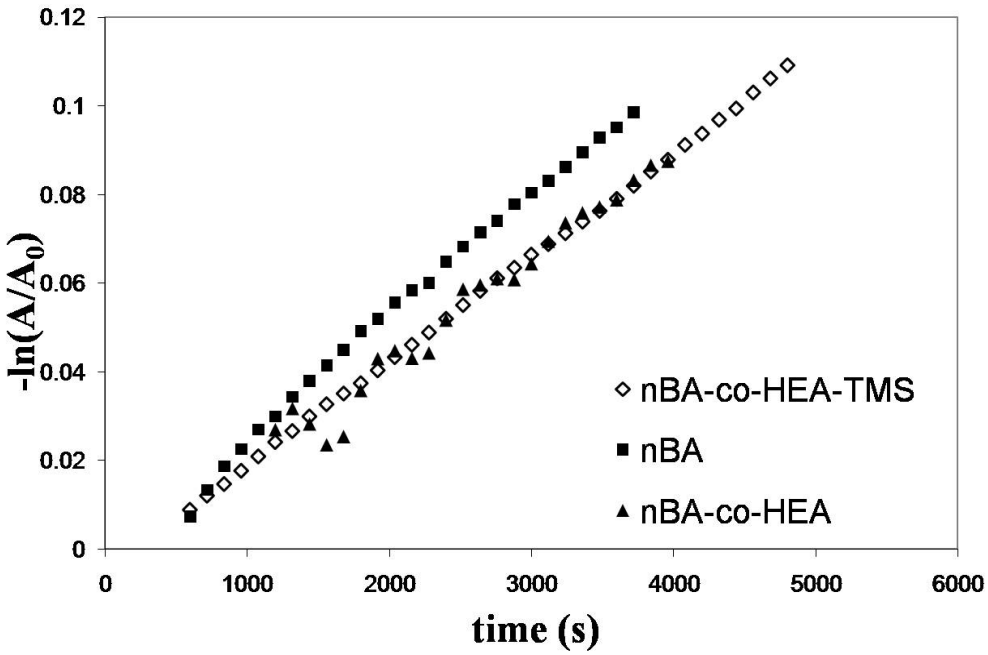

Figure 4.5 Pseudo first order kinetic analysis for DEPN mediated copolymerizations at 988 cm^{-1}. ◊ Copolymerization of nBA and HEA-TMS ■ Hompolymerization of nBA ▲ Copolymerization of nBA and HEA.

Table 4.2 Pseudo first order rate constants for the DEPN-mediated polymerization of nBA, nBA/HEA, and nBA/HEA-TMS.

Monomer Composition	k_{obs} 10^{-5} s^{-1}
nBA	2.82
nBA/HEA	2.41
nBA/HEA-TMS	2.35

4.4.3 Synthesis and Characterization of Block Copolymers

One advantage of NMP is the facile synthesis of block copolymers in two steps. Block copolymerization is a true test of the control afforded in the copolymerizations of nBA and HEA

already discussed. Addition of styrene to poly(nBA-*co*-HEA-TMS) was attempted to prove chain end integrity with a well-known system that is often controlled using DEPN. Poly(nBA) is soluble in styrene, and consequently the copolymer with 13 mol % HEA-TMS was also soluble in styrene. The poly(nBA-*co*-HEA-TMS) macroinitiator (M_n 85,700 g/mol) was dissolved in an excess of styrene monomer with excess DEPN and heated to 125 °C for 70 minutes. SEC of the macroinitiator and the product revealed a significant increase in molecular weight after styrene addition while maintaining a relatively low molecular weight distribution (Figure 4.6). A slight broadening in the chromatogram for the block copolymer (b) is evident in the low molecular weight tail that likely correlates to a small concentration of terminated chains of poly(nBA-*co*-HEA-TMS). Molecular weight characterization of the block copolymers are summarized in Table 4.3. The successful addition of styrene to the poly(nBA-*co*-HEA-TMS) macroinitiator demonstrated the concept of living polymerization and block addition for HEA-containing polymers.

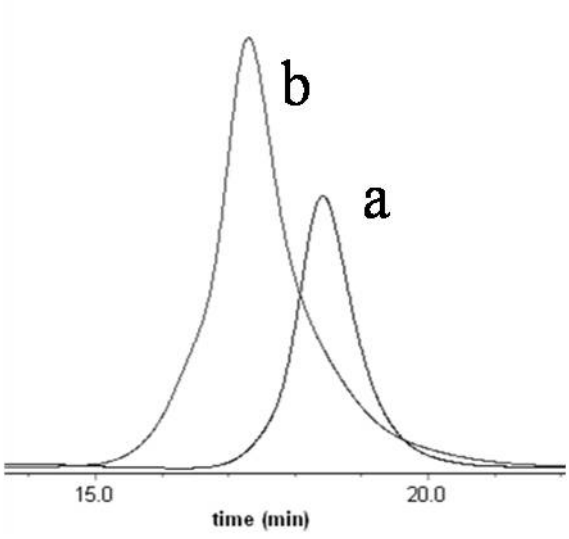

Figure 4.6 SEC chromatograms showing the block addition of styrene to poly(nBA-*co*-HEA-TMS) (a), where (b) is the block copolymer product

The desired block copolymer structures for this study are amphiphilic with HEA functionality concentrated in one block, rather than dispersed throughout the chain. This type of architecture may lead to the synthesis of new families of polymers following chemical modification of the HEA block. Cunningham and Bian previously reported the synthesis of poly(nBA-*b*-HEA) copolymers using DEPN mediated polymerization.[20] Synthesis of the nBA block was performed first because poly(HEA) was not soluble in nBA. Therefore, poly(nBA) macroinitiator was prepared according to the previously used method, and conversion was kept below 50% to avoid loss of chain end DEPN for subsequent block addition. The macroinitiator was isolated through precipitation and dried prior to block addition.

The poly(nBA) macroinitiators prepared in this work were not soluble in HEA, likely due to significantly higher molecular weights than reported in the previous study (M_n ~5300-23000 g/mol).[20] DMF was identified as a suitable solvent for both poly(nBA) and poly(HEA) and was applied as the polymerization solvent for block addition. Poly(nBA) macroinitiator and HEA were dissolved in DMF at 30 wt % solids, and excess DEPN was added to the solution because it was removed during precipitation in the isolation of the macroinitiator. Block addition was carried out at 120 °C for both HEA and HEA-TMS block addition. The polymerization scheme for the addition of HEA-TMS is shown in Scheme 4.3.

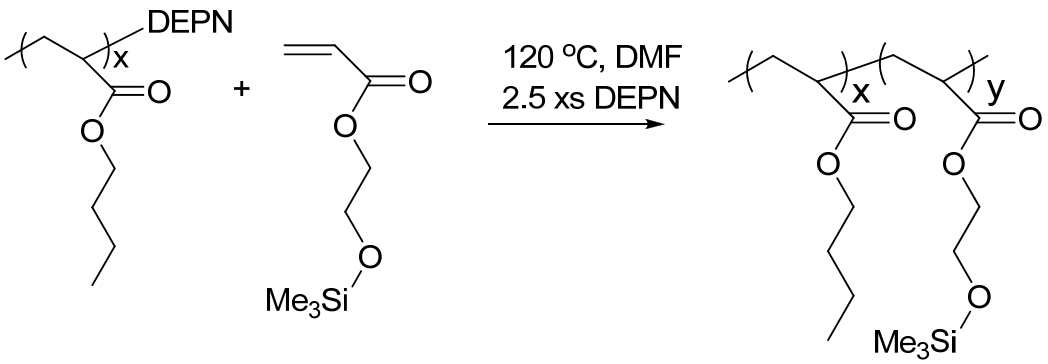

Scheme 4.3 Synthesis of diblock copolymer, poly(nBA-*b*-HEA-TMS)

In the case of HEA block addition, the reaction proceeded for 2 hours prior to termination. Precipitation was attempted in various methanol:water mixtures, which were successful for the precipitation of random copolymerizations. However, only a few milligrams of product were recovered. Precipitation trials in many other polar organic solvents were also unsuccessful. Centrifugation, according to the methods of Bian and Cunningham,[20] also yielded no isolatable polymer. These issues with isolation of the amphiphilic poly(nBA-*b*-HEA) diblock reaffirmed the need for the silyl-protected monomer for synthetic ease.

The block addition of HEA-TMS to PnBA macroinitiator (M_n 39,000 g/mol) was performed under the same conditions as HEA addition. Polymerization proceeded for 90 minutes prior to termination. Unlike the product containing HEA, poly(nBA-*b*-HEA-TMS) diblock copolymer readily precipitated in 5:1 methanol:water and was isolated for characterization. SEC traces of the PnBA macroinitiator (a) and poly(nBA-*b*-HEA-TMS) diblock are shown in Figure 4.7. A shift to higher molecular weight was observed without the clear presence of a low molecular weight tail corresponding to uninitiated PnBA chains. A narrower molecular weight distribution (1.10) was measured after block addition. This effect is likely due to fractionation during the precipitation and isolation of the amphiphilic copolymer.

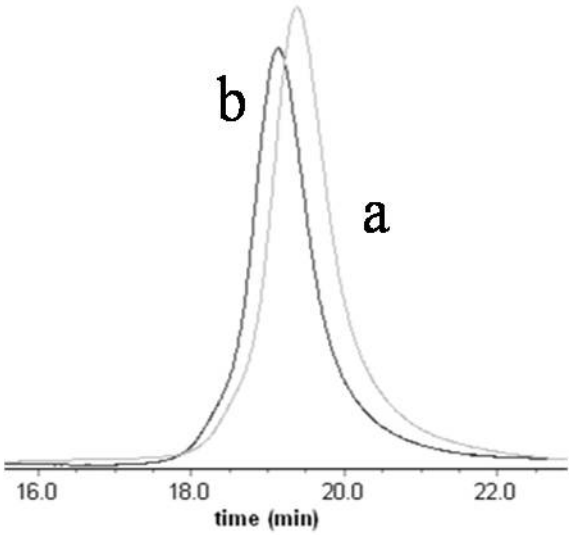

Figure 4.7 SEC chromatograms showing successful block addition to poly(nBA) (a), to form poly(nBA-*b*-HEA-TMS) (b)

Table 4.3 Molecular weight characterization of block copolymers.

Target Polymer	**Macroinitiator**		**Diblock Copolymer**	
	M_n (g/mol)	**M_w/M_n**	**M_n (g/mol)**	**M_w/M_n**
Poly((nBA-*co*-HEA-TMS)-*b*-St)	85,700	1.18	151,000	1.26
Poly(nBA-*b*-HEA)	55,100	1.10	--	--
Poly(nBA-*b*-HEA-TMS)	39,100	1.19	51,800	1.10

^{1}H NMR analysis of the purified block copolymer product is shown in Figure 4.8. Integrations were normalized to the terminal –CH3 of nBA units at 0.93 ppm. The incorporation of HEA-TMS is evident based on the appearance of a –TMS peak at 0.12 ppm and two shoulder peaks at 4.20 and 3.79 ppm. Unfortunately, these peaks were not well resolved from the peak at 4.03 corresponding to the methylene next to the ester in nBA. Calculations revealed the block addition corresponded to ~5 mol % of HEA-TMS incorporated on the chain ends. Detection of

this low molecular weight block addition was difficult to detect with 1H NMR, and larger block lengths are needed for more definitive characterization of the block copolymers. This synthetic strategy opens the door for new classes of functional polymers synthesized through chemical modification of poly(nBA-*b*-HEA) precursors.

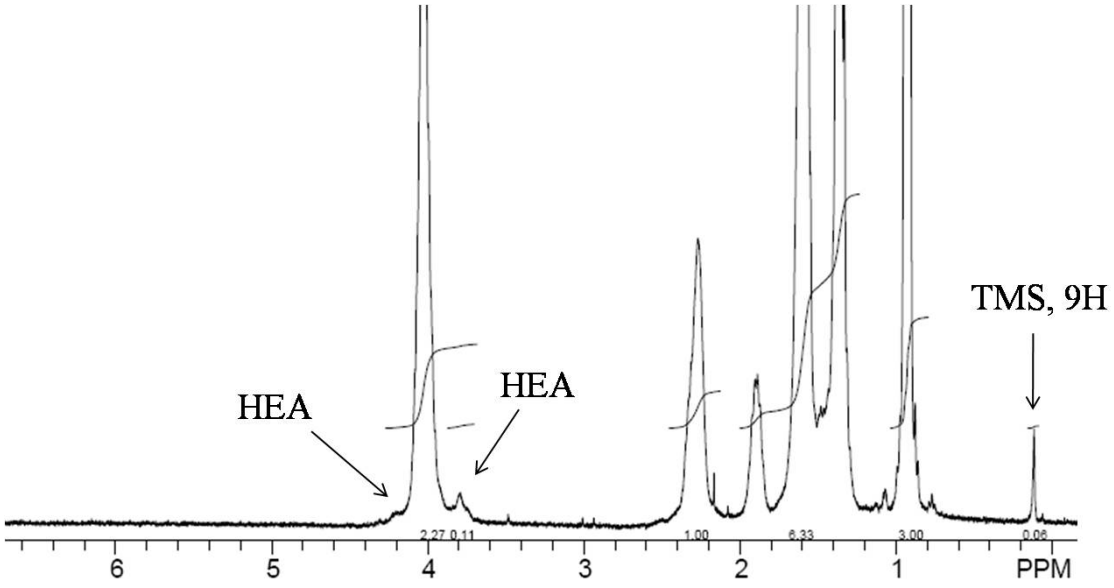

Figure 4.8 ^{1}H NMR of poly(nBA-*b*-HEA-TMS) in $CDCl_3$.

4.5 Conclusions

Controlled polymerization of nBA was demonstrated using DEPN mediated NMP. The copolymerization of nBA with HEA and silyl-protected HEA (HEA-TMS) resulted in linear molecular weight vs. conversion plots and narrow molecular weight distributions, indicating that polymerization control was maintained in the presence of the hydroxyl functionality. Kinetic analysis using in situ FTIR revealed little effect of the hydroxyl on polymerization kinetics at 10 mol % charge, in accordance with previously published results.[21] Living polymerization was further affirmed with the successful block addition of styrene to poly(nBA-*co*-HEA-TMS)

macroinitiator. A shift in the SEC chromatogram toward higher molecular weight confirmed polystyrene growth. Amphiphilic diblock copolymer, poly(nBA-*b*-HEA-TMS) was synthesized from a PnBA macroinitiator in DMF solution. Protection of the monomer hydroxyl alleviated many issues with polymer isolation experienced in the block formation of HEA. SEC revealed growth in molecular weight and a narrow molecular weight distribution, with incorporation of a 5 mol % HEA-TMS block at the end of PnBA. Potential application of these functional diblock copolymers as templates for chemical modification will enable the synthesis of new families of block copolymers.

4.6 Acknowledgements

This material is based upon work supported in part by the Macromolecular Interfaces with Life Sciences (MILES) Integrative Graduate Education and Research Traineeship (IGERT) of the National Science Foundation under Agreement No. DGE-0333378.

4.7 References

(1) La Gatta, A.; Schiraldi, C.; Esposito, A.; D'Agostino, A.; De Rosa, A. *Journal of Biomedical Materials Research Part A* **2009**, *90A*, 292-302.
(2) Chirila, T. V.; Constable, I. J.; Crawford, G. J.; Vijayasekaran, S.; Thompson, D. E.; Chen, Y. C.; Fletcher, W. A.; Griffin, B. J. *Biomaterials* **1993**, *14*, 26-38.
(3) Pourjavadi, A.; Sarnadi, M.; Ghasernzadeh, H. *Starch-Starke* **2008**, *60*, 79-86.
(4) Sagle, A. C.; Ju, H.; Freeman, B. D.; Sharma, M. M. *Polymer* **2009**, *50*, 756-766.
(5) Khutoryanskaya, O. V.; Mayeva, Z. A.; Mun, G. A.; Khutoryanskiy, V. V. *Biomacromolecules* **2008**, *9*, 3353-3361.
(6) Goda, T.; Ishihara, K. *Expert Review of Medical Devices* **2006**, *3*, 167-174.
(7) Mahkam, M. *Designed Monomers and Polymers* **2009**, *12*, 247-255.
(8) Jin, Y.; Yamanaka, J.; Sato, S.; Miyata, I.; Yomota, C.; Yonese, M. *Journal of Controlled Release* **2001**, *73*, 173-181.
(9) Liu, Y. Y.; Lu, J.; Shao, Y. H. *Macromolecular Bioscience* **2006**, *6*, 452-458.
(10) Srivastava, S. *Designed Monomers and Polymers* **2009**, *12*, 1-18.
(11) Montheard, J. P.; Chatzopoulos, M.; Chappard, D. *Journal of Macromolecular Science-Reviews in Macromolecular Chemistry and Physics* **1992**, *C32*, 1-34.

(12) Lowe, A. B.; McCormick, C. L. *Prog. Polym. Sci.* **2007**, *32*, 283-351.
(13) Moad, G.; Rizzardo, E.; Thang, S. H. *Aust. J. Chem.* **2005**, *58*, 379-410.
(14) Matyjaszewski, K.; Spanswick, J.; Sumerlin, B. S. *Living and Controlled Polymerization: Synthesis, Characterization and Properties of the Respective Polymers and Copolymers* **2006**, 1-37.
(15) Tsarevsky, N. V.; Matyjaszewski, K. *Chem. Rev.* **2007**, *107*, 2270-2299.
(16) Chevalier, C.; Guerret, O.; Gnanou, Y. *Living and Controlled Polymerization: Synthesis, Characterization and Properties of the Respective Polymers and Copolymers* **2006**, 51-63.
(17) Hawker, C. J.; Bosman, A. W.; Harth, E. *Chem. Rev.* **2001**, *101*, 3661-3688.
(18) Beers, K. L.; Boo, S.; Gaynor, S. G.; Matyjaszewski, K. *Macromolecules* **1999**, *32*, 5772-5776.
(19) Coca, S.; Jasieczek, C. B.; Beers, K. L.; Matyjaszewski, K. *J. Polym. Sci., Part A: Polym Chem* **1998**, *36*, 1417-1424.
(20) Bian, K.; Cunningham, M. F. *Macromolecules* **2005**, *38*, 695-701.
(21) Lizotte, J. R.; Long, T. E. *Macromol. Chem. Phys.* **2004**, *205*, 692-698.
(22) Grimaldi, S.; Finet, J. P.; Le Moigne, F.; Zeghdaoui, A.; Tordo, P.; Benoit, D.; Fontanille, M.; Gnanou, Y. *Macromolecules* **2000**, *33*, 1141-1147.
(23) Qiang, L. L.; Ma, Z.; Zheng, Z.; Yin, R.; Huang, W. *Macromol. Rapid Commun.* **2006**, *27*, 1779-1786.

Chapter 5: Electrospinning Zwitterion-containing Nanoscale Acrylic Fibers

Brown, R. H.; Hunley, M. T.; Allen, M. H.; Long, T. E. *Polymer* (2009) 50, 4781-4787.

5.1 Abstract

Free radical copolymerization of n-butyl acrylate and a sulfobetaine methacrylamide derivative provided high molecular weight zwitterionic copolymers containing 6-13 mol % betaine functionality, and the electrospinning of low T_g zwitterionomers was explored for the first time. Copolymerizations were performed in dimethylsulfoxide (DMSO) rather than fluorinated solvents previously reported in the literature. Dynamic mechanical analysis of zwitterionomer films revealed biphasic morphology and featured a rubbery plateau and two distinct thermal transitions. Electrospinning from chloroform/ethanol (80/20 v/v) solutions at low concentrations between 2 and 7 wt % afforded nanoscale polymeric fibers with diameters near 100 nm. The presence of only 6 mol % zwitterion allowed the formation of low T_g, free-standing, non-woven mats, and we hypothesize that zwitterionic aggregation rather than chain entanglements facilitated electrospinning at these relatively low solution concentrations. To our knowledge, this is the first report of electrospun zwitterionic polymers and these non-woven membranes are expected to lead to new applications for sulfobetaine copolymers.

5.2 Introduction

The electrospinning process employs an electrostatic potential to form micro- and nanoscale fibers, resulting in thin fibrous mats with high surface area and submicron pores.[1-4] Electrospinning occurs when a charged polymer solution or melt emits a jet in the presence of an electric field.[5] The jet travels rapidly in a chaotic, whip-like motion to a grounded target where solid fibers collect in the form of three-dimensional, non-woven mats.[6] Several important factors, including solution conductivity, viscosity, applied voltage, and tip-to-target distance, dictate the size and morphology of collected fibers.[7,8] Solution concentration has the largest effect on fiber diameter, where higher polymer concentrations lead to the formation of thicker fibers. Applications of electrospun fibers include filtration devices, membranes, protective clothing, tissue scaffolds, and nanofiber-based sensors and electrodes.[9-14]

Previous reports demonstrated that successful electrospinning requires the presence of chain entanglements within the polymer solution.[15,16] The electrospinning behavior of neutral polyesters as a function of molecular weight and solution concentration was previously studied in our laboratories.[15] The critical concentration for entanglements (C_e) was the minimum concentration needed for fiber formation, while defect-free fibers required concentrations above $2C_e$. Later, Wnek and coworkers[16] developed a semi-empirical model for predicting the limits of fiber formation for a range of polymers in good solvents without the presence of polymer-polymer interactions. Fiber formation was correctly predicted to occur in the presence of more than 2.5 entanglements per polymer chain, while one entanglement per chain led to beaded morphologies. While sufficient chain entanglements encourage fiber formation, entanglements are not a required condition to form uniform fibers. Rutledge et al.[17] evaluated the role of fluid elasticity, independent of other fluid properties, in electrospinning a series of non-entangled

aqueous solutions of poly(ethylene glycol) containing small amounts of high molecular weight poly(ethylene oxide). Bead-on-string and uniform fibers were collected for the elastic solutions electrospun at low concentrations and low shear viscosities (<0.30 Pa·s), and bead formation did not occur under any condition. The researchers concluded that fluid elasticity sufficiently stabilized the polymer jet on the short time scale of electrospinning, leading to uniform fiber formation in the absence of chain entanglements.

For ion-containing polymers, the presence of intramolecular electrostatic interactions significantly affects the solution conformation, leading to differences in entanglement behavior. Long et al.[3] studied the electrospinning of poly(2-(dimethylamino)ethyl methacrylate hydrochloride) in water/methanol, and found that concentrations of $8C_e$ were required to form defect-free fibers. The charges in the polyelectrolyte side chains created instabilities in the electrospinning jet that required much higher viscosities to suppress. The high electrical conductivity of the polyelectrolyte solutions led to fibers 2-3 orders of magnitude smaller than neutral polymers electrospun from solutions of similar viscosity and concentration. The addition of NaCl to polyelectrolyte solutions resulted in the screening of electrostatic interactions and a decrease in the normalized concentration required for fiber formation. Ionic aggregation also drastically alters solution conformation and polymer chain dynamics. Elabd et al.[18] explored the electrospinning behavior of Nafion® under various conditions, and discovered that pure Nafion® solutions were highly aggregated and lacked sufficient entanglements to stabilize the electrospinning jet. Blending Nafion® with poly(acrylic acid) suppressed ionic aggregation, and nanoscale Nafion® fibers were collected. Understanding the interplay of viscosity, concentration, and aggregation in electrospun charged polymers remains a fundamental interest.

Polybetaines are a class of zwitterionic polymers featuring a covalently bound cation and anion on each repeating unit. Sulfobetaines feature a quaternized ammonium and a sulfonate group tethered through an alkylene spacer. Polybetaines mimic lipid structures found in biological membranes, which has led to numerous biological applications, including anti-biofouling and protein resistant coatings, biomedical devices, and antimicrobial surfaces.[19-21] Incorporation of sulfobetaine monomers into various polymer matrices offers many potential advantages, including water dispersibility or solubility and mechanical toughness resulting from ionic aggregation.

Galin and coworkers[22] copolymerized sulfobetaine-based monomers with *n*-butyl acrylate (nBA) and 2-ethoxyethyl acrylate (EEA). When placed in a nonpolar matrix with a low T_g, the polar zwitterions aggregated to form strong physical crosslinks similar to classic ionomers. Thermal and mechanical analysis revealed a biphasic morphology consisting of the nonpolar matrix and an ion-rich phase. Later, Gauthier and coworkers also copolymerized a series of different sulfobetaine monomers with nBA and EEA to explore the effects of zwitterionic structure on aggregation behavior.[23] Dynamic mechanical analyses revealed an increased rubbery modulus at higher sulfobetaine concentrations, which was consistent with an increased degree of ionic crosslinking.

To our knowledge, electrospinning of betaine-containing copolymers is unprecedented. In this work, we synthesized a series of *n*-butyl acrylate-based low T_g copolymers containing low concentrations of a zwitterionic monomer (6-13 mol %). We report the effects of zwitterion concentration on the mechanical properties and electrospinning behavior of the copolymers. Incorporation of zwitterionic functionalities offers a method to electrospin nanoscale fibers from

very low solution concentrations. Zwitterion-containing fibers enable potential applications in membrane technologies, antimicrobial surfaces, and protective clothing.

5.3 Experimental

5.3.1. Materials.

N-(3-sulfopropyl)-N-methacryloylamidopropyl-N,N-dimethylammonium betaine (SBMAm) was provided by Raschig GmbH (Germany) and used without purification. Dimethylsulfoxide (DMSO, 99.9+%), azobisisobutyronitrile (AIBN), and *n*-butyl acrylate (nBA) were purchased from Sigma-Aldrich Chemical Co. AIBN was recrystallized from methanol. nBA was passed through a neutral alumina column to remove inhibitors and then distilled under reduced pressure from CaH_2. Chloroform, ethanol, and ethyl acetate were purchased from VWR and used without further purification.

5.3.2. Synthesis of poly(n-butyl acrylate-*co*-sulfobetaine methacrylamide) (PnBA-*co*-PSBMAm).

A typical copolymerization is described. nBA (5.0 g, 0.039 mol) and SBMAm (1.27 g, 0.004 mol) were added to a 100-mL, round-bottomed flask with a magnetic stir bar. The reaction mixture was diluted with DMSO (51 mL, 90 wt %), and AIBN (31.4 mg, 0.50 wt %) was added to the reaction vessel. The reaction mixture was sparged with nitrogen for 15 min and placed in an oil bath at 60 °C for 24 h. The polymer was precipitated into approximately 4 L of water and dried under reduced pressure. Residual DMSO was further removed using either Soxhlet extraction in ethyl acetate or vacuum distillation at 60 °C. The isolated polymer was dried under reduced pressure at 80 °C for 48 h and stored in a desiccator. Isolated yields after precipitation and extraction were typically 75%.

5.3.3. Synthesis of poly(*n*-butyl acrylate) (PnBA).

nBA (25 g, 0.195 mol), AIBN (170 mg, 0.001mol), and ethyl acetate (110 mL, 80 vol %) were added to a 250-mL, round-bottomed flask equipped with a magnetic stir bar. The reaction was sparged with nitrogen for 15 min and placed in an oil bath at 65 °C for 22 h. The reaction solution was diluted with 150 mL ethyl acetate, and added drop wise to 5 L of 9:1 methanol:water solution. The isolated polymer was dried at reduced pressure at 60 °C for 18 h to yield 22.6 g (90 % yield).

5.3.4. Electrospinning.

Zwitterionic copolymers were dissolved in 80/20 v/v chloroform/ethanol at 7 wt %. Subsequent concentrations were achieved through a series of dilutions. PnBA was dissolved in 80/20 v/v chloroform/ethanol at concentrations of 5 and 30 wt %. The polymer compositions and concentration ranges analyzed are summarized in Table 5.1. The solutions were placed in a 20-mL syringe that was mounted in a syringe pump (KD Scientific Inc). The positive lead of a high voltage power supply (Spellman CZE1000R, Spellman High Voltage Electronics Corp.) was connected to an 18-gauge syringe needle using an alligator clip. A grounded metal target (304 stainless steel mesh screen) was placed 20 cm from the needle tip. The syringe pump delivered the polymer solution at a controlled flow of 3 mL/h, and the voltage was maintained at 25 kV. Constant electrospinning conditions were maintained in order to isolate the effect of zwitterion content on the fiber morphology and diameter. Electrospun mats were stored in a desiccator until SEM images were obtained.

Table 5.1 Summary of polymers and concentration ranges for electrospinning study

Polymer Composition	Concentration Range (wt %)
$PnBA_{94}$-*co*-$PSBMAm_6$	2.0 – 6.7
$PnBA_{90}$-*co*-$PSBMAm_{10}$	1.5 – 7
$PnBA_{87}$-*co*-$PSBMAm_{13}$	2.0 – 6.8
PnBA	5, 30

5.3.5. Instrumentation.

^{1}H NMR spectra of the polymers were obtained on a Varian Unity 400 spectrometer in $CDCl_3$ at 399.95 MHz. Molar compositions were determined using resonance integrals at 0.94 ppm for the $–CH_3$ of nBA and the $–CH_3$ groups on the quaternary ammonium of SBMAm at 3.33 ppm, according to previous methods.[23] Size exclusion chromatography (SEC) was used to determine the molecular weights of zwitterionomers at 50 °C in *N*,*N*-dimethyformamide (DMF) with 0.01M lithium bromide (LiBr) at 1 mL min^{-1}. DMF SEC was performed on a Waters SEC equipped with two Waters Styragel HR5E (DMF) columns, a Waters 717plus autosampler, and a Waters 2414 differential refractive index detector. Reported molecular weights are relative to polystyrene standards. SEC of PnBA was performed in tetrahydrofuran at 40 °C and 1 mL min^{-1} on a Waters SEC equipped with three Polymer Laboratories PLGel 5μm Mixed-C columns. THF SEC instrumentation included a Waters 717plus autosampler, Waters 2414 differential refractive index detector, and a Wyatt Technologies miniDAWN multiangle laser light scattering (MALLS) detector. Absolute molecular weight is reported, using a dn/dc of 0.07.

Dynamic mechanical analysis (DMA) was conducted on a TA Instruments Q800 dynamic mechanical analyzer in tension mode at a frequency of 1 Hz and a temperature ramp of 3 °C/min.

All films were solution cast from chloroform on Teflon® molds and dried for 72 h at 70 °C at reduced pressure (0.4 mm Hg) prior to analysis. Steady shear rheological experiments were performed with a TA Instruments AR-G2 rheometer at 25 °C using concentric cylinder geometry. Copolymer solutions in chloroform/ethanol (80/20 v/v) were analyzed using shear rate sweeps from 0.01 to 1000 s^{-1}. The lower torque limit was set at 0.01 μN·m, and the error of the measurement was determined to be ± 2%.

Electrospun fiber diameter and morphology were analyzed using a Leo 1550 field emission scanning electron microscope (FESEM). Fibers for FESEM analysis were collected on a ¼ in. × ¼ in stainless steel mesh, mounted on a SEM disk, and sputter-coated with an 8 nm Pt/Au layer to reduce electron charging effects. Twenty measurements on random fibers for each electrospinning condition were performed using the provided SEM software package to determine average fiber diameters and standard deviations. Error bars shown represent one standard deviation.

5.4 Results and Discussion

5.4.1. Synthesis of Zwitterionic Copolymers.

Copolymers consisting of nBA and SBMAm were synthesized via AIBN-initiated free radical copolymerization (Scheme 5.1). Identification of a suitable solvent to afford homogeneous reactions posed a synthetic challenge due to the drastic polarity differences between the two monomers. Ehrmann and Galin reported using ethanol as the reaction solvent for the copolymerization of SBMAm and nBA; however, reactions became heterogeneous for $f_{SBMAm} < 0.1$.[22] Gauthier and coworkers used 2,2,2-trifluoroethanol for the copolymerization of nBA and a sulfobetaine methacrylate derivative with feed compositions of 1-70 mol %

zwitterion, while maintaining homogeneous solutions only to 30% monomer conversion.[24] Other solvents with their monomer system, including DMSO, tetrahydrofuran, and DMF, resulted in heterogeneous reactions as both zwitterion and total monomer concentrations increased.[24] In this work, polymerizations in DMSO afforded homogeneous reactions to complete conversion with zwitterion monomer feed compositions up to 13 mol % and total monomer concentration maintained at 10 wt %. This strategy offers a viable alternative to more expensive fluorinated solvents commonly used in the literature.

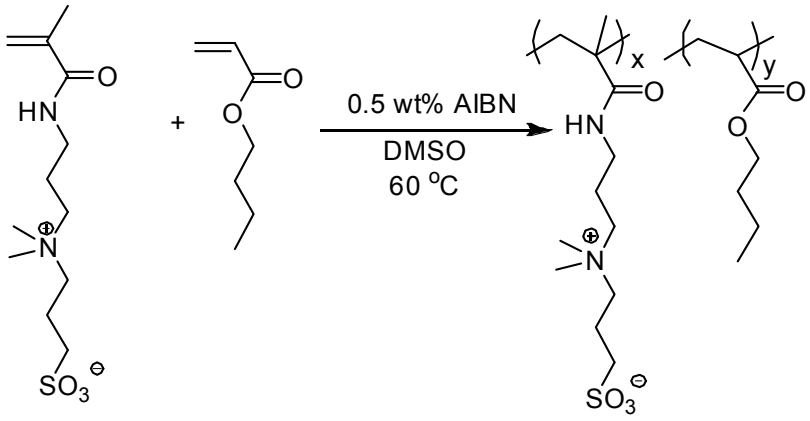

Scheme 5.1 Synthesis of poly(n-butyl acrylate-*co*-sulfobetaine methacrylamide) (PnBA-*co*-PSBMAm)

Isolated zwitterionic copolymers were insoluble in most organic solvents except chloroform, hot DMSO, and DMF. Chloroform was utilized in this study for film casting and electrospinning. Copolymer compositions were determined with ^{1}H NMR spectroscopy in $CDCl_3$, and results agreed well with the monomer feed ratios (±1 mol %). Zwitterion contents of 6, 10, and 13 mol % were achieved. The zwitterionic content was designed to systematically

explore the effects of sulfobetaine on the mechanical properties and electrospinning behavior. In addition, molecular weight characterization was achieved using SEC in DMF with 0.01M LiBr, where the salt content effectively inhibited aggregation and screened polymer-column interactions for reproducible results. Representative chromatograms exhibiting reproducibility of three consecutive injections are shown in Figure 5.1 for $PnBA_{90}$-*co*-$PSBMAm_{10}$. Copolymer molecular weights relative to polystyrene standards are shown in Table 5.2.

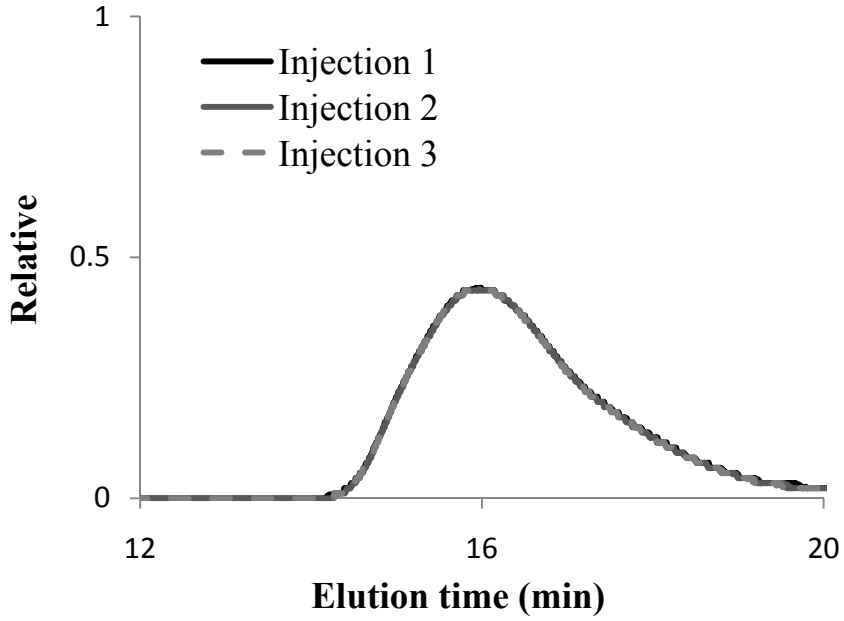

Figure 5.1 Reproducible SEC chromatograms of $PnBA_{90}$-*co*-$PSBMAm_{10}$

Table 5.2 Relative molecular weights of zwitterionic copolymers

Copolymer	M_w (g/mol)	M_w/M_n
$PnBA_{94}$-*co*-$PSBMAm_6$	519,000	2.42
$PnBA_{90}$-*co*-$PSBMAm_{10}$	344,000	2.65
$PnBA_{87}$-*co*-$PSBMAm_{13}$	259,000	2.75

5.4.2. Dynamic Mechanical Analysis of Zwitterionic Copolymers.

Ionomers are known to form biphasic morphologies exhibiting two glass transition temperatures. These distinct thermal transitions represent ion-rich and ion-poor regions formed through the aggregation of ionic groups. DMA measurements of zwitterionic copolymer films were performed in order to monitor the effect of zwitterion concentration on the thermal transitions and mechanical properties. Copolymer films were dried at reduced pressure for 72 h at 70 °C prior to analysis in order to minimize the effects of water absorption.

The storage moduli as a function of temperature for a series of PnBA-*co*-PSBMAm compositions are shown in Figure 5.2. An increase in both the T_g of the ion-poor matrix phase and the breadth of the transition was observed as the SBMAm content increased from 6 to 13 mol %. This trend was also observed in previous studies of SBMAm copolymers with poly(nBA)[25] and poly(EEA)[26], as well as nBA-based copolymers with sulfobetaine methacrylate derivatives.[24] All of the zwitterionomers also exhibited a rubbery plateau region, which was attributed to thermally labile physical crosslinks formed within the ionic aggregates.[24] The modulus of the rubbery plateau region increased with zwitterion content, representing an increased number of crosslink sites. A second thermal transition, attributed to the T_g of the ion-

rich phase, occurred at approximately 80 °C for all three copolymers. DMA of PnBA-*co*-PSBMAm films with only 6 mol % zwitterion content is in sharp contrast to low T_g poly(nBA), which is a viscous liquid at room temperature that does not form films and could not be analyzed using DMA. Previous reports of the thermal properties of PnBA using a dynamic mechanical thermal analyzer showed only one transition at the T_g of PnBA with flow at 0 °C, and no presence of a rubbery plateau region.[25] This major difference in mechanical properties demonstrated the electrostatic interaction between zwitterionic groups, which allowed the formation of free-standing films.

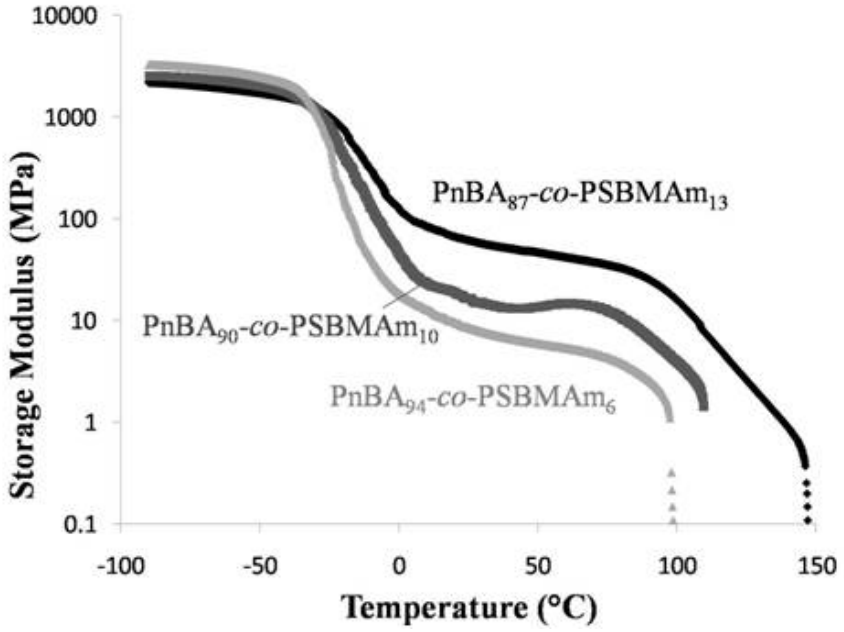

Figure 5.2 Storage modulus at 1 Hz as a function of temperature for PnBA-*co*-PSBMAm containing 6, 10, and 13 mol% SBMAm

5.4.3. Electrospinning Nanoscale Fibers.

Electrospinning studies of PnBA-*co*-PSBMAm at three zwitterion contents were performed at constant conditions (25 kV, 3 mL/h, 20 cm tip-to-target distance) in order to isolate the effects of concentration on fiber formation. To our knowledge, electrospinning of zwitterion-containing copolymers was not reported earlier. The copolymers were electrospun from 80/20 v/v chloroform/ethanol solutions at concentrations below 7 wt %. Ethanol was added as a cosolvent for electrospinning to decrease solvent volatility and prevent clogging of the syringe tip.

5.4.3.1. Effect of Solution Concentration on Fiber Morphology.

Many studies have demonstrated the effect of solution concentration on fiber diameter and morphology during the electrospinning process. Figure 5.3 shows the effect of solution concentration on the fiber morphology of $PnBA_{90}$-*co*-$PSBMAm_{10}$ electrospun fibers. At the lowest concentration of 1.5 wt %, polymer beads or droplets were observed with very few fibers present. Polymer droplets form when insufficient elasticity is present to withstand the Raleigh instabilities and stabilize the charged electrospun jet.[2] The phenomenon of droplet formation is known as electrospraying.

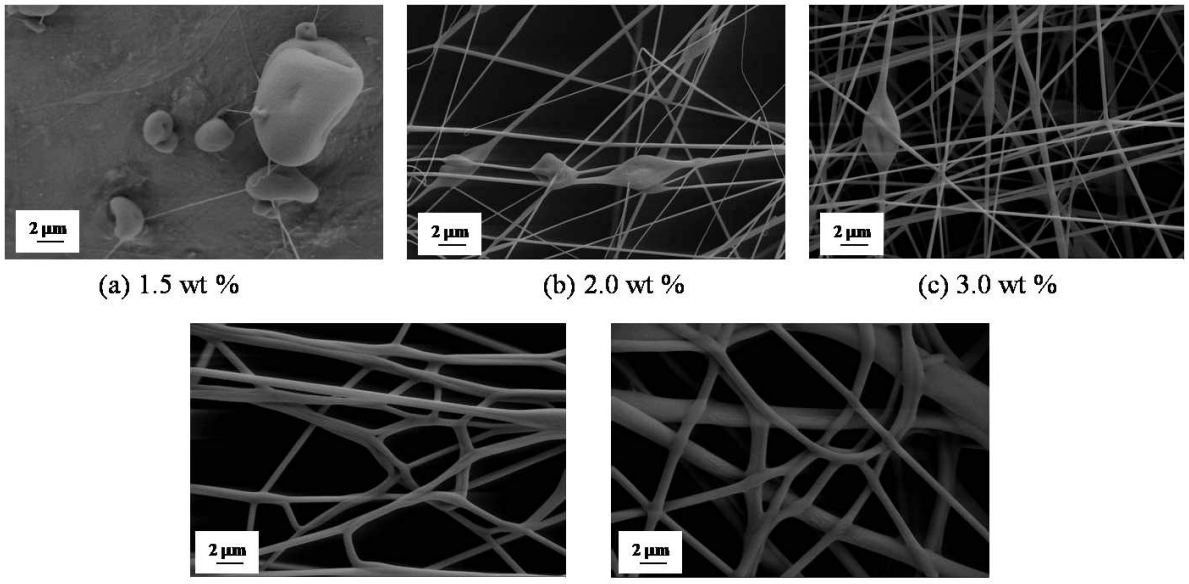

Figure 5.3 FESEM images of $PnBA_{90}$-*co*-$PSBMAm_{10}$ electrospun fibers at various solution concentrations in chloroform/ethanol (80/20 v/v)

Electrospinning of $PnBA_{90}$-*co*-$PSBMAm_{10}$ occurred at solution concentrations greater than 1.5 wt % to form nanometer- to micron-sized fibers. Beaded fiber morphologies formed between 2 and 3 wt %, while uniform bead-free fibers formed above 4 wt %. Similar trends in fiber morphology were observed for $PnBA_{94}$-*co*-$PSBMAm_6$ and $PnBA_{87}$-*co*-$PSBMAm_{13}$, as shown for selected concentrations in Figure 5.4. The minimum concentration required for uniform electrospun fibers was correlated to C_e for linear and branched neutral polyesters in our laboratories,[27] and for poly(vinyl alcohol) by Shivkumar et al.[28] In the case of neutral polymers, uniform fibers were commonly observed at concentrations above $2C_e$. For zwitterionomers, the onset of fiber formation occurred at 2 wt % regardless of zwitterion content, and bead-free fibers were collected at 4 wt % for all compositions.

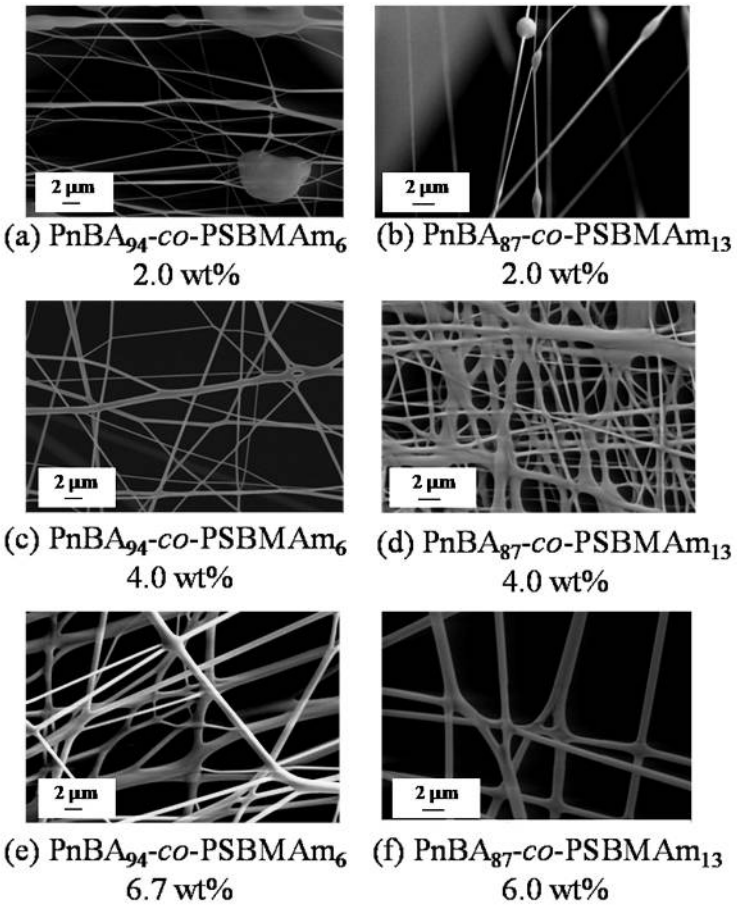

Figure 5.4 FESEM images of electrospun fibers of $PnBA_{94}$-*co*-$PSBMAm_6$ and $PnBA_{87}$-*co*-$PSBMAm_{13}$ at increasing solution concentrations in chloroform/ethanol (80/20 v/v)

The fusion of electrospun thin fibers was observed periodically throughout the study for each of the copolymer compositions. This phenomenon was most prominent in the thicker fibrous mats where fibers were collected on the target for longer times. Fiber fusion likely occurred due to a combination of insufficient solvent evaporation during the jet lifetime and the low T_g matrix of nBA-based copolymers. Areas where distinct fibers fused together after collection are clearly visible in Figure 5.4d.

5.4.3.2. Effect of Solution Concentration on Fiber Diameter.

Continuous fibers approximately 1-2 μm in diameter were collected after electrospinning from 7 wt % solutions. Fiber diameters systematically decreased with solution concentration, reaching average diameters of approximately 100 nm at the lowest concentration for fiber formation (2 wt %). Figure 5.5 shows the fiber diameter as a function of solution concentration for all three copolymer compositions. Fiber diameters are reported as the average of 20 measurements from different areas of the fibrous mat, and the error bars represent one standard deviation of this average. The chaotic nature of the electrospinning process typically causes variations in fiber diameter of approximately 30%. Larger standard deviations were measured for PnBA-*co*-PSBMAm, partially due to the presence of fused fibers.

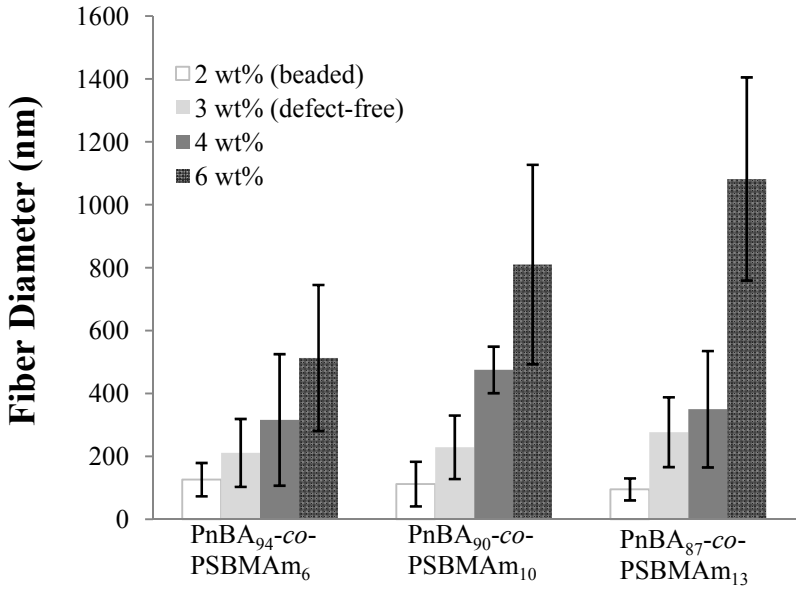

Figure 5.5 Average fiber diameters of $PnBA_{94}$-*co*-$PSBMAm_6$, $PnBA_{90}$-*co*-$PSBMAm_{10}$, and $PnBA_{87}$-*co*-$PSBMAm_{13}$ as a function of solution concentration in chloroform/ethanol (80/20 v/v)

The concentration dependence of $PnBA_{90}$-*co*-$PSBMAm_{10}$ electrospun fiber diameter is shown in Figure 5.6. The fiber diameter exhibited a 2.0 power law dependence on concentration. A slight variation in power law dependence was observed with changing SBMAm content. The fiber diameter scaling exponents as a function of zwitterion content are tabulated in Table 5.3. Despite a much larger M_w of $PnBA_{94}$-*co*-$PSBMAm_6$ compared to $PnBA_{90}$-*co*-$PSBMAm_{10}$ and $PnBA_{87}$-*co*-$PSBMAm_{13}$, the power law dependence increased with zwitterion content. While equivalent molecular weights at each zwitterion concentration are required to isolate the effect of charge, this trend indicated that ionic interactions were the primary dominant factors during electrospinning.

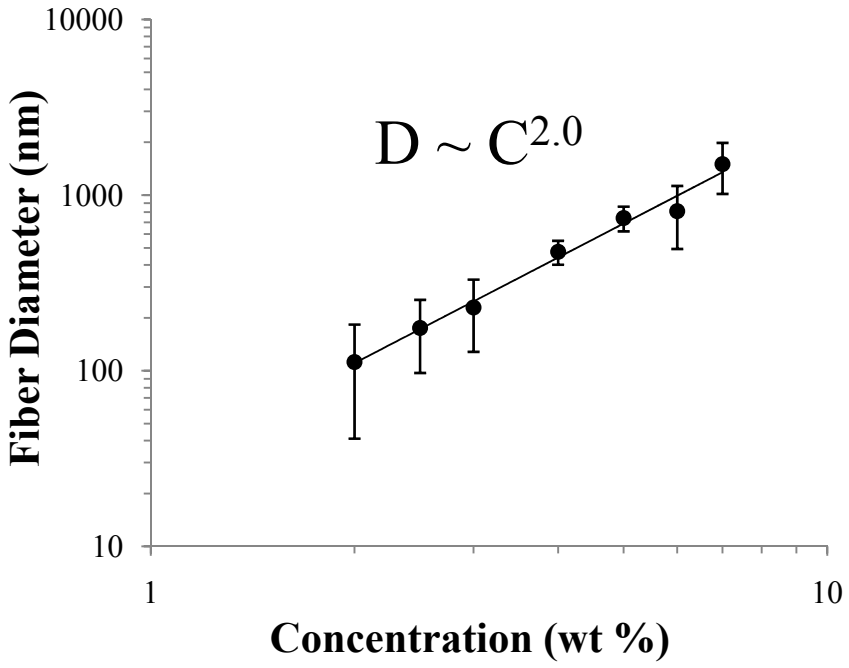

Figure 5.6 Dependence of fiber diameter on solution concentration for $PnBA_{90}$-*co*-$PSBMAm_{10}$

Table 5.3 Fiber diameter scaling exponents for copolymers of various zwitterion concentrations

Copolymer	Power Law Dependence	Avg. Fiber diameter at 3.0 wt%
$PnBA_{94}$-*co*-$PSBMAm_6$	1.3	211 ± 108
$PnBA_{90}$-*co*-$PSBMAm_{10}$	2.0	229 ± 101
$PnBA_{87}$-*co*-$PSBMAm_{13}$	2.3	277 ± 111

5.4.3.3. Influence of Zwitterion Aggregation on the Electrospinning Process Compared to Neutral PnBA.

The ability to form mechanically robust non-woven fibrous mats from low T_g copolymers containing low zwitterion loadings is a significant result that demonstrates the strong interaction between zwitterion functionalities. For comparison, electrospinning of high molecular weight (M_w 283,000 g/mol) PnBA was attempted at two different solution concentrations as shown in Figure 5.7. At 5 wt % (Figure 5.7a), a concentration analogous to the electrospinning conditions for zwitterionic copolymers, fibers did not form and polymer droplets were collected on the grid. Electrospinning was also performed at a much higher concentration of 30 wt %, which corresponds to a concentration of approximately $2C_e$ (where C_e was measured as 15 wt % in chloroform for PnBA of M_w 278,000 g/mol using previously reported rheological techniques[15]). At 30 wt %, a large continuous fiber jet was visible during the electrospinning process as expected based on previous results for neutral polymers. However, fibers were not observed in the FESEM because the low T_g polymer flowed onto the collection grid prior to microscopy characterization. A PnBA fiber can be seen after flowing to cover one strand of the stainless steel mesh in Figure 5.7b. This result shows that the incorporation of only 6 mol % zwitterionic

functionality in a low T_g polymer matrix enabled the formation of stable, free-standing non-woven mats at room temperature without the need for post-processing conditions (ex. UV crosslinking) to maintain fiber structure.

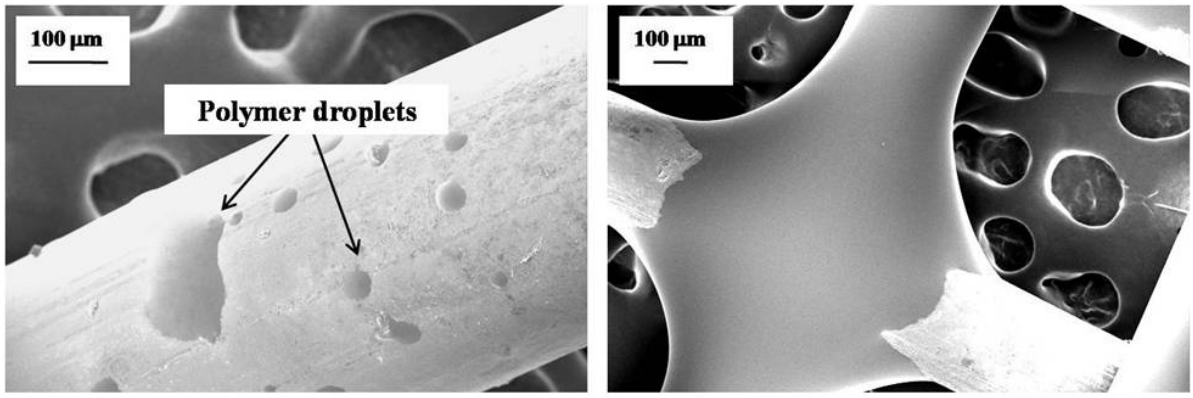

Figure 5.7 FESEM images of low T_g PnBA (M_w 278,000 g/mol, M_w/M_n = 2.56) after attempted electrospinning from chloroform/ethanol (80/20 v/v) at different solution concentrations: (a) at 5.0 wt%, electrospraying of droplets onto collection grids occurred; (b) at 30 wt%, fibers were initially collected but flowed onto grid prior to analysis

In addition to drastic differences in concentration required for successful electrospinning between neutral PnBA and zwitterionomers, large differences in solution viscosities were also observed. The dependence of viscosity on shear rate for zwitterionic copolymers and PnBA are shown in Figure 5.8. Flow curves for the zwitterionic copolymers exhibited Newtonian behavior, while PnBA appeared to exhibit shear thinning behavior at higher concentrations. The concentrations shown represent values above the onset of defect-free fiber formation (5 wt %) for PnBA-*co*-PSBMAm, and the rheologically predicted onset for PnBA (30 wt %). The viscosity of PnBA was two orders of magnitude greater than the PnBA-*co*-PSBMAm series,

consistent with the entanglements present in a high concentration polymer solution. Zero-shear viscosities of the PnBA-*co*-PSBMAm series were between 0.022 and 0.032 Pa·s. As expected based on molecular weight, $PnBA_{94}$-*co*-$PSBMAm_6$ (M_w 519,000 g/mol) exhibited the highest viscosity of the series. However, viscosities of $PnBA_{90}$-*co*-$PSBMAm_{10}$ (M_w 344,000 g/mol) and $PnBA_{87}$-*co*-$PSBMAm_{13}$ (M_w 259,000 g/mol) were approximately were similar, but also scaled with molecular weight.

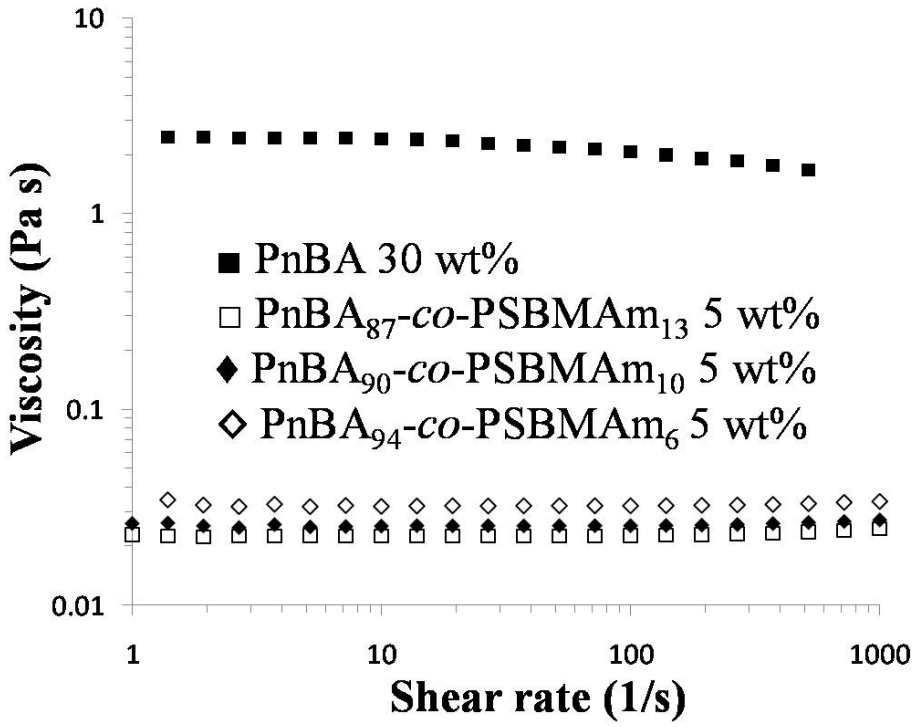

Figure 5.8 Dependence of viscosity on shear rate for zwitterionomers and PnBA at concentrations (in 80/20 v/v chloroform/ethanol) equivalent to defect-free fiber formation

The drastic difference in solution concentrations and solution viscosities required for successful electrospinning of PnBA-*co*-PSBMAm and PnBA demonstrated a fundamental difference in the electrospinning process for these polymers. Acrylic polymers such as PnBA typically have large entanglement molecular weights (M_e), meaning high solution concentrations are required for entanglements and successful electrospinning (such as 30 wt% required to electrospin high molecular weight PnBA). However, continuous fibers were electrospun from PnBA-*co*-PSBMAm at 4 wt %, an order of magnitude lower than the concentration required for PnBA. In addition, the zero-shear viscosities of zwitterionomers at 4 wt % were two orders of magnitude lower than PnBA at $2C_e$. Solution viscosities of approximately 0.02 Pa·s for zwitterionomers are the lowest viscosities observed for successful electrospinning in our laboratories,[15] and are an order of magnitude lower than the low viscosity PEG/PEO solutions reported by Rutledge.[17] These results suggested that ionic associations rather than chain entanglements likely dominated the electrospinning process for zwitterionic copolymers at relatively low concentrations. Rheological studies of the zwitterionomer solutions are underway to confirm this hypothesis.

5.5 Conclusions

Zwitterionic copolymers featuring 6-13 mol % sulfobetaine in a PnBA matrix were electrospun from 80/20 v/v chloroform/ethanol solutions containing 2-7 wt % polymer to form robust nanoscale fibers. The presence of electrostatic interactions between zwitterionic groups in the soft PnBA matrix enabled the formation of free-standing fibers and films at room temperature. To our knowledge, this is the first report of electrospun zwitterionic copolymers. A transition from beaded morphology to uniform continuous fibers occurred at polymer

concentrations of 4 wt % for each copolymer composition. Zwitterion incorporation enabled formation of fibers at low solution concentrations and viscosities below 0.02 Pa·s, resulting in average fiber diameters as small as 100 nm. These viscosity values are the lowest observed for successful electrospinning in our laboratories, and are an order of magnitude lower than the PEG/PEO elastic solutions reported by Rutledge and coworkers.[17] Successful electrospinning of zwitterionic copolymers occurred at solution concentrations and viscosities orders of magnitude lower than those required for high molecular weight PnBA. We hypothesize that intermolecular interactions rather than chain entanglements dominate the electrospinning process in copolymers featuring zwitterion aggregation. This method offers a new approach for the processing of nanoscale fibers at low concentrations with the introduction of a low concentration of strongly dipolar groups. These zwitterionic copolymers may be useful as stimuli responsive materials, electroactive devices, and elastomers, and the formation of non-woven membranes is expected to lead to additional new applications for zwitterionic copolymers.

5.6 Acknowledgements

This material is based upon work supported by the U.S. Army Research Laboratory and the U.S. Army Research Office under grant number W911NF-07-1-0339.

5.7 References

(1) Doshi, J.; Reneker, D. H. *J. Electrost.* **1995**, *35*, 151-60.
(2) Fong, H.; Chun, I.; Reneker, D. H. *Polymer* **1999**, *40*, 4585-4592.
(3) McKee, M. G.; Hunley, M. T.; Layman, J. M.; Long, T. E. *Macromolecules* **2006**, *39*, 575-583.
(4) McKee, M. G.; Layman, J. M.; Cashion, M. P.; Long, T. E. *Science* **2006**, *311*, 353-355.
(5) Reneker, D. H.; Chun, I. *Nanotechnology* **1996**, *7*, 216-223.
(6) Shin, Y. M.; Hohman, M. M.; Brenner, M. P.; Rutledge, G. C. *Polymer* **2001**, *42*, 9955-9967.

(7) Gupta, P.; Elkins, C. L.; Long, T. E.; Wilkes, G. L. *Polymer* **2005**, *46*, 4799-4810.
(8) Greiner, A.; Wendorff, J. H. *Angew. Chem., Int. Ed.* **2007**, *46*, 5670-5703.
(9) Kenawy, E.-R.; Layman, J. M.; Watkins, J. R.; Bowlin, G. L.; Matthews, J. A.; Simpson, D. G.; Wnek, G. E. *Biomaterials* **2003**, *24*, 907-913.
(10) Grafe, T.; Graham, K. *International Nonwovens Journal* **2003**, *12*, 51-55.
(11) Matthews, J. A.; Wnek, G. E.; Simpson, D. G.; Bowlin, G. L. *Biomacromolecules* **2002**, *3*, 232-238.
(12) Wang, X. Y.; Drew, C.; Lee, S. H.; Senecal, K. J.; Kumar, J.; Sarnuelson, L. A. *Nano Lett.* **2002**, *2*, 1273-1275.
(13) Hunley, M. T.; Long, T. E. *Polym. Int.* **2008**, *57*, 385-389.
(14) Gibson, P.; Schreuder-Gibson, H.; Rivin, D. *Colloids Surf., A* **2001**, *187-188*, 469-481.
(15) McKee, M. G.; Wilkes, G. L.; Colby, R. H.; Long, T. E. *Macromolecules* **2004**, *37*, 1760-1767.
(16) Shenoy, S. L.; Bates, W. D.; Frisch, H. L.; Wnek, G. E. *Polymer* **2005**, *46*, 3372-3384.
(17) Yu, J. H.; Fridrikh, S. V.; Rutledge, G. C. *Polymer* **2006**, *47*, 4789-4797.
(18) Chen, H.; Snyder, J. D.; Elabd, Y. A. *Macromolecules* **2008**, *41*, 128-135.
(19) Ward, M.; Sanchez, M.; Elasri, M. O.; Lowe, A. B. *J. Appl. Polym. Sci.* **2006**, *101*, 1036-1041.
(20) Kudaibergenov, S.; Jaeger, W.; Laschewsky, A. *Adv. Polym. Sci.* **2006**, *201*, 157-224.
(21) Lowe, A. B.; McCormick, C. L. *Chem Rev* **2002**, *102*, 4177-89.
(22) Ehrmann, M.; Galin, J. C. *Polymer* **1992**, *33*, 859-65.
(23) Gauthier, M.; Carrozzella, T.; Penlidis, A. *J. Polym. Sci., Part A: Polym. Chem.* **2002**, *40*, 511-523.
(24) Gauthier, M.; Carrozzella, T.; Snell, G. *J. Polym. Sci., Part B: Polym. Phys.* **2002**, *40*, 2303-2312.
(25) Ehrmann, M.; Muller, R.; Galin, J. C.; Bazuin, C. G. *Macromolecules* **1993**, *26*, 4910-4918.
(26) Bazuin, C. G.; Zheng, Y. L.; Muller, R.; Galin, J. C. *Polymer* **1989**, *30*, 654-61.
(27) McKee, M. G.; Park, T.; Unal, S.; Yilgor, I.; Long, T. E. *Polymer* **2005**, *46*, 2011-2015.
(28) Koski, A.; Yim, K.; Shivkumar, S. *Mater. Lett.* **2003**, *58*, 493-497.

Chapter 6: Correlation of Solution Rheological Behavior with Electrospinning for Zwitterionomers

6.1 Abstract

Our recent report showed electrospinning at very low solution concentrations and viscosities for zwitterionic copolymers featuring an amide-linked sulfobetaine at loadings of 6-13 mol %. We hypothesized that the onset of fiber formation correlated to ionic associations rather than chain entanglements. The goal of this work is to explore this hypothesis using solution rheology to determine concentration regimes for a series of zwitterionic copolymers featuring ester-linked sulfobetaine monomers. Free radical copolymerization of n-butyl acrylate and a sulfobetaine methacrylate derivative resulted in high molecular weight polymers incorporating 6 and 9 mol % betaine functionality. Solution rheology of these copolymers in chloroform enabled the analysis of specific viscosity (η_{sp}) dependence on concentration. Two concentration regimes were observed for the copolymer compositions, with a boundary at ~1.5-2 wt %. This transition occurred at an order of magnitude lower solution concentration and η_{sp} than poly(n-butyl acrylate) of similar molecular weight, suggesting the transition does not correlate to chain entanglements. Comparison of experimental data to existing models of polymer solution dynamics determined the transition in zwitterionic copolymers most closely correlated to the transformation of intramolecular associations into intermolecular associations, as modeled for associating polymers. Zwitterionic copolymers were electrospun from chloroform/ethanol solutions to form nano- to micron-scale fibers. Onset of fiber formation occurred above 1.5 wt %, in agreement with rheological observations.

6.2 Introduction

Polybetaines are a class of zwitterionic polymers featuring both a cationic and anionic charge on the same repeating unit. Several classes of polybetaines appear in the literature, including carboxybetaines, phosphobetaines, and sulfobetaines.[1] Phosphobetaines are the most widely studied class of zwitterionic polymers for a variety of biological applications due to the close structural similarity of monomer structures to natural phospholipids.[2] Sulfobetaines, featuring a quarternized ammonium and a sulfonate group separated with an alkyl spacer, also mimic lipid structures and are receiving more attention since affordable sulfobetaine monomers were made commercially available. The tethering of two oppositely charged groups on the same side chain creates a large dipole moment (μ~18.7-27.6 Da),[3] lending many unique properties to betaine-containing polymers.

Galin and workers studied sulfobetaine-containing copolymers in great detail.[4-6] Much of their work focused on the copolymerization of sulfobetaine methacrylate monomers with 2-ethoxyethyl acrylate (EEA) and n-butyl acrylate (nBA) for the synthesis of a new class of low T_g zwitterionic ionomers.[6-13] When incorporated in the low T_g nonpolar matrix of EEA or nBA, the polar zwitterions aggregated to form strong physical crosslinks, as seen in solid state NMR,[7] dynamical mechanical analysis,[9] and x-ray scattering.[8,10] Later, Gauthier and coworkers also copolymerized a series of different sulfobetaine monomers with nBA and EEA to explore the effects of zwitterionic structure on aggregation behavior.[14,15] While a solid understanding of the bulk state properties and morphology of these random copolymers was established through these studies, no attention was given to characterization in the solution state.

Polybetaines exhibit solution behavior known as the antipolyelectrolyte effect, where addition of low molecular weight electrolytes causes chain expansion and an increase in solution viscosity for aqueous solutions. Although properties of zwitterions in water and aqueous salt

solutions are well documented,[1,16-19] characterization of solution properties of zwitterion-containing polymers in organic solvents is lacking. One prominent reason for this lack of study is a limited solubility of polybetaines in organic solvents, especially for sulfobetaines.[1] Organic solvents with the ability to disrupt the strong attraction between ionic groups are needed, and these are commonly fluorinated acids and alcohols that have the strong ability to donate hydrogen bonds. When betaine functionalities are incorporated at low concentrations into organic soluble polymers through copolymerization techniques, the solubility of the matrix is maintained. The n-butyl acrylate-based copolymers previously discussed were soluble in chloroform with up to 10 mol % betaine incorporation,[6] allowing for solution characterization in non-aqueous solvents for this class of organic soluble sulfobetaine copolymers.

Electrospinning from solution forms polymeric fibers on the order of 100 nm to 5 μm in diameter,[20,21] resulting in thin fibrous mats with high surface area and submicron pores which lend themselves to a variety of applications including filtration devices, membranes, protective clothing, and optical devices.[11,22] Fibers form when a charged polymer solution or melt emits a jet in the presence of an electric field. The jet travels chaotically in a whip-like motion toward a grounded target, during which time the solvent evaporates and solid fibers collect in the form of three-dimensional, non-woven mats.[23] Many reports demonstrated that successful electrospinning requires the presence of chain entanglements within the polymer solution through correlations of electrospinning behavior to solution rheological studies.[24,25] Concentrations of $2C_e$ (where C_e is the entanglement concentration) were required for the formation of defect-free fibers for neutral polyesters in our laboratories.[24] More recently, Rutledge et al.[26] found that aqueous solutions of poly(ethylene glycol) containing small amounts of high molecular weight poly(ethylene oxide) formed fibers in the absence of chain

entanglements. They concluded that sufficient fluid elasticity could also stabilize the jet over the short timescale of electrospinning, leading to the formation of fibers without entanglements.

Previously, we reported the electrospinning of PnBA-*co*-PSBMAm at low concentrations and viscosities to form nanoscale fibers.[27] Analysis of zero shear viscosity of both zwitterionic copolymer solutions and PnBA solutions at concentrations analogous to fiber formation indicated that electrospinning occurred through a different mechanism for zwitterionic copolymers than classically accepted for neutral polymers. We proposed the observed behavior correlated to ionic interactions of the zwitterionic functionalities rather than chain entanglements. In this work, we continue to explore this hypothesis with zwitterionic copolymers of similar structure to those previously reported. Concentration regimes and scaling relationships were determined for this unique class of charged polymers utilizing solution rheology. Electrospinning of copolymers of two different zwitterion contents were explored, and correlations between solution rheology and electrospinning behavior will be discussed.

6.3 Experimental

6.3.1 Materials

Zwitterionic monomer *N*-(3-sulfopropyl)-*N*-methacryl-oxyethyl-*N,N*-dimethylammonium betaine (SBMA) was generously provided by Raschig GMBH and used without purification. Dimethylsulfoxide (DMSO, 99.9+%), azobisisobutyronitrile (AIBN), and n-butyl acrylate (nBA) were purchased from Sigma-Aldrich Chemical Co. AIBN was recrystallized from methanol. n-Butyl acrylate (nBA) was passed through a neutral alumina column and distilled under reduced pressure from CaH_2. Chloroform (Optima grade, Fisher Scientific) and ethanol (95%) were used as received.

6.3.2 Synthesis of sulfobetaine methacrylate-*co*-butyl acrylate copolymers

A typical copolymerization is described. nBA (13.4 g, 0.105 mol) and SBMA (3.26 g, 0.012 mol) were added to a 250-mL, round-bottomed flask equipped with a magnetic stir bar. The reaction mixture was diluted with DMSO (137 mL, 90 wt %), and AIBN (83 mg, 0.50 wt %) was added to the reaction vessel. The reaction was sparged with nitrogen for 15 min and placed in an oil bath at 60 °C for 24 h. The polymer was precipitated into 4 L of water and dried under reduced pressure. Residual DMSO was removed via vacuum distillation at 60 °C. The isolated polymer was dried under reduced pressure at 80°C for 48 h and stored in a desiccator. Isolated yields were typically >75%. A series of molecular weights were synthesized using varying AIBN concentrations of 0.1, 0.5, and 1.0 wt%.

6.3.3 Synthesis of poly(*n*-butyl acrylate) (PnBA)

nBA (25 g, 0.195 mol), AIBN (170 mg, 0.001mol), and ethyl acetate (110 mL, 80 vol %) were added to a 250-mL, round-bottomed flask equipped with a magnetic stir bar. The reaction was sparged with nitrogen for 15 min and placed in an oil bath at 65 °C for 22 h. The reaction solution was diluted with 150 mL ethyl acetate, and added drop wise to 5 L of 9:1 methanol:water solution. The isolated polymer was dried at reduced pressure at 60 °C for 18 h to yield 22.6 g (90 % yield).

6.3.4 Electrospinning

Copolymers were dissolved in 80/20 v/v chloroform/ethanol at 7 wt %, and subsequent concentrations were achieved through dilutions. The solutions were placed in a 20-mL syringe

that was mounted in a syringe pump (KD Scientific Inc). The positive lead of a high voltage power supply (Spellman CZE1000R, Spellman High Voltage Electronics Corp.) was connected to a blunt 18-gauge syringe needle using an alligator clip. A grounded metal target (304 stainless steel mesh screen) was placed 20 cm from the needle tip. The syringe pump delivered the polymer solution at a controlled flow of 3 mL/h, and the voltage was maintained at 25 kV. Constant electrospinning conditions were maintained in order to isolate the effect of zwitterion content on the fiber morphology and diameter. Electrospun mats were stored in a desiccator until FESEM images were obtained.

6.3.5 Instrumentation

^{1}H NMR spectra of the polymers were obtained on a Varian Unity 400 MHz spectrometer in $CDCl_3$. Molar compositions of the polymers were determined by comparison of shifts at 1.0 ppm for the $–CH_3$ on nBA with the $–CH_3$ groups on the quaternary ammonium of the sulfobetaine unit at 3.20 ppm.[14] Size exclusion chromatography (SEC) was used to determine the molecular weights of zwitterionomers at 50 °C in *N*,*N*-dimethyformamide (DMF) with 0.01M lithium bromide (LiBr) at 1 mL min^{-1}. DMF SEC was performed on a Waters SEC equipped with two Waters Styragel HR5E (DMF) columns, a Waters 717plus autosampler, and a Waters 2414 differential refractive index detector. Reported molecular weights are relative to polystyrene standards. SEC of PnBA was performed in tetrahydrofuran at 40 °C and 1 mL min^{-1} on a Waters SEC equipped with three Polymer Laboratories PLGel 5μm Mixed-C columns. THF SEC instrumentation included a Waters 717plus autosampler, Waters 2414 differential refractive index detector, and a Wyatt Technologies miniDAWN multiangle laser light scattering (MALLS) detector. Absolute molecular weight is reported, using a dn/dc of 0.07.

Steady shear rheological experiments were performed on a TA Instruments AR-G2 rheometer at 25 ±0.2 °C using concentric cylinder geometry. Copolymer solutions in chloroform with concentrations of 1-7 wt % were prepared individually and subsequently analyzed with shear rate sweeps from 0.01 to 1000 s^{-1}. Electrospun fiber diameter and morphology were analyzed using a Leo 1550 field emission scanning electron microscope (FESEM). Fibers for FESEM analysis were collected on a ¼ in. × ¼ in stainless steel mesh, mounted on a SEM disk, and sputter-coated with an 8 nm Pt/Au layer to reduce electron charging effects. Twenty measurements on random fibers for each electrospinning condition were performed to determine average fiber diameters.

6.4 Results and Discussion

6.4.1 Synthesis and Characterization of Zwitterionomers

We previously reported the synthesis of copolymers containing *n*BA and N-(3-sulfopropyl)-N-methacryloylamidopropyl-N,N-dimethylammonium betaine (SBMAm) using AIBN-initiated free radical copolymerization in DMSO. Copolymers containing *n*BA and 3-9 mol % of zwitterion methacrylate functionality (SBMA) were synthesized through a similar method to afford high molecular weight copolymers (Scheme 6.1). ^{1}H NMR spectroscopy confirmed the copolymer structure, and compositions matched the feed within ±1 mol % for up to 10 mol % SBMA. The synthetic method afforded a series of copolymers containing 3, 6-7, and 9 mol % SBMA. Additionally, altering the initiator concentration led to a series of molecular weights for copolymers containing 6-7 or 9 mol % SBMA. The copolymer with the lowest zwitterion content, 3 mol%, formed a soft, tacky film. Higher zwitterion contents

produced self-standing pliable films with properties similar to the PnBA-*co*-PSBMAm copolymers reported previously.

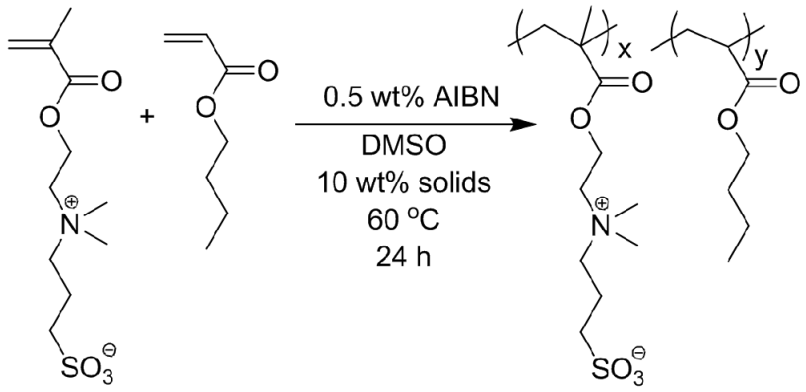

Scheme 6.1. Synthesis of P*n*BA-*co*-PSBMA copolymers

Zwitterionic copolymers were soluble in chloroform and *N,N*-dimethylformamide (DMF), but were insoluble in most other organic solvents. DMF solubility allowed for molecular weight characterization with size exclusion chromatography (SEC) using DMF with 0.01M LiBr as the eluent. This LiBr concentration was determined as the optimal salt concentration to inhibit aggregation in DLS, while also possibly screening interactions of the charged polymer with the column. Chromatography of $PnBA_{97}$-*co*-$PSBMA_3$ and poly(nBA) homopolymer resulted in broad distributions and very low intensity, indicating that the SEC conditions were not ideal for these copolymers. Therefore, $PnBA_{97}$-co-$PSBMA_3$ was not further characterized for this study. Copolymer molecular weights relative to polystyrene standards for the remaining copolymers are shown in Table 6.1.

Table 6.1 Relative molecular weights of PnBA-*co*-PSBMA

Copolymer Composition	M_w (g/mol)	M_w/M_n
$PnBA_{91}$-*co*-$PSBMA_9$	324,000	2.3
$PnBA_{91}$-*co*-$PSBMA_9$	265,000	2.5
$PnBA_{91}$-*co*-$PSBMA_9$	165,000	3.0
$PnBA_{94}$-*co*-$PSBMA_6$	447,000	3.1
$PnBA_{93}$-*co*-$PSBMA_7$	391,000	3.1
$PnBA_{93}$-*co*-$PSBMA_7$	274,000	3.4

6.4.2 Solution Rheology and Determination of Concentration Regimes for Zwitterionomers

The concentration dependence of viscosity for zwitterionic copolymers was explored to determine the corresponding concentration regimes, using solution rheology methods reported by Colby et al.[28] Figure 6.1 shows a plot of viscosity vs. shear rate for $PnBA_{91}$-*co*-$PSBMA_9$ (M_w = 265,000 g/mol) at various concentrations. All polymer solutions exhibited Newtonian behavior over the shear rate range tested. The zero shear rate viscosity (η_0) increased from 1.09 mPa·s to 1500 mPa·s with increasing concentrations from 1.0 to 7.0 wt %.

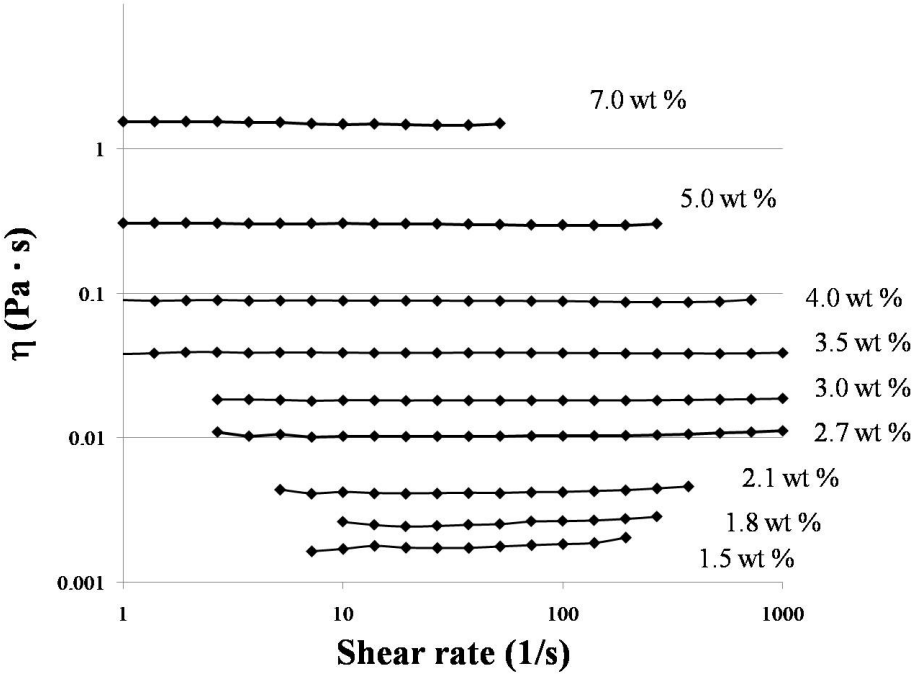

Figure 6.1 Dependence of viscosity on shear rate for $PnBA_{91}$-*co*-$PSBMA_9$ (M_w = 265,000 g/mol) in chloroform at various concentrations.

Zero shear viscosities were normalized for solvent contribution using the specific viscosity, η_{sp}, defined as:

$$\eta_{sp} = (\eta_o - \eta_s)/ \eta_s \qquad (1)$$

where η_s is the solvent viscosity. The use of η_{sp} in the place of η_o allows the isolation of the polymer contribution to solution dynamics for comparison in other solvent systems. Much work has been dedicated to predicting the scaling relationships between polymer concentration (*c*) and solution viscosity in polymer solutions.[29-34] In the case of neutral, non-associating polymers, de Gennes[30] predicted four concentration regimes that were subsequently observed experimentally for a variety of linear polymers. In a good solvent, $\eta_{sp} \sim c^{1.0}$ in dilute solution, $\eta_{sp} \sim c^{1.25}$ in the semidilute unentangled regime, $\eta_{sp} \sim c^{3.75}$ in the semidilute entangled regime, and $\eta_{sp} \sim c^{3.6}$ in the

concentrated regime. Special consideration for the theta (Θ) condition predicts slightly higher exponents in the semidilute regimes, where $\eta_{sp} \sim c^{2.0}$ in the semidilute unentangled regime and $\eta_{sp} \sim c^{4.67}$ in the semidilute entangled regime.[29] η_{sp} is plotted as a function of concentration for the neutral, non-associating PnBA (M_w = 283,000 g/mol) in Figure 6.2. Chloroform is known as a good solvent for PnBA. The rheological properties of PnBA in chloroform are presented first in order to set a basis for subsequent analysis of zwitterionic copolymers with relatively low zwitterion contents.

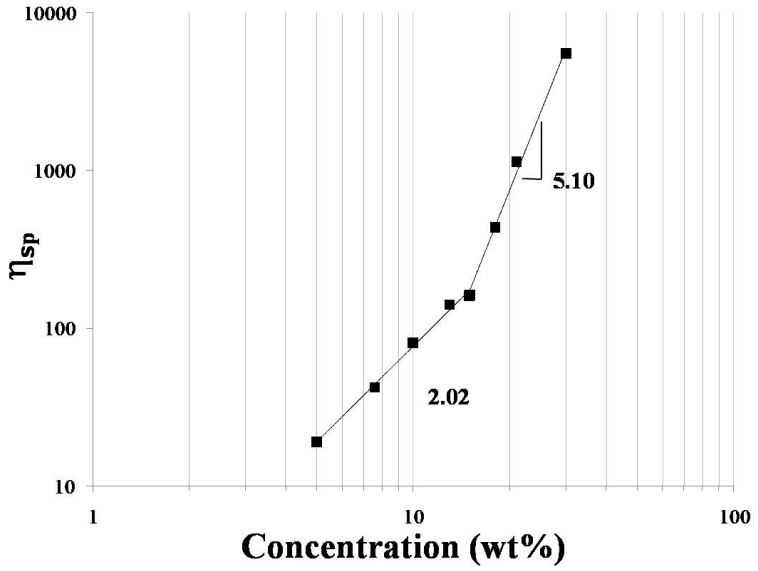

Figure 6.2 Dependence of specific viscosity on concentration for PnBA (M_w = 283,000 g/mol)

Over the concentration range tested (5-30 wt%), two concentration regimes were clearly observed with a change in slope occurring at 15 wt %. The boundary between the two regimes represents the concentration at which significant chain overlap topologically constrains chain

motion, and is defined as the entanglement concentration (C_e).[35] A large C_e in the range of 15-20 wt % was expected based on the relatively large molecular weight of entanglement (M_e) for poly(alkyl acrylates).[36,37] The slopes of the two observed concentration regimes corresponded to the semidilute unentangled and semidilute entangled regimes, respectively. The observed exponent in the semidilute entangled regime showed good agreement with predicted values, while the exponent of the semidilute unentangled regime was larger than predicted for good solvent conditions (2.02 vs 1.25).[30]

Concentration regimes for $PnBA_{91}$-*co*-$PSBMA_9$ at three different molecular weights (164, 265, and 324 kg/mol) were subsequently determined for solution concentrations up to 7 wt % in chloroform, utilizing the same experimental methods. While chloroform is a good solvent for PnBA, the major component of the copolymers, it is not a good solvent for the polar zwitterions. An overlay of the viscosity dependence on concentration for this series of copolymers appears in Figure 6.3. Good linear fits were achieved for both regimes in all three samples. The observed slopes of the upper and lower regimes, as well as the transition for each molecular weight, are summarized in Table 6.2. The boundary of the upper and lower regimes occurred at ~1.5-2.0 wt %. The specific viscosity at equivalent solution concentrations increased with molecular weight, as expected. This trend is clearly seen when comparing samples with molecular weights of 165,000 and 324,000 g/mol. The solution viscosities of the two higher molecular weight polymers (M_w= 265,000 and 324,000 g/mol) are within error of the measurement and therefore not significantly different.

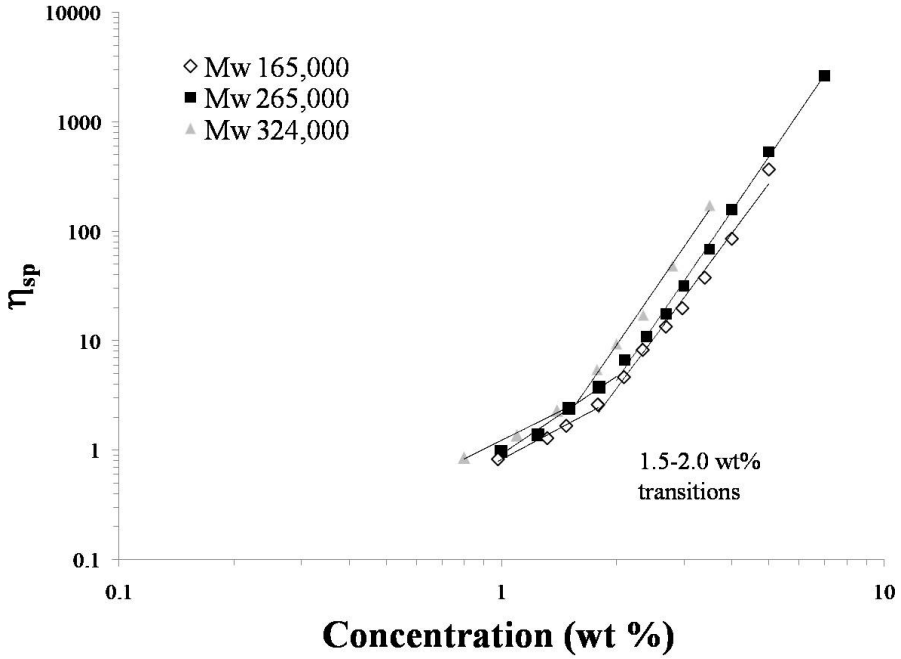

Figure 6.3 Dependence of specific viscosity on concentration for $PnBA_{91}$-*co*-$PSBMA_9$ of varying molecular weights

Table 6.2 Concentration regimes for $PnBA_{91}$-*co*-$PSBMA_9$ as a function of molecular weight

M_w (g/mol)	Slope Upper regime	Slope Lower regime	Transition (wt%)
165,000	4.69	1.88	1.8
265,000	5.13	2.36	2.0
324,000	5.09	1.75	1.5

Similarly, $PnBA_{94}$-*co*-$PSBMA_6$ (M_w= 274,000) and $PnBA_{93}$-*co*-$PSBMA_7$ (M_w= 447,000) were analyzed, and two concentration regimes were observed (Figure 6.4). Good linear fits were also achieved for this series of copolymers. At an M_w = 274,000 g/mol, $\eta_{sp} \sim c^{2.20}$ at lower concentrations, and $\eta_{sp} \sim c^{4.31}$ above the transition at 2.0 wt %. Solution viscosities increased with molecular weight at equivalent concentrations, as expected. $\eta_{sp} \sim c^{2.13}$ at lower

concentrations for M_w = 447,000 g/mol, and $\eta_{sp} \sim c^{4.70}$ at concentrations above the transition at ~1.7 wt%. The observed scaling relationships and transitions were very similar to the behavior of $PnBA_{91}$-*co*-$PSBMA_9$, although the scaling relationships of the upper regime were lower for $PnBA_{94}$-*co*-$PSBMA_6$. In a comparison of similar molecular weights, $PnBA_{91}$-*co*-$PSBMA_9$ (M_w = 265,000) and $PnBA_{94}$-*co*-$PSBMA_6$ (M_w = 274,000), the larger zwitterion content led to scaling exponents of 2.36 and 5.13 for the lower and upper regimes, respectively, compared to the 6 mol % zwitterion content with scaling exponents of 2.20 and 4.31. Despite different slopes, the boundary between the two regimes occurred at ~2.0 wt % regardless of zwitterion content. A higher scaling in the more concentrated regime for $PnBA_{91}$-*co*-$PSBMA_9$ may be explained based on the increased interactions and drag forces on polymer chain dynamics in the presence of more zwitterion functionality, or sticky groups. More ionic groups are available to interact with nearby chains and contribute to drag forces at higher zwitterion contents. This phenomenon leads to restricted mobility of flowing chains and a significantly higher scaling relationship based on solution concentration.

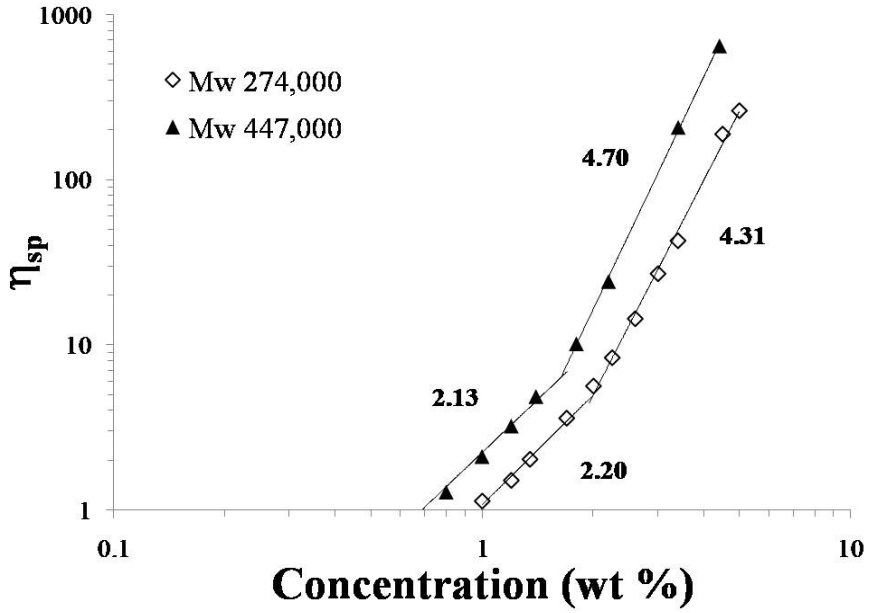

Figure 6.4 Dependence of specific viscosity on concentration for ◊ $PnBA_{94}$-*co*-$PSBMA_6$ M_w = 274,000 g/mol and ▲ $PnBA_{93}$-*co*-$PSBMA_7$ M_w= 447,000 g/mol

Solvent characteristics also have a large influence on the dynamics of flow and therefore the concentration dependence of viscosity for polymer solutions. Ethanol serves as a solvent for sulfobetaines, and was added to the chloroform solutions at 20 vol % to explore the effects of a polar additive on rheological behavior. The specific viscosity dependence on concentration for $PnBA_{91}$-*co*-$PSBMA_9$ (M_w = 265,000) for both chloroform and chloroform/ethanol 80/20 v/v solutions is shown in Figure 6.5. In the presence of ethanol cosolvent, scaling relationships drastically decreased in both concentration regimes, from 2.36 to 1.37 in the lower concentration regime, and from 5.13 to 2.37 in the upper concentration regime. However, the concentration at the slope transition remained at 2.0 wt %. This drastic shift in rheological behavior is likely due to a change in solvation of the zwitterionic functionalities in the presence of the polar solvent

ethanol. Ethanol may serve to disrupt zwitterionic interactions through competitive dipole interactions with zwitterion-zwitterion associations, effectively screening inter-zwitterionic associations. This behavior is similar to the screening of charge in polyelectrolytes with salt.[38,39] The screening effect with a polar additive would reduce the strength of ionic associations, leading to fewer mobility restrictions along the polymer chains (ie. fewer interactions and corresponding drag forces) and a smaller dependence of viscosity on concentration. In this case, the transition between regimes remained the same, while only the magnitude of the scaling relationships changed in the presence of ethanol.

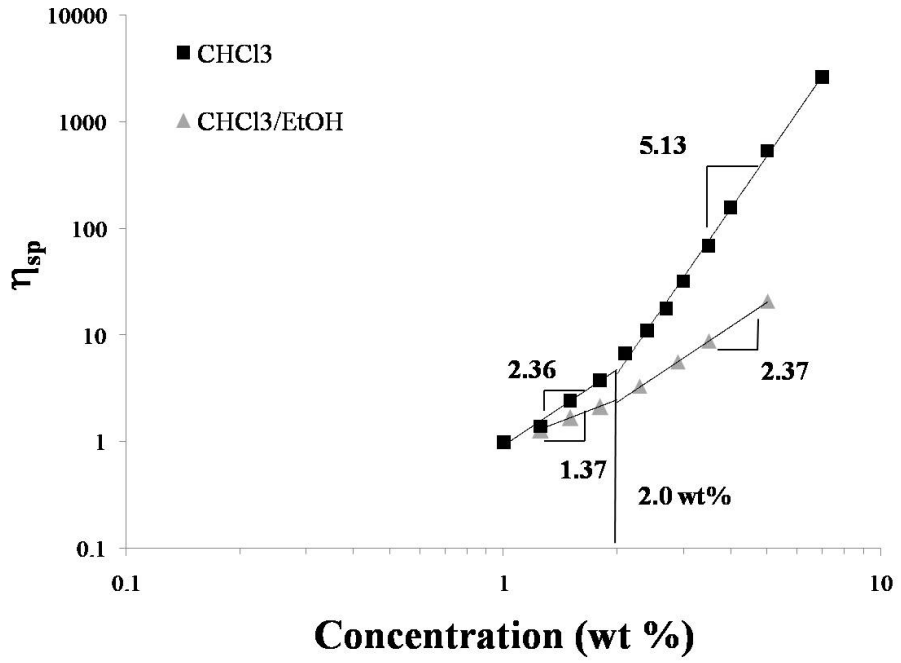

Figure 6.5 Dependence of specific viscosity on concentration for $PnBA_{91}$-*co*-$PSBMA_9$ (M_w = 265,000 g/mol) under different solvent conditions. ■ chloroform; ▲ chloroform/ethanol 80/20 v/v

The same chloroform/ethanol cosolvent composition was previously used for the successful electrospinning of zwitterionic copolymers into nanoscale nonwoven membranes.[27] PnBA-*co*-PSBMA copolymers were also successfully electrospun using this solvent composition, as shown in a later section. Previous reports have shown good correlations between concentration regimes studied with rheology and fiber formation through electrospinning.[24,38,40] Because the transition did not change for $PnBA_{91}$-*co*-$PSBMA_9$ in either chloroform or chloroform/ethanol 80/20 v/v solutions, we believe a correlation between the reported rheological analysis of both $PnBA_{91}$-*co*-$PSBMA_9$ and $PnBA_{94}$-*co*-$PSBMA_6$ in chloroform with electrospinning results from chloroform/ethanol solutions is validated.

The most striking observation from the rheological analysis of zwitterionic copolymers is the comparison of dependence of specific viscosity on concentration to that of PnBA homopolymer (Figure 6.2). The zwitterionic copolymers, regardless of zwitterion content, exhibited both specific viscosities and solution concentrations an order of magnitude lower at the slope transition than those values at the C_e for PnBA. The specific viscosity at C_e (15 wt %) for PnBA was ~200, while the specific viscosities of the zwitterionic copolymers at the transition (~2 wt %) were ~ 2-4. These observations led us to believe that the transitions observed for the zwitterionic copolymers were not defined as the same C_e observed for neutral, non-associating polymers (ie. PnBA). The boundary between concentration regimes is likely due to a different phenomenon than chain entanglements in the presence of zwitterions.

The current models for scaling dynamics in polymer solutions do not adequately account for the nature of the zwitterionic copolymer, featuring highly polarized zwitterionic groups with no net charge in a nonpolar nBA matrix. de Gennes derived a scaling law for neutral, non-associating polymers in a good solvent that models viscosity as a function of c/c^*, where c is the

monomer concentration per unit volume, and c^* is the concentration where individual chains begin to overlap.[30] This simple one-parameter model breaks down in a Θ solvent, where a clear dependence of viscosity on molecular weight is observed.[29] These models are based on a collection of binary contacts between polymer chains that constitute an entanglement. In the presence of ionic or "sticky" groups, the definition of chain overlap and entanglement are redefined, so that this simple model for neutral polymers does not apply to the zwitterionic copolymer system.

Scaling theories for polyelectrolytes (PEs) were also developed according to de Gennes,[41] Pfeuty,[42] and Rubinstein.[43] PEs in salt-free solutions are extended in a rod-like configuration due to charge repulsion of ionic groups along the backbone. Rod-like PE chains repel each other, and entanglements occur at much higher concentrations than neutral analogs. The semidilute unentangled regime ($c>c^*$) for PEs spans three orders of magnitude in concentration with a concentration dependence of only 0.5.[43] Higher scaling relationships (~3.75) are not observed until the concentrated regime. This model is inappropriate for the case of zwitterionic copolymers where charge content is quite low and significant chain interactions are observed at very low concentrations < 2 wt %. Also, a strong dependence on concentration is observed in both regimes for the zwitterionic copolymers, with much larger scaling exponents than predicted for PEs.

A more appropriate model for zwitterion-containing polymers would account for strong associations between polymer chains that increase chain interactions. Rubinstein and Semenov developed a model to describe associating polymers that applies to network structures with many interaction sites in solution.[32] The forming and breaking of bonds between friction centers or "stickers" dominate the dynamics of associating polymers and are the primary consideration of

this model. Two major concepts are addressed: the effect of intramolecular vs intermolecular interactions on solution dynamics, and the lifetime of a sticker association. The semidilute unentangled regime is described according to a sticky Rouse model, while a sticky reptation model describes the entangled regime. Under dilute conditions, all stickers are involved in intramolecular associations and concentration dependence is minimal. As solution concentration increases, intramolecular associations transform to intermolecular associations and a drastic change in concentration dependence is observed ($\eta \sim c^{4.2}$) in the semidilute regime. Above the entanglement concentration, the majority of sticker associations are intermolecular and dynamics are dominated by the effective bond lifetimes, which are long in the absence of free stickers to form new associations. This phenomenon hinders polymer chain movement with increased friction at the sticker sites, resulting in increased scaling relationships ($\eta \sim c^{6.8}$).

The associating polymer model seems to be in fair agreement with the concentration dependence for zwitterionic copolymers in the upper concentration regime ($\eta \sim c^{4.3\text{-}5.1}$), correlating to the transformation of intramolecular into intermolecular associations between zwitterions on separate polymer chains. Such behavior correlates to the semidilute unentangled regime. However, scaling in the lower regime ($\eta \sim c^{1.7\text{-}2.2}$) does not match the model for dilute solution. One shortcoming of this model in application to the zwitterionic system is the assumption of pairwise associations. Zwitterions are known to form aggregates with strong associations, theoretically incorporating >2 sticky groups per association. Differences in zwitterion association number as well as the strength of interaction that could drastically affect the effective bond lifetime of the association may account for differences in the lower concentration regime. The associating polymer model appears to be the best fit of the models considered for zwitterionic copolymers; however, better models to predict the lower regime are

still needed for a complete picture of solution dynamics. Rheological measurements over a broader range of concentrations, molecular weights, and zwitterion contents are needed to ensure a good fit over all concentration regimes in this unique copolymer system.

6.4.3 Electrospinning of Ester-linked Zwitterionomers to Form Nanoscale Fibers

We previously reported the formation of nanoscale zwitterionic fibers through electrospinning of PnBA-*co*-PSBMAm containing 6-13 mol % zwitterion functionality.[27] Fibers as small as 100 nm diameter were formed at polymer concentrations of only 2 wt % and very low solution viscosities. This was the first report of electrospinning betaine-containing copolymers. Electrospinning success with the SBMAm-containing copolymers led us to explore the electrospinning behavior of SBMA-containing copolymers of similar zwitterion contents.

Electrospinning was performed at constant conditions (25 kV, 3 mL/h, 20 cm tip-to-target distance) in order to isolate the effects of concentration on fiber formation. These conditions also match those used for PnBA-*co*-PSBMAm so that a direct comparison to the previously reported data is valid. Copolymers were electrospun from 80/20 v/v chloroform/ethanol solutions at concentrations below 7 wt %. The addition of ethanol decreased solvent volatility sufficiently for electrospinning to occur without clogging of the syringe tip. The polymers selected for this study include $PnBA_{91}$-*co*-$PSBMA_9$ with M_w 324,000 g/mol, and $PnBA_{94}$-*co*-$PSBMA_6$ with M_w 447,000 g/mol.

FESEM images of collected fibers over the concentration range of 1.5-7 wt % are shown in Figures 6.6 and 6.7 for $PnBA_{91}$-*co*-$PSBMA_9$ and $PnBA_{94}$-*co*-$PSBMA_6$, respectively. Polymer droplets formed at the lowest concentration of 1.5 wt %, as seen in the top left image of Figure 6.6. Droplet formation results when insufficient entanglements or fluid elasticity is present to stabilize the polymer jet.[21] Droplet formation was also observed at 1.5 wt % for $PnBA_{90}$-*co*-

PSBMAm$_{10}$ (M_w = 344,000 g/mol) in our previous study.[27] Fiber morphology changed with increasing solution concentration, lending beaded fibers at 2-2.5 wt %, and defect-free fibers above 3.0 wt % for PnBA$_{91}$-*co*-PSBMA$_9$ (Figure 6.6). Similar morphological transitions were observed for PnBA$_{94}$-*co*-PSBMA$_6$, with beaded fibers at 2.0 wt % and uniform fibers above 2.5 wt %. The transition from beaded to uniform fibers occurred at 4.0 wt % for the PnBA-*co*-PSBMAm series, regardless of zwitterion content.[27]

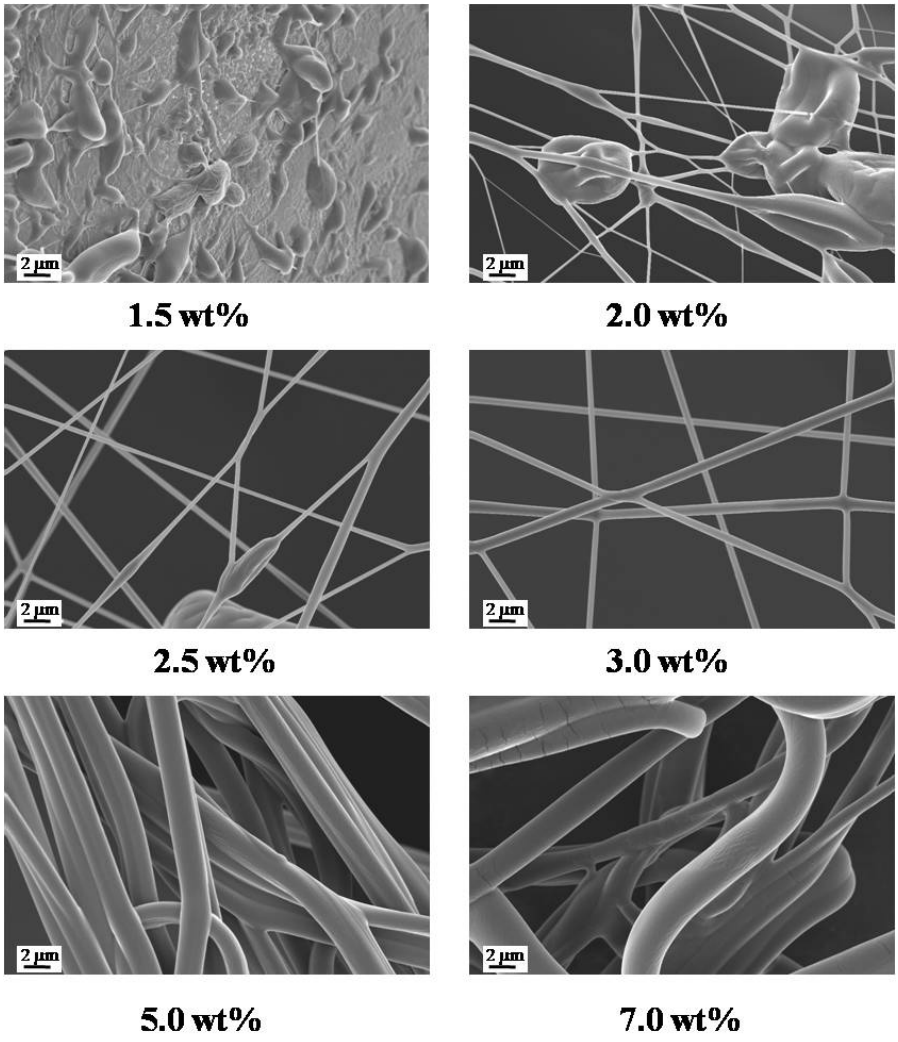

Figure 6.6 FESEM images of PnBA$_{91}$-*co*-PSBMA$_9$ (M_w = 324,000) electrospun fibers at various solution concentrations in chloroform/ethanol (80/20 v/v)

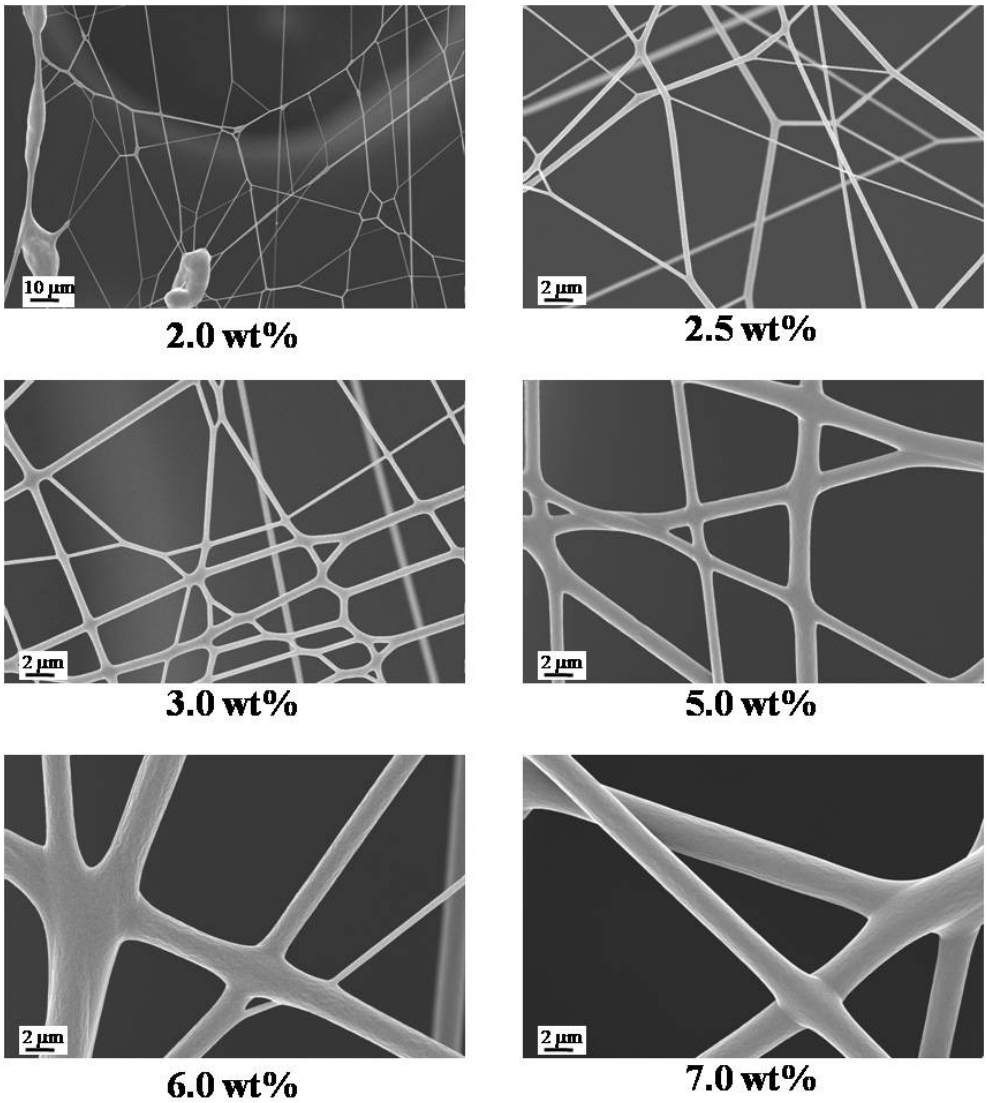

Figure 6.7 FESEM images of $PnBA_{94}$-*co*-$PSBMA_6$ (M_w = 447,000) electrospun fibers at various solution concentrations in chloroform/ethanol (80/20 v/v)

The morphological transitions observed through electrospinning of $PnBA_{91}$-*co*-$PSBMA_9$ and $PnBA_{94}$-*co*-$PSBMA_6$ correlated to the transitions observed in the rheological behavior of copolymer solutions in chloroform. The boundary between concentration regimes for $PnBA_{91}$-*co*-$PSBMA_9$ occurred at ~1.5 wt %, where polymer droplets were collected in electrospinning.

All concentrations above 1.5 wt % led to fiber formation, with uniform fibers at 3 wt %. This trend corresponds well to previous studies in our laboratory where uniform fibers formed at concentrations much greater than the rheological transition (C_e in the case of polyelectrolytes and neutral polymers), usually more than double the transition concentration.[24,38] The boundary between concentrations for $PnBA_{94}$-*co*-$PSBMA_6$ was observed at ~1.7 wt %, and beaded fibers were collected at 2.0 wt %. Uniform fibers formed at concentrations above 2.5 wt %. The transitions in fiber morphology correlate well to the transition concentration observed with solution rheology within the limited data set of electrospinning concentrations studied. Electrospinning of more solution concentrations in the range of ~1.3-2.5 wt % are needed to more specifically identify the actual onset of fiber formation for correlation to rheological transitions.

Continuous electrospun fibers with diameters of ~2-3 microns were collected at the highest solution concentration, 7 wt %. Fiber diameters decreased with concentration, and a minimum average diameter of 250-300 nm was observed at the lowest concentration for fiber formation of 2.0 wt %. A plot of the average fiber diameter as a function of solution concentration for both zwitterionic copolymers is shown in Figure 6.8. The concentration dependence of fiber size exhibits a power law relationship, where the scaling exponent represents the slope of the line in the linear region on a log-log plot. A slight variation in power law dependence was observed with changing SBMA content. Moreover, these scaling relationships matched closely to those reported for the SBMAm series: $D \sim C^{2.0}$ for $PnBA_{90}$-*co*-$PSBMAm_{10}$ and $D \sim C^{1.3}$ for $PnBA_{94}$-*co*-$PSBMAm_6$.

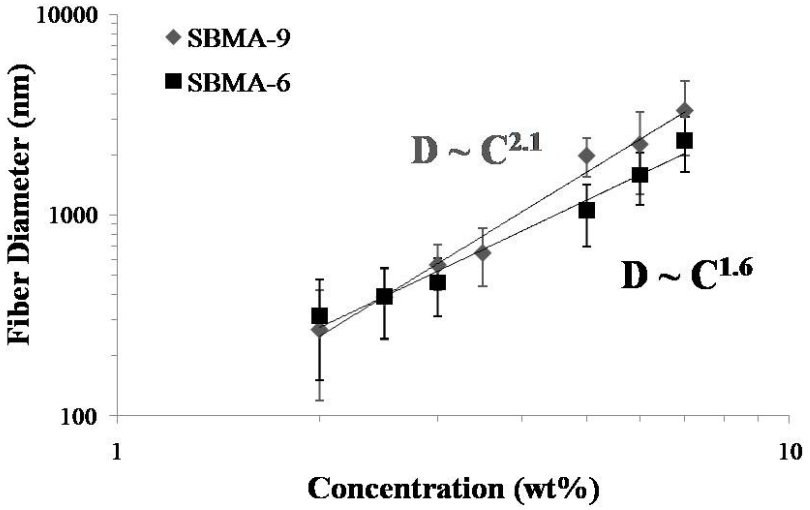

Figure 6.8 Dependence of fiber diameter on solution concentration for $PnBA_{91}$-*co*-$PSBMA_9$ and $PnBA_{94}$-*co*-$PSBMA_6$

In a direct comparison of $PnBA_{91}$-*co*-$PSBMA_9$ and $PnBA_{90}$-*co*-$PSBMAm_{10}$, where zwitterion concentrations are equal within error of NMR measurement and molecular weights match within 10%, $PnBA_{91}$-*co*-$PSBMA_9$ fiber diameters measured 2-3 times larger. Both copolymers exhibited very similar electrospinning behavior in respect to morphology, concentration dependence, and transition concentrations. The concentration dependence of fiber diameter for both copolymers were the same, ~2.0 (Figure 6.9). These observations reveal a marked effect of zwitterion structure on fiber size during electrospinning. The structural differences between SBMA and SBMAm are one methylene spacer between the backbone and the dimethylammonium group, and incorporation of an amide linkage capable of hydrogen bonding versus an ester linkage between the zwitterionic side chain and the polymer backbone. The influence of an increased side chain length of one methylene spacer on fiber diameter is too small to be responsible for a significant increase in fiber diameter, so the influence of the amide bond is more likely involved. One possibility for this phenomenon is that ethanol is more tightly

associated with SBMAm through hydrogen bonding, leading to an increased screening effect of zwitterionic interactions. This proposed screening effect, which was observed through a drastic change in concentration dependence for rheological measurements in chloroform/ethanol (Figure 6.5), leads to a decreased interaction between polymer chains within the electrospinning jet, through either entanglements or ionic aggregates, and therefore smaller fibers. There are also a number of parameters in the electrospinning process that are shown to have large effects on fiber diameter.[11] For example, the presence of the amide bond may have an effect on solution conductivity, resulting in smaller diameters due to increased charge repulsions in the jet. Analysis of the various electrospinning parameters involved in dictating fiber size is beyond the scope of this study and are offered here only as a possible explanation for the observed behavior.

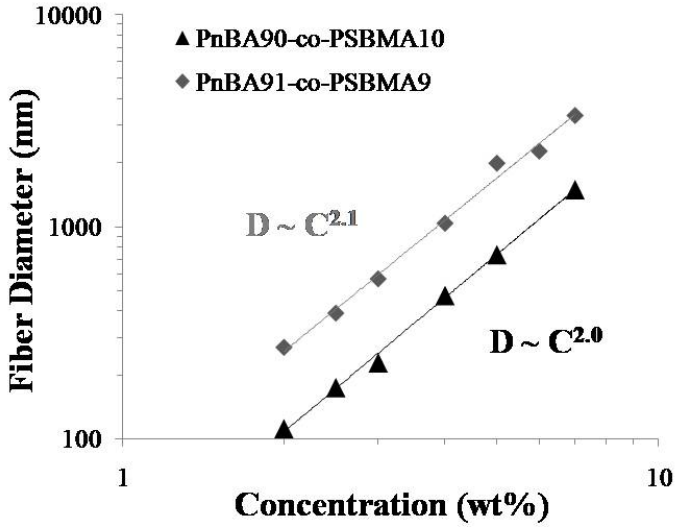

Figure 6.9 Comparison of fiber diameter dependence on solution concentration for $PnBA_{91}$-*co*-$PSBMA_9$ (M_w = 324,000) and $PnBA_{90}$-*co*-$PSBMAm_{10}$ (M_w = 344,000)

6.5 Conclusions

Solution properties of sulfobetaine-containing polymers in non-aqueous solutions are not well studied in the current literature. The present study identified this void for a series of PnBA-*co*-PSBMA copolymers. PnBA-*co*-PSBMA copolymers were synthesized via free radical polymerization in DMSO to afford ionomers containing 6 and 9 mol % zwitterion functionality. Steady shear experiments over a range of solution concentrations in chloroform revealed two concentration regimes and boundary transitions at ~2.0 wt %. A slight influence of zwitterion content on scaling behavior was observed. $PnBA_{94}$-*co*-$PSBMA_6$ showed a smaller dependence on concentration in the upper regime compared to $PnBA_{91}$-*co*-$PSBMA_9$, due to less mobility restrictions on polymer chains in the presence of fewer stickers of zwitterion groups.

Solution properties of the neutral homopolymer PnBA fit the predicted scaling for neutral non-associating polymers with a C_e at 15 wt %. The transition for PnBA was an order of magnitude higher in both specific viscosity and concentration than the transition observed for zwitterionic copolymers. The large difference in properties at the transition for the neutral homopolymer versus the zwitterionic copolymers indicates the transitions are not due to the same physical phenomenon. The solution behavior of zwitterionic copolymers was compared to several different scaling models of polymer dynamics in solution in an attempt to identify the observed transition. Models describing neutral non-associating polymers and polyelectrolytes were inappropriate for the zwitterionic copolymer because they failed to consider the dynamic interactions of the strongly associating zwitterions. Rubinstein and Semenov's model for associating polymers based on sticky Rouse and sticky reptation models sufficiently described zwitterionic copolymer behavior in the upper concentration regime, but poorly correlated to the lower concentration regime. A major shortcoming of the model is the condition of pairwise

association of stickers because zwitterions are known to form aggregated structures consisting of more than two ionic groups.

Electrospinning from chloroform/ethanol (80/20 v/v) solutions led to similar results observed previously for PnBA-*co*-PSBMAm copolymers.[27] Fiber morphology changed with increasing concentration, with the onset of fiber formation occurring above 1.5 wt % for both copolymers. The onset of fiber formation correlated to the transition observed in rheological measurements, tentatively identified as the transition between dilute and semidilute unentangled regimes. Fiber diameter increased with concentration over the range of 2-7 wt %, ranging from ~300 nm to ~2 μm. A direct comparison of $PnBA_{91}$-*co*-$PSBMA_9$ and $PnBA_{90}$-*co*-$PSBMAm_{10}$ at equivalent molecular weights revealed similar scaling relationships for the dependence of fiber diameter on concentration, but drastic differences in fiber size. $PnBA_{91}$-*co*-$PSBMA_9$ fiber diameters were 2-3 times larger than $PnBA_{90}$-*co*-$PSBMAm_{10}$. A hydrogen bonding effect of the amide bond likely contributed to this phenomenon.

6.6 Acknowledgement This material is based upon work supported by the U.S. Army Research Laboratory and the U.S. Army Research Office under grant number W911NF-07-1-0339. Matthew T. Hunley contributed significantly to this work with expertise in electrospinning and rheology, and valuable discussions concerning data analysis.

6.7 References

(1) Lowe, A. B.; McCormick, C. L. *Chem Rev* **2002**, *102*, 4177-4189.
(2) Nakaya, T.; Li, Y. J. *Prog. Polym. Sci.* **1999**, *24*, 143-181.
(3) Galin, M.; Chapoton, A.; Galin, J. C. *J. Chem. Soc. Perkin Trans.* **1993**, *2*, 545-553.
(4) Galin, M.; Marchal, E.; Mathis, A.; Galin, J. C. *Polym. Adv. Technol.* **1997**, *8*, 75-86.
(5) Galin, M.; Marchal, E.; Mathis, A.; Meurer, B.; Soto, Y. M. M.; Galin, J. C. *Polymer* **1987**, *28*, 1937-1944.

(6) Ehrmann, M.; Galin, J. C. *Polymer* **1992**, *33*, 859-865.
(7) Ehrmann, M.; Galin, J. C.; Meurer, B. *Macromolecules* **1993**, *26*, 988-993.
(8) Ehrmann, M.; Mathis, A.; Meurer, B.; Scheer, M.; Galin, J. C. *Macromolecules* **1992**, *25*, 2253-2261.
(9) Ehrmann, M.; Muller, R.; Galin, J. C.; Bazuin, C. G. *Macromolecules* **1993**, *26*, 4910-4918.
(10) Galin, M.; Mathis, A.; Galin, J. C. *Macromolecules* **1993**, *26*, 4919-4927.
(11) Greiner, A.; Wendorff, J. H. *Angew. Chem., Int. Ed.* **2007**, *46*, 5670-5703.
(12) Mathis, A.; Zheng, Y. L.; Galin, J. C. *Makromol. Chem., Rapid Commun.* **1986**, *7*, 333-337.
(13) Mathis, A.; Zheng, Y. L.; Galin, J. C. *Polymer* **1991**, *32*, 3080-3085.
(14) Gauthier, M.; Carrozzella, T.; Penlidis, A. *J. Polym. Sci., Part A: Polym. Chem.* **2002**, *40*, 511-523.
(15) Gauthier, M.; Carrozzella, T.; Snell, G. *J. Polym. Sci., Part B: Polym. Phys.* **2002**, *40*, 2303-2312.
(16) Georgiev, G. S.; Karnenska, E. B.; Vassileva, E. D.; Kamenova, I. P.; Georgieva, V. T.; Iliev, S. B.; Ivanov, I. A. *Biomacromolecules* **2006**, *7*, 1329-1334.
(17) Huglin, M. B.; Radwan, M. A. *Makromol. Chem., Macromol. Chem. Phys.* **1991**, *192*, 2433-2445.
(18) Kudaibergenov, S.; Jaeger, W.; Laschewsky, A. *Adv. Polym. Sci.* **2006**, *201*, 157-224.
(19) Lowe, A. B.; McCormick, C. L. In *Symposium on Polyelectrolytes and Polyzwitterions held at the 228 ACS National Meeting*; Lowe, A. B., McCormick, C. L., Eds. Philadelphia, PA, 2004, p 65-78.
(20) Doshi, J.; Reneker, D. H. *J. Electrost.* **1995**, *35*, 151-60.
(21) Fong, H.; Chun, I.; Reneker, D. H. *Polymer* **1999**, *40*, 4585-4592.
(22) Kenawy, E.-R.; Layman, J. M.; Watkins, J. R.; Bowlin, G. L.; Matthews, J. A.; Simpson, D. G.; Wnek, G. E. *Biomaterials* **2003**, *24*, 907-913.
(23) Shin, Y. M.; Hohman, M. M.; Brenner, M. P.; Rutledge, G. C. *Polymer* **2001**, *42*, 9955-9967.
(24) McKee, M. G.; Wilkes, G. L.; Colby, R. H.; Long, T. E. *Macromolecules* **2004**, *37*, 1760-1767.
(25) Shenoy, S. L.; Bates, W. D.; Frisch, H. L.; Wnek, G. E. *Polymer* **2005**, *46*, 3372-3384.
(26) Yu, J. H.; Fridrikh, S. V.; Rutledge, G. C. *Polymer* **2006**, *47*, 4789-4797.
(27) Brown, R. H.; Hunley, M. T.; Allen, M. H.; Long, T. E. *Polymer* **2009**, *In Press*.
(28) Colby, R. H.; Fetters, L. J.; Funk, W. G.; Graessley, W. W. *Macromolecules* **1991**, *24*, 3873-3882.
(29) Colby, R. H.; Rubinstein, M. *Macromolecules* **1990**, *23*, 2753-2757.
(30) de Gennes, P. G. *Scaling Properties in Polymer Physics*; Cornell University Press: Ithaca, NY, 1979.
(31) Krause, W. E.; Tan, J. S.; Colby, R. H. *Journal of Polymer Science Part B-Polymer Physics* **1999**, *37*, 3429-3437.
(32) Rubinstein, M.; Semenov, A. N. *Macromolecules* **2001**, *34*, 1058-1068.
(33) Semenov, A. N.; Rubinstein, M. *European Physical Journal B* **1998**, *1*, 87-94.
(34) Semenov, A. N.; Rubinstein, M. *Macromolecules* **2002**, *35*, 4821-4837.
(35) Graessley, W. W. *Polymer* **1980**, *21*, 258-262.
(36) Tobing, S. D.; Klein, A. *J. Appl. Polym. Sci.* **2001**, *79*, 2230-2244.

(37) Tong, J. D.; Jerome, R. *Macromolecules* **2000**, *33*, 1479-1481.
(38) McKee, M. G.; Hunley, M. T.; Layman, J. M.; Long, T. E. *Macromolecules* **2006**, *39*, 575-583.
(39) Dobrynin, A. V.; Rubinstein, M. *Prog. Polym. Sci.* **2005**, *30*, 1049-1118.
(40) Wang, C.; Hsu, C.-H.; Hwang, I.-H. *Polymer* **2008**, *49*, 4188-4195.
(41) de Gennes, P. G.; Pincus, P.; Velasco, R. M.; Brochard, F. *J. Phys. (Paris)* **1976**, *37*, 1461.
(42) Pfeuty, P. *J. Phys., Collog.* **1978**, *39*, C2-149.
(43) Dobrynin, A. V.; Colby, R. H.; Rubinstein, M. *Macromolecules* **1995**, *28*, 1859-1871.

Chapter 7: Effect of Ionic Liquid on Mechanical Properties and Morphology of Zwitterionic Copolymer Membranes

Brown, R.H.; Duncan, A.J.; Choi, J-H.; Park, J.K.; Wu, T.; Leo, D.J.; Winey, K.I.; Moore, R.B.; Long, T.E. *Macromolecules* (submitted).

7.1 Abstract

Ionomers containing less than 13 mol % zwitterion functionality were synthesized using free radical copolymerization of n-butyl acrylate (nBA) and sulfobetaine monomers. X-ray scattering results revealed a two-phase morphology, which is typical of random ionomers with an ionomer peak at ~1.5 nm^{-1}. Swelling studies in the ionic liquid (IL), 1-ethyl-3-methylimidazolium ethyl sulfate (EMIm ES), showed an influence of zwitterionic structure on IL uptake. Zwitterionomer membranes were swollen to various IL contents, and the influence of IL on mechanical properties, morphology, and ionic conductivity were explored through dynamic mechanical analysis (DMA), x-ray scattering, and impedance spectroscopy, respectively. Results revealed that IL preferentially swelled the zwitterionic domains, but was excluded from the matrix phase. Significant changes in mechanical properties and ionic conductivity were observed above a critical uptake of IL. Fundamental explorations of the interaction of ILs with sulfobetaine-containing copolymers may lead to the use of zwitterionomers in emerging membrane applications.

7.2 Introduction

Polybetaines are a class of zwitterionic polymers featuring a covalently bound cation and anion on each repeating unit. The presence of two oppositely charged groups bound in close proximity creates a large dipole moment, lending many unique properties to the betaine structure. Zwitterionic structures based on ammonioalkanesulfonates (sulfobetaines) have received significant attention from Galin and others due to their high dipole moments, reported as $\mu \sim 18.7\text{-}27.6$ D.[1] These chemical structures are stable over a wide range of temperatures and feature permanent charge over a large pH range. Polymeric betaines exhibit remarkable miscibility with various inorganic and metal salts up to stoichiometric quantities.[2-4] These salt-polyzwitterion mixtures formed amorphous blends due to strong ion-dipole interactions that precluded salt segregation or crystallization within the zwitterion matrix for a variety of different inorganic salts. This unique ability to dissolve large amounts of salts has sparked interest in polyzwitterions as polymeric host matrices for polar guest molecules.[4]

While polymeric betaines are well studied in the literature,[5,6] much less attention has been devoted to random copolymers featuring zwitterionic sites. Galin and coworkers[7,8] introduced copolymers of sulfobetaines with 2-ethoxyethyl acrylate as a new class of low T_g ionomers for biphasic materials with properties potentially better than cationic ionomers of similar structure. Subsequent studies with copolymers incorporating a poly(n-butyl acrylate) (PnBA) matrix confirmed these zwitterionic copolymers exhibited mechanical properties and morphologies similar to classical ionomers.[9-12] Detailed structural and morphological analysis revealed a morphology in agreement with the EHM model,[13] where increasing zwitterionic content led to development of a phase separated system with a second high temperature T_g representing overlapping regions of restricted mobility surrounding phase-separated multiplets.[11]

Ionic liquids (ILs) have become increasingly important in recent years for applications spanning many fields of chemistry. ILs are molten salts that are liquids below 100 °C and exhibit excellent properties including chemical and thermal stability, low vapor pressure, and high ionic conductivity.[14] Although widely used as solvents for synthesis and extractions, ILs are also used as diluents in polymer membranes to afford high conductivities for applications including lithium batteries,[15,16] solar cells,[14,17,18] and electromechanical transducers.[19-23] For example, replacing water with an IL as the diluent in Nafion™ membranes for ionic polymer transducers resulted in an increase from 30,000 cycles to more than 250,000 cycles.[24] This drastic change was due to a lack of solvent evaporation for ILs, which led to deterioration of transducer performance after 30,000 cycles with water as the diluent.

The goal of the present study is to explore the interaction of ionic liquids with low T_g ionomers featuring moderate loadings of dipolar sulfobetaine-based zwitterions. ILs are expected to interact with the zwitterion functionality in a similar fashion to inorganic salts or polar liquids (water, glycerol, ethylammonium nitrate) as previously reported.[25] DMA, SAXS, and impedance spectroscopy are employed to determine the partitioning of IL within the zwitterionic membrane, as well as its effects on polymer morphology. Incorporation of ILs with high ionic conductivities into zwitterion-containing copolymers may have implications in the use of zwitterionomer membranes in electronic devices, where the lack of mobile counterions in the membrane serves as a fundamental difference from current ionomers.

7.3 Experimental

7.3.1 Materials

Zwitterionic monomers, *N*-(3-sulfopropyl)-*N*-methacryl-oxyethyl-*N,N*-dimethyl-ammonium betaine (SBMA) and N-(3-sulfopropyl)-N-methacryloylamidopropyl-N,N-dimethylammonium betaine (SBMAm), were generously provided by Raschig GMBH and used without purification. Dimethylsulfoxide (DMSO, 99.9+%), azobisisobutyronitrile (AIBN), and n-butyl acrylate (nBA) were purchased from Sigma-Aldrich Chemical Co. AIBN was recrystallized from methanol. n-Butyl acrylate (nBA) was passed through a neutral alumina column and distilled under reduced pressure from CaH_2. Chloroform (Optima grade) was purchased from Fisher Scientific and used without further purification. 1-Ethyl-3-methylimidazolium ethylsulfate (EMIm ES) was purchased from Alfa Aesar and stored over molecular sieves.

7.3.2 Synthesis of sulfobetaine methacrylate-*co*-butyl acrylate copolymers

A typical copolymerization is described. nBA (13.4 g, 0.105 mol) and SBMA (3.26 g, 0.012 mol) were added to a 250-mL, round-bottomed flask equipped with a magnetic stir bar. The reaction mixture was diluted with DMSO (137 mL, 90 wt %), and AIBN (83 mg, 0.50 wt %) was added to the reaction vessel. The reaction was sparged with N_2 for 15 min and placed in an oil bath at 60 °C for 24 h. The polymer was precipitated into 4 L of water and dried under reduced pressure. Residual DMSO was removed with reduced pressure (0.4 mm Hg) at 60 °C. The isolated polymer was dried under reduced pressure at 80 °C for 48 h and stored in a desiccator. Sulfobetaine methacrylamide-*co*-butyl acrylate copolymers (PnBA-*co*-PSBMAm)

were synthesized and purified under similar conditions, according to previously reported methods.[26]

7.3.3 Membrane Preparation and Swelling in Ionic Liquid

Films were solution cast from chloroform (0.1 g/mL) into Teflon molds to achieve a thickness of 0.25-0.30 mm. Films were dried at room temperature overnight, then heated at 80 °C for 72 h under vacuum prior to characterization or treatment. Dry films were cut into strips approximately 20 mm x 5 mm. Films pieces were immersed in EMIm ES and stored in sealed glass vials inside a desiccator maintained at 20% relative humidity (RH). Film pieces were periodically weighed to determine the uptake of IL. Films were removed using forceps and blotted with a Kimwipe to remove excess EMIm ES on the polymer surface. IL uptake was calculated according to the following equation: % uptake = $(m- m_o)/m_o$, where m_o is the initial dry film mass and m is the mass of the swollen film at a given time. IL uptake is also reported as a molar ratio of EMIm ES relative to the number of zwitterionic units in the membrane.

7.3.4 Instrumentation

^{1}H NMR spectra of the polymers were obtained on a Varian Unity 400 MHz spectrometer in $CDCl_3$. Molar compositions of the polymers were determined by comparison of shifts at 1.0 ppm for the $–CH_3$ on nBA with the $–CH_3$ groups on the quaternary ammonium of the sulfobetaine unit at 3.20 ppm.[27] Size exclusion chromatography (SEC) was used to determine the molecular weights of zwitterionomers at 50 °C in *N*,*N*-dimethyformamide (DMF) with 0.01M lithium bromide (LiBr) at 1 mL min^{-1}. DMF SEC was performed on a Waters SEC equipped with two Waters Styragel HR5E (DMF) columns, a Waters 717plus autosampler, and a

Waters 2414 differential refractive index detector. Reported molecular weights are relative to polystyrene standards. Dynamic mechanical analysis (DMA) measurements were performed on a TA Instruments Q800 dynamic mechanical analyzer in tension mode at a frequency of 1Hz and a temperature ramp of 3 °C min^{-1} over the range -90 to 150 °C. Transitions are reported as peak values in the loss modulus.

Electrical impedance spectroscopy (EIS) was performed with an Autolab PGSTAT12 Potentiostat/Galvanostat with FRA2 Impedance Module from 1 MHz – 0.1 Hz. The instrument was operated in potentiostatic mode to apply a single 100 mV rms sine wave while measuring the complex impedance response of the sample. A custom fixture aligned two parallel rectangular brass rods at a defined separation of 0.3 cm to allow for in-plane impedance measurements. Ionic conductivity values (σ, S/cm) were calculated according to $\sigma = t/(R\ l\ w)$, where R is the bulk membrane resistance (Ohms), t (cm) is the sample thickness, l (cm) is the sample length, and w (cm) is the sample width. The kinetic portion of the complex impedance data (Nyquist plot) was fit with a semicircle to extrapolate the membrane resistance as the low frequency x-intercept where the imaginary impedance equals zero.

Scattering measurements were performed with a multiangle X-ray scattering system (MAXS) equipped with a Nonius FR 591 rotating-anode Cu X-ray generator operated at 40 kV and 85 mA. The beam was focused with Confocal Max-Flux optics in an integral vacuum system. Scattering data were collected over a 1 h interval using a Bruker Hi-Star multiwire detector with a sample-to-detector distance of 11, 54, and 150 cm. 2-D data reduction and analysis were performed using *Datasqueeze* software.

7.4 Results and Discussion

7.4.1 Synthesis and Characterization of Zwitterionomers

Zwitterionic copolymers containing 6 and 9 mol % of SBMA or 6, 10, and 13 mol % of SBMAm (Figure 7.1) were synthesized using free radical copolymerization in DMSO to afford high molecular weight zwitterionomers. ^{1}H NMR spectroscopy confirmed the copolymer composition matched the feed within 1 mol % for all compositions. Copolymer molecular weights were determined using SEC in DMF with 0.01M LiBr, and values relative to polystyrene standards are reported in Table 7.1. Dynamic light scattering was performed prior to SEC to indentify the optimal solvent composition and ensure minimal aggregation in DMF with LiBr. The purified polymers were soluble in chloroform and membranes were solution cast from chloroform into Teflon molds to form ductile, free-standing membranes. Copolymer membranes were dried thoroughly under vacuum at 80 °C to remove residual chloroform and absorbed water, then stored in a desiccator prior to swelling or analysis.

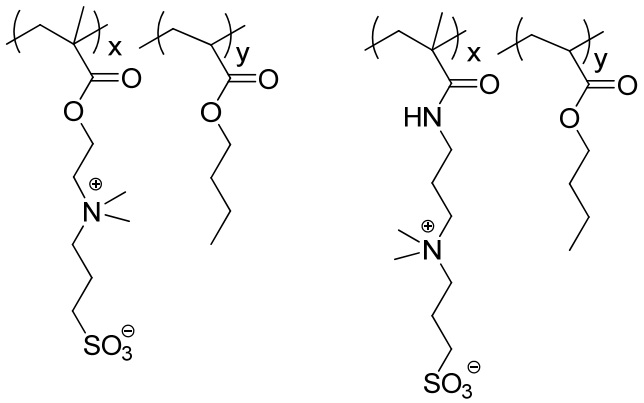

Figure 7.1 Structure of zwitterionic copolymers, (a) PnBA-*co*-PSBMA and (b) PnBA-*co*-PSBMAm

Table 7.1 Relative molecular weights of zwitterionomers

Copolymer	M_n (g/mol)	M_w (g/mol)	M_w/M_n
$PnBA_{94}$-*co*-$PSBMA_6$	165,000	460,000	2.78
$PnBA_{91}$-*co*-$PSBMA_9$	141,000	324,000	2.31
$PnBA_{91}$-*co*-$PSBMA_9$	105,000	265,000	2.51
$PnBA_{94}$-*co*-$PSBMAm_6$	214,000	519,000	2.42
$PnBA_{90}$-*co*-$PSBMAm_{10}$	134,000	344,000	2.65
$PnBA_{90}$-*co*-$PSBMAm_{10}$	141,000	295,000	2.11
$PnBA_{87}$-*co*-$PSBMAm_{13}$	94,100	259,000	2.75

Previous DMA studies showed that PnBA-*co*-PSBMA and PnBA-*co*-PSBMAm zwitterionomer membranes exhibited two-phase morphologies indicative of ionic aggregation.[12,26,28] In our current study, X-ray scattering results revealed the bulk morphology of zwitterionic membranes, and all samples exhibited isotropic rings in the 2D scattering patterns. Figure 7.2 shows the multi-angle X-ray scattering profiles for a series of PnBA-*co*-PSBMA copolymers and corresponding homopolymers as a log-log plot of scattering intensity versus the scattering vector q. Three primary scattering peaks were observed for the zwitterionic copolymers. A peak at ~14 nm^{-1} was observed for the zwitterionomers as well as both homopolymers. This peak is characteristic of amorphous polymers and is attributed to local ordering of pendant chains due to van der Waals forces.[29] A peak at ~5 nm^{-1} was observed in both PnBA and the zwitterionomers, and this peak was attributed to local ordering of chain segments or the distance between polymer main chains, in accordance with assignments made earlier by Miller and Boyer.[29]

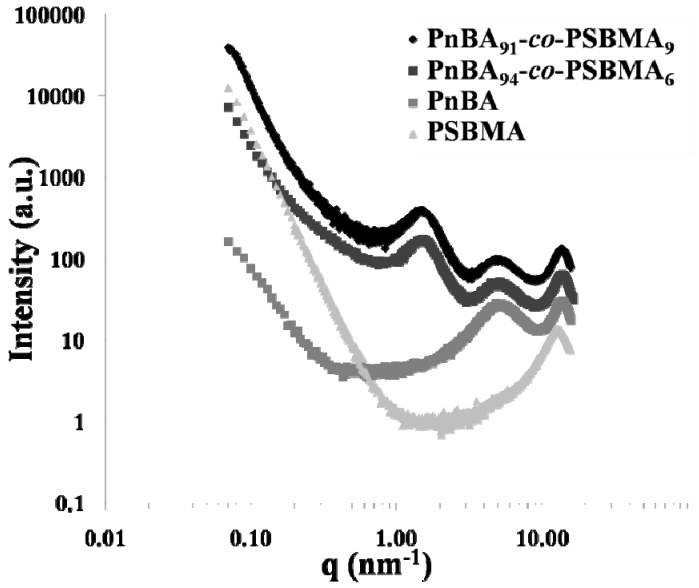

Figure 7.2 X-ray scattering intensity vs. scattering vector (q) for PnBA-*co*-PSBMA (9 and 6 mol%), PnBA, and PSBMA

The broad peak at ~1.5 nm^{-1} was observed only in the zwitterionic copolymers and may be classified as an ionomer peak, which confirmed the presence of a second ionic phase that was observed in DMA.[12,26] The ionomer peak is typically broad in random ionomers due to a range of spacings between ionic domains. This scattering peak at low q corresponded to a Bragg spacing (d) of approximately 4 nm and exhibited a slight dependence on ion content as the peak maximum shifted slightly to higher q with increasing SBMA content. This spacing was consistent with other zwitterionic copolymers[8,11] as well as random ionomers[13,30-32] reported in the literature. Similar results were also obtained for the PnBA-*co*-PSBMAm copolymers as shown in Figure 7.3. Ionomer peak positions as a function of zwitterionomer content and the corresponding d spacings are summarized in Table 7.2.

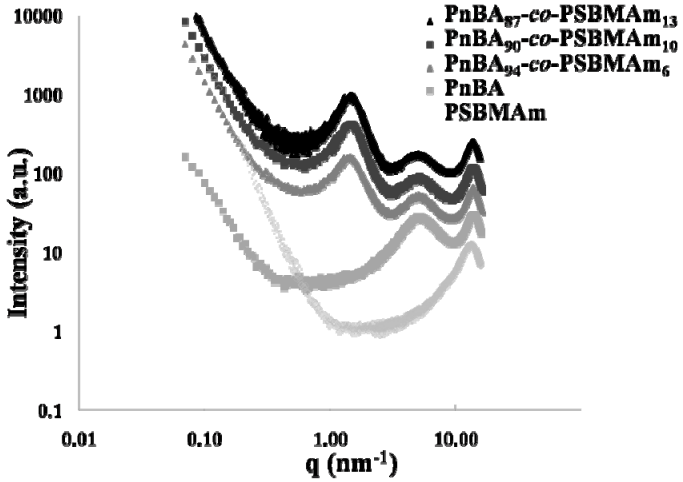

Figure 7.3 X-ray scattering intensity vs. scattering vector (q) for PnBA-*co*-PSBMAm (13, 9, and 6 mol%), PnBA, and PSBMAm

Table 7.2 Summary of scattering peaks and d-spacings for zwitterionomers, PnBA, and zwitterionic homopolymers

Polymer Composition	**Peak Position (nm^{-1})**			**d spacing, ionomer peak (nm)**
$PnBA_{91}$-*co*-$PSBMA_9$	13.7	4.92	1.52	4.13
$PnBA_{94}$-*co*-$PSBMA_6$	13.7	4.92	1.45	4.33
$PnBA_{87}$-*co*-$PSBMAm_{13}$	13.7	4.97	1.54	4.08
$PnBA_{90}$-*co*-$PSBMAm_{10}$	13.7	4.97	1.46	4.30
$PnBA_{94}$-*co*-$PSBMAm_6$	13.7	4.97	1.39	4.52
PnBA	13.7	5.2	--	--
PSBMA	12.8	--	--	--
PSBMAm	13.2	--	--	--

7.4.2 Swelling of Zwitterionomers in Ionic Liquid

While the affinity of polybetaines for water and inorganic salts are well documented, their interactions with ILs have received little attention.[33] The IL chosen for this study was 1-ethyl-3-methylimidazolium ethylsulfate (EMIm ES), as shown in Figure 7.4. EMIm ES is a water-miscible IL with a melting point of -65 °C and bulk conductivity (σ) of 3.82 mS cm^{-1} at 298K.

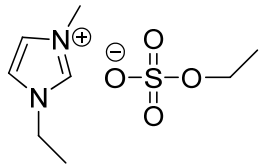

Figure 7.4 Chemical **s**tructure of 1-ethyl-3-methylimidazolium ethylsulfate (EMIm ES).

Copolymer membranes were placed in scintillation vials of EMIm ES and stored in a desiccator at constant RH for the duration of the swelling study. The original dry mass was recorded, and the uptake of IL was measured as a function of weight gain over a period of several months. Initial studies of membrane swelling in EMIm ES were performed on all SBMA and SBMAm copolymers that contained 6-13 mol % zwitterion. These preliminary data showed a significant effect of zwitterion loading on the amount of IL uptake. Very low swelling levels were observed for copolymers with 6 mol % zwitterion, and the IL uptake was difficult to accurately measure using gravimetric techniques. Copolymers with 9 or 10 mol % zwitterion content showed moderate swelling, while the 13 mol % SBMAm copolymer exhibited the largest swelling capacity. These results showed that the IL had a large affinity for the polar zwitterionic phase, leading to higher swelling levels at increasing zwitterion concentrations. The inability to swell the membranes with a significant amount of ionic liquid at zwitterion contents of only 6

mol % suggested the absence of a percolated ionic phase throughout the membranes, which limited the transport of ionic liquid.

This preliminary study also highlighted the influence of sample dimensions, sample history, and swelling conditions on the reproducibility of swelling measurements. When swelling was conducted in closed containers on the benchtop without control of temperature or humidity, much larger increases in weight were observed reaching >100%, suggesting a synergistic effect of water with IL in the swelling process. Also, drastic differences in the kinetics of swelling were observed among membranes of various sizes and thicknesses. Therefore, constant conditions for film formation, annealing, and swelling were adopted to minimize variations in swelling times.

For the purpose of this study, we chose to focus on $PnBA_{91}$-*co*-$PSBMA_9$ (M_w 324,000) and $PnBA_{90}$-*co*-$PSBMAm_{10}$ (M_w 295,000) in more depth in order to maintain a good comparison between these two zwitterionomer classes. Swelling results for the zwitterionomers containing ~10 mol % betaine functionality , were plotted as percent weight gain versus time as shown in Figure 7.5. It is readily apparent that despite similar zwitterion loadings, molecular weights, and solid state properties, these membranes exhibited significantly different swelling behaviors. The maximum uptake observed for $PnBA_{91}$-*co*-$PSBMA_9$ within the period of this study was 40 wt %, while $PnBA_{90}$-*co*-$PSBMAm_{10}$ plateaued at 14 wt %. Small differences in film thickness (0.23 mm and 0.28 mm) were not sufficient to explain this drastic difference in behavior. We propose that the presence of synergistic hydrogen bonding in the amide-linked zwitterionomer provided additional ionic aggregate stability, causing a decrease in the overall IL uptake within the polar ionic phase. Further studies to confirm this hypothesis are needed. This controlled swelling data were used to determine the swelling time for copolymer membranes to reach various swelling

levels; comprehensive characterization of the influence of IL uptake on membrane mechanical properties, morphology, and conductivity was performed.

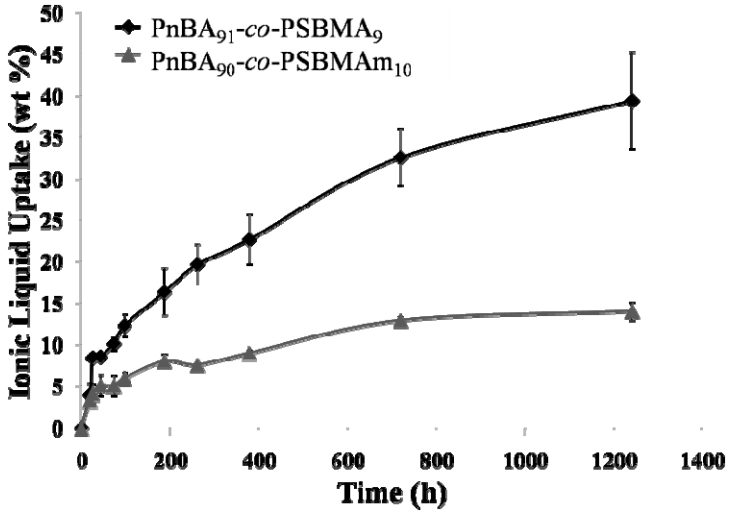

Figure 7.5 Swelling behavior of $PnBA_{91}$-*co*-$PSBMA_9$ and $PnBA_{90}$-*co*-$PSBMAm_{10}$ in EMIm ES as a function of time.

7.4.3 Mechanical Properties of Ionic Liquid Swollen Membranes

The thermal and mechanical properties of both neat state and swollen zwitterionic membranes were characterized using DMA. Gauthier and coworkers reported DMA behavior of PnBA-*co*-PSBMA of varying compositions.[28] At low zwitterion contents, two thermal transitions were observed in DMA, as well as the presence of a rubbery plateau due to physical ionic crosslinking within the zwitterionic domains. Similar behavior was observed for $PnBA_{91}$-*co*-$PSBMA_9$ (M_w 265,000) in the neat state, as shown in Figure 7.6 (solid line). The first transition corresponded to the T_g of the ion-poor matrix phase of the copolymer, i.e. PnBA. The second transition, which occurs between 80 and 90 °C at the end of the rubbery plateau, may be attributed to the T_g of the ion-rich phase.

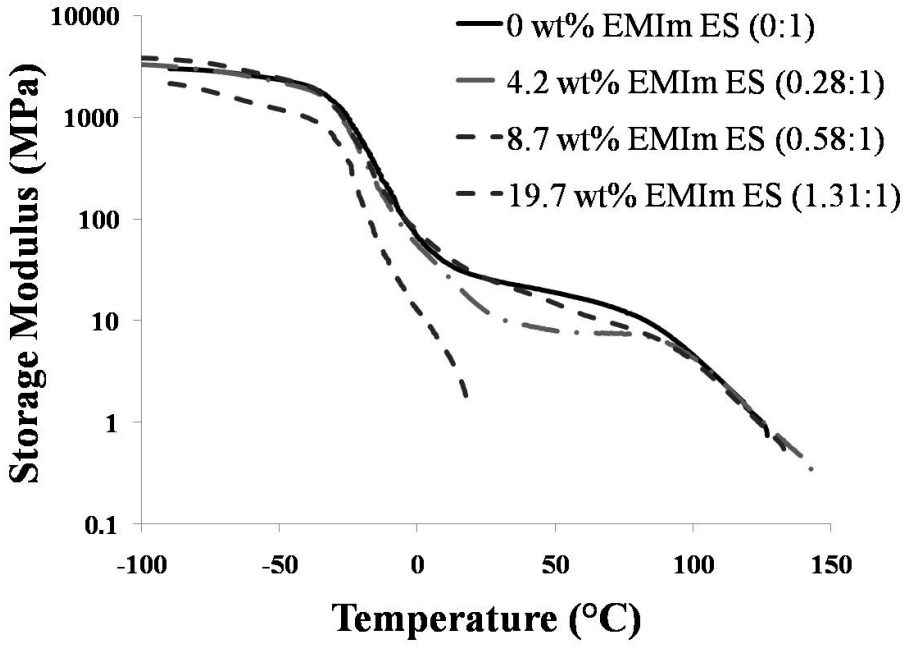

Figure 7.6 DMA storage modulus as a function of temperature for $PnBA_{91}$-*co*-$PSBMA_9$ (M_w 265,000 g/mol) at various levels of swelling in EMIm ES

Upon swelling with EMIm ES, the matrix phase T_g decreased within experimental error from -26 °C without IL present to -28 °C at 19.7 wt % swelling. However, the rubbery plateau region and the ion-rich phase T_g revealed substantial differences with increasing IL content. At low swelling levels below 10 wt % IL, corresponding to less than 0.65 mol EMIm ES per mol SB, mechanical properties remained virtually unchanged within the experimental error. At 19.7 wt % IL (1.31 mol IL: mol SBMA), a rubbery plateau was not observed and flow occurred below 25 °C. The insignificant change in T_g of the PnBA phase at increasing levels of IL uptake indicated that the water-miscible IL did not significantly influence the hydrophobic PnBA matrix. The disappearance of the rubbery plateau at higher swelling levels indicated that the ion-rich domains were preferentially swollen with IL. Galin and coworkers[25] studied the

plasticization of zwitterionic copolymers consisting of a PnBA matrix with plasticizers of drastically different polarities. Dibutyl phthalate (DBP), which has a high affinity for PnBA, was incorporated homogeneously into both phases of the copolymer. However, incorporation of ethylammonium nitrate (EAN) or water, which have high affinities for the dipolar zwitterions, resulted in the plasticization of only the ion-rich phase.[25] For IL swelling, EMIm ES was expected to have a high affinity for the ionic domains, and only the matrix T_g as determined using DMA was observed at 19.7 wt % EMIm ES. This drastic decrease in the T_g of the zwitterionic phase is also in agreement with the observed plasticization behavior of ionomers.[34,35] Polar plasticizers are known to selectively incorporate into the ionic phase (multiplets), which reduces the electrostatic interaction between ion pairs and increases the mobility of the polymer chains attached to the ionomer multiplets.[35]

Similar mechanical properties for swelling levels up to ~10 wt % were also observed for $PnBA_{90}$-*co*-$PSBMAm_{10}$ (M_w 295,000). Storage modulus as a function of temperature is plotted in Figure 7.7 for $PnBA_{90}$-*co*-$PSBMAm_{10}$ at swelling levels of 0, 5, and 10 wt % EMIm ES. The observed similarity of mechanical properties at low swelling levels in both copolymer membranes suggested the presence of a critical IL uptake level, and significant changes in polymer morphology and mechanical performance were expected above this critical level. This critical uptake level was estimated between 10.1 and 19.7 wt % (0.62-1.31 mol IL:SB), and the drastic change in behavior at 19.7 wt % may indicate the exact transition occurred at a composition closer to 10.1 wt %. This assumption is further correlated with ionic conductivity data presented later. Galin et al.[25] suggested the presence of a transition or plateau region between 0.7 and 1.5 mol EAN/mol SB in the plasticization of PnBA-*co*-PSBMAm copolymers, which was tentatively related to observed behavior in the plasticization of ionomers with polar

diluents. A large shift in Bragg spacing to lower q in the SAXS profile was attributed to a rearrangement of the ionic domains, presumably involving the coalescence of ionic regions into fewer, larger aggregates.[13,25] We studied the relevance of this morphological change to zwitterionic membranes with IL using x-ray scattering analysis as a function of IL content.

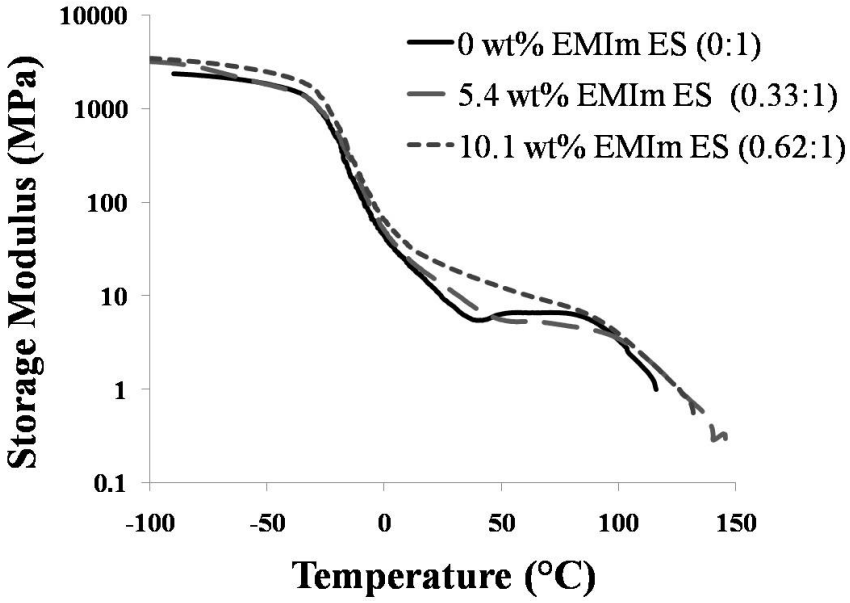

Figure 7.7 Storage modulus vs. temperature profiles for $PnBA_{90}$-*co*-$PSBMAm_{10}$ (M_w 295,000 g/mol) at various swelling levels

7.4.4 Morphological Changes in the Presence of Ionic Liquid

Swelling of the membrane zwitterionic domains was expected to cause changes in the zwitterionomer morphology, especially in the ionomer peak of the SAXS profile. X-ray scattering profiles, plotted as intensity vs scattering vector q on a log-log plot, at various IL swelling levels of $PnBA_{91}$-*co*-$PSBMA_9$ are shown in Figure 7.8. The scattering profile in the absence of IL is identical to Figure 7.2. The ionomer peak systematically shifted to lower q as the ionic liquid content increased, i.e. 1.49 nm^{-1} at 0 wt % to 0.87 nm^{-1} at 46 wt % EMIm ES.

This highest swelling level corresponded to 3.13 mol EMIm ES per mol of SB functionality. The other two peaks in the MAXS profiles at 4.9 and 13.7 nm^{-1} remained unchanged with increasing IL content. The shift of the ionomer peak and the lack of change in the peak representing the ordering of the polymer matrix (~4.9 and 13.7 nm^{-1}) confirmed our hypothesis that the water-miscible EMIm ES swelled the zwitterionic domains preferentially without affecting the matrix phase, and supported the dynamic mechanical behavior. Furthermore, a similar shift of the ionomer peak with increasing IL content was observed for $PnBA_{90}$-*co*-$PSBMAm_{10}$, as shown in Figure 7.9 for swelling levels of 0, 5, and 10 wt % EMIm ES. The scattering peak locations, corresponding Bragg spacings of the ionomer peaks, and the ionic liquid contents are summarized in Table 7.3.

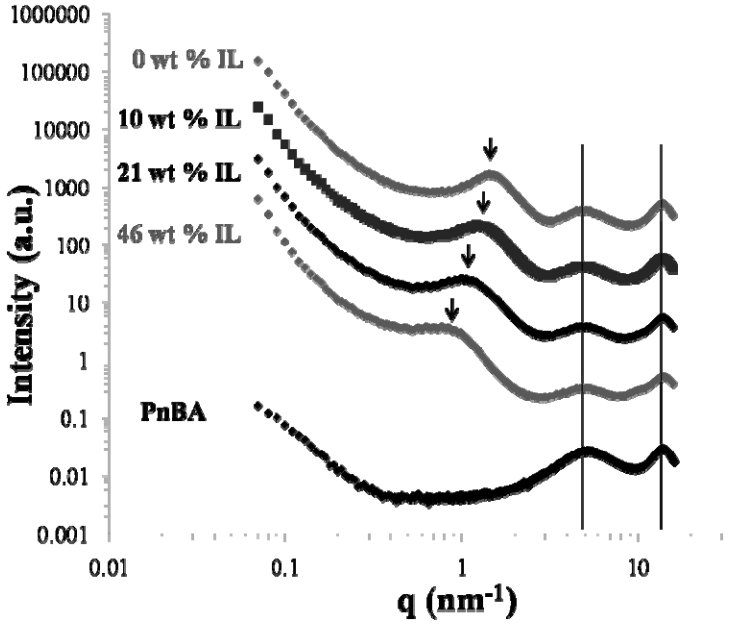

Figure 7.8 X-ray scattering intensity vs. scattering vector (q) for $PnBA_{91}$-*co*-$PSBMA_9$ at increasing levels of IL content showing the shift in the ionomer peak; PnBA is also plotted for comparison of the high q region

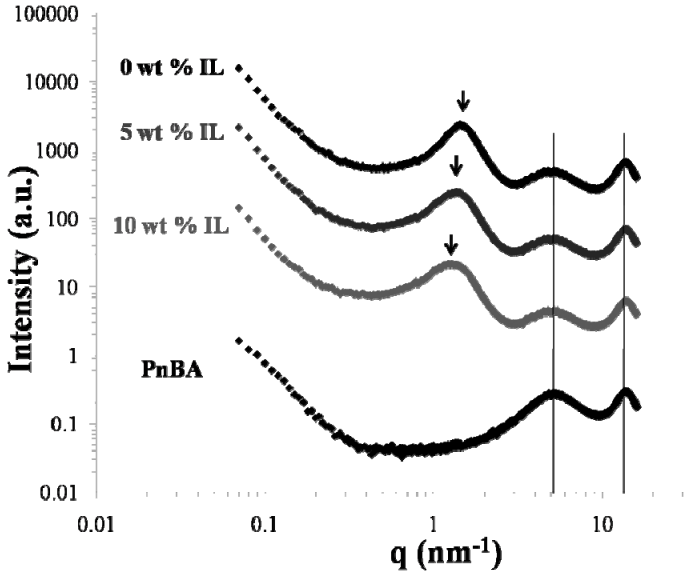

Figure 7.9 X-ray scattering intensity vs. scattering vector (q) for $PnBA_{90}$-*co*-$PSBMAm_{10}$ at three swelling levels of IL showing a shift in the ionomer peak; PnBA is also plotted for comparison of the high q region

Table 7.3 Summary of scattering peaks and d-spacings for zwitterionomers swollen in IL

Copolymer	IL Content (wt %)	IL Content (mol IL:mol SB)	Peak Position (nm^{-1})			d spacing (nm)
$PnBA_{91}$-*co*-$PSBMA_9$	0	0:1	13.7	4.91	1.49	4.22
	10	0.64:1	13.7	4.91	1.28	4.91
	15	1.0:1	ND	ND	1.07	5.87
	21	1.40:1	13.7	4.91	1.06	5.93
	46	3.13:1	13.7	4.91	0.87	7.22
$PnBA_{90}$-*co*-$PSBMAm_{10}$	0	0:1	13.7	5.04	1.43	4.39
	5	0.31:1	13.7	5.04	1.38	4.55
	10	0.62:1	13.7	5.04	1.28	4.91
PnBA	0	0	13.7	5.18	--	--

Gierke et al. first proposed a cluster-network model for Nafion™ ionomers, then Eisenberg[13] and others modified this general model to account for various other experimental observations for ionomers. In general, these models feature a spherical ionic cluster phase within a continuous matrix phase.[36] Based on this model, the angular position of the ionomer peak in the SAXS profile represents the average spacing between centers of ionic clusters. Swelling studies of ionomers with polar diluents have supported this proposed morphology. Gierke et al. observed an increase in the average intercluster spacings with increasing water content in Nafion™.[36] Leo and coworkers[19,37] also observed similar increases upon swelling Nafion™ with two different ionic liquids. The increase in spacing was larger for swelling with the water-miscible IL EMI-Tf than for the hydrophobic IL EMI-Im. Similarly, a sizeable increase in the spacing was observed for swelling of zwitterionomers with EMIm ES in the present work. This increase in intercluster spacing likely corresponded to an increase in cluster size through plasticization with IL. An increase in d spacing was generally observed for many ionomers in the literature, and the multiplet-cluster morphology is well-documented. Unfortunately, modeling of the MAXS data for spherical domains using the Kinning-Thomas model[38] was not in agreement with the data in Figures 7.8 and 7.9. Future microscopy imaging of the ionic domains are needed to further understand the structure of the ionic domains and changes in domain size with increasing IL content.

7.4.5 Effect of IL Swelling on Membrane Conductivity

Electrical properties of the neat and IL-swollen zwitterionic copolymer membranes were analyzed using electrical impedance spectroscopy. Ionic conductivity was calculated from the resistance, as revealed from the x-intercept of a semi-circle fit on a Nyquist plot. Figure 7.10

shows the ionic conductivity as a function of both weight % IL uptake and molar ratio of IL to SBMA for $PnBA_{91}$-*co*-$PSBMA_9$. Conductivity values of the neat membranes were expected to be very low due to the absence of mobile counterions; ionic conductivities on the order of 10^{-9} S cm^{-1} are typical for synthetic polymers without diluent. Ionic conductivity increased with the addition of EMIm ES, reaching values on the order of 10^{-4} S cm^{-1} at 10-20 wt % or 0.7- 1.2 mol IL: SBma, and approaching the conductivity of pure EMIm ES, 3.82 mS cm^{-1}.

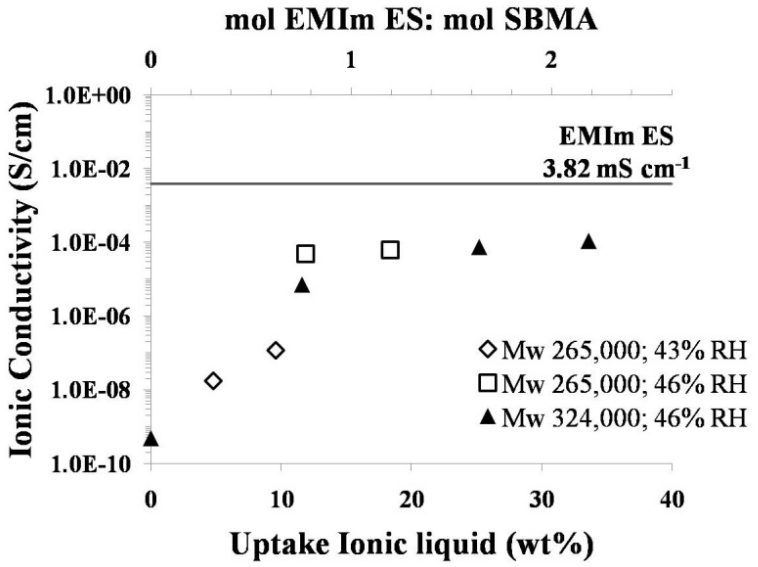

Figure 7.10 Semi-log plot of ionic conductivity vs. IL uptake for $PnBA_{91}$-*co*-$PSBMA_9$ membranes in EMIm ES.

The same conductivity results were also plotted on a linear scale to reveal the presence of a critical uptake point, above which a sizeable change in properties was observed (Figure 7.11). IL uptake between 0 and ~10 wt % resulted in very small differences in ionic conductivity, while a drastic increase occurred above 11.6 wt % IL. A critical uptake value between 10 and 12 wt %

was inferred from impedance analysis, in good agreement with the small influence of IL below 10 wt % on mechanical properties in DMA. More data points are necessary to further pinpoint the exact critical uptake, but there is reasonable evidence from both impedance spectroscopy and DMA that this change in behavior occurred just above 10 wt %.

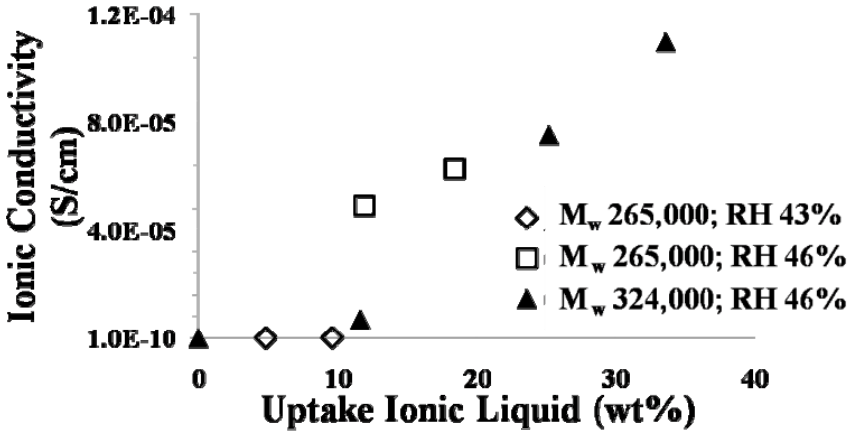

Figure 7.11 Ionic conductivity of $PnBA_{91}$-*co*-$PSBMA_9$ membranes in EMIm ES, plotted as a function of IL uptake, revealing a critical uptake transition

Ionic conductivity of $PnBA_{90}$-*co*-$PSBMAm_{10}$ membranes containing 5 and 10 wt %, 0.31 and 0.62 mol IL:SB, respectively, were also measured under the same conditions as $PnBA_{91}$-co-$PSBMA_9$ (265,000 g/mol), as shown in Figure 7.12. Ionic conductivities for both zwitterionomer families were comparable, measured within one order of magnitude at equivalent swelling levels. These results correlated well to DMA results, where similar mechanical properties were also observed at equivalent swelling levels for both zwitterionomer families.

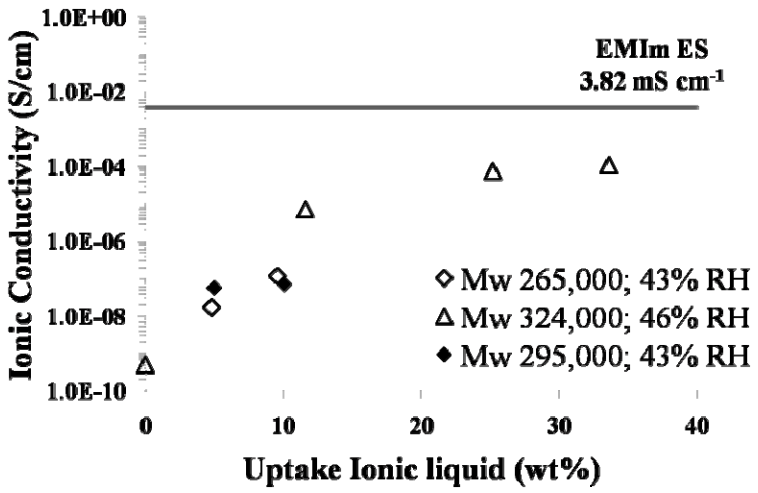

Figure 7.12 Semi-log plot of ionic conductivity vs IL uptake for $PnBA_{91}$-*co*-$PSBMA_9$ (◊, Δ) and $PnBA_{90}$-*co*-$PSBMAm_{10}$ (▲) membranes in EMIm ES

Impedance spectroscopy and subsequent resistance values are highly dependent on the environmental conditions during sample testing. Small differences in relative humidity of the testing chamber led to noticeable changes in ionic conductivity, as seen for the membrane of M_w 265,000 g/mol for two testing periods with differences of 3% RH. Testing with 3% higher RH led to conductivities about a half of an order of magnitude larger than expected based on the increasing trend. This trend is consistent with a higher water content for the membranes with larger conductivities. Ionic conductivity is also highly dependent upon sample preparation, water content, sample history, and electrode content. Relatively good agreement between membranes of different molecular weights and testing conditions was encouraging and indicated reproducibility of results.

7.5 Conclusions

Copolymers containing sulfobetaine-type zwitterions in a poly(n-butyl acrylate) matrix were synthesized using conventional free radical copolymerization in DMSO. X-ray scattering revealed a two-phase morphology of the neat membranes, with a characteristic ionomer peak at ~1.5 nm^{-1}. Zwitterionic membranes containing 9 or 10 mol % sulfobetaine were solution cast from chloroform and swollen in the water-miscible IL, EMIm ES. Zwitterion structure influenced the swelling behavior of the membranes, where IL uptake in ester-linked zwitterionic films was more than double the uptake for amide-linked zwitterionic films over equivalent swelling times. DMA revealed the disappearance of the rubbery plateau as the ion-rich phase was plasticized with increasing amounts of IL above 10 wt % IL. MAXS analysis showed a systematic shift to lower q with increasing IL uptake, without corresponding changes in scattering profiles at q ~4.9 nm^{-1}, corresponding to the local ordering of the polymer matrix chains. These results confirmed that the IL was preferentially swollen into the ionic domains without affecting the morphology of the nonpolar matrix. Ionic conductivity also increased with IL uptake, approaching the conductivity of pure IL. DMA and conductivity results for $PnBA_{91}$-co-$PSBMA_9$ indicated a critical uptake of IL near 11 wt %, above which significant changes in mechanical properties and increases in conductivity occurred. Ester- and amide-linked zwitterionomers at equivalent IL swelling levels exhibited very similar mechanical and electrical properties below 10 wt % IL. The observed critical IL content of ~11 wt %, or ~0.7 mol EMIm ES per mol of zwitterion functionality, is in agreement with Galin's hypothesis that a morphological change occurred at higher swelling levels.[25] Microscopy imaging is needed to fully understand the structure and changes in domain size and shape with increasing IL content.

7.6 Acknowledgements

This material is based upon work supported by the U.S. Army Research Laboratory and the U.S. Army Research Office under grant number W911NF-07-1-0339. Andrew J. Duncan and Prof. Donald Leo in the Mechanical Engineering Department at Virginia Tech allowed the use of equipment for impedance spectroscopy and assisted with data collection and analysis. Multi-angle x-ray scattering results were provided through a generous collaboration with Prof. Karen Winey and Jae-Hong Choi at The University of Pennsylvania. SAXS results were performed at Pohang Light Source (Korea) by Prof. Robert Moore and Jung-Keun Park of Virginia Tech.

7.7 References

(1) Galin, M.; Chapoton, A.; Galin, J. C. *J. Chem. Soc. Perkin Trans.* **1993**, *2*, 545-553.
(2) Koberle, P.; Laschewsky, A. *Macromolecules* **1994**, *27*, 2165-2173.
(3) Galin, M.; Marchal, E.; Mathis, A.; Meurer, B.; Soto, Y. M. M.; Galin, J. C. *Polymer* **1987**, *28*, 1937-1944.
(4) Galin, M.; Marchal, E.; Mathis, A.; Galin, J. C. *Polym. Adv. Technol.* **1997**, *8*, 75-86.
(5) Kudaibergenov, S.; Jaeger, W.; Laschewsky, A. *Adv. Polym. Sci.* **2006**, *201*, 157-224.
(6) Lowe, A. B.; McCormick, C. L. *Chem Rev* **2002**, *102*, 4177-4189.
(7) Mathis, A.; Zheng, Y. L.; Galin, J. C. *Makromol. Chem., Rapid Commun.* **1986**, *7*, 333-337.
(8) Mathis, A.; Zheng, Y. L.; Galin, J. C. *Polymer* **1991**, *32*, 3080-3085.
(9) Ehrmann, M.; Galin, J. C. *Polymer* **1992**, *33*, 859-865.
(10) Ehrmann, M.; Galin, J. C.; Meurer, B. *Macromolecules* **1993**, *26*, 988-993.
(11) Ehrmann, M.; Mathis, A.; Meurer, B.; Scheer, M.; Galin, J. C. *Macromolecules* **1992**, *25*, 2253-2261.
(12) Ehrmann, M.; Muller, R.; Galin, J. C.; Bazuin, C. G. *Macromolecules* **1993**, *26*, 4910-4918.
(13) Eisenberg, A.; Hird, B.; Moore, R. B. *Macromolecules* **1990**, *23*, 4098-4107.
(14) Lu, J. M.; Yan, F.; Texter, J. *Prog. Polym. Sci.* **2009**, *34*, 431-448.
(15) Luo, S. C.; Zhang, Z. X.; Yang, L. *Chin. Sci. Bull.* **2008**, *53*, 1337-1342.
(16) Galinski, M.; Lewandowski, A.; Stepniak, I. *Electrochimica Acta* **2006**, *51*, 5567-5580.
(17) Yang, S. C.; Yoon, H. G.; Lee, S. S.; Lee, H. *Mater. Lett.* **2009**, *63*, 1465-1467.
(18) Mishra, A.; Fischer, M. K. R.; Bauerle, P. *Angew. Chem., Int. Ed.* **2009**, *48*, 2474-2499.
(19) Bennett, M. D.; Leo, D. J.; Wilkes, G. L.; Beyer, F. L.; Pechar, T. W. *Polymer* **2006**, *47*, 6782-6796.

(20) Duncan, A. J.; Leo, D. J.; Long, T. E. *Macromolecules* **2008**, *41*, 7765-7775.
(21) Ding, J.; Zhou, D.; Spinks, G.; Wallace, G.; Forsyth, S.; Forsyth, M.; MacFarlane, D. *Chem. Mater.* **2003**, *15*, 2392-2398.
(22) Lu, W.; Fadeev, A. G.; Qi, B.; Smela, E.; Mattes, B. R.; Ding, J.; Spinks, G. M.; Mazurkiewicz, J.; Zhou, D.; Wallace, G. G.; MacFarlane, D. R.; Forsyth, S. A.; Forsyth, M. *Science* **2002**, *297*, 983-987.
(23) Vidal, F.; Plesse, C.; Teyssie, D.; Chevrot, C. *Synth. Met.* **2004**, *142*, 287-291.
(24) Bennett, M. D.; Leo, D. J. *Sens. Actuators, A* **2004**, *115*, 79-90.
(25) Galin, M.; Mathis, A.; Galin, J. C. *Macromolecules* **1993**, *26*, 4919-4927.
(26) Brown, R. H.; Hunley, M. T.; Allen, M. H.; Long, T. E. *Polymer* **2009**, *In Press*.
(27) Gauthier, M.; Carrozzella, T.; Penlidis, A. *J. Polym. Sci., Part A: Polym. Chem.* **2002**, *40*, 511-523.
(28) Gauthier, M.; Carrozzella, T.; Snell, G. *J. Polym. Sci., Part B: Polym. Phys.* **2002**, *40*, 2303-2312.
(29) Miller, R. L.; Boyer, R. F. *J. Polym. Sci.: Polym. Phys.* **1984**, *22*, 2021-2041.
(30) Moore, R. B.; Gauthier, M.; Williams, C. E.; Eisenberg, A. *Macromolecules* **1992**, *25*, 5769-5773.
(31) Benetatos, N. M.; Winey, K. I. *Macromolecules* **2007**, *40*, 3223-3228.
(32) van der Mee, M. A. J.; l'Abee, R. M. A.; Portale, G.; Goossens, J. G. P.; van Duin, M. *Macromolecules* **2008**, *41*, 5493-5501.
(33) Strehmel, V.; Wetzel, H.; Laschewsky, A.; Moldenhauer, E.; Klein, T. *Polym. Adv. Technol.* **2008**, *19*, 1383-1390.
(34) Bazuin, C. G.; Eisenberg, A. *J. Polym. Sci., Part B: Polym Phys. Ed.* **1986**, *24*, 1137-1153.
(35) Kim, J.-S.; Roberts, S. B.; Eisenberg, A.; Moore, R. B. *Macromolecules* **1993**, *26*, 5256-5258.
(36) Gierke, T. D.; Munn, G. E.; Wilson, F. C. *ACS Symp. Ser.* **1982**, *180*, 195-216.
(37) Bennett, M.; Leo, D. *Proc. SPIE-Int. Soc. Opt. Eng.* **2005**, *5759*, 506-517.
(38) Kinning, D. J.; Thomas, E. L. *Macromolecules* **1984**, *17*, 1712-1718.

Chapter 8: Nitroxide Free Radicals in Synthetic and Biological Macromolecules

8.1 Scientific Rationale and Perspective

Free radicals are recognized as important reactive intermediates in numerous chemical and biological pathways. Oxygen-centered radicals are of special interest due to the widespread effects of oxidation. Many oxygen-centered radicals can serve as both pro- and anti-oxidants, and some are stable enough to serve as probes and mediators of chemical reactions. One such class of oxygen-centered radicals is the nitroxyls, sterically hindered derivatives of nitric oxide with a basic structure as shown in Figure 8.1.[1] These persistent free radicals are now used in a variety of applications and may be useful in understanding radical reactions and mechanisms, in addition to monitoring dynamics of larger molecular structures.

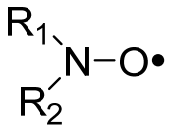

Figure 8.1 General structure of nitroxyl radicals, where R_1 and R_2 represent bulky alkyl substituents

The free radical nature of nitroxyls was first recognized by Wieland in 1914,[2] but the importance of nitroxide chemistry was not fully recognized until the 1960s when Hamilton and McConnell successfully used nitroxides for spin labeling in biological systems with EPR spectroscopy.[3] Since that time, the area of nitroxide chemistry has developed significantly

along with the field of free radical chemistry, leading to vast improvements and numerous discoveries in terms of synthesis and applications.

In addition to their utility as spin labels in EPR spectroscopy, nitroxides have emerged as an increasingly important class of compounds employed in a broad range of applications. Nitroxides are utilized as efficient free radical scavengers in biological and polymeric systems,[4] long-lived spin labels for probing both *in vivo* and *ex vivo* radical reactions,[5, 6] drugs in antioxidant therapy,[6-8] and effective mediating species in polymerization processes,[9] among other uses. This work focuses on the implications of nitroxide use in the synthesis and characterization of macromolecules, especially the chemical characteristics of nitroxyl radicals allowing effective use in mediating polymerizations and monitoring motions of biomacromolecules such as proteins and DNA.

8.2 Chemistry of Nitroxide Radicals

8.2.1 Structural requirements of nitroxides as stable free radicals

The majority of interest in nitroxides stems from the long lifetime of the free radical. Persistence in this field is a kinetic term referring to those compounds which are "living", that exist for at least several minutes at room temperature without employing any additional precautions. Classification as a stable free radical requires an activation energy above 20-25 kcal/mol and a degradation rate constant < 10^{-4} sec^{-1}.[2]

Nitroxide persistence stems from both the stability of the nitroxyl group and steric effects of the substituents surrounding the radical. Nitroxides are a derivative of nitrogen oxide, containing disubstituted nitrogen bonded to monovalent oxygen. The fundamental source of stability is the strong, resonance stabilized, three-electron N-O bond (Figure 8.2). With a high delocalization energy of ~32 kcal/mol, the radical center N-O bond exhibits greater

thermodynamic stability and lower energy content than a typical free radical.[2] The high delocalization energy also accounts for the lack of dimerization for most nitroxides. The loss of delocalization from the combination of two nitroxides is much greater than the energy gained from formation of the O-O bond, leading to a net energy loss for dimerization.[10] However, the effect of high delocalization energy is substantially weaker than that of the steric hindrance from alkyl substituents.[11]

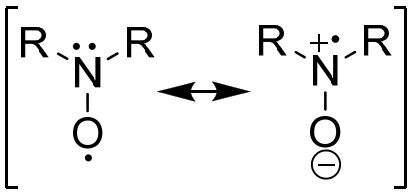

Figure 8.2 Resonance contributors of a stable nitroxide.

The structure surrounding the radical center, namely the nature of the pendant alkyl groups attached to the nitrogen, has a significant effect on the persistence of nitroxide compounds. The substituents on the nitroxide influence the degradation pathways available to the compound and increase compound lifetime through steric hindrance and neighboring group effects. However, these pendant groups may also decrease radical lifetime through introduction of additional pathways for degradation.[2] For example, a pendant benzene ring offers conjugation to the radical center to lower the energy state, but also places a higher spin density on the ring carbons, allowing for new reactive centers and disproportionation to form new non-radical products. Therefore, the kinetic effect is of greater importance than the thermodynamic effect, requiring that the structure surrounding the radical center is carefully designed for maximum stability and persistence.[12]

There are several different classes of stable free nitroxides, separated according to the composition of the aliphatic or alicyclic components. The simplest class includes nitroxides with acyclic, aliphatic substituents. One of the most common members of this class is di-tert-butyl nitroxide (DBN), **1**, Figure 8.3. Acyclic nitroxides are the least stable and most reactive class of the stable nitroxides overall, mainly due to less steric hindrance around the radical center than the cyclic nitroxides.[2, 11] While not useful in a variety of applications which exploit nitroxide stability, the high reactivity of the acyclic nitroxides has proven advantageous in nitroxide-mediated polymerizations. Some highly effective polymerization mediators include *N*-tert-butyl-*N*-[1-diethylphosphono-(2,2-dimethylpropyl)]-oxyl (DEPN) (**2**) and *N*-tert-butyl-*N*-[2-methyl-1-phenylpropyl)]-*N*-oxyl (TIPNO) (**3**).

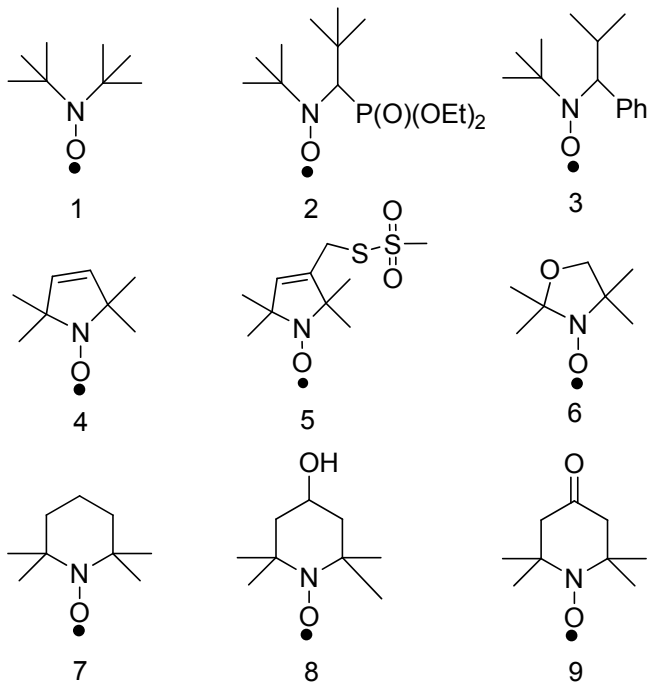

Figure 8.3 Examples of common stable nitroxides.

Most of the common nitroxides currently used and studied are alicyclic structures including five-membered and six-membered rings, as these compounds are three to four orders of magnitude less reactive than acyclic nitroxides.[11] The cyclic five-membered ring structures include derivatized pyrroles, pyrrolines, and pyrrolidines, each differing in the degree of saturation on the ring. The most common of these include the mono-unsaturated pyrrolines, derivatives of 2,2,5,5-tetramethylpyrroline-1-oxyl, more commonly referred to as PROXYL (Figure 8.3, **4**). A common substituted PROXYL used with biomacromolecules in EPR spectroscopy is (1-oxy-2,2,5,5-tetramethylpyrroline-3-methyl)methane thiosulfonate (MTSSL) (Figure 8.3, **5**), which is discussed in Section 4. In addition, some five-membered ring structures contain an extra heteroatom, including oxazolidines and imidazoles, such as 2,2,4,4-tetramethyloxazolidine-*N*-oxyl, known as Doxyl (Figure 8.3, **6**). PROXYL radicals are commonly used as spin probes in EPR spectroscopy and in antioxidant therapy,[13, 14] but are also utilized in a limited number of polymerizations.[15] Oxazolidines are less common in practical applications due to reduction rates ~1-2 orders of magnitude larger than those of the pyrroline derivatives.[16]

Nitroxides composed of six-membered alicyclic rings are classified as piperidines. The most studied compound of this class is 2,2,6,6-tetramethylpiperidinyloxy, commonly referred to as TEMPO (Figure 8.3, **7**). Other common nitroxides of this class are often functionalized at the 4-position and are referred to using the TEMPO nomenclature. Examples include the 4-hydroxy-substituted TEMPOL (Figure 8.3, **8**) and 4-oxo-TEMPO (Figure 8.3, **9**). TEMPO derivatives are used extensively in polymerizations, as well as a wide variety of other applications, including antioxidant therapy and spin traps for EPR spectroscopy.[17]

As previously stated, all of the stable nitroxides listed in Figure 3 contain aliphatic α-carbon substituents, which act as electron donating groups. These substituents offer steric hindrance and increased electron density to further stabilize the radical center and decrease the kinetic reactivity. In addition, all of the nitroxides mentioned with the exception of DEPN and TIPNO lack the presence of β-hydrogens which are particularly susceptible to abstraction reactions. Radical abstraction of a β-hydrogen is a prominent degradation pathway in these systems, leading to degradation of the nitroxide compound.

8.2.2 Reactivity of nitroxide free radicals

The relative reactivities of nitroxides is extremely structure dependent, with significant effects exhibited based on the nature of the substituents, as well as the presence of functional groups. Malievskii and Shapiro summarized these effects in a large study of over ninety nitroxides with various structures and pendant groups based on a standard set of reaction conditions for effective comparisons.[11] The reactivities were measured based on the rate constant k_1 in the reaction of a nitroxide radical with hydrazobenzene at room temperature in hexane, as shown below.

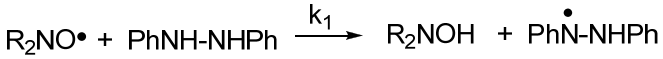

The results of this study proved a general trend of increasing reactivity in the order pyrroline < pyrrolidine < piperidines. However, this trend is greatly influenced by other properties such as the electron withdrawing capability of functional groups at least two σ bonds removed from the nitroxyl center. Of the compounds measured, nitroxides of the pyrroline series had k_1 values of 1.37-2.69, pyrrolidines had values ranging 1.7-3.6, and piperidine values ranged from 5.15 to 67.0 L mol^{-1} sec^{-1}. In the case of piperidines, changing the substituent in the 4-

position from hydrogen to amino-, oxo-, hydroxyl-, and phenyl ester results in k_1 values increasing from 8.70 L mol^{-1} sec^{-1} to 12.00, 13.90, 14.15, and 14.60, respectively. Additionally, the relationship between rate constants of hydrogen addition to stable nitroxides with the bond dissociation energies of the subsequent hydroxylamine (NO-H) revealed that more reactive nitroxides had stronger NO-H bonds in the hydroxylamine form.[11, 18]

Nitroxides are involved in a number of common reactions, the most common of which is the cycling among oxidation states of the nitroxyl (Scheme 8.1). At least four possible oxidation states exist for any given nitroxide, namely amine, hydroxylamine **a**, nitroxide **b**, and oxoammonium cation **c**, all of which come about via one electron transfer reactions.[6] A one-electron oxidation leads to the oxoammonium cation, which is subsequently reduced again through reaction with another reducing agent. This redox cycle effectively regenerates the nitroxide allowing the antioxidant protection and detoxification desired in biological systems. The nitroxide can also undergo a one-electron reduction, through either hydrogen abstraction or transition metal oxidation, to form the corresponding hydroxylamine. Both oxidation and reduction reactions are highly solvent dependent, and the rate of oxidation is increasingly impeded with more electron withdrawing capabilities of substituents.[11] Furthermore, comproportionation reactions, the reaction between a hydroxylamine and oxoammonium cation to form two nitroxides, are much faster at pH 12 than pH 3.[19]

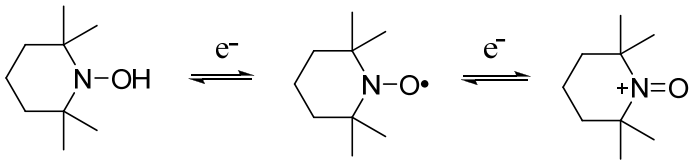

a **b** **c**

Scheme 8.1 Different oxidation states of nitroxides (adapted from ref. 20).[20]

The rate at which these oxidation and reduction reactions occur determines the antioxidant efficiency of a given nitroxide. Krishna and coworkers evaluated the efficiency of several different nitroxides as protectors against hydrogen peroxide insult through the redox midpoint potentials, an electrochemical measurement of a compound's oxidizing ability relative to the standard hydrogen electrode.[21] The results were in agreement with previous reports, stating TEMPO and related six-membered ring nitroxides, with the lowest midpoint potentials, exhibit more oxidative protection than five-membered ring nitroxides. PROXYL derivatives are more resistant to bioreduction than TEMPO derivatives,[5] so that TEMPO is more reactive with other radicals and more easily reduced to the hydroxylamine. However, α-substituents were shown to have a significant effect on the antioxidant capability, as some substituted PROXYLs exhibited protection effects similar to TEMPO. This data correlates well with the more recent study by Malievskii and Shapiro.[11]

Reaction of a nitroxide with an alkyl or other carbon-centered radical produces an alkylated nitroxide, or an alkoxyamine. Nitroxides scavenge alkyl and benzyl radicals effectively, with high rate constants for the coupling reaction determined by the nitroxide structure and following the trend PROXYL > TEMPO > open chain.[22, 23] This coupling reaction forms the thermally labile C-ON bond, allowing for reverse coupling at elevated temperatures, where the homolysis rate depends on various factors including bulkiness and

polarity of the nitroxide substituents.[24] Homolysis rates are fastest for the acyclic nitroxides, and increase with increasing ring size.[23] While alkoxyamines are poorly studied, these compounds are increasingly used as both unimolecular initiators and mediators in controlled polymerizations.[9, 25, 26]

8.3 Nitroxides as Mediators in the Synthesis of Macromolecules

8.3.1 Nitroxide Mediated Polymerization

The controlled synthesis of high molecular weight polymers with narrow polydispersities is a challenging process in high demand in the field of polymer chemistry. The development of "living" systems, defined as polymerizations completely devoid of termination and chain transfer reactions, mediated with persistent radicals has allowed the synthesis of controlled polymers with narrow molecular weight distributions and well-defined architectures.[9, 27-31] The reversible termination of the propagating species with a persistent radical, which suppresses bimolecular termination, dictates these systems. Bachmann and coworkers explained this effect, termed the persistent radical effect (PRE), in 1936 and Otsu and Rizzardo et al. eventually applied PRE to polymer systems in the 1980s.[32]

A persistent radical, as defined, does not self-terminate but may only disappear through cross-reaction with another radical species. Therefore, the presence of a persistent radical in a radical reaction diminishes the occurrence of self-termination reactions.[32] In the case of polymerizations, the persistent radical acts as a reversible endcapper of the polymer chain, which creates a thermally labile alkoxyamine, and in theory, allows the chain to grow until the monomer supply is depleted (Scheme 8.2). However, self-termination of transient alkyl radicals is competitive with the cross coupling of nitroxide with initiator fragments or chain ends in the early stages of polymerization, so that an excess of nitroxide builds up. This excess helps control

the reaction in later stages via diminishing the presence of active radicals, but polymerizations are not taken to quantitative conversion to avoid the loss in control from inevitable dead chain end formation. Regardless, this endcapping method effectively minimizes the occurrence of termination steps through maintenance of a very low concentration of the propagating radical compared to the dormant chain, based on the relative rates of activation (k_{act}), deactivation (k_{deact}), and propagation (k_p).[9, 32] In a model study of various polymeric alkoxyamines, values of k_{act} determined using Fukuda's chromatographic method[33] were ~10^{-3} s^{-1}, while k_{deact} values determined with flash photolysis[34, 35] are ~10^5 – 10^8 M^{-1} s^{-1}.[32] General trends show a dependence on nitroxide structure with k_{act} increasing in the order PROXYL < TEMPO < DEPN < DBN.[23]

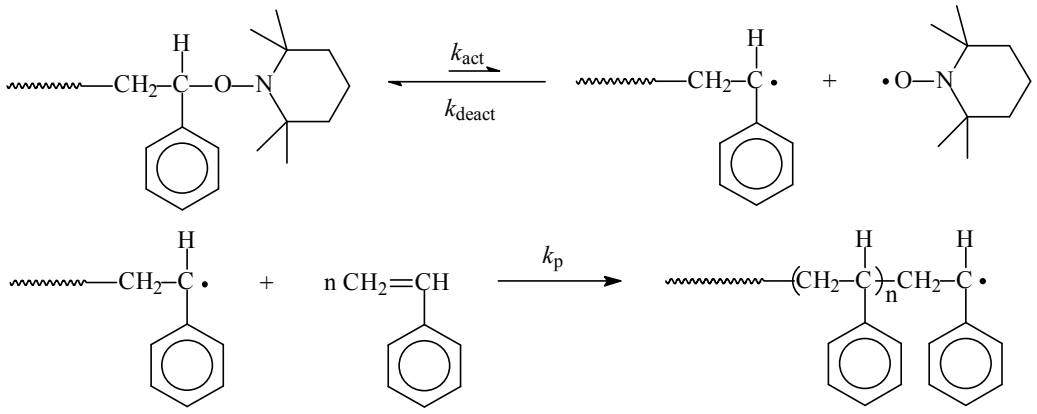

Scheme 8.2 Three reaction rates (k_{act}, k_{deact}, and k_p) govern the TEMPO-mediated polymerization of styrene. Propagation occurs through the activated state, which exists at low concentrations due to an equilibrium favoring the deactivated form.

In order for the polymer to be living, the mediating radical must undergo reversible termination of the propagating chain end without acting as an initiator of an additional chain.[31] Successful mediating radicals are characterized with delocalized systems, the presence of

heteroatoms, and high degrees of steric hindrance around the radical center. While several different classes of persistent radicals were employed for controlled polymerizations,[36-38] the stable nitroxides and alkoxyamines have proven the most successful.[9, 31, 32]

8.3.2 Commonly used nitroxides in NMP

Derivatives of both TEMPO and PROXYL, as well as various acyclic nitroxides such as DEPN and TIPNO, are used for NMP. The polymerization of styrene using TEMPO is the most studied and well understood NMP process, producing living polymer at temperatures of 125-145 °C and reaction times of 24-72 h.[9] These high temperatures and long reaction times are not ideal for industrial processes, and Georges et al. realized that TEMPO was not suitable for other systems due to the low equilibrium constant between dormant and active species ($K \sim 10^{-11}$ M) and the lack of thermally induced autopolymerization for non-styrenic monomers.[15]

Early attempts at improved nitroxides continued to rely on TEMPO derivatives. Veregin and coworkers at XEROX successfully polymerized acrylates at 145-155 °C in the presence of 4-oxo-TEMPO, but at the expense of low polydispersities and the living nature of the system.[39] The same group later demonstrated that 3-carboxy-PROXYL used in conjunction with benzoyl peroxide initiator gave significantly increased polymerization rates of styrene when compared to TEMPO. EPR studies indicated a C-O homolysis activation energy approximately 20 kcal/mol lower for a model PROXYL than the corresponding TEMPO. This same PROXYL derivative also successfully polymerized n-butyl acrylate at faster rates, but with significantly broader polydispersities.[40] Cameron and Reid reported similar results using a 2-phenyl-PROXYL derivative to mediate n-butyl acrylate polymerization.[15] The PROXYL-mediated

polymerization proceeds at more than twice the rate of the TEMPO-mediated process, but with much less control.

The limitations of monomer choices in NMP were overcome with the development of acyclic nitroxides with a hydrogen atom on an α-carbon, a property normally associated with instability. However, these traditionally less stable nitroxides exhibited vastly improved polymerization properties over TEMPO.[9] Successful polymerization with acyclic mediators such as DEPN and TIPNO are reported for styrenes as well as acrylates,[41, 42] acrylamides,[43] 1,3-dienes,[44] and acrylonitrile[15, 45] at faster rates and polydispersities as low as 1.05. Additionally, these nitroxides can tolerate amino, carboxyl, and glycidyl functionalities unlike previously studied compounds. These less stable acyclic nitroxides exhibit equilibrium constants on the order of 10^{-8}, several orders of magnitude higher than TEMPO, allowing controlled polymerization of various monomer systems under living conditions.[15]

More recently, various researchers have studied the additional advantages of using alkoxyamines as unimolecular initiators in place of bimolecular systems for NMP.[45-49] Using an alkoxyamine as the initiator allows the addition of only one component to the polymerization system, seemingly making this the simplest controlled radical polymerization process.[50] These unimolecular initiators are designed to thermally decompose into the mediating radical and initiator fragment, and often the initiating fragment is chosen to resemble a monomer in the system. The biggest advantage of using alkoxyamines as initiators is the accurate control over molecular weight demonstrated with these systems, given the assumption that one polymer chain is initiated for every alkoxyamine present in the solution.[45] In addition, bisaminooxy compounds such as Bis-TIPNO were synthesized and shown to efficiently control the polymerization of A-B-A block systems in two steps with efficient chain growth from both

sides.[51, 52] Some examples of alkoxyamine initiators described in the literature appear in Figure 8.4.

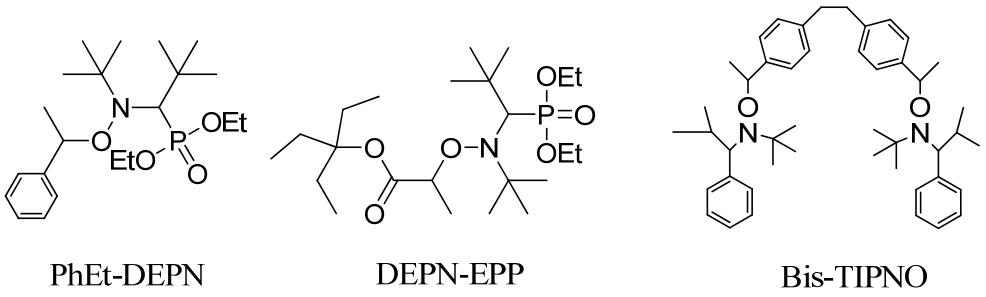

Figure 8.4 Alkoxyamine unimolecular initiators for NMP.

As expected from earlier reactivity discussions, k_a values for alkoxyamines based on DEPN are usually larger than those based on TEMPO.[53] Therefore, most of the unimolecular initiators appearing in the literature are based on DEPN structures. Benoit, Hawker, and coworkers defined PhEt-DEPN (Figure 8.4) as one of two universal alkoxyamines developed in an effort to expand the applicability of nitroxide mediated polymerization to nonstyrenic monomers.[45] This compound successfully polymerized styrene up to molecular weights of 200,000 g mol^{-1} and acrylates were polymerized to moderate conversion maintaining polydispersities below 1.1. Controlled polymerizations of acrylamides, acrylonitrile, and other functionalized monomers were also achieved with Ph-Et-DEPN.

8.3.3 Advantages of control with nitroxide mediators

Nitroxide mediated polymerization is defined as a living process in which ideally all chains are initiated with the desired initiating species and growth occurs in a linear fashion.[9]

Many monomers are polymerized via the nitroxide mediated method, including acrylates,[54, 55] styrenes,[9, 41, 47] acrylamides,[56, 57] 1,3-dienes,[44, 58] and acrylonitrile.[59, 60] Polystyrenes produced using this method are the most studied, but fine tuning of the reaction conditions and nature of the nitroxide and initiating species have allowed more recent development with a broader range of monomers. Polydispersities on the order of ~1.1 are readily achieved, and the upper weight average molecular weight limit reported is ~150,000 to 200,000 g mol^{-1}.[31]

Additional advantages of NMP include control of polymer architecture and polymerization rates through the alteration of the nitroxide structure. Hawker and coworkers have developed methods of synthesizing graft, star, comb, and hyperbranched polymers in addition to the more traditional statistical, gradient, and block copolymer architectures.[9, 61-63] In addition, Matyjaszewski observed that the addition of hydrogen bonding functionalities on the nitroxide increased the rate of polymerization.[31] Nitroxides containing phosphonate groups allow the use of NMP in a broader range of monomer units with interesting effects on polymerization control.[43, 47, 64]

8.4 Nitroxides as Tags on Biological Macromolecules

8.4.1 Site directed spin labeling and EPR spectroscopy

For several decades, researchers studying biomacromolecules have accepted the notion that proteins and DNA are dynamic molecules, but the connection among conformation, stability, and biological function was recognized only recently.[65] Recent studies show local and global motions of dynamic molecules directly affect molecular function and performance, as well as intermolecular interactions. Determining the specific motional dynamics and structure of these macromolecules is central to many fields of chemistry, biology, and other bio-related fields

in order to attain a complete understanding of factors determining protein function, DNA expression, and other biological functions. While X-ray crystallography is often used to determine the structure of biomacromolecules, the crystal structure alone is not sufficient to determine dynamic effects since it only represents one conformation of the molecule. Therefore, electron paramagnetic spectroscopy (EPR) is commonly used in conjunction with crystallography to probe the structure and motional dynamics of biological molecules.[66, 67]

EPR spectroscopy is a common method used to detect and identify free radical species through detection of a magnetic moment of an unpaired electron exhibited when placed in a high-power magnetic field.[68] Several advances in technology allow for sophisticated EPR experiments using high field EPR (HF-EPR) techniques such as continuous wave (CW-EPR), pulsed (P-ENDOR), or time domain (TD-EPR).[69] These techniques render increased sensitivity as well as the ability to determine real-time motions of dynamic molecules. CW-EPR is a saturation technique which uses a dependence on microwave power to determine relaxation rates and correlation times of the free radical species. Pulsed techniques also measure relaxation rates and serve as a good complementary method to increase accuracy and sensitivity of rate measurements.[70]

In order to use these methods to probe biomacromolecules, a stable free radical, known as a spin label, must be incorporated into the chain. The prominent spin labels used in EPR spectroscopy are the stable nitroxides, and the ability to study real-time motions by EPR spectroscopy led to the development of site directed spin labeling (SDSL) as the preferred method to study folding and conformational changes of proteins and DNA.[71] In this technique, a nitroxide spin label is covalently attached to the biomacromolecule and serves as a probe to study the surrounding structure. Backbone and side chain motion, morphology, and other

dynamic properties are deduced from the hyperfine splitting and changes in the real time spectra obtained. In addition, adducts formed through radical reaction with the nitroxide label give insight to the type of environment and other species present in the area surrounding the label.

The major disadvantage of SDSL is that it involves mutagenesis of the protein or DNA strand followed by attachment of a nitroxide group. In proteins, attachment occurs through the sulfhydryl group of cysteine residues (Figure 8.5), and all native cysteines must be replaced with other amino acids, such as alanine and glycine, to ensure site selectivity of the spin label. Otherwise, synthesis of an alternate sequence to mimic the original is required.[71] In the case of DNA, the nitroxide label is attached to a nucleotide via the nitrogenous base through a variety of tethers. Because of this limitation, SDSL is impractical for *in vivo* analysis and therefore can still only approximate motional dynamics of the true macromolecule. Regardless, EPR spectroscopy lends valuable information and remains the most used and most effective tool for probing motional dynamics and conformation switching of biological macromolecules.

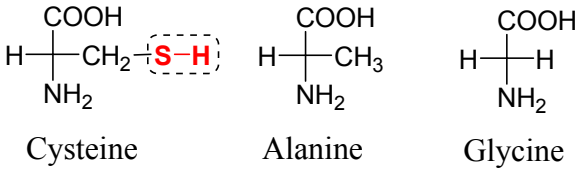

Figure 8.5 Spin labels are attached to proteins through the sulfhydryl group of cysteine. In order to maintain site label specificity, all native cysteines in a protein sequence which are not meant for spin label attachment must be replaced with amino acids of a similar size, mainly alanine and glycine.

8.4.2 Features of common tags used for biological macromolecules

Nitroxides are effective spin labels due to their longevity, low reactivity, and high selectivity. In order to serve as an effective probe, the spin label is expected to remain in its

radical form or rapidly associate and disassociate with other species throughout the experiment. Good selectivity is desirable in order to minimize reaction with other radical species so that the paramagnetic species does not disappear. Redox cycling of nitroxides both regenerates the paramagnetic species and gives information about the surrounding environment. Therefore, the most stable nitroxide to bioreduction, PROXYL, would be expected to serve as the ideal spin label.

However, probe longevity is not the only consideration when dealing with biomacromolecules, as proteins and DNA are highly sensitive to structural changes and the surrounding environment. Spin labels for biomolecules must also be evaluated based on the extent of perturbations created in macromolecular structure or dynamics.[72] For example, a poor choice of DNA spin label may result in widening of the major groove, diminishing helical twist, and increased displacement of base pairs.[73, 74] Undesirable polarity and steric effects may interfere with the dynamic motions of the molecule and misrepresent the DNA dynamics as a result. Also, a probe with a large effective size may disrupt secondary and tertiary structure of the molecule. In the probing of proteins, (1-oxy-2,2,5,5-tetramethylpyrroline-3-methyl)methane thiosulfonate (MTSSL) is used most often,[66, 67, 75] with attachment to the protein chain through the sulfhydryl group of cysteine residues, as shown in Figure 8.6. Some researchers have used other pyrroline derivatives[76] as well as TEMPO derivatives[77] with some success for this purpose.

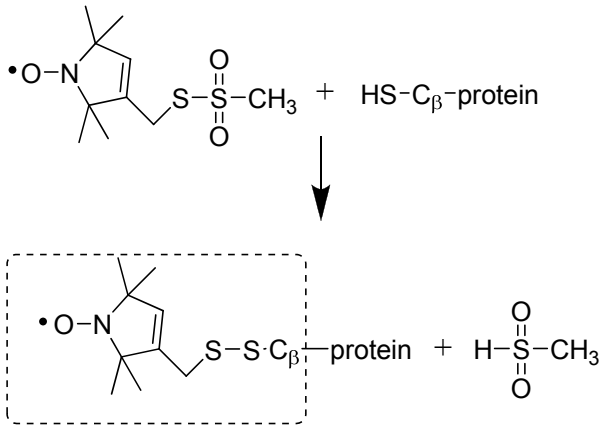

Figure 8.6 Attachment of MTSSL to protein backbone through cysteine residues (adapted from ref. 71).[71]

In the case of DNA, or more specifically oligonucleotides, more attention is given to the mode of attachment than to the actual nitroxide structure. Spin probes based on derivatives of TEMPO[78-80] and PROXYL[72, 74, 80] are most commonly utilized, although others have been explored.[73] These spin labels are attached to guanidine, thymidine, cytosine, or other derivatives of DNA bases through a variety of linking chemistries, including amides, diamines, and acetylenic tethers. The tether type and flexibility determines the nitroxide motion and freedom, which is important when considering backbone motion relative to nitroxyl side chain rotation. An example of nitroxide attachment to an oligonucleotide appears in Figure 8.7.

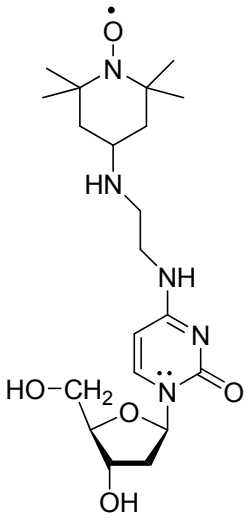

Figure 8.7. TEMPO-labeled uracil linked by a flexible ethyldiamino tether (adapted from ref. 79).[79]

Two main methods of covalent attachment of the spin label are used. Bobst and coworkers explored flexible tethers consisting of two to five atoms, and used the dynamic cylinder and base disk models to separate global and local dynamics.[80, 81] On the other hand, Robinson and coworkers utilized rigid two or four atom tethers consisting of acetylenic linkages.[72, 82] This tether type serves to minimize local probe motion for more direct measurement of base motion. EPR spectra of unhindered spin label motion are predominantly isotropic, while the corresponding spectra of constrained labels are anisotropic, lending structural and local environment information.[83] Therefore, more rigidly attached labels show larger changes between bound and unbound DNA forms, effectively spacing out the time scale and allowing easier distinction of different environments of the spin probe.[73] Spin labels attached by flexible tethers or attached directly to the DNA backbone also show differences between single- and double-stranded states, but to a much smaller degree.[84-86]

The nitroxide-labeled oligonucleotide with rigid attachment can also be treated with multi-frequency EPR using a slowly relaxing local structure model.[80] This model separates the fast motions of internal dynamics and the slow motions of global tumbling. The result of such an experiment is the observation of two EPR spectra types representing both a highly restricted site of slow motion and a less restricted site of fast motions, assuming a very short tether is used.

8.4.3 Probing molecular dynamics and motion with nitroxide tags

8.4.3.1 Studying protein structure and function relationships

The use of specialized EPR techniques and SDSL, in conjunction with crystal structure from X-ray crystallography, allows the accurate analysis of conformational switching and local backbone fluctuations in proteins, two dynamic modes known to affect protein function.[65] Combined, these techniques provide a broad range of information including the determination of complex dynamics and structure of soluble and membrane proteins, discrimination between bulk and boundary domains in lipids, interchain distances, fluctuations in backbone dihedral angles and α-helical rigid-body motions, and local interactions of solvent.[65, 69] Without the crystal structure, the EPR spectra are too complicated to deduce many of these valuable properties, and EPR studies of proteins are limited to well-defined proteins and biological systems at the present time.

Using MTSSL as the probe, solvent accessibility, nitroxide-labeled side chain mobility, local environment polarity index, and distance between the spin label and another paramagnetic species are deduced from the EPR spectrum.[66] These changes in mobility, accessibility, and distance provide clues for the rigid body motions of and changes in secondary structures, as well as relative domain movements. These events are monitored on the micro- to milli-second

timescale so that it is possible to observe structural changes as they relate to protein function. In order to perform the most complete analysis, the use of two spin labels on the protein chain is advised. This allows the observance of magnetic dipolar spin-spin interactions which provide precise information concerning global structure and constraints of the molecule, especially peptide conformation and helical stability at the intrahelix residue-residue level.[87] Use of only one label limits the analysis to the immediate environment surrounding the probe, but spectral analysis of this system is also much less complicated.[67]

Conformational studies are performed according to two extreme limits: rigid body motion with frozen samples, and rapid tumbling of proteins at room temperature. Neither of these methods exactly matches biomolecules under physiological conditions. Altenbach and coworkers validated the rigid body method by showing that it sufficiently estimates distances at physiological temperatures, in accord with other techniques.[67] They also determined that solvent exposed nitroxides have little effect on protein structure and the effects of nitroxide side chain motions on estimated distances are small, so that analysis is simplified based on these assumptions.

Most EPR dynamic studies are performed under rigid body motion conditions with α-helical structures. Some well-studied systems in the literature which demonstrate the direct effect of conformation on protein function include helix motion in rhodopsin which causes activation,[65, 88] domain movement in T4 lysozyme,[66, 67] secondary structure fluctuations in bacterial porin BtuB upon substrate binding,[65, 66, 89] and structural changes in KcsA baterial K+ channel caused by pH.[65, 66, 90, 91] In addition, Lietzow and coworkers reported the first attempt to explore structure-function relationships of β-sheet structures with a study of a cellular retinol-binding protein, showing that edge strands showed similar effects to α-helical structures.[75]

Dynamics of labeled sites on interior strands, however, were greatly influenced by neighboring strands, resulting in a much more complicated spectral analysis. All of these studies effectively correlate protein dynamics with protein function through nitroxide spin label attachment and sophisticated EPR experiments.

8.4.3.2 Monitoring DNA dynamics through spin-labeled oligonucleotides

Similarly, SDSL and EPR spectroscopy are used to monitor the structure and dynamics of DNA using oligonucleotides of varying length, from 5 up to 100 base pairs.[78, 92] Sequence-specific spin labeled DNA are synthesized to study structure-function relationships based on internal dynamics, including long-range bending and twisting of bases, individual base oscillations, and spin label motion.[80] These dynamics effect DNA-protein complexation,[82] formation and denaturation of DNA structures,[73] genetic code expression,[80] and properties of the microenvironment surrounding the probe.[93] Koudekla and coworkers reported a strong dependence of DNA operation and affinity for protein binding on the nucleotide sequence in 1987.[94] Affinity of phage 434 repressor protein for its DNA operator sequence was reduced 50-fold by alterations in sequence at the operator center, where the DNA and protein never experience direct contact. This discovery led to a peaked interest in the probing of the relationship among DNA sequence, conformation, and performance

Nitroxide spin label sensitivity allows the detection of small variations in the microenvironment surrounding the spin label, allowing the determination of probe location within the DNA conformation. The hyperfine coupling constant describes the micropolarity of the probe environment, while the rotational correlation time τ_c relates to the variations in viscosity around the spin label.[93] Assuming some basic knowledge of secondary and tertiary

structure, these measurable parameters can distinguish between probe presence in the shielded minor groove or the solvent exposed exterior, for example. Microenvironmental sensitivity also allows the probing of biologically significant DNA structural formations such as loops, duplex structures, and triplex structures.

Probing local dynamics of DNA is essential to the complete understanding of the role of DNA complexes. Gannett and coworkers, as well as other researchers, have reported the monitoring of duplex and triplex DNA through covalent attachment of a spin probe on the 5-position of uracil.[73, 93] Similar probe attachments are preferred for other DNA bases as well, especially guanine due to the known biological significance of duplex and quadruplex structures for G-rich sequences. Therefore, Okamoto and coworkers developed a spin-labeled guanine derivative, ^{TEMPO}G, to easily monitor the local environments of various G-rich DNA.[93]

Because local dynamics are known to influence DNA function, spin labeling and EPR spectroscopy are also very useful tools in probing DNA interaction with proteins or enzymes. Kolaczkowski and coworkers were the first to observe a spin-labeled 23-mer oligonucleotide interacting with AP endonuclease by high field EPR.[79] AP endonuclease, the key enzyme in abasic site DNA repair, successfully binds and cleaves when the spin label is located at the 3' position, but not when labeled at the 5' position from the abasic site. This demonstrates that the position of bases surrounding the active site is critical to DNA-protein function, and confirms that EPR is a useful tool for examining biomacromolecular interactions.

8.5 Conclusions

Nitroxides have emerged as a very useful class of stable free radicals in monitoring and probing both synthetic polymers and natural biomacromolecules. The resonance stability of the

N-O bond, as well as the steric hindrance surrounding the radical center, renders these compounds the flexibility and kinetic stability needed for many applications in various environments. Acyclic nitroxides are especially useful as mediators in polymer synthesis, while nitroxides based on five- and six-membered rings prove useful in probing motional dynamics and structure in proteins and DNA. New advances in the design and synthesis of stable nitroxides continue to improve the utility of nitroxides in various fields. The range of monomers and polymerization conditions available for synthesis of controlled architectures and well-defined macromolecules has greatly expanded since the first introduction of TEMPO for nitroxide-mediated polymerization. Additionally, advances in EPR spectroscopy instrumentation and tethering chemistries for attaching nitroxides to biological macromolecules continue to bring scientists closer to understanding the dynamics and functions of proteins and DNA in their native environments.

8.6 References

[1] K. Hensley, T. Tabatabaie, C. A. Stewart, Q. Pye, R. A. Floyd, *Chem. Res. Toxicol.* **1997**, *10*, 527.
[2] L. B. Volodarsky, V. A. Reznikov, V. I. Ovcharenko, "*Synthetic Chemistry of Stable Nitroxides"*, CRC Press, Boca Raton, 1994.
[3] C. L. Hamilton, H. M. McConnell, "Spin Labels", in *Structural Chemistry and Molecular Biology*, A. Rich and N. Davidson, Eds., W. H. Freeman, San Francisco, 1968.
[4] E. T. Denisov, *Polymer Degradation and Stability* **1991**, *34*, 325.
[5] L. J. Berliner, "*In Vivo EPR (ESR)"*, Kluwer Academic/Plenum Publishers, New York, 2003.
[6] J. B. Mitchell, M. C. Krishna, A. Samuni, P. Kuppusamy, S. M. Hahn, A. Russo, "Clinical uses of nitroxides as superoxide-dismutase mimics", in *Toxicology of the Human Environment*, C.J. Rhodes, Ed., Taylor & Francis, London, 2000.
[7] Z. D. Raikov, R. E. T, A. T. Atanasov, *Medical Hypotheses* **2001**, *57*, 302.
[8] S. M. Hahn, Z. Tochner, M. C. Krishna, J. Glass, L. Wilson, A. Samuni, M. Sprague, D. Venzon, E. Glatstein, *Cancer Research* **1992**, *52*, 1750.
[9] C. J. Hawker, A. W. Bosman, E. Harth, *Chem. Rev.* **2001**, 3661.
[10] H. G. Aurich, "Nitroxides", in *Nitrones, Nitronates, and Nitroxides*, S. Patai and Z. Rappoport, Eds., John Wiley & Sons, Chichester, England, 1989.
[11] A. D. Malievskii, A. B. Shapiro, *Kinetics and Catalysis* **2005**, *46*, 506.

[12] P. F. Alewood, S. A. Hussain, T. C. Jenkins, M. J. Perkins, A. H. Sharma, N. P. Y. Siew, P. Ward, *J Chem. Soc., Perkin Trans 1* **1978**, *1066*.
[13] S. Liu, G. S. Timmins, H. Shi, C. M. Gasparovic, K. J. Liu, *NMR in Biomedicine* **2004**, *17*, 327.
[14] P. Twomey, J. Taira, W. DeGraff, J. B. Mitchell, A. Russo, M. C. Krishna, O. H. Hankovszky, L. Frank, K. Hideg, *Free Radical Biology & Medicine* **1997**, *22*, 909.
[15] N. R. Cameron, A. J. Reid, *Macromolecules* **2002**, *35*, 9890.
[16] S. Morris, G. Sosnovsky, B. Hui, C. O. Huber, N. U. M. Rao, H. M. Swartz, *J. Pharm. Sciences* **1991**, *80*, 149.
[17] J. Fuchs, N. Groth, T. Herrling, G. Zimmer, *Free Radical Biology & Medicine* **1997**, *22*, 967.
[18] A. D. Malievskii, A. B. Shapiro, *Kinetics and Catalysis* **2005**, *46*, 472.
[19] A. Israeli, M. Patt, M. Oron, A. Samuni, R. Kohen, S. Goldstein, *Free Radical Biology & Medicine* **2005**, *38*, 317.
[20] A. M. Samuni, W. DeGraff, M. C. Krishna, J. B. Mitchell, *Molecular and Cellular Biochemistry* **2002**, *234/235*, 327.
[21] M. C. Krishna, W. DeGraff, O. H. Hankovszky, C. P. Sa´r, T. Ka´ lai, J. Jeko, A. Russo, J. B. Mitchell, K. Hideg, *J. Med. Chem.* **1998**, *41*, 3477.
[22] V. W. Bowry, K. U. Ingold, *J. Am. Chem. Soc.* **1992**, *114*, 4992.
[23] G. Moad, E. Rizzardo, *Macromolecules* **1995**, *28*, 8722.
[24] D. Bertin, D. Gigmes, S. Marque, R. Maurin, P. Tordo, *Journal of Polymer Science: Part A: Polymer Chemistry* **2004**, *42*, 3504.
[25] R. Braslau, L. C. Burrill, M. Siano, N. Naik, R. K. Howden, L. K. Mahal, *Macromolecules* **1997**, *30*, 6445.
[26] K. Matyjaszewski, S. Gaynor, D. Greszta, D. Mardare, T. Shigemoto, *Macromol. Symp.* **1995**, *98*, 73.
[27] C. J. Hawker, *J. Am. Chem. Soc.* **1994**, *116*, 11185.
[28] M. K. Georges, R. Veregin, P. M. Kazmaier, G. K. Hamer, *Macromolecules* **1993**, *26*, 2987.
[29] A. Goto, T. Fukuda, *Prog. Polym. Sci.* **2004**, *29*, 329.
[30] K. Matyjaszewski, "Controlled/Living Radical Polymerization", American Chemical Society, Washington, D.C., 2000, p. 768/.
[31] G. Odian, "*Principles of Polymerization"*, 4th edition, John Wiley & Sons, Hoboken, 2004.
[32] H. Fischer, *Chem. Rev.* **2001**, 3581.
[33] T. Fukuda, A. Goto, *Macromol. Chem. Phys.* **2000**, *201*, 2138.
[34] A. L. J. Beckwith, V. W. Bowry, K. U. Ingold, *J. Am. Chem. Soc.* **1992**, *114*, 4983.
[35] J. Sobek, R. Martschke, H. Fischer, *J. Am. Chem. Soc.* **2001**, *123*, 2849.
[36] M. Steenbock, M. Klapper, K. Muellen, C. Brauer, M. Hubrich, *Macromolecules* **1998**, *31*, 5223.
[37] M. Klapper, T. Brand, M. Steenbock, K. Mullen, *ACS Symposium Series* **2000**, *768*, 152.
[38] U.S. 726,238 (1989), inv. A. H. Janowicz;
[39] B. Keoshkerian, M. K. Georges, M. Quinlan, R. Veregin, R. Goodbrand, *Macromolecules* **1998**, *31*, 7559.
[40] R. P. N. Veregin, M. K. Georges, G. K. Hamer, P. M. Kazmaier, *Macromolecules* **1995**, *28*, 4391.
[41] D. Benoit, S. Grimaldi, S. Robin, J. P. Finet, P. Tordo, Y. Gnanou, *J. Am. Chem. Soc.* **2000**, *122*, 5929.

[42] G. Ananchenko, K. Matyjaszewski, *Macromolecules* **2002**, *35*, 8323.
[43] T. Diaz, A. Fischer, A. Jonquieres, A. Brembilla, P. Lochon, *Macromolecules* **2003**, *36*, 2235.
[44] D. Benoit, E. Harth, P. Fox, R. M. Waymouth, C. J. Hawker, *Macromolecules* **2000**, *33*, 363.
[45] D. Benoit, V. Chaplinski, R. Braslau, C. J. Hawker, *J. Am. Chem. Soc.* **1999**, *121*, 3904.
[46] J. Nicolas, B. Charleux, O. Guerret, S. Magnet, *Angewandte Chemie, International Edition* **2004**, *43*, 6186.
[47] B. Mather, J. Lizotte, T. E. Long, *Macromolecules* **2004**, *37*, 9331.
[48] J. R. Lizotte, S. G. Anderson, T. E. Long, *Journal of Polymer Science: Part A: Polymer Chemistry* **2004**, *42*, 1547.
[49] T. Krause, W. D. Habicher, M. Messerschmidt, B. I. Voit, *Designed Monomers and Polymers* **2004**, *7*, 391.
[50] J. F. Lutz, P. Lacroix-Desmazes, B. Boutevin, C. Le Mercier, D. Gigmes, D. Bertin, P. Tordo, *Polymer Preprints* **2002**, *43*, 287.
[51] M. Bothe, G. Schmidt-Naake, *Macromol. Rapid Commun.* **2003**, *24*, 609.
[52] M. Bothe, G. Schmidt-Naake, *Macromol. Chem. Phys.* **2004**, *205*, 208.
[53] G. Ananchenko, S. Marque, D. Gigmes, D. Bertin, P. Tordo, *Org. Biomol. Chem.* **2004**, *2*, 709.
[54] E. Drockenmuller, J. Lamps, J. M. Catala, *Macromolecules* **2004**, *37*, 2076.
[55] M. K. Georges, J. L. Lukkarila, A. R. Szkurhan, *Macromolecules* **2004**, *37*, 1297.
[56] H. Gotz, E. Harth, S. M. Schiller, C. W. Frank, W. Knoll, C. J. Hawker, *J. Polym. Sci., Part A: Polym. Chem.* **2002**, *40*, 3379.
[57] K. Schierholz, M. Givehchi, P. Fabre, F. Nallet, E. Papon, O. Guerret, Y. Gnanou, *Macromolecules* **2003**, *36*, 5995.
[58] M. K. Georges, G. K. Hamer, N. A. Listigovers, *Macromolecules* **1998**, *31*, 9087.
[59] C. Detrembleur, V. Sciannamea, C. Koulic, M. Claes, M. Hoebeke, R. Jerome, *Macromolecules* **2002**, *35*, 7214.
[60] C. Tang, T. Kowalewski, K. Matyjaszewski, *Macromolecules* **2003**, *36*, 1465.
[61] C. J. Hawker, J. M. J. Frechet, R. B. Grubbs, J. Dao, *J. Am. Chem. Soc.* **1995**, *117*, 10763.
[62] A. W. Bosman, A. Heumann, G. Klaerner, D. Benoit, J. M. J. Frechet, C. J. Hawker, *J. Am. Chem. Soc.* **2001**, *123*, 6461.
[63] A. W. Bosman, R. Vestberg, A. Heumann, J. M. J. Frechet, C. J. Hawker, *J. Am. Chem. Soc.* **2003**, *125*, 715.
[64] P. Lacroix-Desmazes, J. F. Lutz, F. Chauvin, R. Severac, B. Boutevin, *Macromolecules* **2001**, *34*, 8866.
[65] L. Columbus, W. L. Hubbell, *TRENDS in Biochemical Sciences* **2002**, *27*, 288.
[66] W. L. Hubbell, D. S. Cafiso, C. Altenbach, *Nature Structural Biology* **2000**, *7*, 735.
[67] C. Altenbach, K.-J. Oh, R. J. Trabanino, K. Hideg, W. L. Hubbell, *Biochemistry* **2001**, *40*, 15471.
[68] R. A. Towner, "Chemistry of Spin-trapping", in *Toxicology of the Human Environment: The critical role of free radicals*, C.J. Rhodes, Ed., Taylor & Francis, London, 2000.
[69] P. P. Borbat, A. J. Costa-Filho, K. A. Earle, J. K. Moscicki, J. H. Freed, *Science* **2001**, *291*, 266.
[70] R. D. Nielsen, S. Canaan, J. A. Gladden, M. H. Gelb, C. Mailer, B. H. Robinson, *Journal of Magnetic Resonance* **2004**, *169*, 129.

[71] H.-J. Steinhoff, B. Suess, *Methods* **2003**, *29*, 188.
[72] E. J. Hustedt, J. J. Kirchner, A. Spaltenstein, P. B. Hopkins, B. H. Robinson, *Biochemistry* **1995**, *34*, 4369.
[73] P. M. Gannett, E. Darian, J. Powell, E. M. J. II, C. Mundoma, N. L. Greenbaum, C. M. Ramsey, N. S. Dalal, D. E. Budil, *Nucleic Acids Research* **2002**, *30*, 5328.
[74] E. Darian, P. M. Gannett, *J. Biomol. Struc. Dyn.* **2005**, *22*, 579.
[75] M. A. Lietzow, W. L. Hubbell, *Biochemistry* **2004**, *43*, 3137.
[76] S. Cavalu, G. Damian, *Biomacromolecules* **2003**, *4*, 1630.
[77] V. P. Timofeev, Y. V. Tkachev, V. V. Novikov, V. A. Alyoshkin, V. A. Lapuk, *J. Biomol. Struc. Dyn.* **2005**, *23*, 175.
[78] D. E. Budil, S. V. Kolaczkowski, A. Perry, C. Varaprasad, F. Johnson, P. R. Strauss, *Biohpysical Journal* **2000**, *78*, 430.
[79] S. V. Kolaczkowski, A. Perry, A. Mckenzie, F. Johnson, D. E. Budil, P. R. Strauss, *Biochemical and Biophysical Research Communications* **2001**, *288*, 722.
[80] Z. Liang, J. H. Freed, *J Phys Chem B* **2000**, *104*, 5372.
[81] O. K. Strobel, D. D. Kryak, E. V. Bobst, A. M. Bobst, *Bioconjugate Chem* **1991**, *2*, 89.
[82] A. Spaltenstein, B. H. Robinson, P. B. Hopkins, *Biochemistry* **1989**, *28*, 9484.
[83] M. Bennati, T. F. Prisner, *Rep. Prog. Phys.* **2005**, *68*, 411.
[84] R. S. Keyes, A. M. Bobst, *Biophys Chem* **1993**, *45*, 281.
[85] O. K. Strobel, R. S. Keyes, R. R. Sinden, A. M. Bobst, *Arch. Biochem. Biophys.* **1995**, *324*, 357.
[86] P. Z. Qin, S. E. Butcher, J. Feigon, W. L. Hubbell, *Biochemistry* **2001**, *40*, 6929.
[87] A. Polese, D. J. Anderson, G. Millhauser, F. Formaggio, M. Crisma, F. Marchiori, C. Toniolo, *J. Am. Chem. Soc.* **1999**, *121*, 11071.
[88] D. L. Farrens, C. Altenbach, K. Yang, W. L. Hubbell, H. G. Khorana, *Science* **1996**, *274*, 768.
[89] H. J. Merianos, N. Cadieux, C. H. Lin, R. J. Kadner, D. S. Cafiso, *Nat Struct Biol* **2000**, *7*, 205.
[90] E. Perozo, D. M. Cortes, L. G. Cuello, *Science* **1999**, *285*, 73.
[91] Y. Liu, P. Sompornpisut, E. Perozo, *Nat Struct Biol* **2001**, *8*, 883.
[92] T. M. Okonogi, A. W. Reese, S. C. Alley, P. B. Hopkins, B. H. Robinson, *Biohpysical Journal* **1999**, *77*, 3256.
[93] A. Okamoto, T. Inasaki, I. Saito, *Bioorg. Med. Chem. Lett.* **2004**, *14*, 3415.
[94] G. B. Koudelka, S. B. Harrison, M. Ptashne, *Nature* **1987**, *326*, 846.

Chapter 9: Overall Conclusions

The influence of functionality (nitroxyl radical and hydroxyl group) and charge (carbanion and zwitterion) on the synthesis and properties of acrylic copolymers was described. First, stabilizing the anion in living polymerization with bulky aluminum compounds enabled the synthesis of (meth)acrylic polymers at ambient temperatures with syndiotacticity control, in stark contrast to the low temperatures (-78-95 °C) required for the preparation of isotactic structures in the absence of aluminum. Previous work by Ballard and Hadddleton inspired the exploration of the upper limits of temperature conditions useful in the controlled anionic polymerization of methyl methacrylate in the presence of triisobutylaluminum ($^{i}Bu_3Al$). Syndiorich PMMA was synthesized via screened anionic polymerization at temperatures ranging from 0 to 50 °C using a mixed $^{i}Bu_3Al$/1,1-diphenylhexyllithium (DPHL) initiator. Polymerization control was monitored as a function of Al:Li and temperature using parameters including yield, tacticity, and molecular weight distribution. At Al:Li ratios < 2, moderate molecular weight control was observed and the structure was predominantly isotactic. However, control of both molecular weight distribution and syndiotacticity were achieved at Al:Li >2. The glass transition temperature (T_g) of PMMA homopolymers also revealed the degree of tacticity control afforded in the presence of $^{i}Bu_3Al$. At Al:Li = 1.1, a T_g of 81.4 °C was observed. At the highest ratio tested, Al:Li = 6, 66% syndiotactic PMMA was achieved with a significantly increased T_g of 126.2 °C. This study reveals the advantages of controlling stereotacticity in the tailoring of polymer properties, where the T_g of PMMA can be tuned from ~50 °C for fully isotactic structures, to >130 °C for fully syndiotactic structures.

Polymerizations were carried out at temperatures ranging from 0 to 50 °C at Al:Li = 2.1 in order to discern the temperature limits of control. Effectiveness of polymerization control decreased markedly above room temperature. Narrow molecular weight distributions <1.2 were achieved at 0 and 25 °C, but increased to 1.5-1.6 at elevated temperatures. Higher temperature polymerizations also resulted in less than quantitative yields that decreased with increasing temperature to only 58% at 50 °C. Analysis with MALDI-TOF spectroscopy revealed an increasing contribution of the product resulting from back-biting termination with increasing temperature. At 50 °C, only chains with the cyclic chain terminated endgroup were detected, without any signals for the desired product with a proton endgroup. This study revealed a limit of control between 0 and 25 °C for the polymerization of PMMA using $^{i}Bu_3Al$/DPHL initiator, depending on desired application and endgroup control.

Nitroxide mediated polymerization was utilized for the preparation of functional random and block copolymers incorporating hydroxy-functional 2-hydroxyethyl acrylate. Polymerization conditions were established for the DEPN-mediated polymerization of nBA, and were applied to the synthesis of random copolymers. The copolymerization of nBA with HEA and silyl-protected HEA (HEA-TMS) resulted in linear molecular weight vs. conversion plots and narrow molecular weight distributions, indicating that polymerization control was maintained in the presence of the hydroxyl functionality. Kinetic analysis using in situ FTIR revealed little effect of the hydroxyl on polymerization kinetics at 10 mol % HEA in the feed, in accordance with previously published results. The living nature of the chain end was confirmed with the successful block addition of styrene to poly(nBA-*co*-HEA-TMS). A shift in the SEC chromatogram toward higher molecular weight confirmed polystyrene growth. Amphiphilic diblock copolymer, poly(nBA-*b*-HEA-TMS) was synthesized from a poly(nBA) macroinitiator

in DMF solution. Protection of the monomer hydroxyl alleviated many issues with polymer isolation experienced for block copolymers with HEA. SEC revealed growth in molecular weight and a narrow molecular weight distribution, with incorporation of a 5 mol % HEA-TMS block at the end of poly(nBA). Potential application of these functional diblock copolymers as templates for chemical modification may enable the synthesis of new families of block copolymers.

Zwitterionic functionality of the sulfobetaine type was incorporated into a low T_g n-butyl acrylate matrix through free radical copolymerization techniques to afford high molecular weight zwitterionomers with sulfobetaine contents of 6-13 mol %. DMSO was identified as the copolymerization solvent to maintain homogeneous reactions up to quantitative monomer conversion. This solvent replaced the fluorinated alcohols previously used in the literature. SEC in DMF with 0.01M LiBr afforded reproducible, monomodal chromatograms and molecular weights relative to polystyrene standards. Solid state and solution properties of copolymers containing two different sulfobetaine monomers, the amide-linked SBMAm and ester-linked SBMA, were subsequently characterized using various methods.

Zwitterionic copolymers were electrospun for the first time from 80/20 v/v chloroform/ethanol solutions containing 2-7 wt % polymer to form robust nanoscale fibers. The presence of strong ionic crosslinks between zwitterionic groups in the soft PnBA matrix enabled the formation of free-standing fibers and films at room temperature. Zwitterion incorporation enabled formation of fibers at low solution concentrations and viscosities below 0.02 Pa·s, resulting in average fiber diameters as small as 100 nm for PnBA-*co*-PSBMAm copolymers. These viscosity values are the lowest observed for electrospinning in our laboratories. Successful electrospinning of zwitterionic copolymers occurred at solution concentrations and

viscosities orders of magnitude lower than those required for high molecular weight PnBA. We hypothesized that intermolecular interactions rather than chain entanglements dominated the electrospinning process in copolymers featuring zwitterion aggregation.

Electrospinning of PnBA-*co*-PSBMA copolymers also resulted in nanoscale to micron size fiber diameters for polymer concentrations of 2-7 wt %. Fiber morphology changed with increasing concentration in a similar manner for both copolymer series. Polymer droplets formed at 1.5 wt %, while the onset of fiber formation occurred at ~2 wt %, and uniform fibers formed above 2.5-3 wt % for PnBA-*co*-PSBMA and at 4 wt % for PnBA*co*-PSBMAm. Fiber diameter increased with concentration over the range of 2-7 wt %, and fiber diameters of ~100 nm to ~2 μm were collected. A direct comparison of $PnBA_{91}$-*co*-$PSBMA_9$ and $PnBA_{90}$-*co*-$PSBMAm_{10}$ at equivalent molecular weights revealed similar scaling relationships for the dependence of fiber diameter on concentration, but drastic differences in fiber size. $PnBA_{91}$-*co*-$PSBMA_9$ fiber diameters were 2-3 times larger than $PnBA_{90}$-*co*-$PSBMAm_{10}$. A hydrogen bonding effect of the amide bond was offered as a preliminary explanation for this phenomenon.

Steady shear solution rheological measurements were carried out in chloroform for 1-7 wt % solutions of PnBA-*co*-PSBMA in order to identify the concentration dependence of solution viscosity for zwitterionic copolymers. Two concentration regimes were identified with a boundary transition at ~2.0 wt %. A slight influence of zwitterion content on scaling behavior was observed. $PnBA_{94}$-*co*-$PSBMA_6$ showed a smaller dependence on concentration in the upper regime compared to $PnBA_{91}$-*co*-$PSBMA_9$, due to less mobility restrictions on polymer chains in the presence of fewer stickers or zwitterion groups. Solution properties of the neutral homopolymer PnBA fit the predicted scaling for neutral non-associating polymers with a C_e at 15 wt %. The transition for PnBA was an order of magnitude higher in both specific viscosity

and concentration than the transition observed for zwitterionic copolymers. The large difference in properties at the transition for the neutral homopolymer versus the zwitterionic copolymers suggested the transitions were not due to the same physical phenomenon, as previously hypothesized in the electrospinning of PnBA-*co*-PSBMAm copolymers.

The solution behavior of zwitterionic copolymers was compared to several different scaling models of polymer dynamics in solution in an attempt to identify the observed transition. Models describing neutral non-associating polymers and polyelectrolytes were inappropriate for the zwitterionic copolymer because they failed to consider the dynamic interactions of the strongly associating zwitterions. Rubinstein and Semenov's model for associating polymers based on sticky Rouse and sticky reptation models sufficiently described zwitterionic copolymer behavior in the upper concentration regime, but poorly correlated to the lower concentration regime. Based on the model of associating polymers, the transition observed at ~2 wt % for zwitterionic copolymers corresponded to the boundary between dilute and semidilute unentangled regimes, representing the concentration at which intramolecular zwitterion associations transformed to intermolecular associations. In addition, this transition observed in rheological measurements correlated to the onset of fiber formation for electrospinning results, adding credence to the hypothesis that electrospinning was dominated by electrostatic interactions between zwitterions rather than chain entanglements.

Characterization of solid-state properties of zwitterionomers, including mechanical performance and morphology, is important for their potential use in high performance materials. n-Butyl acrylate-based zwitterionic copolymers exhibited a two-phase morphology with properties similar to classical ionomers. A rubbery plateau that increased with zwitterion content was observed in dynamic mechanical analysis, along with two transitions representing the T_g of

the n-butyl acrylate matrix and a transition associated with zwitterion aggregates. The biphasic morphology was confirmed with multi-angle x-ray scattering which revealed a characteristic ionomer peak at q ~ 1.5 nm^{-1}. This peak correlated to a Bragg spacing of ~ 4 nm.

The interaction of zwitterionic copolymers with ionic liquids (ILs) was also explored for potential application of zwitterions in electromechanical devices. Zwitterionic membranes containing 9 or 10 mol % sulfobetaine were solution cast from chloroform and swollen in the water-miscible IL, EMIm ES. Zwitterion structure influenced the swelling behavior of the membranes, where IL uptake in ester-linked (SBMA) zwitterionic films was more than double the uptake for amide-linked (SBMAm) zwitterionic films over equivalent swelling times. The local effects of swelling on zwitterionomer properties were studied with x-ray scattering, DMA, and ionic conductivity measurements. DMA revealed the disappearance of the rubbery plateau as the ion-rich phase was plasticized with increasing amounts of IL above 10 wt % IL. SAXS analysis showed a shift in the ionomer peak of 0.3 nm^{-1} to larger spacings with 15 wt % IL. Additional scattering results from multi-angle x-ray scattering (MAXS) showed systematic shift of the ionomer peak to lower q with increasing IL content, and no change in the other peaks at higher q that correlate to the matrix polymer. These results confirmed the IL preferentially swelled the ionic domains without affecting the matrix polymer. The appearance of a shoulder at 9.3 nm^{-1} and the broadening of the ionomer peak at 75 wt % IL content indicated a change in morphological structure at very high swelling. Ionic conductivity also increased with IL uptake, approaching the conductivity of pure IL. DMA and conductivity results for $PnBA_{91}$-co-$PSBMA_9$ indicated a critical uptake of IL around 11 wt %, above which significant changes in mechanical properties and increases in conductivity occurred. Ester- and amide-linked zwitterionomers at equivalent IL swelling levels exhibited very similar mechanical and electrical properties below

10 wt% IL. These results confirmed the IL was preferentially swollen in the zwitterion-rich domains, and we hypothesized that a morphological change due to an increased size and decreasing number of ionic domains occurred above a critical IL content of ~11 wt %.

Chapter 10: Suggested Future Work

10.1 Living Polymerization of Functional Triblock Copolymers

The main advantage of using living polymerization techniques throughout this work was the ability to form block copolymer architectures with controlled molecular weights. Thermoplastic elastomers (TPEs) based on styrene-butadiene systems are a prototypical example of high performance block copolymers synthesized through living polymerization. However, these systems suffer from poor oxidative and UV-stability and low service temperature.[1] All-acrylic triblock copolymers offer an attractive alternative to traditional styrene-butadiene TPEs with enhanced stability and a broad range of glass transition temperature possibilities based on acrylate choice. Screened anionic polymerization offers a synthetic approach for the controlled synthesis of acrylic block copolymers with control of stereotacticity to tailor the T_g. Suggested copolymers to achieve this goal include poly(MMA-*b*-isoprene-*b*-MMA) and poly(MMA-*b*-nBA-*b*-MMA) using reported strategies in Chapter 2. Substitution of a low T_g block with *t*-butyl methacrylate (tBMA) leads to the synthesis of functional block copolymers following hydrolysis to form methacrylic acid. The use of aluminum mediators in the controlled polymerization of tBMA is significantly less studied than MMA and other common methacrylates in the literature. A proposed synthetic scheme for the formation of poly(MMA-*b*-tBMA) is shown in Scheme 10.1.

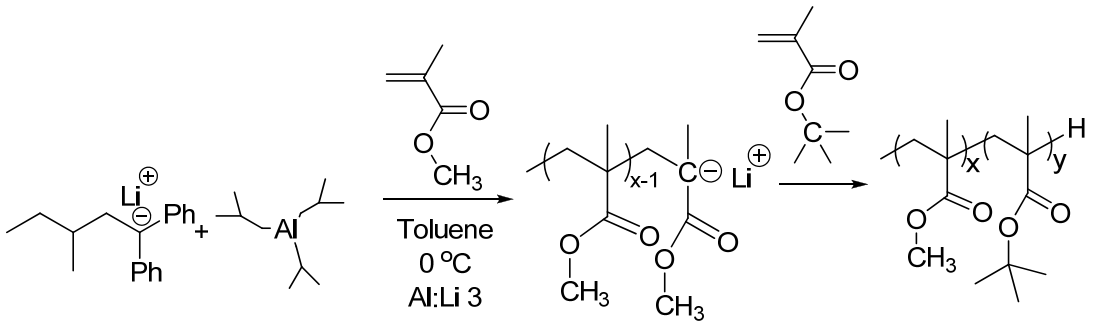

Scheme 10.1 Sequential block addition of MMA and tBMA to form acrylic diblock copolymer using screened anionic polymerization.

Nitroxide mediated polymerization is another facile technique for the synthesis of functional block copolymers. Successful formation of poly(nBA-*b*-HEA-TMS) was demonstrated in Chapter 3. Formation of functional, telechelic triblock copolymers is the next step in this study. Mather and Long et al.[2] previously reported the synthesis of a difunctional alkoxyamine initiator based on DEPN for the formation of triblock acrylic copolymers. Good control of molecular weight and polydispersity in the formation of an nBA center block was exhibited, with good crossover to form triblock copolymers featuring multiple hydrogen bonding groups. Preliminary synthetic experiments demonstrated the controlled polymerization of nBA in the bulk using $DEPN_2$, as shown in Scheme 10.2. SEC results exhibiting narrow polydispersities at low conversions are summarized in Table 10.1.

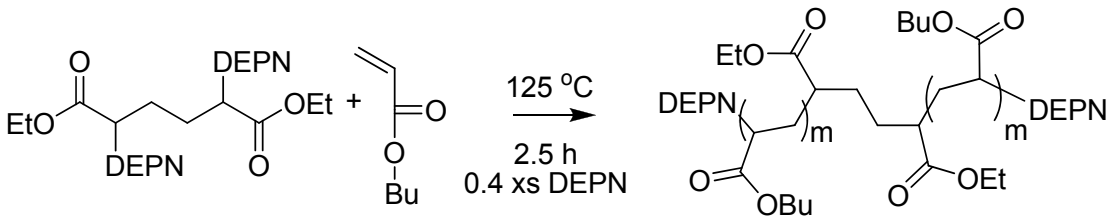

Scheme 10.2 Synthesis of difunctional poly(nBA) using $DEPN_2$ difunctional alkoxyamine.[2]

Table 10.1 Molecular Weight Characterization of Poly(nBA) prepared with $DEPN_2$.

M_n (g/mol)	M_w/M_n	% Conv
24,500	1.12	13
39,700	1.09	21
54,500	1.10	15

Well controlled poly(nBA) macroinitiators prepared in the first step were used for the synthesis of triblock copolymers through the block addition of HEA-TMS. To date, issues with solubility and isolation of these amphiphilic triblock copolymers have led to difficulties in product characterization and confirmation of block addition. A proposed synthetic route at 20 wt % solids in DMF is shown in Scheme 10.3. Optimization of reaction conditions and isolation procedures are expected to result in the successful synthesis of amphiphilic triblock copolymers.

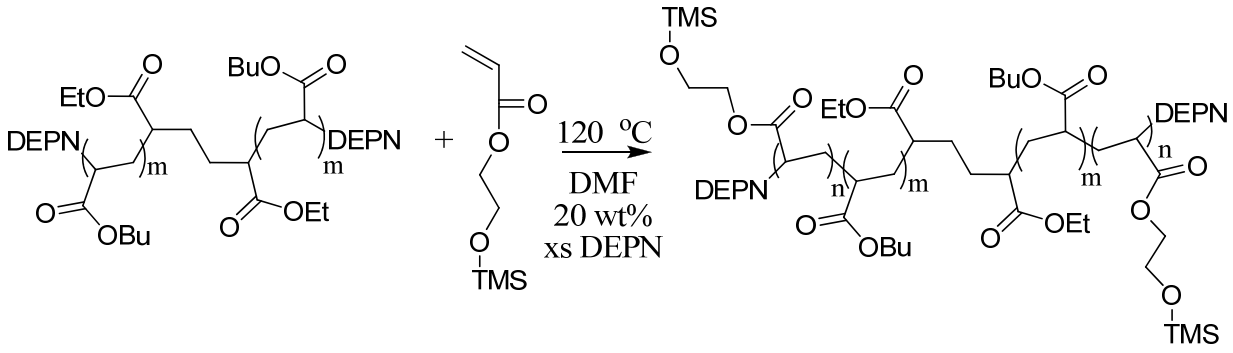

Scheme 10.3 Proposed synthesis of triblock copolymer through addition of HEA-TMS to poly(nBA) macroinitiator.

Reversible addition-fragmentation chain transfer (RAFT) polymerization has emerged as one of the most versatile controlled radical polymerization techniques. Controlled polymerization with RAFT chain transfer agents are successful for a variety of monomer functionalities and under a broad range of reaction conditions, from the bulk to aqueous conditions.[3] Facile synthesis of block copolymers with narrow molecular weight distributions, controlled architecture, and defined endgroups and block lengths have been achieved. Lowe and McCormick have performed extensive studies on the RAFT polymerization of functional monomers, including zwitterions.[4,5] Therefore, RAFT is a feasible approach for the synthesis of well-defined block copolymer structures containing sulfobetaine and nBA blocks. This particular architecture is desirable to induce an ordered morphology for exploration of zwitterionic copolymers in electroactive devices. Block copolymers are known to form well-ordered bulk morphologies, and a block copolymer structure analogous to the random copolymers previously discussed may lead to the formation of ion channels or larger ionic domains for interaction with ionic liquids.

Yusa and coworkers[6] previously reported the synthesis of zwitterionic block copolymers with n-butyl methacrylate, where the zwitterion block was synthesized in water, and chain extension with n-butyl methacrylate was performed in methanol. A similar synthetic pathway is proposed for the synthesis of triblock zwitterion-containing copolymers, using a difunctional RAFT chain transfer agent synthesized in our laboratories, according to literature methods.[7] Issues with block copolymer solubility and characterization are a major factor in the successful isolation of the triblock copolymer, as solubility of the block system is significantly different from the random copolymers that maintained the matrix polymer solubility properties.

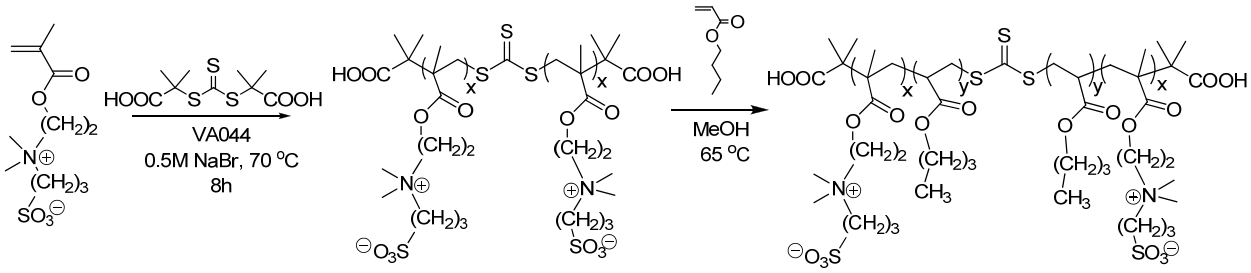

Scheme 10.4 Proposed synthetic route for the formation of zwitterionic block copolymers with n-butyl acrylate center block.

Formation of zwitterionic copolymers of well-defined molecular weights and structures may also be accessible through nitroxide mediated polymerization. Phan and Bertin recently reported the aqueous nitroxide mediated polymerization of several water-soluble monomers, including neutral, anionic, and cationic monomers using an aqueous soluble derivative of BlocBuilder unimolecular initiator.[8] This same water soluble alkoxyamine was applied in the polymerization of SBMA under aqueous conditions to afford homopolymers with quantitative

yields (Scheme 10.5). To our knowledge, zwitterions have not been polymerized using nitroxide mediators previously. Preliminary results show that polymerization control is improved in the presence of excess DEPN, resulting in a more narrow molecular weight distribution of 1.5 in the presence of 100 mol % excess DEPN to BlocBuilder. No conversion of monomer to polymer occurred in the absence of BlocBuilder. Aqueous SEC results in Figure 10.1 show the improvement in control with increasing amounts of DEPN, with the peak shape changing from bimodal to monomodal, and polydispersity decreasing from 2.6 to 1.5 when control was achieved. Continued efforts in this area include block addition to prove the living nature of the chain end, as well as optimization of DEPN:BlocBuilder to achieve superior polymerization control.

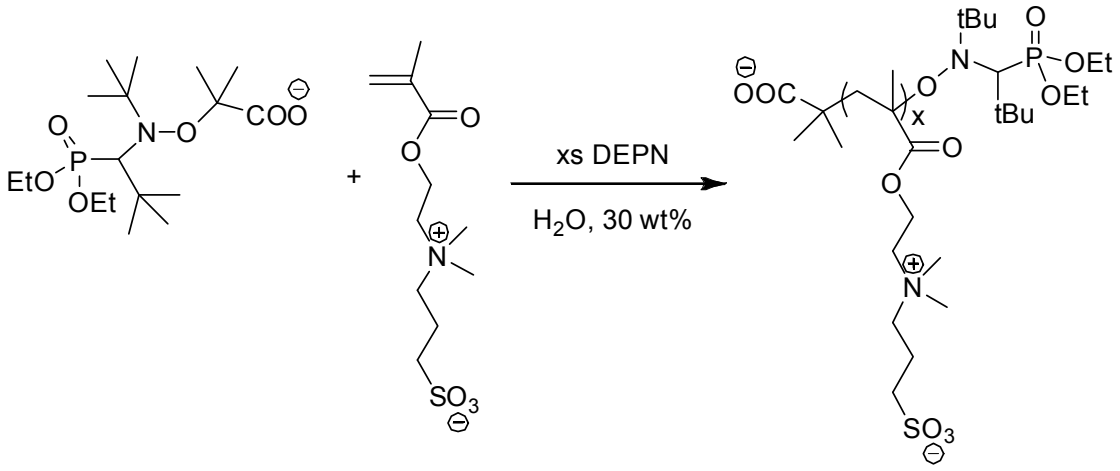

Scheme 10.5 Aqueous nitroxide mediated polymerization of SBMA using deprotonated BlocBuilder.

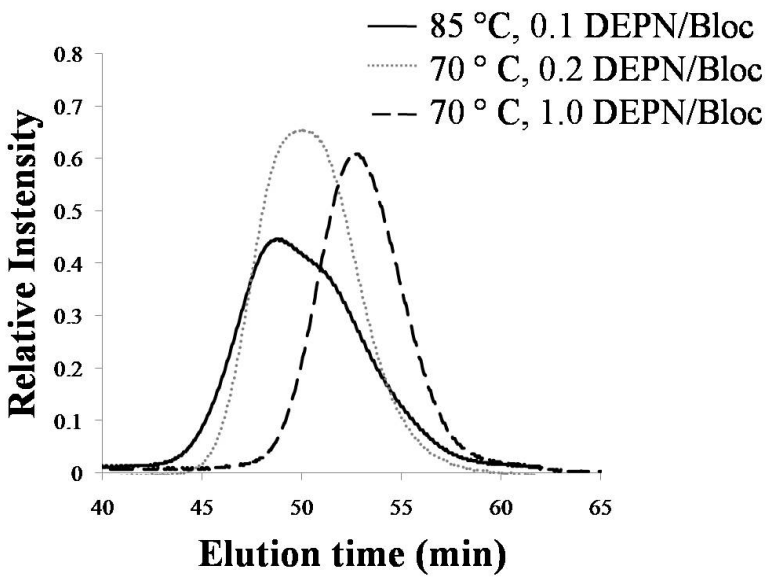

Figure 10.1 Aqueous SEC of Poly(SBMA) synthesized using various DEPN:BlocBuilder ratios.

10.2 Application of Zwitterionic Copolymers in Electroactive Devices

Ion-containing polymers such as Nafion and other ionomers are state-of-the-art materials for the design of new electroactive devices and alternative energy sources. The introduction of ionic liquids as conductive diluents in polymer membranes has greatly improved the applicability and service lifetime of polymeric ionomer transducers and other electronic devices, due to their low volatility and large voltage windows.[9,10] Achieving a better understanding of the interaction of zwitterionic copolymers with ionic liquids may also lead to their application in a number of electronic applications, including ionic polymer transducers (IPTs).

Use of zwitterionomers in electroactive devices first requires a deeper understanding of the effect of ionic liquid on polymer properties and morphology. One limiting factor in the reported work with zwitterionomers is relatively low swelling levels over long swelling times. A comprehensive study to optimize swelling conditions for reproducible and targeted IL contents is

warranted. Swelling membranes at various temperatures and agitation mechanisms, such as stirring or shaking, may lead to faster swelling times and higher swelling levels. Casting in the presence of ionic liquid rather than swelling cast membranes may also lead to higher IL contents and better control of incorporated amounts, although drastic differences in morphology have been observed between casting and swelling methods. Swelling in a range of other ionic liquids with higher conductivities and lower viscosities is also needed in order to determine the best ionic liquid for the desired electronic device. The swelling behavior of zwitterionomers with zwitterionic ionic liquids would also be fundamentally interesting in this study.

Achieving higher swelling levels and better reproducibility of swelling times across samples will provide a larger sample set for the detailed study of mechanical properties, ionic conductivity, and morphology as a function of IL content for both amide- and ester-linked zwitterionic copolymers. More IL contents over a larger range are needed in order to confirm the presence of a critical uptake point above which drastic changes in polymer properties occurred. Additional work in the modeling of x-ray scattering data and the imaging of ionic aggregates using microscopy will also help elucidate the zwitterionomer morphology in the presence of ionic liquids and the meaning of d-spacing within this system. Imaging using high angle annular dark field (HAADF) scanning transmission electron microscopy (STEM) may provide the necessary contrast for the size resolution needed to visualize the size and shape of zwitterionic aggregates. Staining of the ionic liquid may also allow visualization of the percolation dimensions to show the uniformity of swelling throughout the membranes.

Additional characterization of swollen membranes may also enhance the understanding of zwitterion interactions and strength of the aggregates in both swollen and neat membranes. FTIR studies of swollen and neat zwitterionic membranes may elucidate the strength of

interaction between zwitterion functionalities and the competitive binding of IL in the swollen state based on changes in absorbance of the zwitterion functionality as a function of IL content. Additional DSC experiments are needed to probe the presence of a higher thermal transition in the neat membranes. The importance of ionic associations vs. dipole-dipole interactions is also an important distinction when comparing zwitterionomers to classical ionomers. The nature of the associations within zwitterionic aggregates may be probed through blending studies of the zwitterion-containing copolymers with a sulfonated polystyrene or other sulfonated anionic ionomer analog.

The next step in the application of zwitterionomers and ionic liquids in electronics involves the fabrication of electroactive devices. Through collaborations with the Leo Group in Mechanical Engineering, our group has experience in the fabrication of IPTs using novel ionomers as the ionic polymer membrane. A schematic of the components of a typical IPT is shown in Figure 10.2.[9] The ionomer membrane and ionic liquid diluents are coated with a high surface area interpenetrating electrode, such as RuO_2, and then covered with a conductive surface layer of gold leaf. Actuation occurs when an electric field is applied across the device, eliciting a mechanical response in the form of bending. Due to the low modulus of n-butyl acrylate-based polymers, actuation mechanisms other than bending may need to be explored.

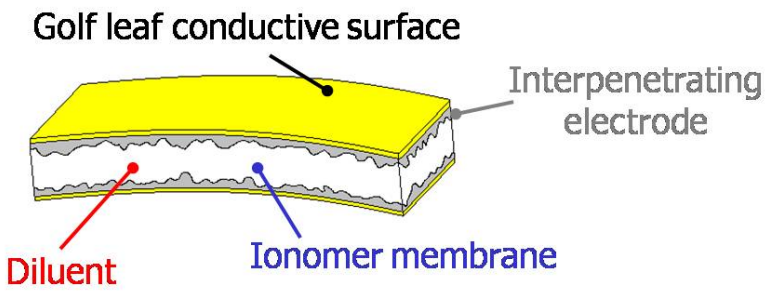

Figure 10.2 Components of an ionic polymer transducer (IPT) device

10.3 Solution Properties of Zwitterionic Copolymers

Rheological behavior of non-aqueous soluble zwitterion-containing polymers is not well studied in the current literature. The contribution of our work is significant, however many questions remain unanswered. The relatively low viscosities of zwitterionic copolymer solutions at concentrations ~1 wt % in chloroform were close to the sensitivity limits of the AR G2 rheometer used in this work. Additional studies at lower concentrations to explore the presence of a dilute regime are desired in order to confirm the identification of concentration regimes for this unique series of copolymers.

In addition to lower instrument sensitivities, a larger range of molecular weights at more zwitterion concentrations are also needed in order to confirm the observed behaviors across polymer compositions. A similar series of copolymers incorporating SBMAm at equivalent loadings were also synthesized in this work, but the rheological properties were not fully characterized. Completion of this work will bolster the hypothesis that zwitterion functionality dominates the rheological behavior. This additional series of copolymers will also provide a larger data set for new modeling studies to explain solution dynamics of zwitterionomers, which

are unlike any other polymer model currently in the literature. In addition to solution rheological behavior, the melt rheology of zwitterionomers is also useful for more sensitive detection of the flow region in mechanical property measurements.

Polyzwitterions exhibit interesting solution behavior known as the antipolyelectrolye behavior in the presence of low molar mass electrolytes. Addition of salts to polyzwitterions leads to chain expansion. This behavior is opposite of polyelectrolyes where increasing electrolyte concentration screens the charges on the rigid rod-like polyelectrolytes, leading to a more coil-like structure. The responsiveness of zwitterions to electrolyte concentration allows changes in polymer properties as a function of salt concentration. This behavior may allow salt triggered solubility changes in polyzwitterion solutions at various polymer and salt concentrations.

10.4 Comparison of Zwitterionomers and Ammonium Cationic Polyelectrolyte Analogs

A head-to-head comparison of sulfobetaine and a closely related cationic analog will reveal the true advantages of the dipolar zwitterion in comparison to weaker interactions present in polyelectrolytes. This comparison is very important in order to fully understand the differences in performance and properties of these two vastly different, but structurally similar, ion-containing polymer classes. Sulfobetaines are synthesized through alkylation of 2-dimethylaminoethyl methacrylate (DMAEMA) using a sultone of varying ring sizes. Therefore, a close structural analog results from the alkylation of DMAEMA using an alkyl halide to form the cationic analog. Furthermore, anion exchange of the halide results in more relevant structural analogs. Two proposed structures that have been synthesized in our laboratories are shown in Figure 10.3, where the methyl sulfonate counterion closely matches the SBMA composition.

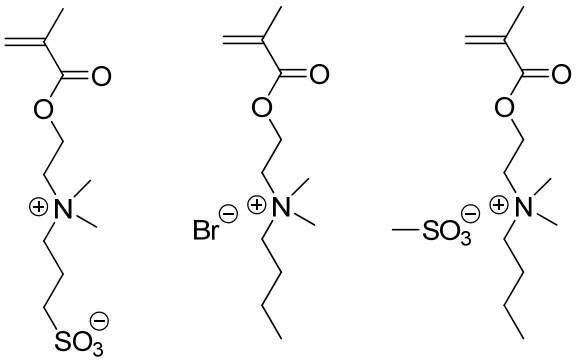

Figure 10.3 Monomers for comparison of zwitterion with structurally similar cationic monomers

A detailed study of the mechanical behavior, morphology, thermal properties, electrical properties, and interaction with ionic liquids is expected to show marked differences in the properties of these ion-containing polymers, where the only difference should result from counterion mobility. These studies are currently underway, and copolymers containing the cationic analog exhibit very different mechanical and thermal properties, presumably based on weaker ionic interactions and a lesser extent of phase separation.

10.5 References

(1) Tong, J. D.; Moineau, G.; Leclere, P.; Bredas, J. L.; Lazzaroni, R.; Jerome, R. *Macromolecules* **2000**, *33*, 470-479.
(2) Mather, B. D.; Baker, M. B.; Beyer, F. L.; Berg, M. A. G.; Green, M. D.; Long, T. E. *Macromolecules* **2007**, *40*, 6834-6845.
(3) Lowe Andrew, B.; McCormick Charles, L. *Prog. Polym. Sci.* **2007**, *32*, 283-351.
(4) Lowe, A. B.; McCormick, C. L. *Chem Rev* **2002**, *102*, 4177-89.
(5) Lowe, A. B.; McCormick, C. L. In *Symposium on Polyelectrolytes and Polyzwitterions held at the 228 ACS National Meeting*; Lowe, A. B., McCormick, C. L., Eds. Philadelphia, PA, 2004, p 65-78.
(6) Yusa, S. I.; Fukuda, K.; Yamamoto, T.; Ishihara, K.; Morishima, Y. *Biomacromolecules* **2005**, *6*, 663-670.
(7) Lai, J. T.; Filla, D.; Shea, R. *Macromolecules* **2002**, *35*, 6754-6756.
(8) Phan, T. N. T.; Bertin, D. *Macromolecules* **2008**, *41*, 1886-1895.
(9) Duncan, A. J.; Leo, D. J.; Long, T. E. *Macromolecules* **2008**, *41*, 7765-7775.
(10) Bennett, M. D.; Leo, D. J. *Sens. Actuators, A* **2004**, *115*, 79-90.